

Mechanical Engineering, Materials Science Research and Applications



EDITORS

Prof. Dr. Yusuf ŞAHİN

Prof. Dr. Adrian OLARU

Assist.Prof. Senai YALÇINKAYA

MECHANICAL ENGINEERING, MATERIALS SCIENCE RESEARCH AND APPLICATIONS

EDITORS

Prof. Dr. Yusuf ŞAHİN
Prof. Dr. Adrian OLARU
Assist. Prof. Senai YALÇINKAYA

MECHANICAL ENGINEERING, MATERIALS SCIENCES RESEARCH AND APPLICATIONS

EDITORS

Prof. Dr. Yusuf ŞAHİN

Prof. Dr. Adrian OLARU

Assist. Prof. Senai YALÇINKAYA

Güven Plus Group Inc. Publications: 21/2022
20 DECEMBER 2022

Publisher Certificate No: 52866

E-ISBN: 978-625-7367-37-0

Güven Plus Group Inc. Publications

All kinds of publication rights of this scientific book belong to GÜVEN PLUS GROUP CONSULTANCY INC. PUBLICATIONS. Without the written permission of the publisher, the whole or part of the book cannot be printed, broadcast, reproduced or distributed electronically, mechanically or by photocopying. **Responsibility for each chapter and article in the book, visuals, graphics, direct quotations, and the permission of the ethics committee and institution belong to the respective authors. In case of any legal negativity that may occur in this direction, the institutions that support the preparation of the book, especially the Publishing House, the institution(s) responsible for the arrangement and design of the book, and the book editors, referees, organizing committee, scientific committee and other boards, the publishing house do not accept any "material and moral" liability and legal responsibility in any matter and cannot be taken under legal obligation. All kinds of legal obligations and responsibilities belong to the author(s) of the relevant section in terms of "material and moral". As GROUP CONSULTANCY "PUBLISHING" INC. and on behalf of book science/editor boards, we reserve our rights in this regard materially and morally. In any legal problem/situation TURKEY/ISTANBUL courts are authorized.** This work, prepared and published by Güven Plus Group Consultancy Inc. Co., has ISO: 10002: 2014-14001: 2004-9001: 2008-18001: 2007 certificates. This work is a branded work by the TPI "Turkish Patent Institute" with the registration number "Güven Plus Group Consultancy Inc. Co. 2016/73232" and "2015/03940". This scientific/academic book is of national and international quality and has been officially documented with the information of Istanbul Governorship Provincial Culture and Tourism Directorate Istanbul Printed Letters and Pictures Compilation Directorate No: 37666426-207.01[207.02.02]-E.62175 Date: 21.01.2019. **This scientific/academic book is "within the scope of academic incentive criteria for 2019, and it is evaluated within the scope of the related regulation published in accordance with the Presidential Decision numbered 2043 dated 16/1/2020 and published in the Official Gazette numbered 31011 dated 17/01/2020" and meets the academic incentive criteria.** This multi-author book has E-ISBN and is scanned by the National Libraries of the Ministry of Culture and the E Access system of the National Library, which has an agreement with 18 different World Countries. This book cannot be bought or sold with a monetary value. Provided that the chapter and content in this scientific book is quoted and cited to the relevant book, it can be used by scientific or relevant researchers for reference. **Our publishing house and the editorial board of the book act in accordance with the laws on the protection of personal data and privacy. It obliges the authors of scientific book chapters to act in this direction. Individuals who own this academic/scientific book regarding the protection of personal data are obliged to act in accordance with the relevant laws, regulations and practices. It is deemed to have accepted in advance the legal, material and moral problems and obligations that arise about those who act contrary to this.**

Text and Language Editors

Assoc. Prof. Gökşen ARAS (Turkish – English)

Assist. Prof. L. Santhosh KUMAR (English)

Cover and Graphic Design

Lec. Ozan KARABAŞ

Ozan DÜZ

Page Layout

Burhan MADEN

Print-Binding

GÜVEN PLUS GROUP CONSULTANCY INC. PUBLICATIONS®

Kayaşehir Neighborhood Evliya Çelebi Street Emlakkonut Başakşehir Houses 1/A D Block Floor 4 Number 29 Başakşehir İstanbul - Turkey Phone: +902128014061- 62 Fax: +902128014063 Mobile: +9053331447861

BOOK LICENSEE

GÜVEN PLUS GROUP CONSULTANCY INC. PUBLICATIONS®

Kayaşehir Neighborhood Evliya Çelebi Street Emlakkonut Başakşehir Houses 1/A D Block Floor 4 Number 29 Başakşehir İstanbul - Turkey Phone: +902128014061- 62 Fax: +902128014063 info@guvenplus.com.tr,

www.guvenplus.com.tr

CONTENTS

PREFACE	5
ÖNSÖZ	7
CHARACTERISTIC BEHAVIOR OF AUXETIC STRUCTURES	9
Fevzi BEDİR, Shao-Ho HUANG	
DETERMINATION OF THE EFFECT OF TAILSTOCK AND CHUCK PRESSURE ON VIBRATION AND SURFACE ROUGHNESS IN TURNING OPERATIONS WITH GRAY RELATIONAL ANALYSIS METHOD	43
Hüseyin GÜRBÜZ, Şehmus BADAY	
EXPERIMENTAL INVESTIGATION OF SINGLE PHASE UNCONTROLLED RECTIFIERS	73
Mehmet Ali ÖZÇELİK, Ahmet AYCAN	
RADIATION SHIELDING PROPERTIES OF REINFORCED (BASO₄ AND SIC) AZ91 MATERIALS	106
Gizem YALÇIN, Zübeyde ÖZKAN, Uğur GÖKMEN, Sema Bilge OCAK	
SAVING ENERGY CONSUMPTION IN BUILDINGS BY ADVANCED CONTROL STRATEGIES	132
Masoud TAGHAVI	
UNRELATED PARALLEL MACHINE SCHEDULING WITH SEQUENCE-DEPENDENT SETUP TIMES: AN APPLICATION TO AUTOMOBILE SPARE PART MANUFACTURER	149
Muhammed SÜTÇÜ, İbrahim Tümay GÜLBAHAR, Yakup KAPAR, Fatih İNCE, Nurettin ŞAHİN	
FUNDAMENTALS OF THE NEW CALCULATION METHOD OF THE HYDRODYNAMIC JOURNAL BEARINGS	170
Hüseyn MIRZAYEV	
SELECTION OF PLASTIC INJECTION MACHINE WITH AXIOMATIC DESIGN APPROACH	213
Gürcan ATAKÖK, İzzet ÖZBEK	
FINE-KINNEY RISK ANALYSIS METHOD STUDY AT THE HAZARDOUS WORKPLACE MANUFACTURING METAL MATERIAL FOR THE DEFENSE INDUSTRY	228
Zehra Gülten YALÇIN, Muhammed Bora AKIN, Mustafa DAĞ	

PREFACE

In our world, while there are many negativities in the areas of nature, health, social, etc.; technological developments are becoming a necessity in the industry in general for the solution of these and other problems. Technological developments, triggered by quality competition, desire for comfort, fear and anxiety, emerge as a fact that we face in many and difficult to follow. Academic studies conducted in this context; It is brought together with its interlocutors, sometimes in the form of open-access sites, and sometimes in the form of congresses, panels, periodicals and scientific books.

We wanted to have a finger in the pie with this academic book study called

“Mechanical Engineering, Materials Sciences Research and Applications”

which consists of different chapters and covers the researches of valuable academicians. This book; we present it to you, valuable scientists and industry employees through “Güven Plus Grup Inc. Publications” which a major part of its publications consisting of academic books, has gained a great reputation with its qualified activities in the national and international arena.

This book consists of many engineering subjects and experimental studies and applied academic subjects. In the book;

You will find valuable research and experimental studies on many important subjects.

We believe that the book, which includes chapters dealing with many interesting topics of engineering technologies, will shed light on the academic studies of many researchers, and will find a valuable place in the catalogs of the Higher Education Institution, public libraries and personal archives.

ÖNSÖZ

We would like to express our gratitude to our esteemed editors, writers, referees and you, our dear readers, who have contributed to the realization of this important work, which emerged as a result of the long-lasting and meticulous work. **December 2022**

Prof. Dr.Yusuf ŞAHİN

Prof.Dr.Adrian OLARU

Assist. Prof. Senai YALÇINKAYA

ÖNSÖZ

Dünyamızda doğa, sağlık, sosyal vb. alanlarda birçok olumsuzluk yaşanırken; bunların ve diğer problemlerin çözümüne yönelik olarak genel anlamda endüstride, teknolojik gelişmeler zorunluluk halini almaktadır. Kalite rekabeti, konfor arzusu, korku ve endişenin de tetiklediği teknolojik gelişmeler, takipte zorlanılacak derecede ve çok sayıda yüzleştığımız bir gerçek olarak karşımıza çıkmaktadır. Bu bağlamda yapılan akademik çalışmalar; kimi zaman açık erişimli siteler, kimi zaman da kongre, panel, süreli yayınlar ve bilimsel kitaplar şeklinde muhataplarıyla buluşturulmaktadır.

Biz de, birbirinden kıymetli akademisyenlerin araştırmalarını kapsayan, yirmi altı farklı bölümden oluşan

“Mechanical Engineering, Materials Sciences Research and Applications” adını verdiğimiz bu akademik kitap çalışması ile çorbada tuzumuz olsun istedik. Bu kitabı; yayınlarının önemli bir bölümünü akademik kitaplardan oluşan, Ulusal ve Uluslararası alanda nitelikli faaliyetleriyle oldukça saygınlık kazanmış olan “Güven Plus Grup A.Ş. Yayınları” aracılığı ile siz değerli bilim insanları ve endüstri çalışanlarının hizmetine sunuyoruz.

Bu kitap, birçok mühendislik konuları ve deneysel çalışmalar ile uygulama yapılmış akademik konulardan meydana gelmiştir. Kitapta;

Farklı problemlerin çözümüne kadar birçok önemli konuda değerli araştırma ve deneysel çalışmaları bulacaksınız.

Mühendislik teknolojilerinin birçok ilgi çekici konularına değinilen bölümlerin yer aldığı kitabın, çok sayıda araştırmacının akademik çalışmalarına ışık tutacağına, Yükseköğretim Kurumu kataloglarında, kamu kütüphanelerinde ve kişisel arşivlerde oldukça değerli bir yer bulacağına inanıyoruz.

Uzun zaman alan ve büyük bir titizlikle yapılan çalışmaların sonucu olarak ortaya çıkan bu önemli eserin gerçekleşmesinde emeği geçen saygıdeğer editörlerimize, yazarlarımıza, hakemlerimize ve kitabımızı editen siz sevgili okurlarımıza teşekkürlerimizi sunarız. **Aralık 2020**

ÖNSÖZ

Mechanical Engineering, Materials Sciences Research and Applications

Prof. Dr. Yusuf ŞAHİN
Prof. Dr. Adrian OLARU
Assist. Prof. Senai YALÇINKAYA

CHARACTERISTIC BEHAVIOR OF AUXETIC STRUCTURES

Fevzi BEDİR¹, Shao-Ho HUANG²

Abstract: Auxetic structure or material which obtains negative Poisson's ratio (NPR) gives us a great opportunity to manufacture more fascinating products. Auxetic structure obtains opposite physical characteristics from normal materials which means when under compressive loading auxetic structure would contract rather expand and acts oppositely under tensile. This behaviour performs differently from normal structures and because of this specialty auxetic structure applies spectacular ability for enduring compacts, good indentation resistance, energy absorption capability and shear resistance. Nowadays, many incredible auxetic structure designs have been created to advance our lives, such as medical and sports applications. To achieve improved properties for engineering submissions, there are plenty existed pieces of articles that demonstrated the possibility of auxetic structures. Different material-based specimens, providing subtle differences in composition, or combining different types are the most common methodologies. However, most research only mentioned the behaviours that occur under loading in beam shape or 2D sketches. In real applications, tubular structures are also essential for building significant products. This chapter is to observe the behaviour of auxetic structures that are under impact with the tubular structure which may occur frequently in our realities. Though there are plenty of types of auxetic structure, it was selected the two most studied kinds of auxetic structure cell geometry; tetra-chiral and re-entrant to build the specimen for understanding the behaviour of the auxetic structure under compact loading.

¹ Gebze Technical University, Dept. Mechanical Eng., Kocaeli / Türkiye e-mail: fevizbedir@gmail.com, Orcid Id: 0000-0002-9202-3458

² Gebze Technical University, Dept. Mechanical Eng., Kocaeli / Türkiye e-mail: ppaanny952@gmail.com, Orcid Id: 0000-0002-7481-8695

Keywords: Auxetic Structure, Negative Poisson's Ratio, Tubular Structure, Re-Entrant, Tetrachiral

INTRODUCTION

It was written by Evans for the first time that the concept of auxetic structure can be traced back to 1991(K.E.Evans, 1991). Such a structure exhibits opposite physical behaviour from normal materials due to the negative poisson ratio (NPO). The auxetic structure expands under tensile strain and contracts under compressive strain (M.Mir etc., 2014), resulting in a decidedly different physical performance. Based on our knowledge, the Poisson's ratio (ν) is the negative ratio of transverse strain to axial strain. Axial strain decreases when compressive stress is applied to normal material, while transverse strain increases, and when tensile stress is applied to normal material, axial strain increases, then transverse strain decreases. However, the auxetic structure gains an opposite feature from normal materials. The auxetic structure contracts transversely when subjected to compressive stress and expands transversely when its axial stress increases.

The general deformation can be understood from Figure 1. The left side is the normal side that contracts when pulled. The right side is the auxetic structure, which behaves the opposite of normal expansion when retracted. The feature that performs differently from normal materials is able to implement the distinguishing feature that improves many important features for engineering materials. People have noticed this particular structure for over 30 years due to engineering needs, but there is still not much research in this area, so this topic is still fairly new. The subject is still new, there are plenty of natural auxetic substances that have existed in nature for a long time.

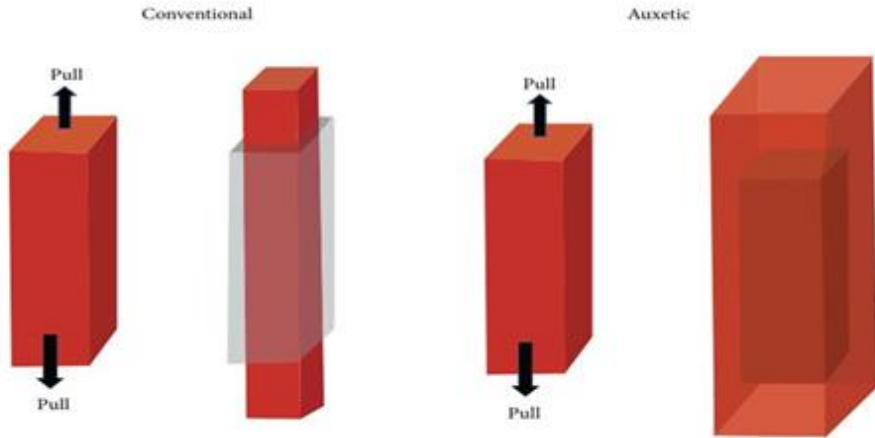


Figure 1. Difference Between Conventional Material and Auxetic Structure Under Tensile Stress (M. Mir etc., 2014)

For example, the salamander's auxetic structural skin gives it a good ability to escape from its predators (C.Santulli and C.Langella, 2016). This feature is also seen in the skin of cats, snakes and cow muzzles and this helps them to make some abnormal movements.

Most auxetic structure articles focus on auxetic behaviour under loading with 2D configurations or beam structures. Because of the structural configuration, each cell influences each other, current research has only shown the auxiliary behaviour where the two extreme edges of the model are not connected. This section is to find out whether the mechanical properties can be improved by permissiveness. Binding to all unit cells and exhibiting more complete NPO behaviour leads to promising mechanical performance. In order to compare the possible different results, the results of the compression test were compared with the results of the simulation by performing the simulation of impact and compression to verify the effects of the samples under the verified loading rates.

AUXETIC MATERIALS/STRUCTURES

People have noticed this particular structure for over 30 years due to engineering needs, but there is still not much research in this area, so this topic is still fairly new. The subject is new, there are plenty of natural

auxetic substances that have been in nature for a long time. For example, the salamander's auxetic structural skin gives it a good ability to escape from its predators (C.Santulli and C.Langella, 2016). This feature is also seen in the skin of cats, snakes and cow muzzles and this helps them to make some abnormal movements.

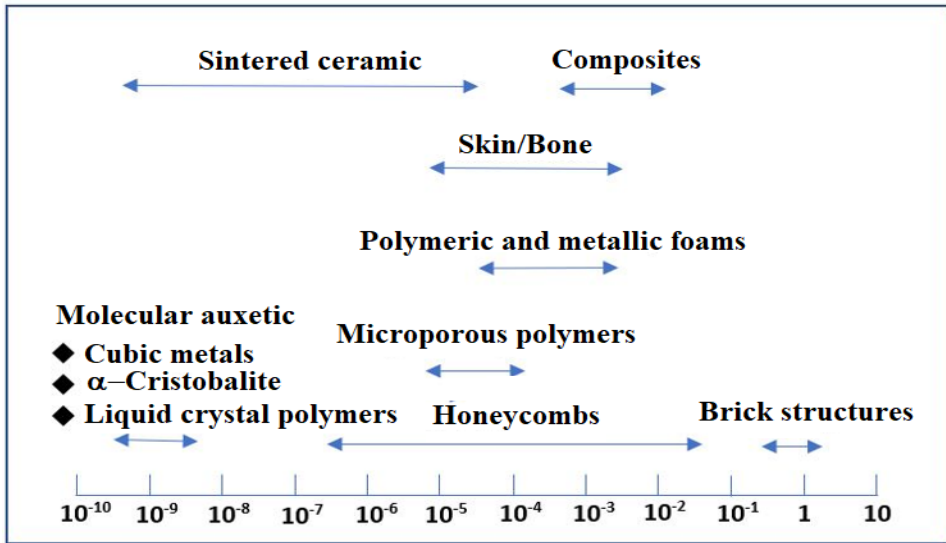


Figure 2. Scales of Auxetic Structure Variations

As we can see in Figure 2, auxetic materials are available in many different sizes. Auxetic materials have been discovered on a wide scale from the nanometer to the meter, so the auxetic structure can be applied to multiple suitable applications. The first designed auxetic structure, “re-entrant honeycomb” was designed by Gibson et al. (L. J.Gibson and M. F.Ashby, 1982). As shown in Figure 3, the figure is simply set to a proportion of the entire geometry. Changing the equal sides can lead to a re-entrant structure that achieves auxetic behaviour.

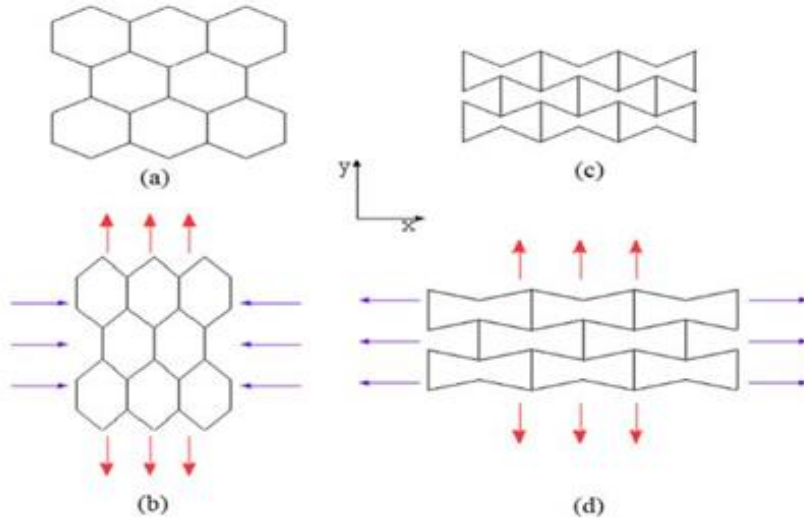


Figure 3. Loading conventional and auxetic materials (M. Ashjari., 2017)

ADVANTAGES and APPLICATIONS of STRUCTURES with NEGATIVE POISSON RATIO

NPO expertise offers us a promising opportunity to manufacture products that are lighter and have better performance during bearing force, as many material properties are related to the ν -value. For example, the indentation resistance developed with an auxetic structure based on the theory that the indentation resistance is proportional to $[(1 - \nu^2)/E]^{-1}$ was discussed (V. L.Coenen and K. L.Alderson, 2012) (I. I.Argatov etc., 2012)

Since ν is only a performing value between -1 and 0.5, and most normal materials only achieve positive Poisson's ratio, this usually means that this fact can slightly affect material properties. However, the auxetic structure can meet the Poisson's ratio of -1 to -1/2 through fine tuning. This causes the poisson ratio to approach the -1, while the $(1-\nu^2)$ value approaches 0, as a result, the indentation resistance can lead to infinity. As shown in Figure 4, the density-changing pattern of the normal material on the left and the density-changing pattern of the auxetic

structure on the right. Low loading reduces the normal material density, but for the auxetic structure, loading causes shrinkage that can increase the indentation of the structure. Negative Poisson's ratio specialization can also improve toughness under compression in re-entrant foam; this sprayed the foam into the preheated metallic cube, imparting an auxetic structure to the foam shape and heating it under compression for a certain period of time (V. L.Coenen and K. L.Alderson, 2012) (I. I.Argatov etc., 2012). The result shown shows that the auxetic structure can promise good application.

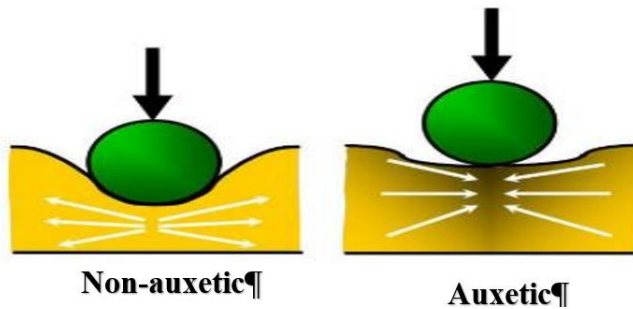


Figure 4. Difference Between Normal and Auxetic Structure Under Indentation Loading (M. Sanami etc., 2014)

It is also justified to increase the localized impact loads achievable in auxetic structures (A.Remennikov etc., 2019) (D.Xiao etc., 2019), which is particularly important for buildings or facilities since the increased accidental detonation. The sample is placed in a sandwich beam with an auxetic structure core to carry the impacts. This result shows that auxetic structure can be advantageous for building construction. Another similar experiment shows an advantage for defense applications (R. S.Underhill and D.Canada, 2014) (C.Qi etc., 2013). Figure 5. shows three different honeycomb core sandwich beam configurations that will be examined for ballistic resistance. Figure 6. shows the velocity under impact loading at 190 m/s, showing that the re-entrant configuration gives the most appreciable ballistic resistance.

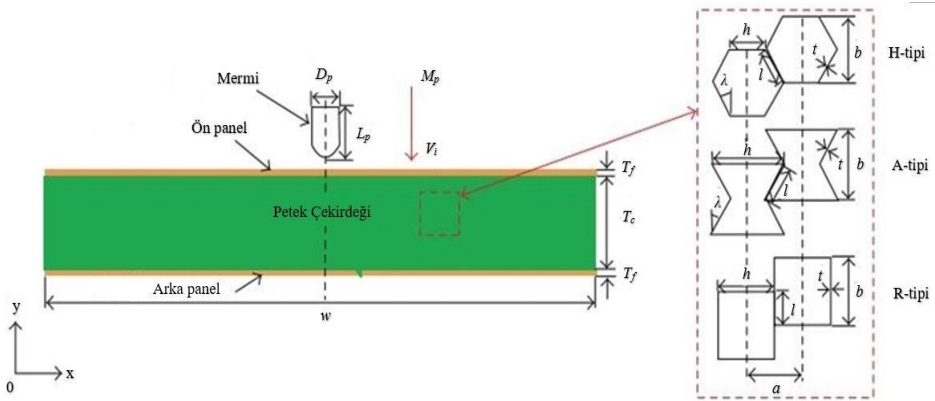


Figure 5. Schematic Outline of Honeycomb Sandwich Panels (Hsps) Under in-Plane Bullet impact (C. Qi etc., 2013)

Thanks to the proven results, it can be understood that it is possible to apply the auxetic structure in military or some high security buildings. Anti-terrorist attacks and prevention of accidental explosions are important studies that can be improved with auxetic structure.

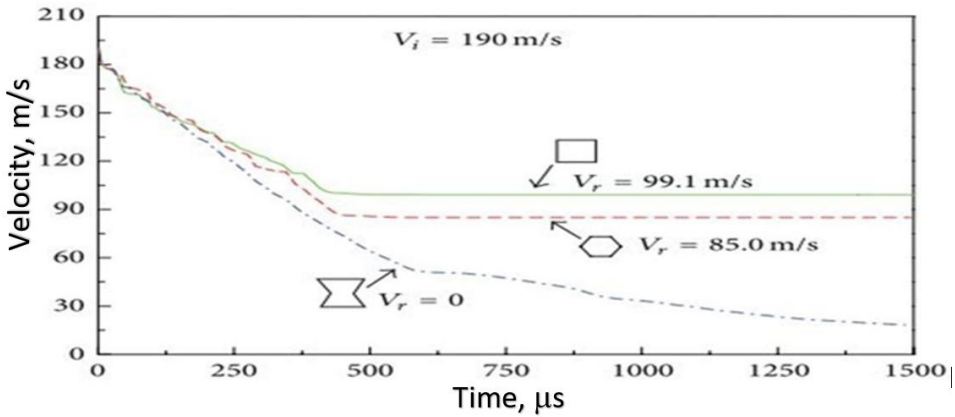


Figure 6. Time History of the Transit Velocity of the Projectile with $V_i = 190$ M/S. Here V_r is the Residual Velocity (C.Qi etc., 2013)

In addition, the auxetic structure can also be applied to knitted composites, which means that expected results can be achieved with simpler modelling. It can save more time and research resources, providing more opportunities to expand the field of application (P.Subramani etc., 2014).

Many more useful applications have been developed with auxetic structures (M.Sanami etc., 2014) on sports applications. For example, as with the geometry shown in Figure 7, the auxetic structure made of chiral arrowhead configuration, compared to conventional ones, gives a distinctive feature that can meet the need for a helmet that requires double curvature.

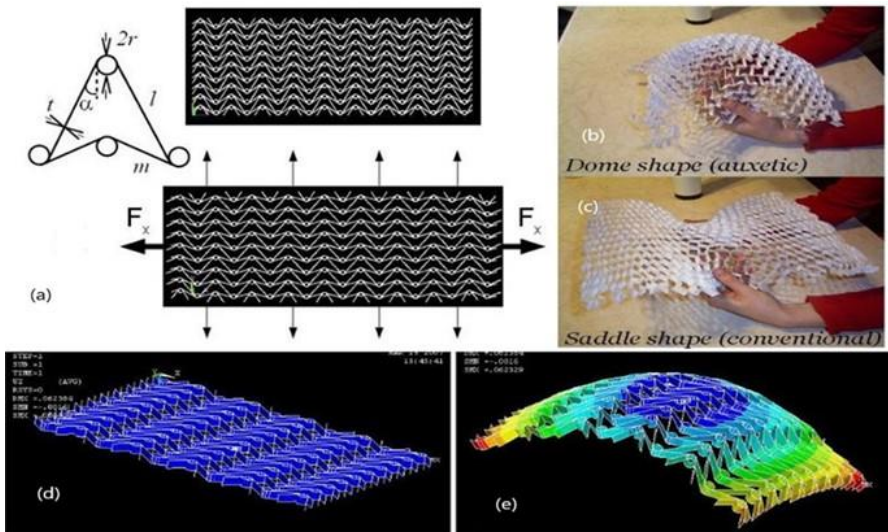


Figure 7. (a) Chiral Arrowhead Honeycomb 9x9 Unit Cell FE Model Before and After Stretching. Curvature of (b) Auxetic and (c) Non-Auxetic Materials. (d) Chiral Arrowhead' Honeycomb: 5x9 Unit Cell FE Model Before and (e) After out-of-Plane Bending Structures (M. Sanami etc., 2014)

Based on this expertise, cylinders combined in the auxetic structure can normally align with the curved surface of the helmet to protect people from accidental crushing or impact. Another improved auxetic structure it can provide in sports applications is the adjustable porosity variation that helps dissipate heat (A.Alderson etc., 2000) and this advantage can be applied to disperse human odor or antiperspirant agents during intense exercise. Also, as we know, there are some sports equipment that require impulsive absorption abilities, such as baseball gloves or baseball pads, which can also benefit from auxetic foam, which has already prov-

en to have better indentation resistance than starting foam. To increase stability and efficiency in flight, the design of the transforming air foil must allow for change at low speed or high speed. As Figure 8 shows, deforming air foils based on chiral geometry are effective sources for fabricating aircraft structures (W.Wu etc., 2019) (P.Bettini etc., 2010). Consequently, the reason why the auxetic structure can be applied to such a large number of applications is that it acquires many good material properties, such as better shear modulus, improved indentation resistance, improved fracture toughness, expanded planar strain resistance and favourable energy absorption measurements. With all these fascinating properties, auxetic structures attract us to further research for them.

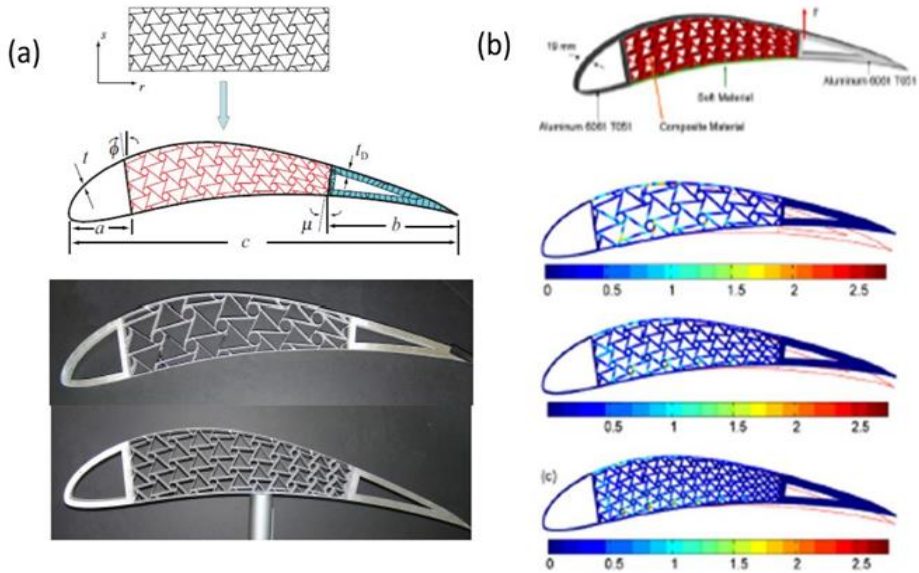


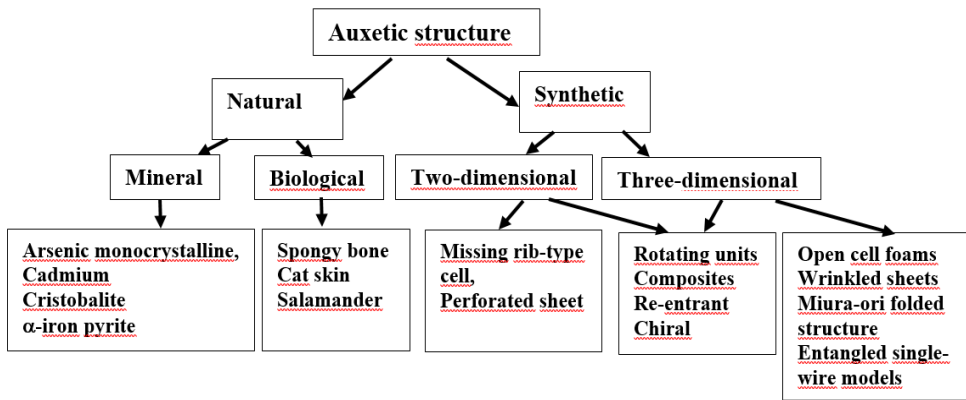
Figure 8. Chiral Airfoil and Aerodynamic Performance Simulation: (a) Design and Fabrication of a Chiral Airfoil Using Waterjet Cutting Techniques; (b) Axial Stress Distribution at the Boundary of the Elastic Regime of the Material for a Carbon Fiber Air Foil (P. Bettini., 2010)

AUXETIC STRUCTURE CATEGORIES

There are many forms of auxetic structures, as shown in Table 1 (I.O.P.C.Series and M.Science, 2020), which shows a general ranking of

auxetic materials. First of all, the auxetic structure can be divided into two types as natural and synthetic according to its source, or it can be called artificial. There are two forms of natural auxetic material: biological and mineral. As for the synthetic auxetic structure, the carrier loads can be divided into two main groups according to the deformation: two-dimensional and three-dimensional. Although natural auxetic materials are important in many ways, the focus of this thesis is the introduction of synthetic structures rather than natural ones.

Table 1. Auxetic Structure Categories (I.O.P.C. Series and M. Science, 2020)



TWO-DIMENSIONAL AUXETIC STRUCTURES

As we can see in Table 1, the first row of the two-dimensional group is the incomplete rib type shown in Figure 9 (C.W.Smith, 2000) consists of connecting the centers of two equal ribs vertically and again connecting perpendicularly to the other rods of their ends, forming an incomplete rectangle. Although this pattern is quite simple, it successfully describes the performance of auxetic polyurethane foam.

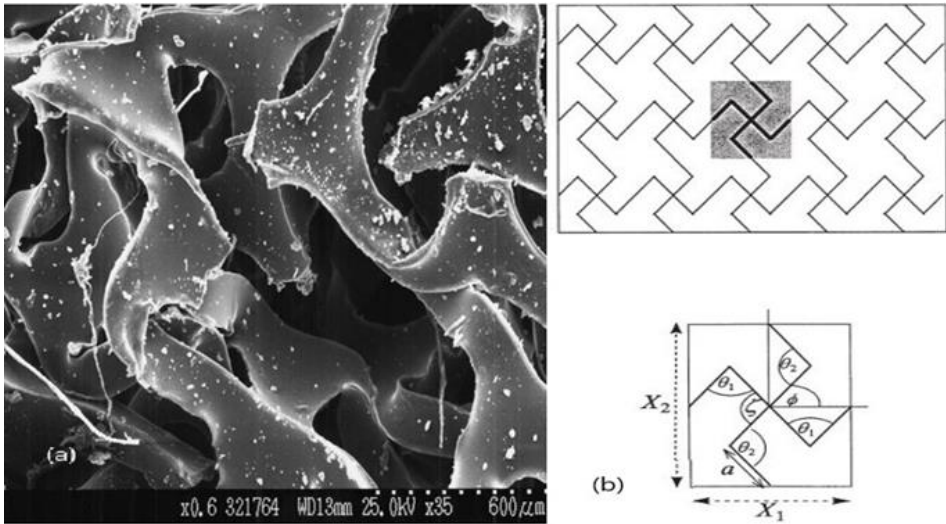


Figure 9. (a) The Cut Surface of a Foam Converted to Auxetic Behavior. Note That There are Cells with Broken Ribs Lying in the Plane of the Cut Surface. (b) Selected Unit Cells for Intact and Truncated Versions, with Their Geometric Parameters (C. W. Smith etc., 2000)

The second one should be perforated sheet type, it is the auxetic structure that manifests itself in the perforated plates (L.Mizzi etc., 2015). As we see in Figure 10, the plates are sequential or randomly oriented notches or meshes. In this case, only some parts of the block or panel need to be cut to construct an auxetic structure, leading to an arrangement with a geometrical formation that has been discovered in many diagrams that have the potential to exhibit auxetic behaviour. Perforated sheet metal has been widely applied to resemble rotating structures based on different shapes, such as squares or rectangles.

Although it is a good method to perform auxetic behaviour, this group is still not fully developed as it means loss of perforated material due to large defect. And this disadvantage will be exacerbated by expensive materials. However, some proposed slit type holes have been created, which are regenerated perforated systems, which means less significant material loss. These renewed techniques not only reduce material

loss, but also show similarities to the deformation behaviour of auxetic systems.

The next type, the rotary system, is a kind of mechanism to achieve an NPR behaviour. As shown in Figure 11, rotating systems are some rigid squares whose vertices are connected by hinges. It can be seen as a certain square arrangement in a two-dimensional structure or as a three-dimensional projection consisting of a certain plane. Such a structure is often discovered from inorganic crystalline materials. An auxetic composite of auxetic property is studied and improvements in some excellent properties such as fracture toughness, low velocity impact performance can be achieved to demonstrate the potential in energy absorbing components.












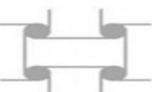


Straight slits		I-Shaped slits	
Slit pattern	Mechanism	Slit pattern	Mechanism
(a) 	 <u>Rotating squares</u>	(e) 	 <u>Fibrils and knots</u>
(b) 	 <u>Type I rotating rectangles</u>	(f) 	 <u>Re-entrant honeycomb</u>
(c) 	 <u>Type alpha rotating rhombus</u>	(g) 	 <u>Anti-tetrachiral</u>
(d) 	 <u>Type I alpha Rotating parallelograms</u>		

Figure 10. Pictorial Representation of the Various Auxetic Mechanisms Expected to be Derived from Relevant Cleft Perforation Patterns (L. Mizzi etc., 2015)

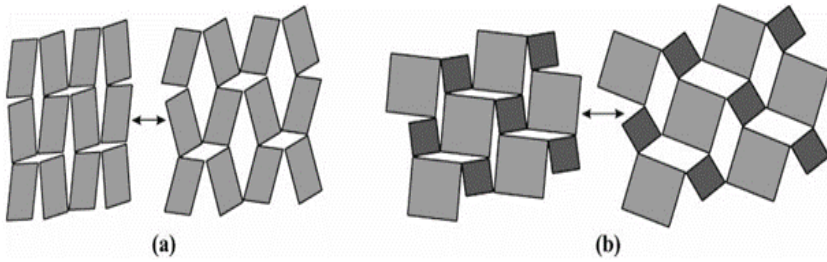


Figure 11. Variations in the "Rotating Squares" Geometry: (a) a More General Rotating Parallelogram Structure and (b) a "Rotating Squares" Structure Formed from Squares of Different Sizes (J. N. Grima and K. E. Evans., 2000)

The re-entrant structure is marked as the stress acting on one side of the solid, resulting in elongation of the adjacent side (L. J.Gibson and M. F.Ashby, 1982). A re-entrant structure is a basic geometry that has an angle greater than 180° or a negative angle in a polygon. The re-entrant structure is one of the most studied auxetic structures. As shown in Figure 12, many different types have been applied to increase the structural strength. For the re-entrant structure, one of the methods applied to strengthen the rigidity of the structure is to add tight ribs to the normal auxetic unit cells in a direction perpendicular to the re-entrant direction (Z.Chen etc., 2020) this article states that it is possible to improve the Young's modulus and shear modulus by adjusting the relative density range. Another study reveals that changing the cavity geometry is also a methodology to improve the energy absorption ability (H.Wang etc., 2019). Or some other subtle differences, such as the angle adjustment applied between cells, may have a chance to increase performance while carrying loads (K.Cai etc., 2016) (K.Meena and S.Singamneni, 2019). In addition, the thickness of the re-entrant structure also plays an important role in influencing the negative Poisson ratio behaviour (Z.Dong etc., 2019). Both thick-walled and thin-walled re-entrant structures exhibit negative Poisson's ratio behavior, but the thickness of the re-entrant structures can affect the deformation mode, which can affect the performance of the structure.

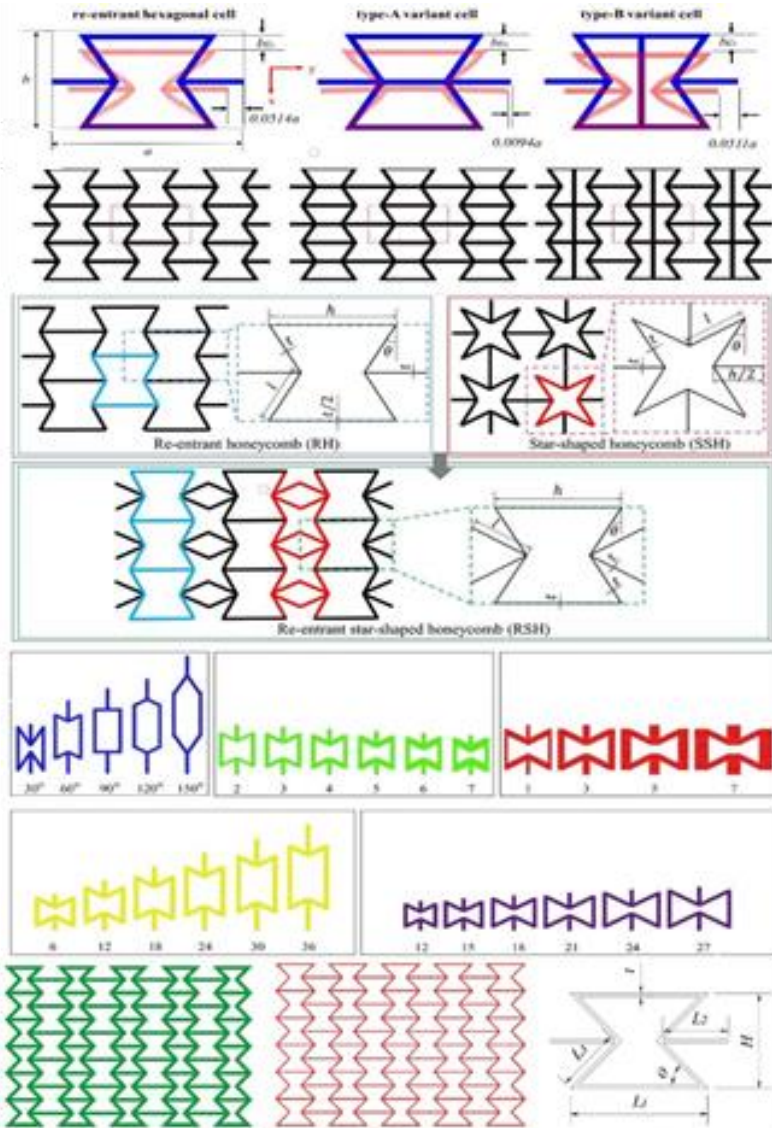


Figure12. (a) A Rigid Ribbed Re-Entrant Structure (Z. Chen etc., 2020). (b) Re-Entrant Structure with Varying Cavity Geometry (H. Wang etc., 2019). (c) Re-Entrant Structure with Different Angles (K. Cai etc., 2016). (d) Re-Entrant Structure at Different Thicknesses (Z. Dong etc., 2019).

If a structure or geometry cannot be superimposed on its mirror image after rotating translation, it can be said to have chirality (W.Wu etc., 2019). Many different design concepts of the chiral type have been intro-

duced since the emergence of the first designed chiral geometry [26]. The chiral structure can show the relationship between local rotation, material deformation, and bending, thus providing this explanation for deriving many unusual performances, such as the negative Poisson ratio of chiral materials. The chiral unit cell consists of an arrangement of cylinders of spherical cross section. Bonds of similar radius, connected by bonds of the same size, are eventually connected tangentially. this type of auxetic structure is the same as the re-entrant structure, which can be applied to both 2D and 3D applications. Even in nature, for example, human left and right hand, DNA, etc. There are many types of chiral structures such as There are many types of chiral structure, such as hexachiral, trichiral, anti-trichiral, tetrachiral, and anti-tetrachiral (A.Alderson, 2010). As shown in Figure 13, the chiral structure can be divided into three main groups: anti-chiral, chiral, and meta-chiral (W.Wu etc., 2019).

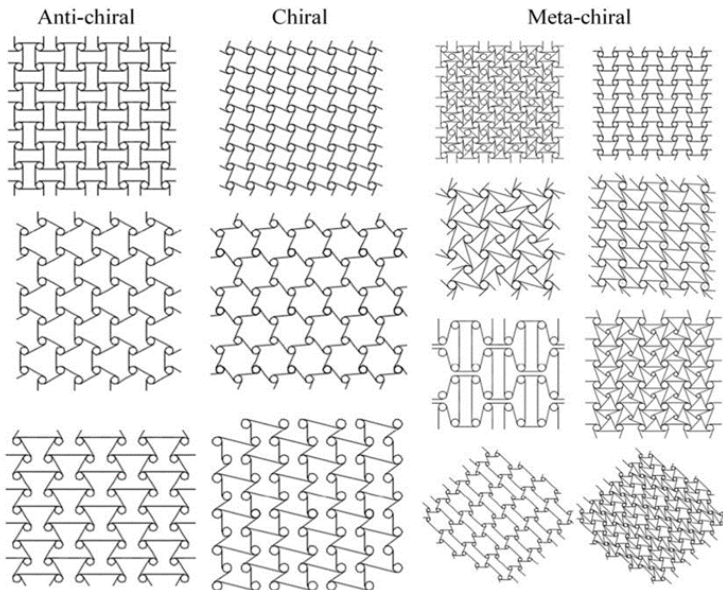


Figure 13. Classification of 2D Chiral Mechanical Metamaterials (W. Wu etc., 2019)

THREE-DIMENSIONAL AUXETIC STRUCTURES

3D auxetic structures are products derived from a 2D structure common to open-cell foams, crumpled sheets, Miura-ori folded structure and entangled single-wire model. Polytetrafluoroethylene is a type of weighted molecular polymer formed by an additional procedure. PTFE acquires a set of complex microstructures; The microstructure comprises an exposed linkage of anisotropic disc-shaped elements held together by a fibril network. This network structure causes complex relationships between transverse and longitudinal strains leading to a large negative major Poisson ratio that can reach -12 (B. D.Caddock and K. E.Evans, 1989). Crumpled materials exhibit a mixed property, with their mechanical behaviour moving between the foams and the entangled single-wire patterns. It shows pure elasticity and low hysteresis like foams, without plateau beyond yield stress. After such materials reach the yield stress, a strain hardening occurs directly (O.Bouaziz etc., 2013). The Miura-ori folded structure is a special structure dominated by the folding reactions of mechanics. This means that such a structure depends only on the geometry it acquires and is scale-independent. The mechanics of the Miura-ori folded structure are of interest because it shows opposite Poisson's ratios for different plane deformations. It achieves negative Poisson's ratio for planar deformation under bending, but becomes a saddle-shaped configuration, meaning positive Poisson's ratio. In addition, these Poisson ratios are equal and opposite to each other (M.Schenk and S. D.Guest, 2013). The entangled single wire contains the properties of helical and steric effect, resulting in transverse expansion during longitudinal tensile or compressive stress. The improved adhesion under loading makes the entangled single-wire model more suitable for the manufacture of anchoring devices than other auxetic structures (D.Rodney etc., 2016).

RE-ENTRANT STRUCTURE ANALYSIS

In this section, simulation results are compared with different applied speeds. The analysis focused on the stress distribution, deformation state and negative Poisson ratio behaviour of the structure in the auxetic cylindrical form. Poisson's ratio is calculated by the following formula (X.Ren etc., 2016).

$$v_i = -\frac{\varepsilon_{xz}}{\varepsilon_y} = -\frac{\Delta r_i/R}{\Delta y_i/Y_i} \quad (1 \leq i \leq 5)$$

$$\bar{v} = \frac{1}{5} \times \sum_1^5 v_i \quad (1 \leq i \leq 5)$$

Here $\Delta r_i = \frac{r_i+r_{i+1}}{2} - R$, $\Delta y_i = y_i - Y.R_i$ is the diameter of the auxetic cylindrical form before deformation, r is the i -th layer diameter after deformation of the auxetic cylindrical form, Y is the unit is the height of the cell before deformation and y_i is the height of the layer after deformation (Figure 14).

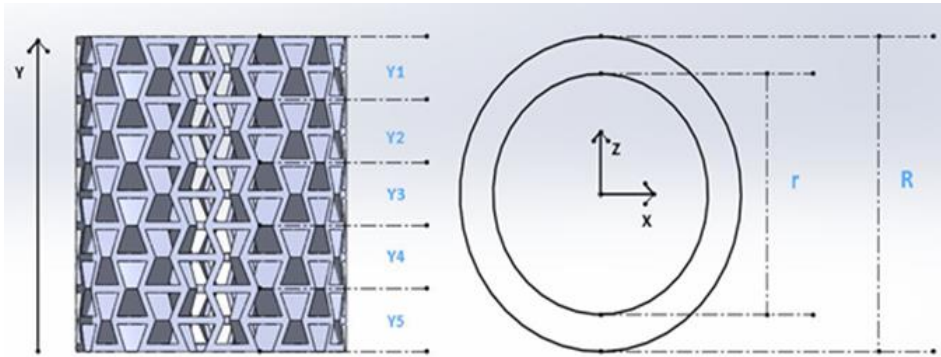


Figure 14. Calculating the Poisson Ratio Using a View Rendering Method from Two Perspective Views: (A) Top View; (B) Front View

The following content discusses the stress distribution of the re-entrant structure, as Figure 15 shows the effective stress curve. The upper layers bear the most stress at the beginning, and after a few minutes the stress is concentrated in the lower part, there is no obvious deformation because the amount of velocity is not very large. However,

through the stress distribution pattern, he can find that the structural behavior follows the beam-shaped auxetic structure under impact, and because of the cylindrical form structure, the stress is concentrated in the center rather than the expansion (Huang H.S etc., 2022).

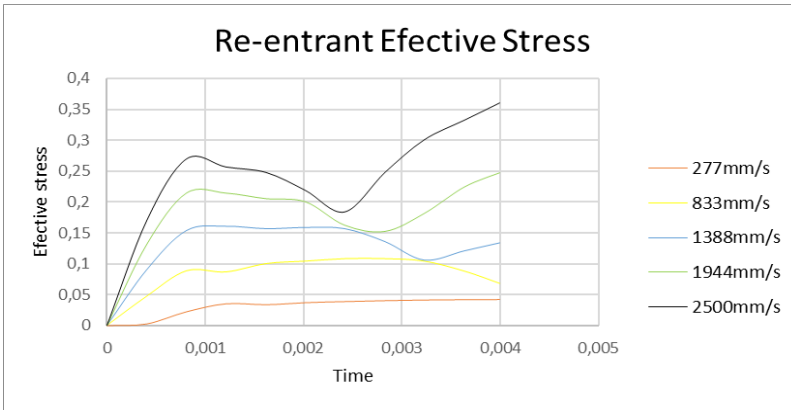


Figure 15. Effective Stress Curves of the Re-Entrant Structure Under Loads

Due to the position, the deformation size of the first layer is higher than the others, while bearing the lower velocity loading, and the deformation size of the last layer gradually meets the first ones. The negative Poisson ratio behaviour causes the central layers to contract when the impulsive wave passes completely to the lower layer. The figures below show the horizontal deformation performances.

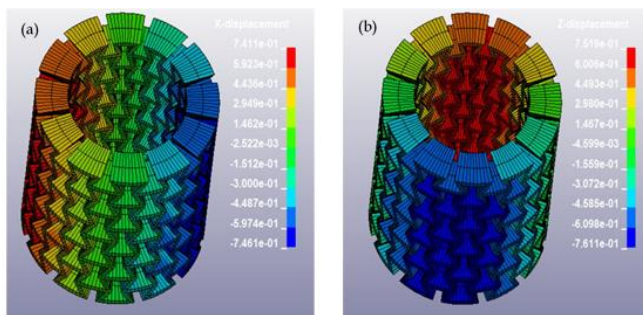


Figure 16. (a) Re-Entrant Enclosure X-Displacement Under Load; and (b) Z-Displacement

Negative Poisson ratio behavior can be observed from the horizontal deformation dimension of the re-entrant structure, except for 2500 mm/s

velocity loading, which causes an excessive deformation within the structure and causes the unit cells to behave abnormally. Malformation of re-entrant structure. Because of this, the most stressed top layer and bottom layer are displayed differently than the smaller velocity load. In the next section, the Poisson ratio, which is the most important part of the auxetic structure, will be discussed (Huang H.S etc., 2022).

The negative Poisson ratio behaviour of the re-entrant structure can be verified by Figure 16, the X and Z directional displacement shows the volume mode narrowing towards the center of the structure, the XZ strain in each layer clearly shows negative Poisson ratio behaviour in the figures shown in figure.

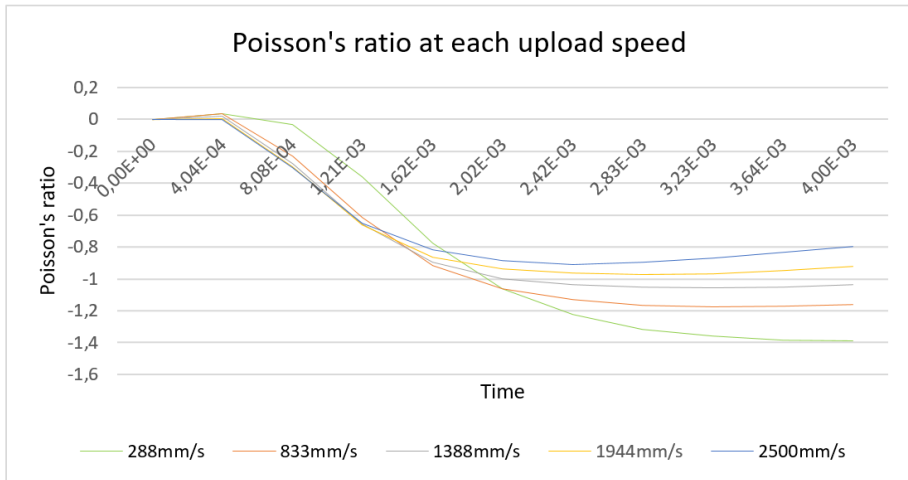


Figure 17. Poisson's Ratio at Each Reload Speed at Impact

As shown in Figure 17, the negative Poisson ratio behavior does not appear at the initial time point, except for the 2500 mm/s loading rate curing, and after a certain time the amount of velocity decides the negative Poisson ratio behaviour in the middle of the time frame. The increasing rate of Poisson's ratio slows down over time. The result shows that the Poisson ratio is inversely proportional to the loading speed. Thanks to the stress distribution figures, a small amount of loading velocity transmits stress to the lower part on average and until the end of the time

period the stress remains in the lower parts and the most severe stress occurs in the intermediate structures, which is the central concentration. The increased velocities lead to additional abnormal deformation of the unit cells, as the greater the velocity, the faster the stress is dissipated to complete the fracture. When the structure condenses up to the unit cell constraint, the horizontal portion of the unit cells is compressed and interferes with the deformation mode of each unit cell. As shown in Figure 18, interference from unit cells leads to a Poisson ratio reduction of the swell structure.

As a result, the re-entrant structure follows the in-plane re-entrant structural negative Poisson's ratio behaviour, the applied loading directs the swelling structure to condense into an X-shape deformation, and the stress collapses into the spacers. At lower velocity loading, the stress is dispersed layer by layer and less stress is distributed to the middle, allowing the bulky structure to achieve a greater Poisson's ratio. Higher velocity loads immediately apply greater pressure to the structure. The pressure causes excessive condensation of the spacer, resulting in abnormal deformation to reduce the rate of Poisson's re-entrant structure (Huang H.S etc., 2022).

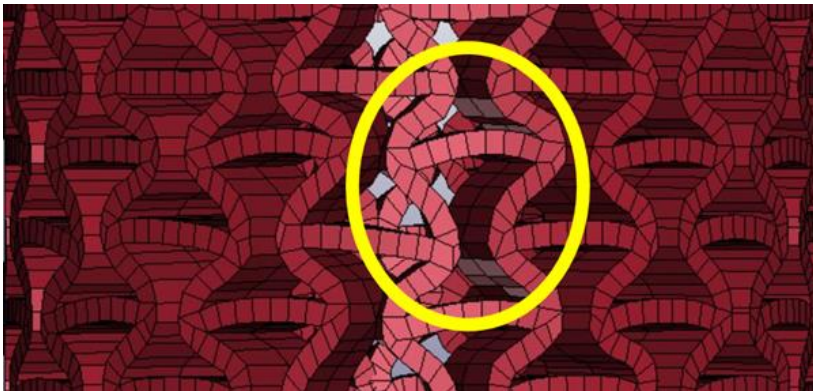


Figure 18. Diagram of the Re-Entrant Structure with Abnormal Deformation

TETRACHIRAL STRUCTURE ANALYSIS

Tetrachiral structure is the main topic discussed in this chapter. The tetrachiral structure, which is the same as the re-entrant structure, is also a well-known auxetic structure that has been proven to perform negative Poisson's ratio behavior under loading. In this section, stress distribution, deformation mode and obtained Poisson ratio are discussed. Figure 19 shows the effective tension of the tetrachiral structure. The figures show a different stress distribution performance from the re-entrant structure, where the deformation model meets the in-plane deformation model. The stress distribution patterns presented below showing that the first layer, which is the first contact layer, withstands the most stress at the initial moment when stress is applied to the structure, however, unlike the re-entrant structure, the tetrachiral structure transfers stress along the intermediate piece to the substrate, which is related to the unit cell deformation pattern. The tetrachiral structure is deformed under loading with the “Z” mode, which is in good agreement with the in-plane crush deformation mode (C.Qi etc., 2019), but the cylindrical structure rotates instead of being crushed. The top layer and bottom layer rotate in opposite directions, causing the middle layers to contract towards the middle, helping to realize the negative Poisson ratio behavior.

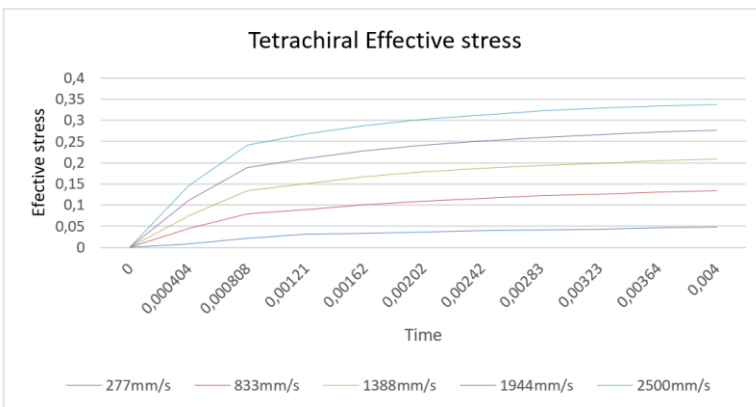


Figure 19. Effective Stress of Tetrachiral Structure Under Different Loads (Huang H.S etc., 2022)

According to the figures shown above, the deformation pattern of the tetrachiral structure shows that the first layer is constantly stressed, the deformation mode is independent of the applied stresses, even if the loading amount is larger, the unit cell deformation patterns maintain a certain mode and last up to a certain range, then the first layer is the single layer deformation, which can be seen more clearly in the figures below.

The results of the longitudinal deformation of the tetrachiral structure show good order, the longitudinal ligaments are deformed layer by layer, this deformation pattern occurs due to the tetrachiral geometry of a cylinder radius and bond length ratio $\alpha = r/l = 0.35$.

As shown in Figure 20, the tetrachiral structure performs the positive Poisson ratio in the initial time frame no matter how large the loading, indicating that the tetrachiral structure requires a certain amount of loading to reach the critical point of negative Poisson ratio behaviour. Before the load reaches the critical point, this is sufficient to bend the longitudinal struts, the unit cells turning only laterally. Also, according to the horizontal deformation data, the tetrachiral structure achieves a limitation in the Poisson ratio. When loading reaches critical speed, unit cells are blocked and stop shrinking. At this moment, the inflation mode begins to expand rather than contract, as shown in Figure 21.

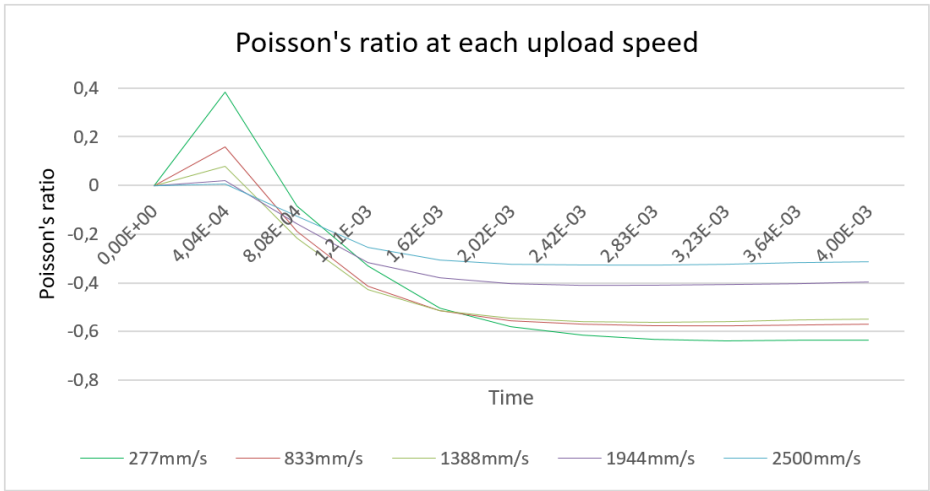


Figure 20. Poisson's Ratio at Each Reload Speed at Impact (Huang H.S etc., 2022)

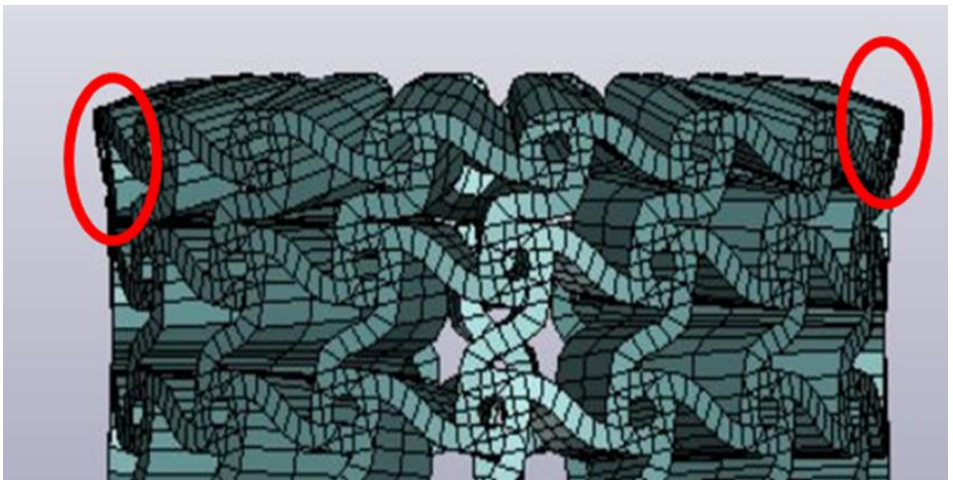


Figure 21. Diagram of Tetrachiral Structure with Expanding Layer

COMPARISON of RE-ENTRANT and TETRACHIRAL STRUCTURE

The difference between the re-entrant structure and the tetrachiral structure under impact loading can be verified from the above data, the unit cell of each structure exhibits a completely different deformation pattern. The stress distribution presents both the re-entrant structure and

the tetrachiral structure, which at first withstands stress with longitudinal bonds, then the re-entrant structure bears stress with horizontal supports, while the tetrachiral structure continues to withstand stress with longitudinal bonds and shows the stress distribution. The re-entrant structure is mainly concentrated in the middle part, but the stress distribution of the tetrachiral structure works evenly over the whole layer, these two performances make the deformation performance different.

After receiving the loading at the first time, the longitudinal struts of the re-entrant structure transform the loading and drive the horizontal struts to crush evenly towards the center for each layer, effectively showing the negative Poisson ratio behaviour, as a result, the re-entrant structure, exhibits at least -0.8 of the Poisson's ratio. The main obstacle to the negative Poisson ratio behaviour of the re-entrant structure is the unit cell contact, when the spacing of each unit cell is compressed beyond the interparticle shrinkage gap limitation, the longitudinal struts of the re-entrant structure begin to stretch and the horizontal struts begin to bend. malformation, which causes the volume structure to expand from the middle and affects the negative Poisson ratio behaviour. The deformation mode of the tetrachiral structure shows a distinct kinematic comparison to the re-entrant structure. When loading is applied to the tetrachiral structure, the greatest stress is distributed only to the longitudinal bonds, causing the swelling structure to rotate towards the slope of the longitudinal bond. The rotation causes the bulk structure to contract towards the middle, and when the loading exceeds 1388 mm/s, it deforms continuously in the horizontal direction except for the first layer, while the remaining layers only deform longitudinally. This phenomenon greatly reduces the negative Poisson ratio behavior of the tetrachiral structure. Also, the tetrachiral structure acts in opposition to the re-entrant structure, as the loading is large enough, the swell structure begins to expand from the upper and lower layers.

COMPRESSION TEST

The result of numerical simulations showed that the structure in auxetic cylindrical form exhibits good agreement with the negative Poisson ratio behaviour. The compression test is performed by applying constant pressure at a velocity of 0.0033 mm/s to the two auxetic cylindrical structures until the structures are elastically deformed. As can be seen in Figure 22, the samples are placed in the center of the hydraulic press, expected to concentrate towards the middle part of the samples showing negative Poisson ratio behaviour.



Figure 22. Image of the Compression Test Using a Hydraulic Press

The figures below show the deformation mode of the two samples. Figure 23 shows the result of re-entrant structural carrier loadings, “V” deformation mode is exhibited when compressive loading is applied. negative Poisson's ratio behaviour is not evident initially, in the same way as for thick-walled cells in the in-plane deformation mode.

The extent of the negative Poisson's ratio behaviour becomes more apparent as the force increases, with one of the unit cells of the substrate breaking, the swelling structure shrinks significantly. It can be distinguished from the in-plane deformation mode by the shrinking core unit cell, the in-plane deformation mode is carried out by relatively shrinking towards the upper parts and gradually concentrating on the lower parts,

but the structure in the auxetic cylindrical form is carried out. It is the deformation mode by breaking the subunit cell as shown below.

Breakage occurs from the arrowheads shown in (a) image, this phenomenon can be monitored by LS-DYNA simulation during the compression test. Both the open dynamic simulation and static simulation show that the stress is distributed to the lower layers and the structure is narrowed to the middle, which exhibits negative Poisson ratio behaviour, but the material does not show enough flexibility and the unit

Breakage occurs from the arrowheads shown in (a) image, this phenomenon can be monitored by LS-DYNA simulation during the compression test. Both the open dynamic simulation and static simulation show that the stress is distributed to the lower layers and the structure is narrowed to the middle, which exhibits negative Poisson ratio behaviour, but the material does not show enough flexibility, causing the unit cell to break. The front view of the tested specimen shows an obvious "V" mode deformation, the distinctive deformation mode occurs due to the shrinkage phenomenon, the normal deformation mode occurs with overhanging edges that allow the stress to be distributed to only one slope edge for each side. The cylindrical shaped structure with no overhanging edge triggers a chain effect when it withstands the compressive force, the unit cells concentrate on the central part on average, resulting in the stress concentrating on a particular unit cell and breaking it. Cells on both sides of the curved edges of the broken cell begin to rupture and eventually form the "V" mode deformation. The result is different from the simulation result because the material characteristic changes after refreezing from the molten filament. The compression test result does not deform as elastically as the simulation result due to the transformation of the material properties, as a result, the deformation mode performs differently between the two results. However, the simulation data corresponds to a compression test, both results show a maximum loading of about 4000 N, which gives a promising time.

The tetrachiral structure deforms as shown in Figure 24, the swell structure rotates with the perpendicular angle and the rotation causes the substrate to break. Compared to the re-entrant structure, the stress distribution and broken parts appear more homogeneous. The fracture mode also shows the torsional behaviour that causes spiral damage in the sample. During the compression test, the upper layer remains stationary and transmits force to the lower layers, which causes the lower parts to bend, when the force reaches the critical value, the lower part immediately breaks along the uprights. Although the tetrachiral structure shows negative Poisson ratio behavior in open dynamic simulation, it shows positive Poisson ratio in both compression test and static excitation. Under quasi-static loading, the tetrachiral structure tends to expand rather than concentrate in the central portion.

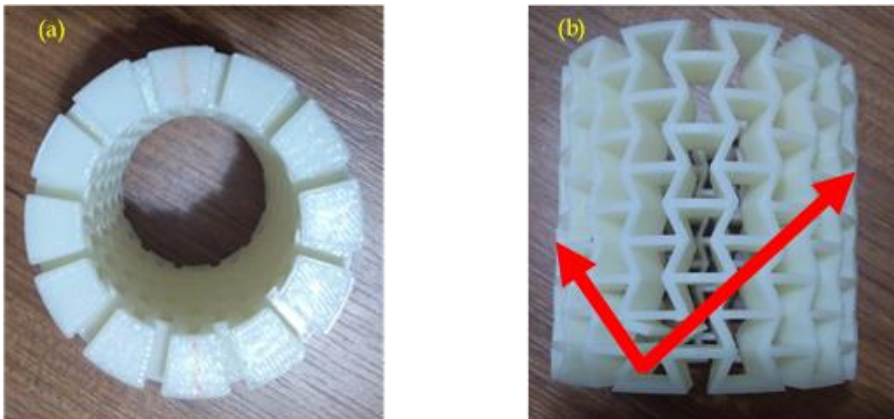


Figure 23. Views of the (a) Bottom View (b) Front View of the Tested Sample

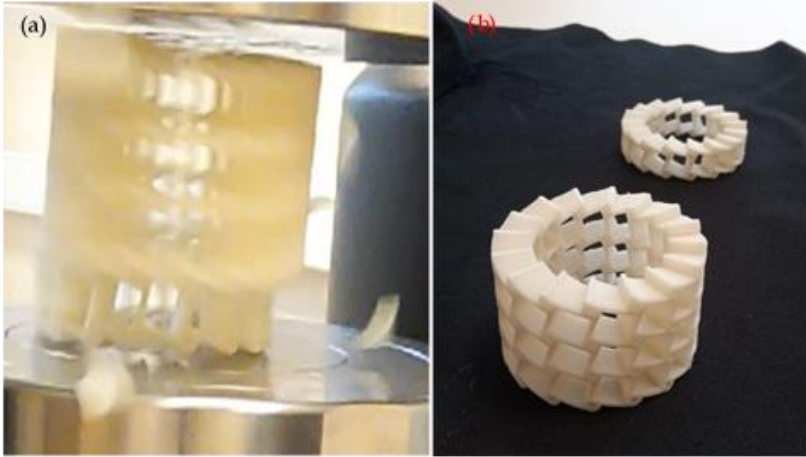


Figure 24. (a) Tetrachiral Image in Destructive Deformation (B) Broken Specimen Diagram

Comparison of numerical and experimental testing

Both static excitation and compression testing are carried out to analyze the behavior of the auxetic cylindrical form structure, in this section the results are compared to understand the properties of the volume-forming structures. Both numerical and experimental tests are performed under 0.0033 mm/s velocity, and with this low velocity loading, the peak withstand force meets a close value as shown Figure 25.

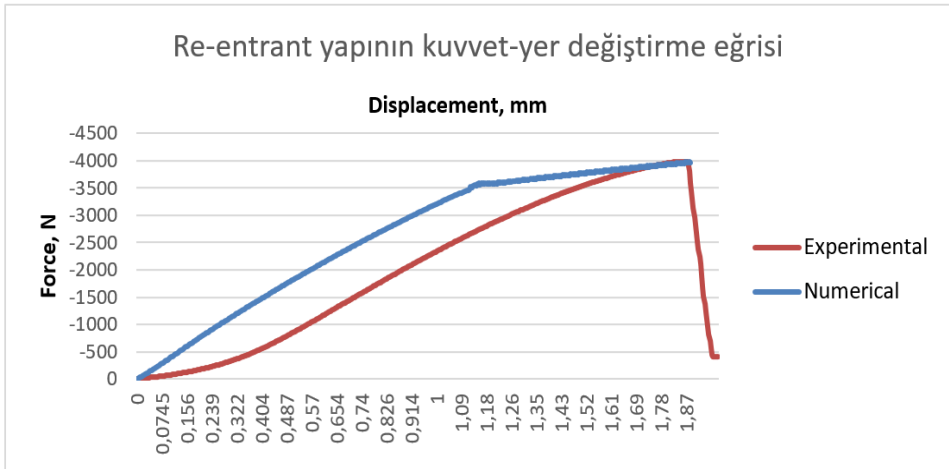


Figure 25. Force-Displacement Curve of Re-Entrant Structure

It is the fact that through the force-displacement curve of the re-entrant structure, the numerical result can fit the experimental result, except for the deviation caused by the initial non-linear behavior time frames. Also, due to the gap between the machine and the sample, the gaps that the 3D molded samples should have lead to the non-linear phenomenon. Except for the non-linear deformation steps, the swelling structure gradually intensifies towards the central part. In addition, the numerical result showed that the material properties changed after melting and resolidification. The material becomes harder but more brittle, unlike the numerical one that achieves plastic deformation, the sample collapses when it reaches the highest strength. The deformation mode of both experimental and numerical results behave similarly in linear deformation time periods when the numerical result meets the plastic deformation step, the swelling structure deforms in a certain direction instead of shrinking towards the middle, and this deformation mode is also suitable for the following. Experimental result that breaks off from one of the subunit cells and creates a “V”-shaped break.

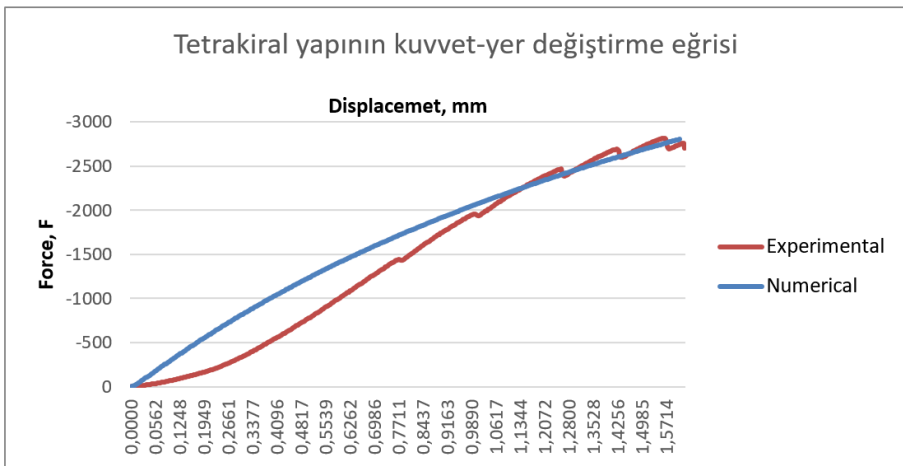


Figure 26. Force-Displacement Curve of Tetrachiral Structure

Figure 26 shows the result of the tetrachiral structure, same as the re-entrant structure, the deviation at the beginning leads to the difference between the two data. However, during the compression test, the defor-

mation pattern of the tetrachiral structure tends to differ from the deformation pattern of the re-entrant structure. The tetrachiral structure tends to deform separately instead of gradually concentrating on the middle part, resulting in a jagged curve unlike the numerical one. The difference is due to the transformation of material properties.

The experimental results of the re-entrant structure and the tetrachiral structure are both in agreement with the numerical results, but the sample production methodology leads to a non-linear result due to the transformation of material properties and minor inhomogeneity of the samples. It is the behavior in the first time periods that causes the results to deviate.

RESULTS

The scope of this chapter examines the mechanical behaviour of auxetic structures manufactured in cylindrical form. Auxetic structures in cylindrical form are responsible for relatively few studies in this field. The arrangement of the unit cells of the auxetic structure is very important, the generally studied auxetic structure forms are mainly with dangling edges, as a result, the cylindrical form structure with all connected unit cells is applied in this paper. With this difference, the specific deformation patterns of the samples are displayed.

Numerical and experimental results show good deformation patterns and live negative Poisson ratio behaviour in both re-entrant structure and tetrachiral structure, but based on the results of the open dynamic method, there is a difference in deformation mode between re-entrant and tetrachiral structure. The main factor affecting the negative Poisson ratio behaviour of the re-entrant structure in open dynamic situations is the heavily deformed unit cell caused by the overvoltage caused by the relatively high velocity. However, the tetrachiral structure behaves opposite to the re-entrant structure when it withstands overloading, when some cells become stable and no longer contract in the horizontal direction, which limits the performance of the negative Poisson

ratio behaviour. Except for the initial bias caused by the samples, the static simulations agree well with the experimental results. According to the results of the re-entrant structure gaining a better property than the tetrachiral structure, this result is due to the kinematics of the unit cells in the structure, the re-entrant structure shows a more flexible performance allowing it to exhibit a better negative Poisson ratio behaviour.

REFERENCES

- K. E.Evans, "Okzetik polymers: a new range of materials," *Endeavour*, vol. 15, no. 4, pp. 170-174, Jan.1991.
- M.Mir, M. N.Ali, J.Sami, andU.Ansari, "Review of Mechanics and Applications of Okzetik Structures," vol. 2014, pp. 1-18, 2014.
- C.Santulli andC.Langella, "Study and development of concepts of okzetik structures in bio-inspired design," *Int. J. Sustain. Des.*, vol. 3, no. 1, p. 20, 2016.
- L. J.Gibson andM. F.Ashby, "The mechanics cellular materials of three-dimensional cellular materials," *Proc. R. Soc. L.*, vol. A382, pp. 43-59, 1982.
- M.Ashjari, "Okzetik Materials Materials with Negative Poisson's Ratio," *Mater. Sci. Eng. Int. J.*, vol. 1, no. 2, pp. 62-64, 2017.
- V. L.Coenen andK. L.Alderson, "Mechanisms of failure in the static indentation resistance of okzetik carbon fibre laminates."
- I. I.Argatov, R.Guinovart-Díaz, andF. J.Sabina, "On local indentation and impact compliance of isotropic okzetik materials from the continuum mechanics viewpoint," *Int. J. Eng. Sci.*, vol. 54, pp. 42-57, 2012.
- A.Remennikov, D.Kalubadanage, T.Ngo, P.Mendis, G.Alici, andA.Whittaker, "Development and performance evaluation of large-scale okzetik protective systems for localised impulsive loads," 2019.
- D.Xiao, X.Chen, Y.Li, W.Wu, andD.Fang, "The structure response of sandwich beams with metallic okzetik honeycomb cores under localized impulsive loading-experiments and fi nite element analysis (a) (b)," *Mater. Des.*, vol. 176, p. 107840, 2019.
- R. S.Underhill andD.Canada, "Defense Applications of Okzetik Materials," no. July, 2014.

C.Qi, S.Yang, D.Wang, and L. J. Yang, "Ballistic resistance of honeycomb sandwich panels under in-plane high-velocity impact," *Sci. World J.*, vol. 2013, 2013.

P.Subramani, S.Rana, D.V.Oliveira, R.Fangueiro, and J.Xavier, "Development of novel okzetik structures based on braided composites," *Mater. Des.*, vol. 61, pp. 286–295, 2014.

M.Sanami, N.Ravirala, K.Alderson, and A.Alderson, "Okzetik materials for sports applications," *Procedia Eng.*, vol. 72, no. September 2018, pp. 453–458, 2014.

A.Alderson, J.Rasburn, S.Ameer-Beg, P. G.Mullarkey, W.Perrie, and K.E.Evans, "An okzetik filter: A tuneable filter displaying enhanced size selectivity or defouling properties," *Ind. Eng. Chem. Res.*, vol. 39, no. 3, pp. 654–665, 2000.

W.Wu, W.Hu, G.Qian, H.Liao, X.Xu, and F.Berto, "Mechanical design and multifunctional applications of chiral mechanical metamaterials: A review," *Mater. Des.*, vol. 180, no. June, p. 107950, 2019.

P.Bettini, A.Airoidi, G.Sala, L.DiLandro, M.Ruzzene, and A.Spadoni, "Composite chiral structures for morphing airfoils: Numerical analyses and development of a manufacturing process," *Compos. Part B Eng.*, vol. 41, no. 2, pp. 133–147, 2010.

I. O. P. C.Series and M.Science, "Okzetiks materials: classification, mechanical properties and applications," 2020.

C. W.Smith, J. N.Grima, and K. E.Evans, "Novel mechanism for generating okzetik behaviour in reticulated foams: Missing rib foam model," *Acta Mater.*, vol. 48, no. 17, pp. 4349–4356, 2000.

L.Mizzi, K. M.Azzopardi, D.Attard, J. N.Grima, and R.Gatt, "Okzetik metamaterials exhibiting giant negative Poisson's ratios," *Phys. Status Solidi - Rapid Res. Lett.*, vol. 9, no. 7, pp. 425–430, 2015.

Z.Chen, X.Wu, Y.Min, Z.Wang, and S.Zhou, "International Journal of Mechanical Sciences Re-entrant okzetik lattices with enhanced stiffness: A numerical study," *Int. J. Mech. Sci.*, vol. 178, no. December 2019, p. 105619, 2020.

H.Wang, Z.Lu, Z.Yang, and X.Li, "A novel re-entrant okzetik honeycomb with enhanced in-plane impact resistance," *Compos. Struct.*, vol. 208, no. May 2018, pp. 758–770, 2019.

K.Cai, J.Luo, Y.Ling, J.Wan, and Q.Qin, "Effects of size and surface on the okzetik behaviour of monolayer graphene kirigami," *Nat. Publ. Gr.*, pp. 1-10, 2016.

K.Meena and S.Singamneni, "A new okzetik structure with signifi cantly reduced stress concentration effects," *Mater. Des.*, vol. 173, p. 107779, 2019.

Z.Dong, Y.Li, T.Zhao, W.Wu, D.Xiao, and J.Liang, "Experimental and numerical studies on the compressive mechanical properties of the metallic okzetik reentrant honeycomb," vol. 182, 2019.

J. N.Grima and K. E.Evans, "Okzetik behavior from rotating squares," *J. Mater. Sci. Lett.*, vol. 19, no. 17, pp. 1563-1565, 2000.

K. W.Wojciechowski, "Two-dimensional isotropic system with a negative poisson ratio," *Phys. Lett. A*, vol. 137, no. 1-2, pp. 60-64, May 1989.

A.Alderson *et al.*, "Elastic constants of 3-, 4- and 6-connected chiral and anti-chiral honeycombs subject to uniaxial in-plane loading," *Compos. Sci. Technol.*, vol. 70, no. 7, pp. 1042-1048, 2010.

B. D.Caddock and K. E.Evans, "Microporous materials with negative Poisson's ratios. I. Microstructure and mechanical properties," *J. Phys. D. Appl. Phys.*, vol. 22, no. 12, pp. 1877-1882, 1989.

O.Bouaziz, J. P.Masse, S.Allain, L.Orgéas, and P.Latil, "Compression of crumpled aluminum thin foils and comparison with other cellular materials," *Mater. Sci. Eng. A*, vol. 570, pp. 1-7, 2013.

M.Schenk and S. D.Guest, "Geometry of Miura-folded metamaterials," *Proc. Natl. Acad. Sci. U. S. A.*, vol. 110, no. 9, pp. 3276-3281, 2013.

D.Rodney, B.Gadot, O. R.Martinez, S. R.DuRoscoat, and L.Orgéas, "Reversible dilatancy in entangled single-wire materials," *Nat. Mater.*, vol. 15, no. 1, pp. 72-77, 2016.

X.Ren, J.Shen, A.Ghaedizadeh, H.Tian, and Y. M.Xie, "A simple okzetik tubular structure with tuneable mechanical properties," *Smart Mater. Struct.*, vol. 25, no. 6, 2016.

Huang H.S., "3D Okzetik Yapıların Farklı Yüklemeler Altında Yapısal Davranışlarının Araştırılması ve Simulasyonu" Gebze Teknik Üniversitesi Fen Bilimleri Enstitüsü, Makine Mühendisliği Anabilim dalı yüksek lisans tezi, 2022 Gebze-Türkiye.

Fevzi BEDİR, Shao-Ho HUANG

C.Qi, F.Jiang, C.Yu, andS.Yang, “International Journal of Impact Engineering In-plane crushing response of tetra-chiral honeycombs,” *Int. J. Impact Eng.*, vol. 130, no. December 2018, pp. 247–265, 2019.

DETERMINATION OF THE EFFECT OF TAILSTOCK AND CHUCK PRESSURE ON VIBRATION AND SURFACE ROUGHNESS IN TURNING OPERATIONS WITH GRAY RELATIONAL ANALYSIS METHOD

Hüseyin GÜRBÜZ¹, Şehmus BADAY²

Abstract: Developing technology creates new needs. One of the most important requirements in the manufacturing industry is how to produce workpiece materials more efficiently and perfectly with the least cost. Today, many machine parts are produced through either traditional or non-traditional manufacturing method. One of the most widely used methods in shaping machine parts is turning. Low surface roughness and vibration values are at the top of the requirements for the workpieces that are desired to be produced by turning method. Because the fact that the workpiece is produced in high surface roughness and vibration values causes it to have short life and low performance. However, this contradicts with the machining efficiency principles. In other words, this does not comply with the low cost and high quality requirement. In order to minimize the high values of surface roughness and vibration, the workpieces must be correctly held to the lathe. The inability of the workpiece to be attached to the workbench between a suitable chuck and tailstock pressure causes it to rotate in an off-axis runout and deteriorates the accuracy of the measurement. Therefore, undesirable high values of vibration and surface roughness occur in the workpiece. The aim of this study is to determine the most suitable tailstock and chuck pressure to obtain the lowest vibration and surface roughness values in turning of AISI 304 steel by using the Grey relations method based on the Taguchi method. Turning operations were performed using 5 different chucks and tail-

¹ Batman Üniversitesi, Mühendislik Mimarlık Fakültesi, Batman / Türkiye, e-mail: huseyin.gurbuz@batman.edu.tr, Orcid No: 10000-0003-1391-172X

² Batman Üniversitesi, Beşiri Organize Sanayi Bölgesi Meslek Yüksekokulu, Batman / Türkiye, e-mail: sehmus.baday@batman.edu.tr, Orcid No: 10000-0003-4208-8779

stock pressures at constant cutting parameters (cutting depth, cutting speed and feed). Taguchi L25 (5^2) orthogonal experiment design array was chosen for turning experiments. The ideal tailstock and chuck pressure for the vibration and surface roughness values were determined with S/N (signal/noise) ratio, the “smaller is better” approach, according to Grey relations method. The chuck and tailstock pressures, which gave the optimum vibration and surface roughness values, were determined as 18 and 11 bars, respectively. According to S/N ratio results in Taguchi experimental design and ANOVA table, it was found that the chuck pressure was more effective than the tailstock pressure on the surface roughness and vibration. As a result, it was understood that Grey relations method based on Taguchi Method is a systematic, simple and efficient method for the optimization of tailstock and chuck pressure parameters.

Keywords: Surface Roughness, Vibration, Chuck Pressure, Tailstock Pressure, ANOVA, Grey Relations, Taguchi Method

INTRODUCTION

Metalworking operation is one of the main manufacturing methods used in the production of machine parts. Performing manufacturing processes at high standards can be possible by holding the workpieces with a suitable chuck and tailstock pressure. Because proper attachment of the workpiece to the workbench improves surface roughness, reduces vibrations and increases machining efficiency. Today, low surface roughness values are at the top of the requirements for the workpieces that are desired to be produced through traditional and non-traditional manufacturing method. The purpose of the manufacturing process is both to shape the workpieces and obtain products with an ideal surface quality according to a certain tolerance and accuracy in terms of geometry and dimension (Gürbüz et al., 2021; Nas et al., 2012; Gürbüz et al., 2019). The low surface roughness value of the workpiece contributes to the longer life of the workpiece. It will also help to reduce the production costs reserved for the manufacture of the workpiece. In addition, a quality machined surface will significantly improve fatigue life, corrosion and wear resistance. However, surface irregularities caused by machining condi-

tions or other problems in the manufacturing process cause undesirable surface roughness. One of these problems is vibration (chattering). The vibration event occurs due to the instantaneous changes that occur while the cutting tool is machining the workpiece (Zhang et al., 2015; Neşeli et al., 2007; Rao et al., 2014). The first step in eliminating undesirable high surface roughness and vibration values when machining workpieces is provided by correctly holding the workpieces to the workbench. Holding a workpiece at the ideal tailstock and chuck pressure will help to obtain the ideal surface quality desired from the workpieces by reducing the eccentric, stretching and vibration that will occur while the workpiece is being machined. In order to determine the effects of cutting parameters on surface roughness and vibration, various experimental and statistical studies were carried out based on experimental design methods using Grey relations method (Mavi, 2018; Zeng et al., 2009; Karthikeyan et al., 2012; Lin et al., 2004; Uzun, 2019; Sarıkaya and Güllü, 2015; Salvi et al., 2013; Çaydas and Hascalik, 2008; Günay and Yücel 2013; Yan and Li, 2013; Debnath et al., 2016; M. Sarıkaya et al., 2015; Rao et al., 2016; Zerti et al., 2018; Nalbant et al., 2007; Ramesh et al., 2019; Bagaber and Yusoff, 2017; Mozammel et al., 2018; Cetin et al., 2011; Bhattacharya et al., 2009). However, no statistical and experimental studies were found to determine the effect of tailstock and chuck pressure on vibration and surface roughness values using Grey relations method. Mavi (2018) investigated the effects of cutting parameters with drills having different types of coatings on drilling performance. Author determined the optimum cutting parameters affecting the surface form properties of duplex stainless steel with the help of Grey relations analysis method. Machining experiments were carried out according to the L18 orthogonal design. By optimizing the deviation values from diameter and cylindricality with the help of grey relational method, he determined that the most suitable cutting parameter was 0.05 mm/rev feed rate, 15 m/min cutting speed and TiN coated drill. Zeng et al., (2009) performed the optimization of the parameters used in turning by using Taguchi and Grey relations analy-

sis. As a result of their analysis, they found that the most effective parameter on the surface roughness was the depth of cut, while the cutting speed was effective on the roundness. They also used ANOVA to determine the effect of parameters on experimental results. Karthikeyan et al. (2012) analyzed micro EDM performance using different statistical tools. They used regression analysis, ANOVA, S/N ratio and Grey relations analysis methods as statistical tools. They found that for single performance study parameters, energy and speed are superior while for multi performance analysis, feed contributes significantly. Lin (2004) used Grey relations and Taguchi method to reveal the effects of cutting parameters on tool life, surface roughness and cutting forces. As a result of the Grey relations method, it was revealed that the most effective parameters on the experimental results are feed, depth of cut and cutting speed, respectively. Uzun (2019) used Grey relations method to determine the relations between cutting forces, tool wear and surface roughness values. Austempering process was applied to vermicular graphite cast iron workpieces subjected to two different temperatures and three different holding times. Machining experiments were carried out on a CNC milling machine using coated cementite carbide cutting tools. According to the grey relationship analysis, the conditions that gave the highest cutting performance were obtained for the austempered sample at 375 °C, and a waiting period of 120 min. Sarıkaya and Güllü (2015) optimized the machining parameters by using Taguchi-based grey relations analysis for turning of Haynes 25 workpiece, which is difficult to machine. According to the results of multiple optimization, the optimum machining parameters were determined as cutting speed (30 m/min), fluid flow rate (180 m/h) and cutting fluid vegetable. Salvi et al. (2013) analyzed the surface roughness values resulting from hard turning using Taguchi orthogonal design method. The authors showed that feed and then cutting speed play an important role in achieving low surface roughness with their results they obtained. Çaydaş and Hasçalık (2008) optimized the parameters used in laser cutting by using the grey relations method. As a

DETERMINATION OF THE EFFECT OF TAILSTOCK AND CHUCK PRESSURE ON VIBRATION AND SURFACE ROUGHNESS IN TURNING OPERATIONS WITH GRAY RELATIONAL ANALYSIS METHOD

result of their analysis, they revealed that the laser power was more effective than the cutting speed on the experimental results. Günay et al. (2013) used Taguchi L18 orthogonal design to determine the optimum surface roughness in turning high alloy white cast iron with two different hardnesses. They determined the optimal cutting conditions according to the "smaller is better" approach used in S/N (signal-to-noise) ratio. They found that feed was effective on the surface roughness values obtained from the workpiece surface with a hardness of 50 HRc, and the cutting speed was effective on the surface roughness values obtained from the workpiece surface with a hardness of 62 HRc. Yan and Li (2013) optimized the parameters used in the milling process using grey relations and surface response method. As a result of the analyses, they found that the most effective parameter among the parameters used in milling on the experimental results was the width of cut. Debnath et al. (2016) investigated the effect of coolant conditions and cutting parameters on tool wear and surface roughness in turning operation using Taguchi method, which is one of the experimental design methods. They found that the optimum cutting conditions for desired surface roughness and tool wear are high cutting speed, medium depth of cut, low feed and low flow high speed coolant. Sarıkaya et al. (2015) demonstrated the effects of milling parameters on experimental results such as vibration signals, cutting force, and surface roughness using Taguchi L18 orthogonal array and grey relationship analysis. According to Taguchi S/N ratios and degree of Grey relations, they found that the optimum parameters on the experimental results were depth of cut of 1 mm, feed rate of 0.05 mm/rev, cutting speed of 308 m/min, and the number of inserts of 1 to minimize simultaneously. Rao et al., (2016) using Taguchi L9 orthogonal design and ANOVA (analysis of variance), investigated the surface roughness values resulting from turning AA7075 workpiece depending on the specified cutting parameters. From Taguchi results, they found that feed rate and cutting speed were the most important parameters affecting the surface roughness and the optimal combination of cutting

parameters for low surface roughness, which were 1000 m/min for cutting speed, 0.2 mm for feed rate and 0.5 mm for depth of cut. Zerti et al. (2018) carried out an experimental and statistical study on the efficacy of machining parameters on the surface quality and productivity results obtained by turning AISI D3 steel with ceramic cutting tools, using grey relations analysis. As a result of their analysis they carried out, they found that the most effective parameters on the experimental results were the depth of cut and the cutting speed. Nalbant et al., (2007) in their study, used Taguchi method and ANOVA to determine the effect of optimum cutting parameters on the surface roughness resulting from turning of AISI 1030 steel. In line with their results, they concluded that the most important effects on the surface roughness are the cutting tool nose radius, feed rate and depth of cut, respectively. Ramesh et al. (2019) used grey relations analysis to determine the effect of machining parameters on cutting tool temperature in turning. According to the analysis results they obtained, they determined that low tool temperature causes low tool wear. Bagaber and Yusoff (2017) optimized the cutting parameters using ANOVA to minimize power consumption and surface roughness in dry turning of AISI 316 stainless steel. At the end of their study, they emphasized that they obtained the minimum power consumption values at the lowest cutting speed, highest feed and depth of cut. They found that the most effective parameters on surface roughness are feed rate and then cutting speed. Mia et al. (2018) performed the optimization of tool-chip interaction parameters using grey relations analysis. According to the results of Grey relations analysis, they found that the most effective parameter on the experimental results was the cutting speed, followed by feed rate. Çetin et al. (2011) performed regression, S/N ratio and ANOVA analysis to see the effect of cutting parameters on cutting force and surface roughness during turning of AISI 304L steel. The authors determined that the values of the regression models they obtained for surface roughness and cutting forces were in good agreement with the experimental values. They also found that feed and depth of cut were

more effective than cutting speed and cutting fluids in improving surface roughness and reducing cutting forces. Bhattacharya et al. (2009) applied Taguchi method and ANOVA to estimate the effect of cutting parameters on surface roughness and power consumption during machining of AISI 1045 steel at high speed. From the results they obtained, they found that the cutting speed had a significant effect on the surface roughness and power consumption, while the other cutting parameters had little effect. As a result of the literature review, it was seen that various experimental and statistical studies based on analyzes and experimental design methods have been carried out to determine the effects of machining parameters on the surface roughness and vibration resulting from conventional and nonconventional machining of various materials (Gürbüz et al., 2021; Nas et al., 2012; Gürbüz and Baday 2019; Zhang et al., 2015; Neşeli and Yıldız 2007; Rao et al., 2014; Mavi, 2018; Zeng et al., 2009; Karthikeyan et al., 2012; Lin et al., 2004; Uzun, 2019; Sarıkaya and Güllü, 2015; Salvi et al., 2013; Çaydas and Hascalık, 2008; Günay and Yücel 2013; Yan and Li, 2013; Debnath et al., 2016; M. Sarıkaya et al., 2015; Rao et al., 2016; Zerti et al., 2018; Nalbant et al., 2007; Ramesh et al., 2019; Bagaber and Yusoff, 2017; Mozammel et al., 2018; Cetin et al., 2011; Bhattacharya et al., 2009). However, it was determined that neither a statistical nor an experimental study has been carried out to determine the effect of tailstock and chuck pressure on vibration and surface roughness in CNC turning. With this experimental and statistical study, it is aimed to ensure that the workpiece material is properly attached to the chuck and tailstock pressures in CNC lathes, and thus to eliminate the negative effects such as high values of vibration and surface roughness that may occur in the workpiece.

MATERIAL and METHOD

Workpiece Material

AISI 304 stainless steel, which is frequently used in the manufacture of machine parts, was used as workpiece material in the experiments.

The dimensions of the workpieces were determined to be 35 mm in diameter and 300 mm in length. This workpiece material has good corrosion resistance due to the high amount of chromium it contains. In addition, the most widely used AISI 304 quality stainless steel in the stainless steel group is preferred because of its very good mechanical properties, chemical composition, corrosion-oxidation resistance and weldability. The hardness and chemical composition values of the workpiece used in the experiments are given in Table 1.

Table 1. Chemical Composition and Hardness Value of the Workpiece Material

% C	% Cr	% S	% N	% Si
0.070-0.024	19.50-17.50	0.030-0.029	0.100-0.085	1.00-0.39
% Mn	% P	% C0	% Ni	Hardness
2.0-1.45	0.045-0.036	0.15(max)	10.50-8.00	215 HB

Cutting Tools and Tool Holder

The cutting tool and tool holder to be used in the machining experiments of AISI 304 austenitic stainless steel on CNC lathe, depending on cutting parameters, were obtained from Fidan Cutting Tool Company, which is the supplier of OKE cutting tool manufacturer. The insert and tool holder are given in Figure 2. In the selection of the insert, double-sided, WNMG 080408-OMM, PVD-coated cutting tool with negative rake angle was selected. This cutting tool is a multi-purpose insert suitable for medium chip removal in both stainless steels and carbon steels. This selected cutting tool was used in machining experiments with the PWLNR 2525M08 tool holder, which is suitable for its geometric structure.



a) PWLNR 2525M08 tool holder

b) WNMG cutting tool

Figure 1. Tool Holder and Cutting Tool Used in the Experiments

Machining experiments and Cutting Parameters

AISI 304 workpieces, which were supplied in 36 mm diameter, were reduced to 35 mm in diameter on the universal lathe in order to eliminate the external negativities on the surface, and after the facets were turned and the center holes were drilled, they were made ready for machining on CNC lathe. TAKISAWA EX-310 brand CNC lathe was used in the processing of machining experiments. The cutting parameters used in the machining experiments were determined by considering ISO 3685 requirements and the recommendations of the manufacturer cutting Tool Company. In the machining experiments, the cutting parameters, feed rate, cutting speed and depth of cut, were determined as 0.2 mm/rev, 250 m/min and 2 mm, respectively. Five different tailstock and chuck pressures were used to see the effect of tailstock and chuck pressure on vibration and surface roughness values. Chuck and tailstock pressure were determined as variable parameters and are shown in figure 1.

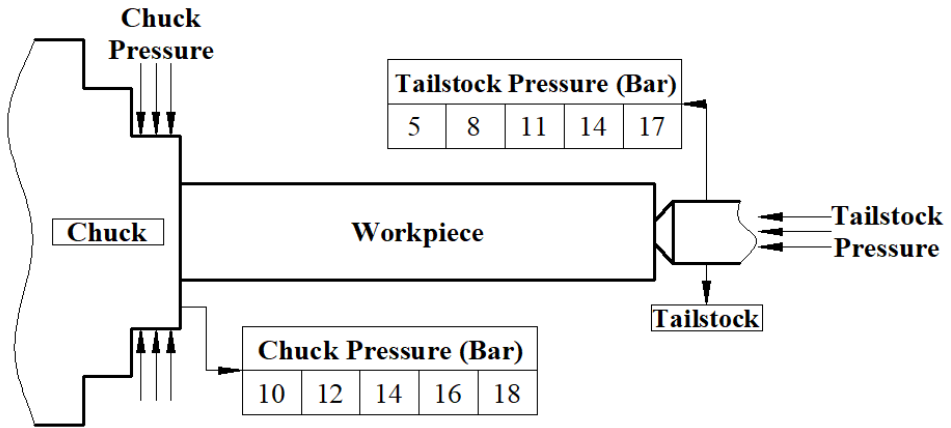


Figure 2. Chuck and Tailstock Pressure Parameters Used in the Experiments

The parameters used in the machining experiments and the numerical values of these parameters are given in Table 2.

Table 2. Cutting Parameters Used in Machining Experiments

Feed rate (mm/rev)	0.2
Cutting Speed, V (m/min)	250
Depth of cut, a (mm)	2
Tailstock Pressure, P (bar)	5, 8, 11, 14, 17
Chuck Pressure, P (bar)	10, 12, 14, 16, 18

Vibration and Surface Roughness Measurement

Vibrations in the workpiece during the turning operation were measured with the NI-9230 accelerometer-measuring device connected to the tool holder, which can measure in X, Y and Z coordinates in a computer-connected way; and the obtained measurement values were transferred to the graphics. The surface roughness values on the workpiece surface resulting from the machining experiments were measured using a portable TR 200 measuring device. Five separate measurement zones were determined on the workpiece surface to determine the surface

DETERMINATION OF THE EFFECT OF TAILSTOCK AND CHUCK PRESSURE ON VIBRATION AND SURFACE ROUGHNESS IN TURNING OPERATIONS WITH GRAY RELATIONAL ANALYSIS METHOD

roughness values. Average surface roughness values were calculated by taking the arithmetic average of five separate measurements at a measuring length of 5.6 mm from the surface of each machined workpiece. The experimental setup is given in Figure 3 to see the effect of tailstock and chuck pressure on the vibration and surface roughness values obtained during turning of AISI 304 stainless steel.

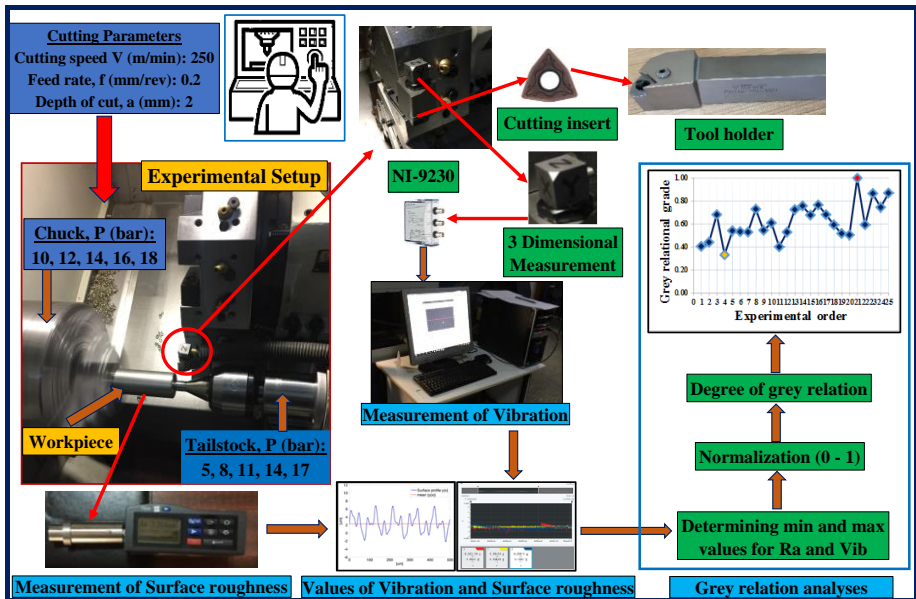


Figure 3. Schematic Representation of Experimental and Statistical Study

GREY RELATIONS ANALYSIS

In this study, Taguchi-based grey relations analysis was used to optimize the effects of the combination of different tailstock and chuck pressures on the vibration and surface roughness values. The first step in gray relations analysis is the normalization of the experimental values (data set). The most important factor to be considered in the normalization of the influencing factors is which approach should be used. If the influencing factor points are desired to be small values, points with small values in linear normalization will take values close to "0" in normaliza-

tion, while points with large values will take values close to “1” (Acir et al., 2017; Palanikumar, 2011). The surface roughness and vibration values obtained as a result of the experiments were normalized between 0-1. The following three different approaches can be made for the normalization of the results obtained in the experiments;

If “Smaller is better”, then the original index is normalized as follows;

$$y_i(k) = \frac{\max x_i^0(k) - x_i^0(k)}{\max x_i^0(k) - \min x_i^0(k)} \quad (1)$$

Here, $y_i(k)$, $x_i^0(k)$, $\max x_i^0(k)$ ve $\min x_i^0(k)$ represent grey relations analysis, normalization value, maximum value and minimum value, respectively. In the grey relations analysis method, while determining the grey relational degree, the relation degree of twenty-five indexes ($y_0(k)$ and $y_i(k)$, $i=1,2,3,\dots,25$; $k=1,2$) is determined. The grey relations coefficient $\xi_i(k)$ is calculated according to the equation 2-5 given below:

$$\xi_i(k) = \frac{\Delta_{min} - \partial \Delta_{max}}{\Delta_{oi}(k) - \partial \Delta_{max}} \quad (2)$$

$$\Delta_{oi}(k) = \|y_o(k) - y_i(k)\| \quad (3)$$

$$\Delta_{max} = \max_{\forall j \in i} \max_{\forall k} \|y_o(k) - y_i(k)\| \quad (4)$$

$$\Delta_{min} = \min_{\forall j \in i} \min_{\forall k} \|y_o(k) - y_i(k)\| \quad (5)$$

Here; the absolute deviation value between $\Delta_{oi}(k)$, $y_o(k)$ ve $y_i(k)$ is taken as ∂ = discriminating coefficient (0-1), and usually $\partial = 0.5$ in literature (Acir et al., 2017; Palanikumar, 2011). Δ_{max} is the maximum value of Δ_{oi} values, and Δ_{min} is the minimum value. Grey relational degree (Yi) is obtained by averaging Grey relational formation coefficients and it can be expressed as in equation 6 below:

$$\begin{aligned} \gamma_i &= \frac{1}{n} \sum_{k=1}^n \xi_i(k) \end{aligned} \tag{6}$$

In Equation 6, the symbol n represents the grey correlation coefficient obtained from the normalized experimental values. A high degree of grey associative occurrence indicates a strong correlation between $y_i(k)$ and $y_o(k)$. If the two compared series have the same values, the gray relational degree is found to be 1.

Taguchi Signal to Noise (S/N) Ratio

In Taguchi, an experimental design method, the most basic criterion used in the analysis of experimental data is S/N ratio. In Taguchi method, "Signal (S)" corresponds to the desired value (average) for the output characteristic, and "Noise (N)" corresponds to the undesired value for the output characteristic. Taguchi S/N ratio has been used by many researchers in the interpretation of experimental data (Gürbüz and Baday 2019; Zeng et al., 2009; Lin et al., 2004; Sarıkaya and Güllü, 2015; Salvi et al., 2013; Günay and Yücel 2013; Debnath et al., 2016; M. Sarıkaya et al., 2015; Rao et al., 2016; Zerti et al., 2018; Nalbant et al., 2007; Ramesh et al., 2019; Mozammel et al., 2018; Cetin et al., 2011; Bhattacharya et al., 2009).

In this experimental study, Taguchi L25 (5^2) orthogonal array S/N ratio equation is used according to "smaller is better" approximation. Because when machining workpieces in manufacturing, low surface roughness and vibration values are desired. According to Taguchi method, the optimum tailstock and chuck pressures required for the lowest vibration and surface roughness values were determined with S/N ratio. Three types of S/N ratio formulas are used to interpret the desired experimental values. These formulas are expressed as larger is better (Equation 7), smaller is better (Equation 8) and nominal is better (Equation 9). The "smaller is better" formula for interpreting the experimental values was used. S/N formulas are shown in Equation 7-9 below.

$$\begin{aligned} S/N \\ &= -10\log \frac{1}{n} \left(\sum_{i=1}^n \frac{1}{y_i^2} \right) \end{aligned} \quad (7)$$

$$\begin{aligned} S/N \\ &= -10\log \frac{1}{n} \left(\sum_{i=1}^n y_i^2 \right) \end{aligned} \quad (8)$$

$$\begin{aligned} S/N \\ &= 10\log \left(\frac{\bar{y}^2}{s^2} \right) \end{aligned} \quad (9)$$

In Equation 7, n represents the number of experiments performed, y_i represents the measured values for vibration and surface roughness, \bar{y} represents the mean of the test results, and s represents standard deviation of the experimental results.

Anova

In ANOVA, there are two types of variables. These variables are control factors and response values. The purpose of ANOVA, which is a statistical method, is to reveal which and how control factor is effective on the response value. An ANOVA table gives these: P values, indicating the significance level of each variable on the results, and mean of squares (MS), degrees of freedom (DF), statistics (F) values, sum of squares (SS) and percentage contribution rates (PCR). The importance of control factors in ANOVA is established by comparing P values of each control factor. In an ANOVA table, if the control factors' P value is less than 0.05, it is considered "statistically significant" in scientific parlance. The reason for this is because of the formulation of ANOVA table is significant with level 5% i.e. Also, it demonstrates how PCR value of each control factor shown in an ANOVA table is effective on the response value (Campo-seco, 2013; Kuntoğlu and Sağlam, 2019; Gürbüz et al., 2020).

EVALUATION of EXPERIMENTAL RESULTS

Evaluation of Surface Roughness and Vibration results

During machining, high surface roughness and undesired vibration values may occur due to an improperly held workpiece. These vibrations, when severe, produce chattering, which results in poor surface quality. Each parameter used during the machining of materials affects the surface quality and vibration. It causes a series of economic losses such as deterioration of workpiece dimensions or insufficient surface quality of the work, which requires a second operation. Therefore, machining the workpieces by holding them at a suitable chuck and tailstock pressure increases the surface quality of the workpiece by reducing the surface roughness values, and also contributes to the reduction of unwanted vibrations. The surface roughness values obtained from the surfaces of the turned workpieces depending on the different combinations of five different chuck and tailstock pressures and constant cutting parameters are given in Figure 4 and Figure 5. When the graphs in Figure 4 and Figure 5 are examined, it is determined that the chuck and tailstock pressure have a significant effect on surface roughness. It is seen in the graph in Figure 4 that the highest surface roughness value is obtained when the workpieces are machined at a chuck pressure of 10 bar and a tailstock pressure of 14 bar, while the lowest surface roughness value is obtained when machining workpieces at a tailstock pressure of 5 bar and a chuck pressure of 18 bar. In addition, from the graph in figure 4, it is determined that the ideal tailstock pressure is 11 bar among five different tailstock pressures in terms of surface roughness.

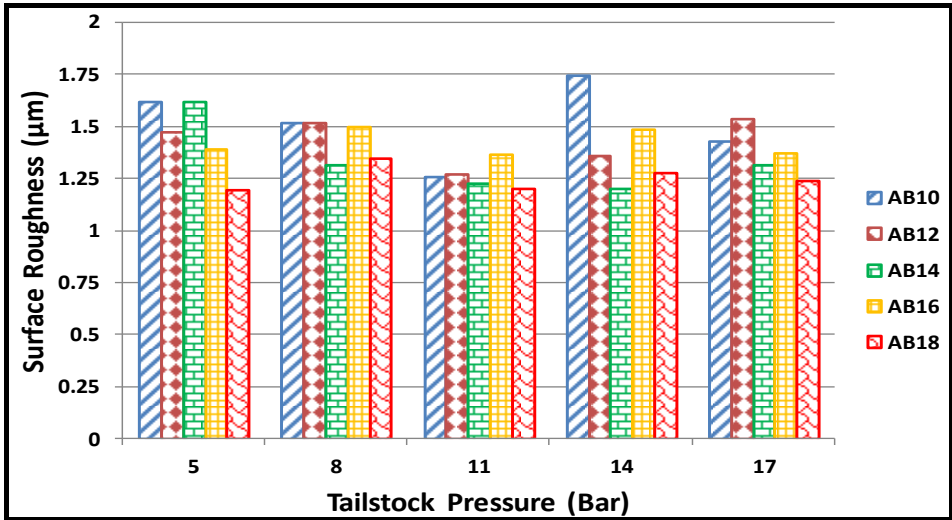


Figure 4. Surface Roughness Values Obtained Depending on Tailstock Pressure

When the surface roughness graph obtained depending on the chuck pressure in Figure 5 is examined, it is determined that the ideal chuck pressure is 18 bar among five different chuck pressures in terms of surface roughness.

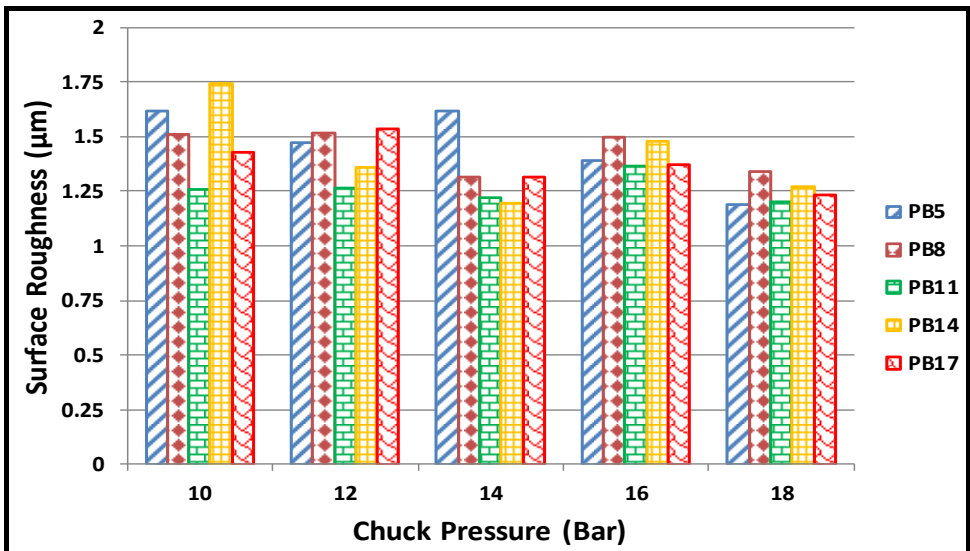


Figure 5. Surface Roughness Values Obtained Depending on Chuck Pressure

DETERMINATION OF THE EFFECT OF TAILSTOCK AND CHUCK PRESSURE ON VIBRATION AND SURFACE ROUGHNESS IN TURNING OPERATIONS WITH GRAY RELATIONAL ANALYSIS METHOD

The vibration values obtained from the turned workpieces depending on the chuck and tailstock pressure at constant cutting parameters are given in Figure 6 and Figure 7. When the vibration graphs in Figure 6 and Figure 7 are examined, it is seen that chuck and tailstock pressure are effective on vibration.

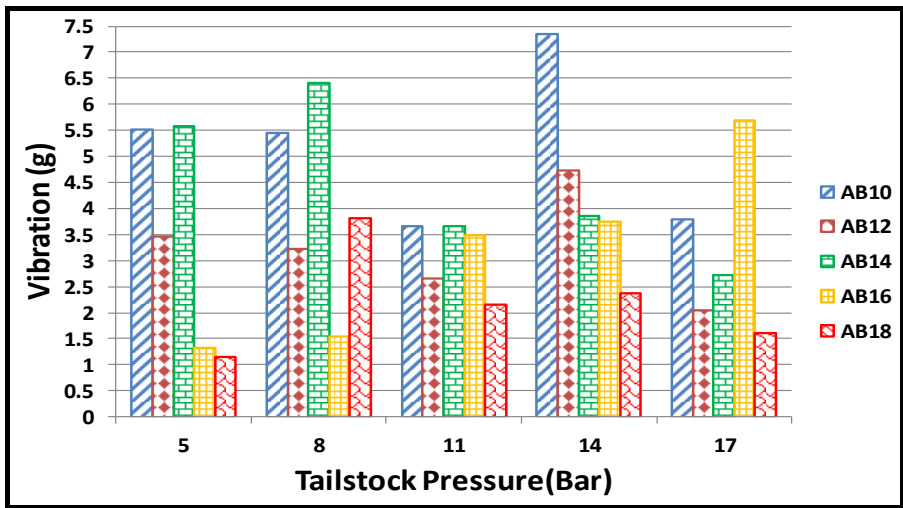


Figure 6. Vibration Values Obtained Depending on Tailstock Pressure

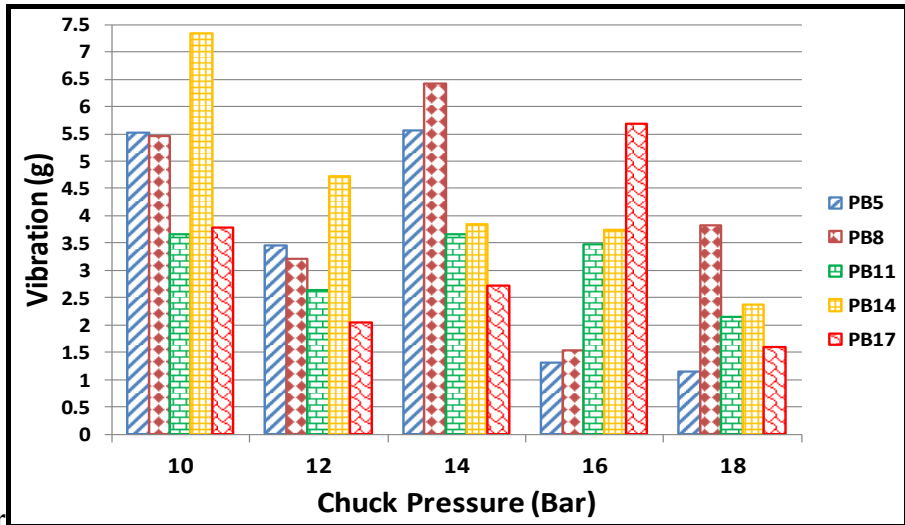


Figure 7. Vibration Values Obtained Depending on Chuck Pressure

Considering the vibration graph obtained depending on the tailstock pressure in Figure 6, the highest vibration value was obtained when the tailstock pressure was 14 bar and the chuck pressure was 10 bar. The lowest vibration value is determined from the graph in Figure 7, which occurs when the workpieces are machined at a tailstock pressure of 5 bar and a chuck pressure of 18 bar. When the graphs in Figure 6 and Figure 7 are examined, it is revealed that the ideal tailstock pressure is 11 bar, while the ideal chuck pressure is 18 bar among all chuck and tailstock pressures in terms of vibration.

STATISTICAL ANALYSIS and DISCUSSION

Grey Relations Analysis

A five-level and two-factor Taguchi orthogonal array L25 (5^2) was designed, corresponding to the experimental results obtained depending on the chuck and tailstock pressure under constant cutting conditions. The Taguchi orthogonal array corresponding to the experiment order performed and the corresponding response variables are shown in Table 3. When the values in Table 3 are examined, it is seen that the vibration and surface roughness values change according to the change of chuck and tailstock pressure factors. It is seen that the most suitable chuck pressure value for the lowest surface roughness and vibration values is 18 bar, while the tailstock pressure value is 11 bar.

Table 3. Taguchi L25 (5^2) Orthogonal Array, Surface Roughness and Vibration Values

Experimental No	Chuck Pressure, Bar	Tailstock Pressure, Bar	Surface Roughness, Ra (μm)	Vibration Amplitude, g
1	10	5	1.61767	5.51
2	10	8	1.51533	5.45
3	10	11	1.257	3.66
4	10	14	1.74633	7.34
5	10	17	1.43	3.78

DETERMINATION OF THE EFFECT OF TAILSTOCK AND CHUCK PRESSURE ON VIBRATION AND SURFACE ROUGHNESS IN TURNING OPERATIONS WITH GRAY RELATIONAL ANALYSIS METHOD

6	12	5	1.47567	3.46
7	12	8	1.51767	3.22
8	12	11	1.26767	2.65
9	12	14	1.36	4.73
10	12	17	1.53633	2.05
11	14	5	1.62033	5.57
12	14	8	1.31733	6.41
13	14	11	1.22433	3.66
14	14	14	1.199	3.85
15	14	17	1.31667	2.72
16	16	5	1.39167	1.32
17	16	8	1.49967	1.54
18	16	11	1.365	3.48
19	16	14	1.48333	3.75
20	16	17	1.37233	5.69
21	18	5	1.19267	1.148
22	18	8	1.34367	3.82
23	18	11	1.20067	2.16
24	18	14	1.274	2.37
25	18	17	1.23667	1.6

The low surface roughness and vibration values that occur while machining the workpieces are desirable to increase productivity in machining. Therefore, according to Grey relations L25 orthogonal design results based on Taguchi, the "smaller is better" array normalization approach is used. Firstly, in determining Grey relations, the average Grey relational degree for that parameter was obtained by summing the same level values for each control factor (surface roughness and vibration) and taking the average. This process is repeated in the second levels to obtain

the response table for the Grey relational degrees. The normalized values of the vibration and surface roughness measurement results and the calculated absolute deviation values, the calculated gray relations degree and order are given in Table 4. For each experiment carried out, grey relational coefficients and as a result of these coefficients, grey relational degrees were obtained. While calculating the coefficients, the discriminating coefficient was taken as $\theta = 0.5$ (Acir et al., 2017; Palanikumar, 2011). The Grey correlation coefficient of 1 given in Table 4 shows the highest correlation between surface roughness and vibration values. Grade of grey relationships in order of experiments is given Figure 8. Looking at Table 4 and Figure 8, it can be clearly seen that the highest value among the Grey relational degrees is experiment with number 21. According to the results for the surface roughness and vibration values, and as a result of the evaluation made with the "smaller is better ", the optimum parameters were determined as chuck pressure (18 bar) and tailstock pressure (5 bar).

Table 4. Normalized Values, Calculated Grey Relational Coefficient, Grey Relational Degree, and Ranks for L25 Orthogonal Array

Experimental Number	Normalized values		Calculated grey relational coefficient		Grey relational degree	Ranks
	Vib	Ra	Vib	Ra		
1	0.2955	0.2324	0.4151	0.3944	0.405	23
2	0.3052	0.4172	0.4185	0.4618	0.440	22
3	0.5943	0.8838	0.5521	0.8114	0.682	9
4	0.0000	0.0000	0.3333	0.3333	0.333	25
5	0.5749	0.5713	0.5405	0.5384	0.539	16
6	0.6266	0.4889	0.5725	0.4945	0.533	17
7	0.6654	0.4130	0.5991	0.4600	0.530	19
8	0.7574	0.8645	0.6733	0.7868	0.730	7

*DETERMINATION OF THE EFFECT OF TAILSTOCK AND CHUCK PRESSURE ON
VIBRATION AND SURFACE ROUGHNESS IN TURNING OPERATIONS WITH GRAY
RELATIONAL ANALYSIS METHOD*

9	0.4215	0.6978	0.4636	0.6233	0.543	15
10	0.8543	0.3793	0.7744	0.4461	0.610	12
11	0.2859	0.2276	0.4118	0.3930	0.402	24
12	0.1502	0.7748	0.3704	0.6895	0.530	18
13	0.5943	0.9428	0.5521	0.8974	0.725	8
14	0.5636	0.9886	0.5340	0.9776	0.756	5
15	0.7461	0.7760	0.6632	0.6906	0.677	11
16	0.9722	0.6406	0.9474	0.5818	0.765	4
17	0.9367	0.4455	0.8876	0.4742	0.681	10
18	0.6234	0.6887	0.5704	0.6163	0.593	13
19	0.5798	0.4750	0.5433	0.4878	0.516	20
20	0.2665	0.6755	0.4053	0.6064	0.506	21
21	1.0000	1.0000	1.0000	1.0000	1.000	1
22	0.5685	0.7273	0.5368	0.6471	0.592	14
23	0.8366	0.9856	0.7537	0.9719	0.863	3
24	0.8026	0.8531	0.7170	0.7729	0.745	6
25	0.9270	0.9205	0.8726	0.8629	0.868	2

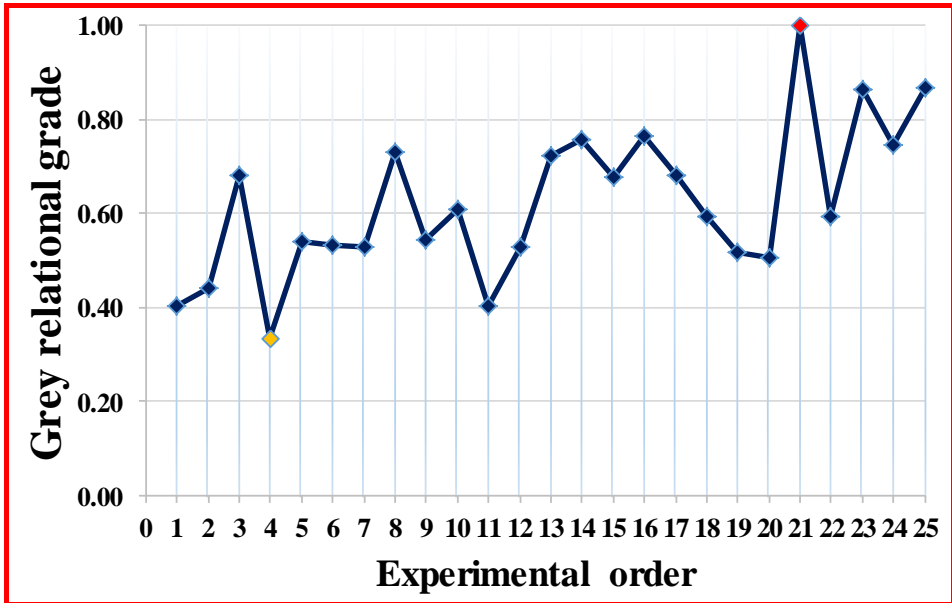


Figure 8. Grade of Grey Relationships in Order of Experiments

S/N RATION RESULTS

In this experimental study, the effects of five different chuck and tailstock pressures on the surface roughness and vibration values were optimized by Taguchi-based Grey relations method. The experiments were carried out according to Taguchi L25 (5^2) orthogonal array and the input parameters were taken as two factors of chuck and tailstock pressure. Five levels were determined for each factor and the output parameters surface roughness and vibration values were optimized according to Taguchi based Grey relations. The effects of tailstock and chuck pressure on the vibration and surface roughness values depending on the S/N ratio and the rankings obtained as a result of the grey relations were investigated. The control factors and levels used in the experiments are given in Table 5. Control factors and levels and their surface roughness and vibration values are given in Table 3. The values of the tailstock and chuck pressure, which optimized the vibration and surface roughness

DETERMINATION OF THE EFFECT OF TAILSTOCK AND CHUCK PRESSURE ON VIBRATION AND SURFACE ROUGHNESS IN TURNING OPERATIONS WITH GRAY RELATIONAL ANALYSIS METHOD

values, were calculated according to S/N ratios obtained from the L25 orthogonal Taguchi method.

Table 5. Control Factors and Their Levels

Control Factors	Levels of factors				
	Level 1	Level 2	Level 3	Level 4	Level 5
Tailstock Pressure (bar)	5	8	11	14	17
Chuck Pressure (bar)	10	12	14	16	18

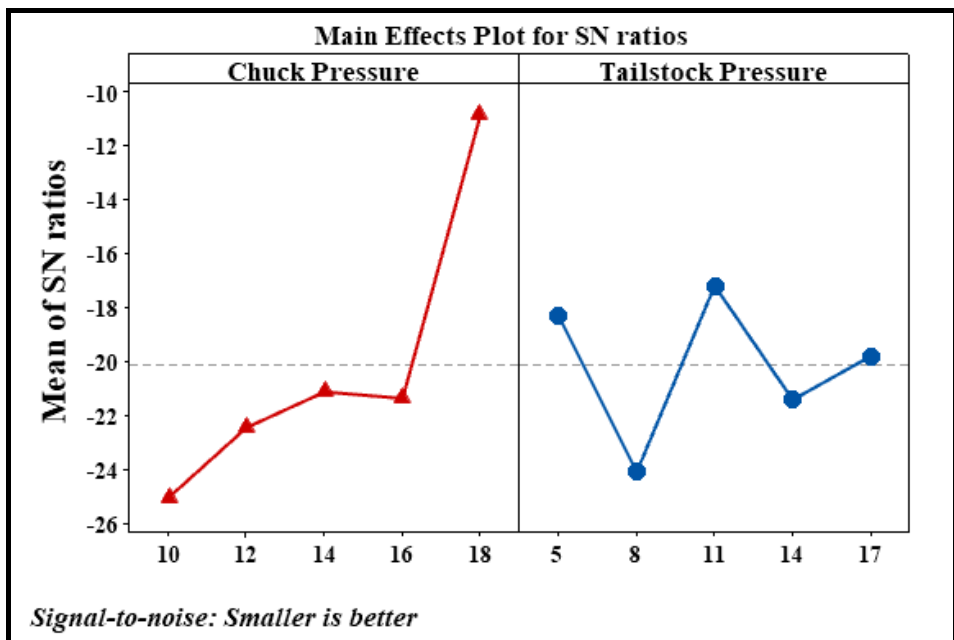


Figure 9. Signal to Noise (S/N) Ratio Main Effect Plot for Surface Roughness and

Vibration Values

The graph obtained according to Taguchi based Grey relations and S/N ratios showing the effects of the relationship between tailstock and chuck pressure on vibration and surface roughness values is given in Figure 9. When the graph in Figure 9 is examined, the optimum paramete-

ters for the surface roughness and vibration values according to the average of the S/N ratios are 18 bar for the chuck pressure and 11 bar for the tailstock pressure. Signal-to-noise ratio values calculated according to the L25 orthogonal array are given in Table 6. When Table 6 is examined, it is determined that S/N values at level 5 for the chuck pressure and at level 3 for the tailstock pressure give the optimum surface roughness and vibration values. When the signal-to-noise ratio values are examined, it is understood with the rank value in Table 6 that the chuck pressure is more effective than the tailstock pressure on the surface roughness.

Table 6. S/N Ratios According to Grey Relations Degrees

Level	Chuck Pressure (Bar)	Tailstock Pressure (Bar)
1	-25.04	-18.30
2	-22.44	-24.09
3	-21.12	-17.17
4	-21.36	-21.41
5	-10.81	-19.79
Delta	14.23	6.92
Rank	1	2

At the same time, the delta value shows the magnitude of the effect parameters on the test results. A large delta value indicates that the control factor is more effective. Looking at the delta values in Table 6, it is understood that the chuck pressure is more effective than the tailstock pressure on the experimental results. From the results given for the surface roughness and vibration values in Figure 9 and Table 6, the optimum chuck pressure value was calculated as level 5 (18 bar), while the tailstock pressure was calculated as level 1 (11 bar). As a result, it is de-

terminated that chuck pressure is more important and effective than tailstock pressure on surface roughness values according to signal-to-noise ratios.

Anova Results

Another statistical tool that reveals the effect of dependent variables on independent variables is ANOVA values. In the evaluation of ANOVA results, the dependent variables are the surface roughness and vibration values calculated according to Grey relations order, while the independent variables are chuck and tailstock pressures. ANOVA results performed depending on five different chuck and tailstock pressures are given in Table 8. In statistical analysis, whether a value is statistically significant or not can be expressed with "P" value. If "P" value is less than 0.05, it is significant. If it is greater than 0.05, it is insignificant (Camposeco, 2013; Kuntoğlu and Sağlam, 2019; Gürbüz et al., 2020; Das et al., 2019). When "P" values in Table 8 were examined to see the effect of the independent variables on the dependent variables, it was concluded that the chuck pressure ($0.012 < 0.005$) was statistically significant and the tailstock pressure ($0.374 > 0.005$) was statistically insignificant.

Table 7. Analysis of Variance for SN Ratios

Source	DF	Seq SS	Adj SS	Adj MS	F	P	Remarks
Chuck Pressure (Bar)	4	594.0	594.0	148.50	4.58	0.012	Significant
Tailstock Pressure (Bar)	4	147.6	147.6	36.91	1.14	0.374	Not Significant
Residual Error	16	518.6	518.6	32.41			
Total	24	1260.2					

RESULTS

In this study, vibration and surface roughness values obtained by turning AISI 304 austenitic stainless steel at different chuck and tailstock pressures under constant cutting conditions were optimized by Taguchi Grey relations method. The effects of the chuck and tailstock pressures used in holding of the workpiece were evaluated, and the experimental and statistical results are given below.

- In general, it was determined that there is a direct proportion between surface roughness values measured on the machined workpieces depending on the chuck and tailstock pressure and the vibration values that occurred during machining.
- In terms of vibration and surface roughness values, the ideal tailstock pressure was seen as 11 bar, while the chuck pressure was 18 bar. Depending on the experimental results, it was determined that chuck and tailstock pressure were effective on vibration and surface roughness values.
- According to the Grey relations order, it was observed that the surface roughness value was the lowest at 18 bar chuck pressure and 5 bar tailstock pressure. The levels that give the optimum surface roughness values according to the signal-noise ratios were obtained as level 5 at chuck pressure 8 bar and level 3 at tailstock pressure 11 bar.
- According to the Taguchi Grey relations degree, the lowest vibration values were calculated as level 5 chuck pressure 18 bar and level 1 tailstock pressure 5 bar. Optimum parameters were obtained at these levels according to S/N ratios.
- It was determined that chuck pressure was the most effective parameter on vibration and surface roughness values, which were dependent variables according to signal-to-noise ratio (S/N) values.

DETERMINATION OF THE EFFECT OF TAILSTOCK AND CHUCK PRESSURE ON VIBRATION AND SURFACE ROUGHNESS IN TURNING OPERATIONS WITH GRAY RELATIONAL ANALYSIS METHOD

- The statistical results obtained once again showed that Taguchi-based Grey relations analysis is an experimental design and analysis that can be successfully applied in metal machining research.

Acknowledges

We would like to thank TÜBİTAK for supporting us in terms of financing within the scope of 2209/B industry-oriented undergraduate thesis support program, Yavuzlar Kardeşler Makine for providing all kinds of support during the experiments and also Batman University Mechanical Engineering Department for the measuring devices.

REFERENCES

- Acir, A., Canlı, M. E., Ata, İ., Çakıroğlu, R. (2017). Parametric optimization of energy and exergy analyses of a novel solar air heater with grey relational analysis. *Applied Thermal Engineering*, 122, 330-338.
- Bhattacharya, A., Das, S., Majumder, P., Batish, A. (2009). Estimating the effect of cutting parameters on surface finish and power consumption during high speed machining of AISI 1045 steel using Taguchi design and ANOVA. *Production Engineering*, 3(1), 31-40.
- Bagaber, S. A., Yusoff, A. R. (2017). Multi-objective optimization of cutting parameters to minimize power consumption in dry turning of stainless steel 316. *Journal of cleaner production*, 157, 30-46.
- Camposeco-Negrete, C. (2013). Optimization of cutting parameters for minimizing energy consumption in turning of AISI 6061 T6 using Taguchi methodology and ANOVA. *Journal of Cleaner Production*, 53, 195-203.
- Cetin, M. H., Ozcelik, B., Kuram, E., Demirbas, E. (2011). Evaluation of vegetable based cutting fluids with extreme pressure and cutting parameters in turning of AISI 304L by Taguchi method. *Journal of Cleaner Production*, 19(17-18), 2049-2056.
- Çaydas, U., Hascalik, A. (2008). Use of the grey relational analysis to determine optimum laser cutting parameters with multi-performance characteristics, *Optics & laser technology*, 40, 987-994.

Das, A., Patel, S. K., Hotta, T. K., Biswal, B. B. (2019). Statistical analysis of different machining characteristics of EN-24 alloy steel during dry hard turning with multilayer coated cermet inserts. *Measurement*, 134, 123-141.

Debnath, S., Reddy, M. M., Yi, Q. S. (2016). Influence of cutting fluid conditions and cutting parameters on surface roughness and tool wear in turning process using Taguchi method. *Measurement*, 78, 111-119.

Günay, M., Yücel, E. (2013). Application of Taguchi method for determining optimum surface roughness in turning of high-alloy white cast iron. *Measurement*, 46(2), 913-919.

Gürbüz, H., Baday, Ş., Sönmez, F. (2021). CNC Takım Tezgahlarında Ayna ve Punta Basıncının Talaşlı İmalat Parametrelerine Etkisinin Yüzey Yanıt Yöntemiyle Değerlendirilmesi. *Bitlis Eren Üniversitesi Fen Bilimleri Dergisi*, 10(1), 160-169

Gürbüz, H., Baday, Ş. (2019). CNC torna tezgâhlarında ayna ve punta basıncının yüzey pürüzlülüğü ve titreşim üzerine etkisinin Taguchi metodu ile optimizasyonu. *Bilecik Şeyh Edebali Üniversitesi Fen Bilimleri Dergisi*, 6(2), 119-134.

Gürbüz, H., Gönülaçar, Y.E., Baday, Ş. (2020). Effect of MQL flow rate on machinability of AISI 4140 steel. *Machining Science and Technology*, 24(5), 663-687.

Karthikeyan, G., Ramkumar, J., Shalabh, Aravindan, S. (2012). Performance analysis of µED-milling process using various statistical techniques. *International Journal of Machining and Machinability of Materials*, 11(2), 183-203.

Kuntoğlu, M., Sağlam, H. (2019). Investigation of progressive tool wear for determining of optimized machining parameters in turning. *Measurement*, 140, 427-436

Lin, C. L. (2004). Use of the taguchi method and grey relational analysis to optimize turning operations with multiple performance characteristics, *Materials and manufacturing processes*, 19 (2), 209-220.

Mavi, A. (2018). Gri ilişkisel analiz yöntemi ile dubleks paslanmaz çeliklerin delinmesinde yüzey form özelliklerini etkileyen optimum kesme parametrelerinin belirlenmesi. *Gazi Üniversitesi Fen Bilimleri Dergisi Part C: Tasarım ve Teknoloji*, 6(3), 634-643.

Mia, M., Rifat, A., Tanvir, M. F., Gupta, M. K., Hossain, M. J., Goswami, A. (2018). Multi-objective optimization of chip-tool interaction parameters using

DETERMINATION OF THE EFFECT OF TAILSTOCK AND CHUCK PRESSURE ON VIBRATION AND SURFACE ROUGHNESS IN TURNING OPERATIONS WITH GRAY RELATIONAL ANALYSIS METHOD

Grey-Taguchi method in MQL-assisted turning, *Measurement*, 129 (2018), 156–166.

Nalbant, M., Gökkaya, H., Sur, G. (2007). Application of Taguchi method in the optimization of cutting parameters for surface roughness in turning. *Materials & design*, 28(4), 1379-1385.

Nas, E., Samtaş, G., Demir, H. (2012). CNC Frezelemede Yüzey Pürüzlülüğüne Etki Eden Parametrelerin Matematiksel Olarak Modellenmesi. *Pamukkale Üniversitesi Mühendislik Bilimleri Dergisi*, 18(1), 47-59.

Neşeli S., Yıldız S. (2007). Tornalamada Yaklaşma Açısı ve Talaş Açısına Bağlı Tırlama Titreşimlerinin Yüzey Pürüzlülüğüne Etkileri. *Politeknik Dergisi*, 10(4), 383-389.

Palanikumar, K. (2011). Experimental investigation and optimisation in drilling of GFRP composites. *Measurement*, 44(10), 2138-2148.

Ramesh, K., Baranitharan P., Sakthivel, R. (2019). Investigation of the stability on boring tool attached with double impact dampers using Taguchi based Grey analysis and cutting tool temperature investigation through FLUKE-Thermal imager. *Measurement* 131 143–155.

Rao, C. M., Venkatasubbaiah, K., Babu, S. P., Srinivas, C. (2016). Optimization of surface roughness in CNC turning using Taguchi method and ANOVA. *International Journal*, 93, 1-14.

Rao K. V., Murthy, B. S. N., Rao, N. M. (2014). Prediction of cutting tool wear, surface roughness and vibration of work piece in boring of AISI 316 steel with artificial neural network. *Measurement*, 51: 63-70.

Salvi, S. B., Deshmukh, R. R., Deshmukh, S. D. (2013). Analysis of surface roughness in hard turning by using Taguchi method. *International Journal of Engineering Science and Technology*, 5(02), 365-370.

Sarıkaya, M., Güllü, A. (2015). Multi-response optimization of minimum quantity lubrication parameters using taguchi-based grey relational analysis in turning of difficult-to-cut alloy haynes 25. *Journal of Cleaner Production*, 91, 347–357.

Sarıkaya, M., Yılmaz, V., Dilipak, H. (2015). Modeling and multi-response optimization of milling characteristics based on taguchi and gray relational

analysis. *Proceedings of the Institution of Mechanical Engineers, Part B: Journal of Engineering Manufacture*, 9, 1-17.

Uzun, G. (2019). Analysis of grey relational method of the effects on machinability performance on austempered vermicular graphite cast irons. *Measurement*, 142, 122-130.

Yan, J., and Li, L. (2013). Multi-objective optimization of milling parameters-the trade-offs between energy, production rate and cutting quality. *Journal of Cleaner Production*, 52, 462-471.

Zeng, T., Lin, C. J., Yang, Y. H., Jeng, M. C. (2009). Optimization of turning operations with multiple performance characteristics using the taguchi method and grey relational analysis. *Journal of materials processing technology*, 209(6), 2753-2759.

Zerti, O., Yallese, M., Zerti, A., Belhadi, S., Girardin, F. (2018). Simultaneous improvement of surface quality and productivity using grey relational analysis based Taguchi design for turning couple (AISI D3 steel/mixed ceramic tool (Al₂O₃+ TiC)). *International Journal of Industrial Engineering Computations*, 9 (2), 173-194.

Zhang, S. J., To, S., Zhang, G. Q., Zhu, Z. W. (2015). A review of machine-tool vibration and its influence upon surface generation in ultra-precision machining. *International Journal of Machine Tools & Manufacture*, 91, 34-42.

EXPERIMENTAL INVESTIGATION OF SINGLE PHASE UNCONTROLLED RECTIFIERS

Mehmet Ali ÖZÇELİK¹, Ahmet AYCAN²

Abstract: Electrical Energy is one of the most popular energy sources today. In general, electricity is divided into alternating current (AC) and direct current (DC). There are forms of transformation during this energy generation, transmission, distribution, and using. Generally, transformers and power electronics components are used in these processes. Raising, lowering and isolation of AC energy are provided with transformers. AC voltage is examined in two parts single-phase and three-phase. With Power Electronics, electrical power can be converted to the desired electrical form and value and controlled with semiconductor static electronic elements. Power Electronics converter systems can be used in places where electrical energy needs to change form and are very popular today. In Power Electronics, the energy range can be increased from milliwatts (mW) to gigawatts (GW). While electric current and voltage are used to carry and transmit information in classical electronic circuits, electrical power is transported and converted into power electronics. It is used by semiconductor switching elements such as diodes, thyristors, and transistors in rotation processes and efficiency is very important. Unlike electronic systems such as communications and signal-data processing, high amounts of electrical power are considered in power electronics and treated accordingly. The conversion of AC electrical energy to DC is within the scope of power electronics, and rectifiers/rectifier circuits are used to achieve this. AC/DC

¹ Gaziantep Üniversitesi, Teknik Bilimler Meslek Yüksekokulu, Elektrik ve Enerji Bölümü, Gaziantep / Türkiye, e-mail: ozcelik@gantep.edu.tr, Orcid No: 0000-0003-0984-5707

² Gaziantep Üniversitesi, Teknik Bilimler Meslek Yüksekokulu, Elektrik ve Enerji Bölümü, Gaziantep / Türkiye, e-mail: aycan@gantep.edu.tr, Orcid No: 0000-0001-9915-9465

converters (rectifier); It is used to power industrial power electronics such as many consumer electronics devices (eg tv, personal computers, battery chargers, etc.) and induction furnaces. Controlled and uncontrolled rectifiers do the rectification process. Diodes for uncontrolled rectifiers and thyristors for controlled rectifiers can be given as examples. A constant DC voltage output can be obtained in uncontrolled rectifiers, while controlled rectifiers are power electronic systems with variable DC output and can be used in speed control. In applications where controlled voltage or power transfer is not required in the industry, the general trend in terms of cost is to use diode rectifiers. In diode rectifiers, the power flow from the mains to the load is only unidirectional. Diode rectifiers are preferred in DC power supplies, AC motor drivers, and many other areas. Although diode rectifiers are preferred in industrial applications in terms of cost, controlled rectifiers, namely thyristors, are used instead of diode rectifiers in cases where an adjustable voltage rather than a constant is required. In the section study, uncontrolled rectifiers for single-phase AC systems; theoretical knowledge, mathematical expressions, waveforms, experimental studies, and example problems have been discussed.

Keywords: Uncontrolled Rectifiers, Diodes, Power Electronics

INTRODUCTION

Today, the increasing use of renewable energy sources such as solar, wind, geothermal, and electric vehicle and unmanned aerial vehicle technologies are on the agenda, increasing the importance of power electronics (Azeem vd., 2019; Özçelik vd., 2019; Özçelik, 2018). The concept of Power Electronics can be defined as the science that examines the control of the electrical energy given to the load and the conversion of these energy forms to each other (Emadi vd., 2006; Özçelik 2017). Power Electronics; It is a very attractive and important branch of Electrical-Electronics Engineering, and it mainly includes Mathematics, Circuit Theory, and Electronics knowledge (Nour vd., 2022; Yılmaz, 2016). The main purpose is to control the electrical power from a source to a load (Eid vd., 2010; Kılıç, 2019). This control is in different ways; it can only be

the amount of power going from the source to the load. In addition, the characteristic of the power supplied to the load or its frequency may need to be changed compared to the characteristic of the power at the source (Kumar and Poddar, 2017; Adak vd.,2021). An example of this is changing an AC source frequency to another frequency that requires motor speed (Kawamura vd., 2017).

The control of the electrical energy supplied to the output load is switched by switching the power on and off, and the energy is adjusted (Chen vd., 2022). Static semiconductor switches are used to provide switching and static semiconductor regulators are used for switching (Meier vd., 2018).

Circuits that convert electrical energy forms to each other in power electronics are generally called converters and they are classified into four sections (Mohammed and Jung, 2021). These converters are expressed in 4 sections as seen in Figure 1.

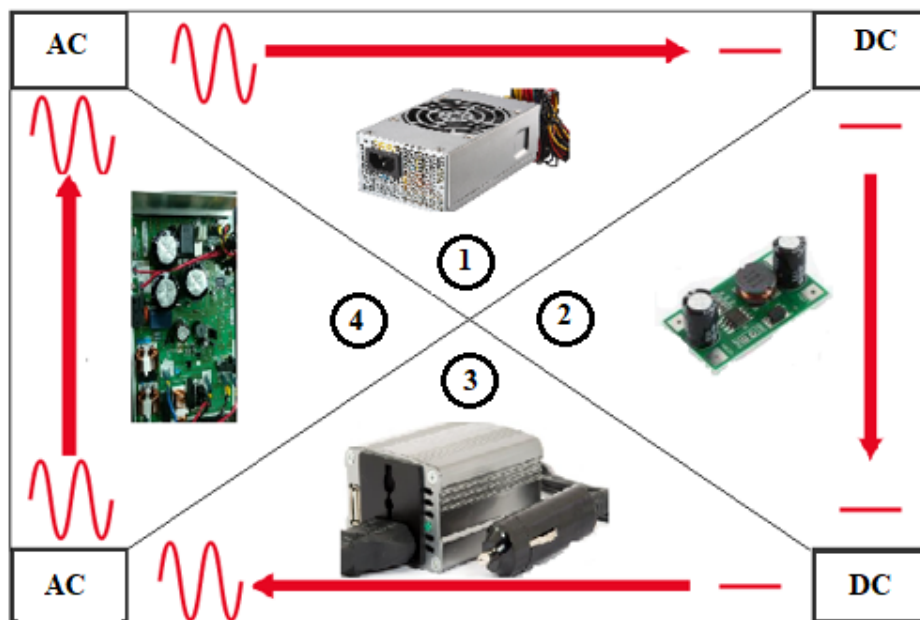


Figure 1. Power Electronics Converters

In Figure 1, Part 1 is AC/DC converters, namely rectifiers, and diodes and thyristors are used for this process. The AC voltage applied to the input has the frequency and the number of phases, and a DC with an average value has been obtained at the output. This structure is generally used in power supplies, DC motor control, and battery chargers.

The second part is DC/DC converters, the amplitude of the input DC is changed to the output. There are Buck, Boost, and Buck-Boost structures. In these circuits, DC amplitude is changed by semiconductor switching elements using a coil, diode, and capacitor. It is used in DC motor control, Photovoltaic energy conversion, Battery charging systems, and DC voltage sources.

The third part is DC/AC converters, that is, inverters. In inverters, the DC applied to the input is converted to AC at the desired frequency and amplitude at the output. Inverters are used in renewable energy systems, uninterruptible power supplies, and AC motor speed control.

Part 4 is AC/AC converters, also known as frequency converters. Thyristors and triacs are implemented with IGBTs. They change the amplitude and frequency of the AC supplied to the input. They are especially used in changing the speed of AC motors.

Efficiency Concept

Considering that efficiency is the most important parameter in power electronics converters, power electronic systems should cause as little power loss as possible. The instantaneous power (P) of a device is equal to the product of the voltage (U) across the device and the current (I), ie $P=U \times I$. As can be seen from here, the power loss of the device is at the minimum level when the voltage is 0 (open state) or when there is no current flow through the device (closed state). Therefore, power electronics converters are designed around one or more devices that can operate in on or off mode. With this type of structure, the energy given from the input of the converter is transferred to the output side via triggers.

EXPERIMENTAL INVESTIGATION OF SINGLE PHASE UNCONTROLLED RECTIFIERS

Comparing the efficiency of a switched control with a linear control can be explained with an example. A 120 Volt DC source shown in Figure 2(a) supplies 120 Watts to a 30Ω load. In this linear control, the value of the resistor R must be 30Ω to provide a current of 2 A to deliver 120 Watts to a 30Ω load. The power of the load is 120 W and 120 W is lost in the load-controlling resistor R. The efficiency in energy transfer from source to load is 50% with 120 W loss.

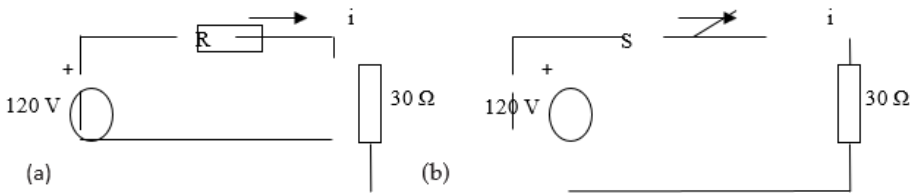


Figure 2. Energy Transfer from Source to Load

As a different operation from the situation in Figure 2(a), power can be transferred by periodically on-off the ideal S switch in Figure 2(b). The switching period is shown in Figure 3.



Figure 3. Switching Period

In this way, the power of the load is 480 Watts in the closed state of the switch and zero in the open state of the switch, this situation is seen in Figure 3. If the switch is closed 25% of the time, the average power will be 25% of 480 Watts or 120 Watts. In this way, almost all the energy of the source can be transferred to the load with ideal switching.

The losses at medium switching frequencies are due to the collector-emitter saturation voltage of the transistor. If this voltage is 2 volts, then the switching conduction losses will be approximately 10 watts. This occurs 20% of the time and causes an average power loss of 2 watts. Thus, to transfer 98 watts to the load, a supply of 100 watts from the source will be required and an efficiency of 98% will be achieved in the control of the power transfer from the source to the load. Of course, this is an ideal assumption, since there are other losses, usually small, in other parts of the switching time, and some power source is needed to feed the control circuits. However, this demonstrates the high yield that can be obtained (Gürdal, 2008).

BASIC SEMI-CONDUCTOR POWER ELEMENTS

A diode is a semiconductor element that acts as a one-way switch for current (Zhenxue vd., 2000). It allows current to flow easily in one direction but severely limits the current flowing in the opposite direction. Diodes are also known as rectifiers because they convert alternating current (AC) to direct current (DC). Diodes are classified according to their types, voltage, and current capacities. Diodes have polarity determined by an anode (positive lead) and a cathode (negative lead). Many diodes only allow current to flow when a positive voltage is applied to the anode. Different combinations of diodes are seen in Figure 4 and they all perform the same function, respectively; It is in the form of metal sheath, nail mounting, tape plastic sheath, channeled plastic sheath, and glass box.

EXPERIMENTAL INVESTIGATION OF SINGLE PHASE UNCONTROLLED RECTIFIERS



Figure 4. Different Diode Combinations

A diode is a two-terminal circuit element made of semiconductor materials that allow an electric current to flow in only one direction. The symbol shown in Figure 5 is used in the circuits.

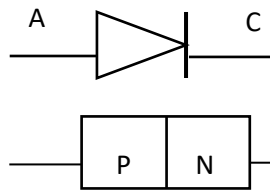


Figure 5. Diode Symbol

If a diode allows current to flow, it is correctly biased. If the diode is reverse-biased, it acts as an insulator and does not allow current to flow. This situation is seen in Figure 6.

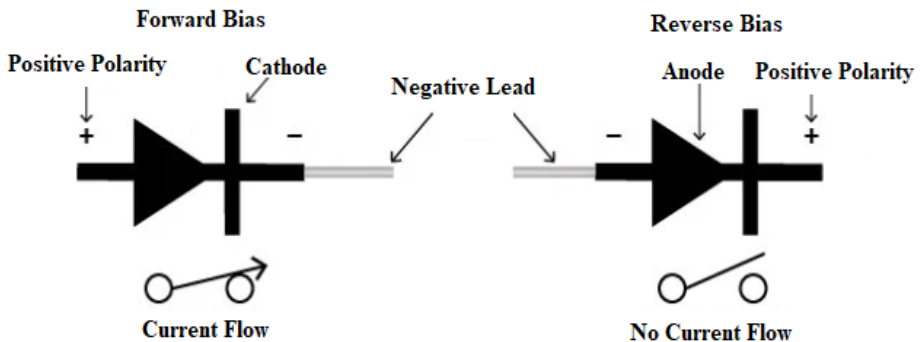


Figure 6. Forward Bias, Reverse Bias

The characteristic curve of the diode is shown in Figure 7 (Lim vd., 2015). In direct polarization, the voltage drop across a typical Silicon diode is about 0.7V (for Germanium the voltage drop is 0.3V). This threshold voltage is called a twist on the diode characteristic curve. Because in this region, the current passing through the diode changes with the voltage falling on the diode. When this threshold voltage value is exceeded, the conduction current "Id" flows. At values lower than this threshold voltage, the diode only allows a small current to pass. If the diode is reverse biased, ideally the diode should not conduct current. But a very small leakage current flows, this current is called "Is" reverse saturation current.

The diode current-voltage connection is given in equation 1. In this equation; Is, VD, n, and VT denote Reverse saturation current, the voltage applied to the diode, de-ideal factor, and Thermal voltage (around 26 mV at room temperature), respectively.

$$I_D = I_S [e^{V_D/nV_T} - 1] \quad (1)$$

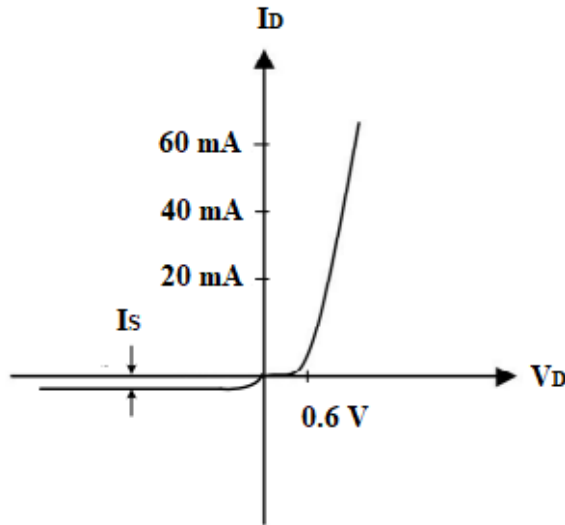


Figure 7. Characteristic Curve of Diode

Since diode rectifiers rectify the voltage in the network, voltage oscillations occur on them at the frequency of the harmonics of the network, depending on the type of rectifier. To reduce them, a capacitor is added to the output before the load. There will be a reduction in voltage fluctuations in the size of the capacitor. One of the disadvantages of diode rectifiers is that they draw very high distortion currents from the network. Since this is limited by harmonic standards, diode rectifiers may not be used in all cases. Instead of these, controlled rectifiers can be used to approach the current sinus curve with various control strategies. We can classify diode rectifiers as single-phase, three-phase, half-wave rectifiers, and full-wave rectifiers. In the book section, single-phase half-wave and full-wave rectifiers will be discussed.

Single Phase Half Wave Rectifier

Although single-phase half-wave rectifiers are not used much, they are a good example for understanding rectifier operation. Figure 8 shows a single-phase half-wave rectifier.

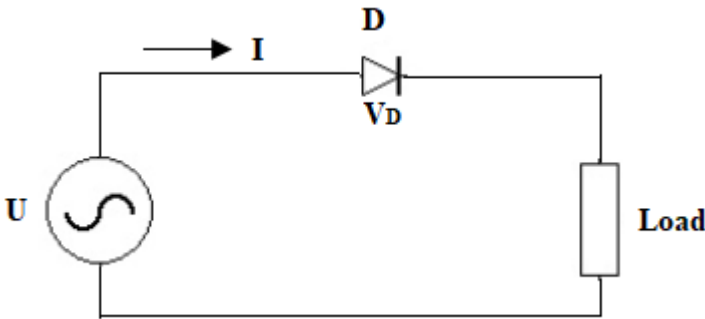


Figure 8. Half-Wave Rectifier at Ohmic Load

The half-wave rectifier will only rectify the positive part of the sinusoidal voltage since it does not transmit the negative voltage on the diode (Chan vd., 2016). The load can be either ohmic or inductive. If the load is ohmic, the diode will only pass the positive alternating of the AC, i.e. rectify. This situation is shown in Figure 9.

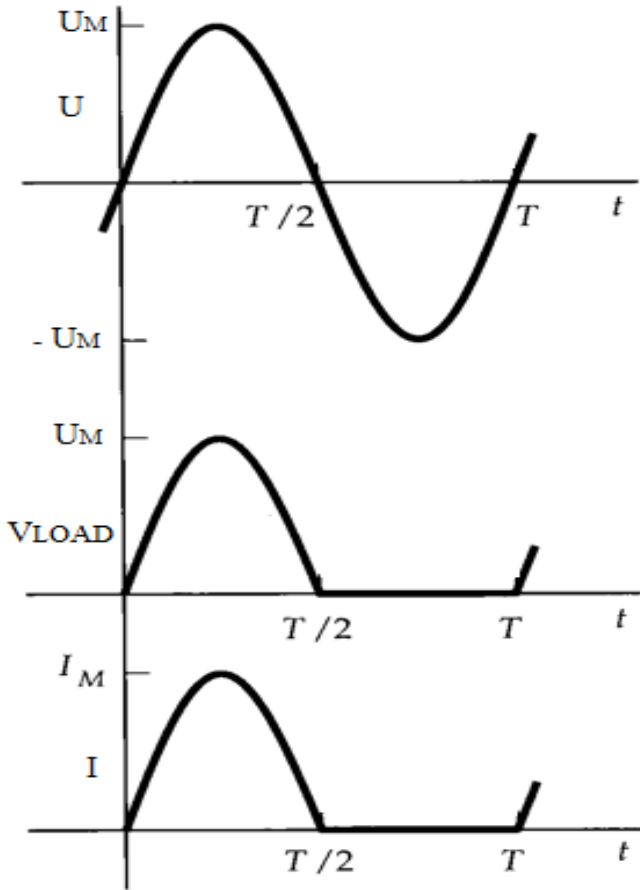


Figure 9. Current, Voltage, Load Waves in Ohmic Load Half-Wave

In the experimental study of the ohmic load half-wave rectifier, the waveform of the ohmic load is given in Figure 10.

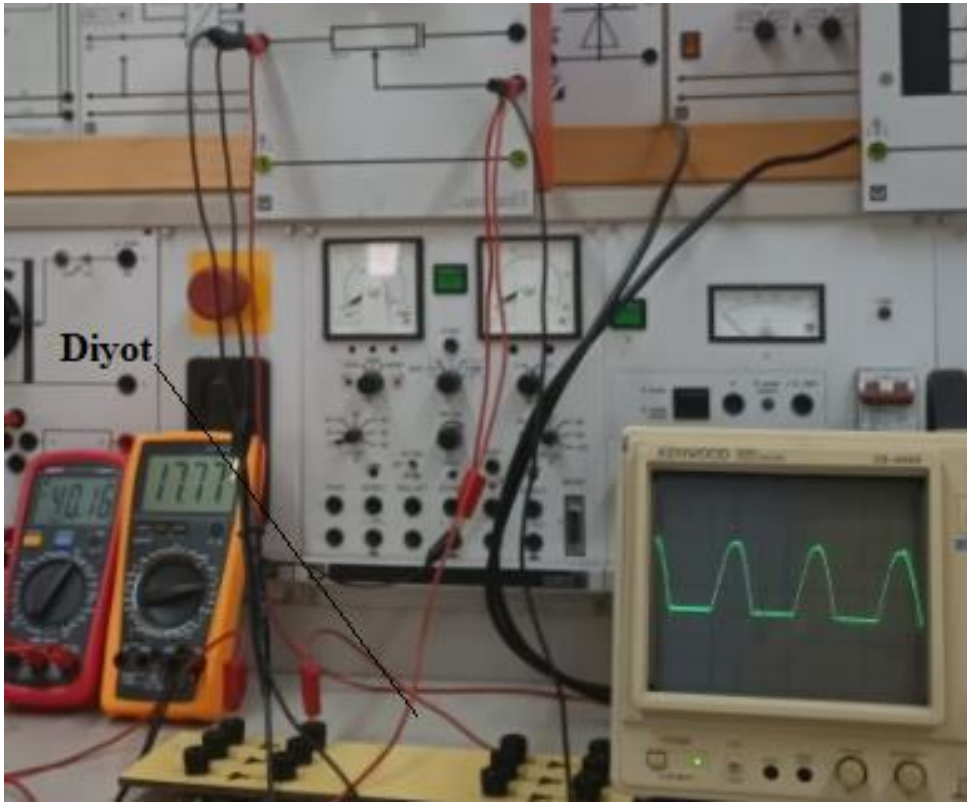


Figure 10. Resistive Load Voltage at Half Wave

Circuit equation,

$$V = V_D + V_{Load} \quad (2)$$

Since $V_D = 0$ for $I(t) = 0$, the current equation is,

$$i(t) = \frac{V}{R} = \frac{V_m \sin \omega t}{R} \quad (3)$$

In equation (2), ω corresponds to the determined source frequency and the equation is valid only for $i(t) > 0$. Thus, the maximum voltage

occurs when V is equal to V_m and is given by eq. 3.

$$I_m = \frac{V_m}{R} \quad (4)$$

During the transmission, the expression (5) is written for the condition $v_D=0$, hence $i(t)$,

$$i(t) > 0 \text{ for } V_R = V \quad (5)$$

For half a cycle when $V < 0$, the diode is reverse-biased. Current is zero and V_R is zero. During this half cycle, there is the equation $V_D = V$. The relevant quantities for this circuit are the average load current and voltage. The average current is found by the integral (6) of $i(t)$ throughout the waveform.

$$I_{average} = \frac{1}{T} \int_0^T i(t) dt \quad (6)$$

Since $i(t) = 0$ for the second half cycle, this integral is evaluated over the half-period $0 - T/2$. Here $w=2\pi f$ is equal to $I_{mean}=I_m/\pi$. Since the waveform of the voltage is the same as the waveform of the current, $V_{mean}=V_m/\pi$ can be written.

$$I_{average} = \frac{1}{T} \int_0^{T/2} I_m \sin wtdt \quad (7)$$

The RMS equation is written with equation (8) from the definition of RMS.

$$I_{RMS} = \sqrt{\left[\frac{1}{T} \int_0^T [i(t)^2] dt\right]} \quad (8)$$

If the integral is evaluated over a half period, equation (9) is obtained.

$$I_{RMS} = \sqrt{\left[\frac{1}{T} \int_0^{T/2} (I_m \sin \omega t)^2 dt\right]} \quad (9)$$

The result of equation (10) is the characteristic of the waveform of the half-wave circuit.

$$I_{RMS} = \frac{I_m}{2} \quad (10)$$

Example 2.1

Since the DC voltmeter measuring the average value connected to the load ends in the half-wave rectifier circuit in Figure 11 shows 30 V, how many volts does the AC voltmeter measuring the effective value at the rectifier input show? (Diode threshold voltage value V_D is neglected)

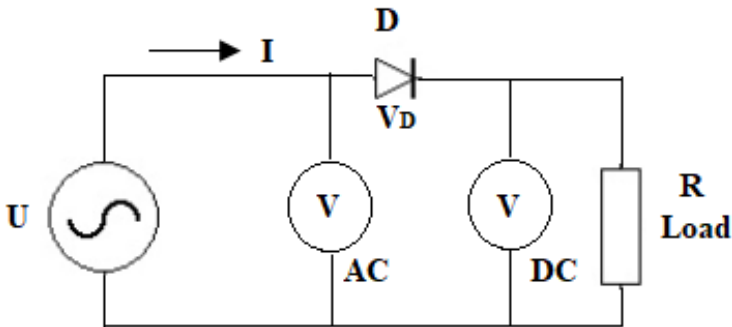


Figure 11. Half Wave Circuit

Solution

Since the period is $T=2\pi$ and $V_m = \sqrt{2}V_{rms}$ and by writing equation

(11), V_m is found.

$$V_{mean} = \frac{1}{T} \int_0^{\pi} V_m \sin \omega t dt = \frac{V_m}{\pi} = 0,318V_m \quad (11)$$

$$a.) = V_m = \frac{V_{average}}{0,318} = \frac{30}{0,318} = 94,33 \text{ V}$$

$$b.) \text{ Effective voltage} = V_{RMS} = \frac{V_M}{\sqrt{2}} = 0.707V_m = 0,707.94,33 = 66,69 \text{ V}$$

has been found..

Half Wave Inductive Load

If the load is inductive, since the load current will continue to flow in the positive direction for a while after the voltage drops to zero, the diode cannot turn off immediately and transmits the negative voltage until the current on it drops to zero.

The half-wave circuit is obtained by adding an inductive load as seen in Figure 12 (Kkelis vd., 2017). The load current may be present for more than half of the entire period. The magnitude of the load's inductance is not important, and the conduction is not the same over the entire period. The load current needs to be zero in some range, which is less than half a period.

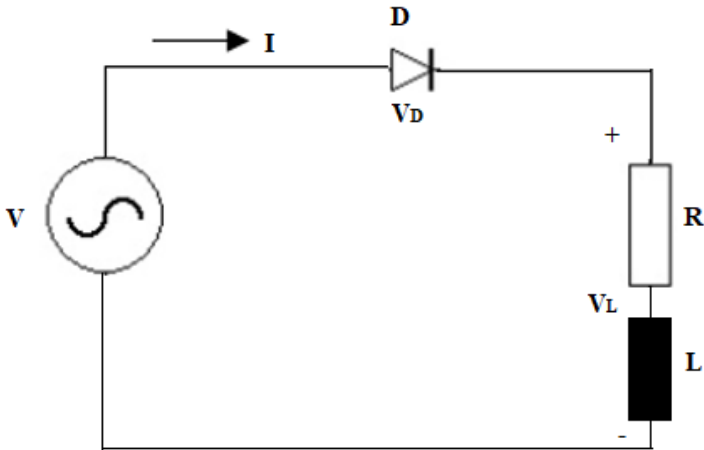


Figure 12. Half-Wave Rectifier with Inductive Load

A solution to the transient load current is as follows. In the waveform in Figure 13, the current is zero at $t=0$. The current relationship is given in equation (12).

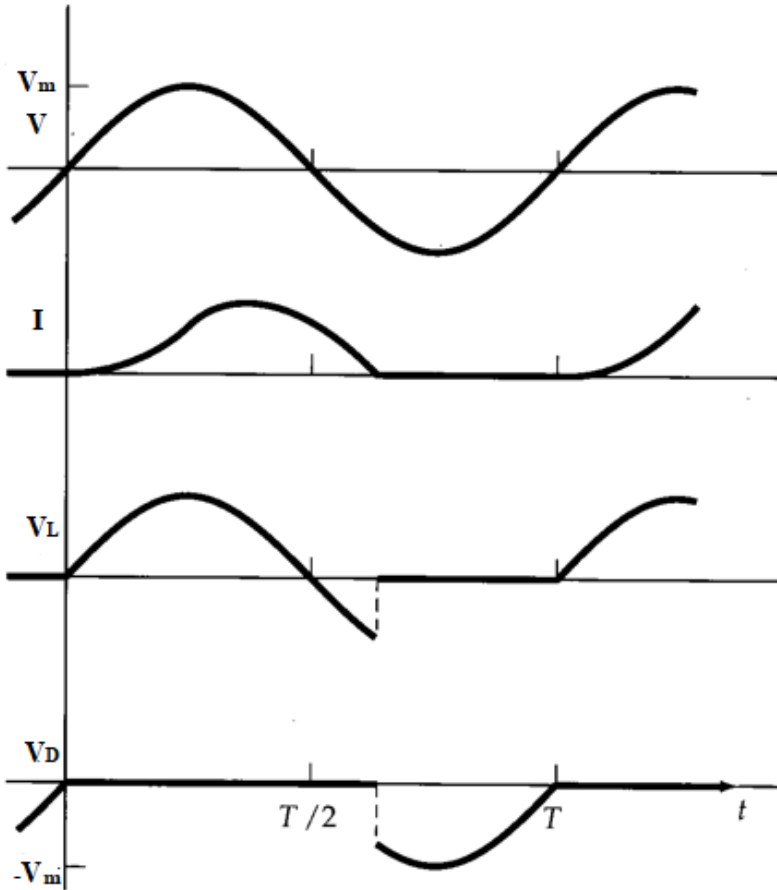


Figure 13. Current, Voltage, and Load Waves in Inductive Load Half-Wave (Gürdal, 2008)

The current in equation (12) becomes zero at a time greater than $T/2$. This time can be found by a numerical analysis of this equation.

$$i = \left(\frac{V_m}{|Z|} \right) \left[\sin(\omega t - \theta) + (\sin\theta)e^{-t/\tau} \right] \quad (12)$$

This method is not useful for large power straightening operations. Any amount of inductance will not produce a non-zero load current for

part of each cycle. Moreover, AC welding current is bidirectional and can cause saturation in a transformer feeding the rectifier circuit, especially if the load current is large. Impedance expression is given in equation (13), and angle expression in equation (14).

$$|Z| = \sqrt{(R^2 + \omega^2 L^2)} \quad (13)$$

$$\theta = \tan^{-1}\left(\frac{\omega L}{R}\right) \quad (14)$$

In the experimental study of half-wave rectifier with inductive load, the waveform of the inductive load is given in Figure 14.

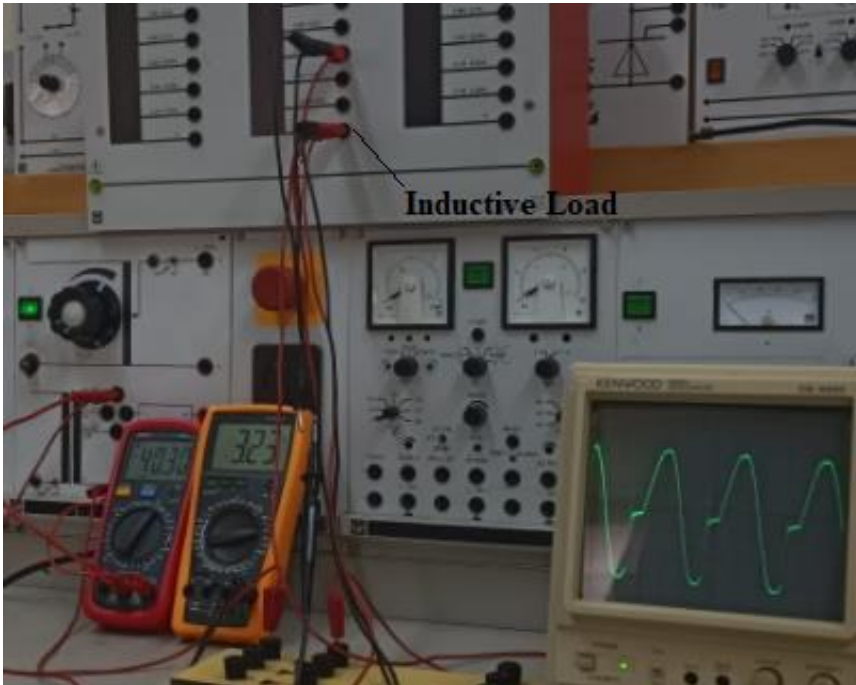


Figure 14. Inductive Load Voltage at Inductive Load Half Wave

The self-induction voltage induced in the inductive circuit is brought back to the inductive load via the diode. While the direction of current passing through the main diode does not change, the polarity of the vol-

EXPERIMENTAL INVESTIGATION OF SINGLE PHASE UNCONTROLLED RECTIFIERS

tage at the load ends changes. A by-pass diode is used in inductive circuits to protect semiconductor elements such as transistors and to avoid reverse polarity. This diode is connected in reverse parallel to the coil. When there is a by-pass diode, the average value of the voltage at the output and the current through the load increase. For example, when a DC motor or Universal motor is connected to the output, and there is no by-pass diode, the output voltage is lower, so the speed and torque of the motor are lower. When the by-pass diode is used, the average value of the voltage at the load ends and the current flowing through the load increase, so the speed and torque of the motor increase. In other words, the induction voltage induced in the coil is brought back to the load via the diode and the main diode goes to cutoff. In the absence of a by-pass diode, the main diode continues to conduct for a while even if the input switches to negative alternate due to the self-induction voltage. The connection of the by-pass diode to the inductive uncontrolled half-wave rectifier circuit is shown in Figure 15.

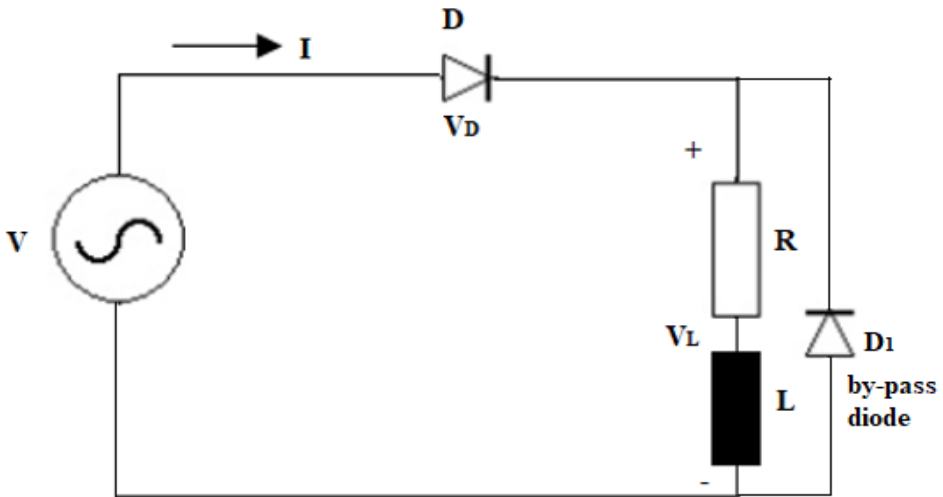


Figure 15. Inductive Load Voltage at Half Wave with By-Pass Diode

The effect of the bypass diode on the inductive uncontrolled half-wave rectifier circuit on the output voltage is seen in Figure 16. Here, in alternans change, the main diode goes cut-off immediately. It is seen that the voltage at the load ends increases because the self-induction voltage induced in the coil is brought back to the load via the diode.

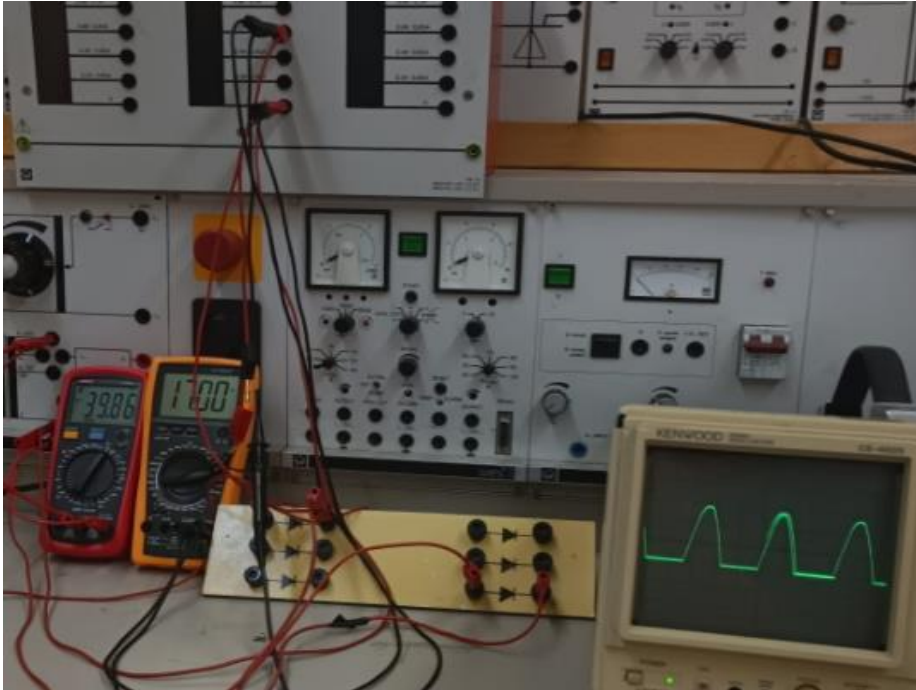


Figure 16. Effect of Bypass Diode on Output Voltage

While the mains current increases in the alternating (+) alternating current, the polarity of the self-induction voltage induced in the coil is (+) and the lower end is (-). As soon as the mains current starts to decrease from the peak value, the polarity of the self-induction voltage induced in the coil is the lower end (+) and the upper end (-). At this moment, the free loop diode, that is, the Bypass diode turns on. The main diode carrying the load current goes off. The (-) alternate of the voltage at the load ends does not appear, but the current continues to flow from the load

EXPERIMENTAL INVESTIGATION OF SINGLE PHASE UNCONTROLLED RECTIFIERS

until the energy accumulated in the inductance is exhausted. Since the voltage at the load ends has no (-) alternate, its average value increases. Therefore, current and power increase. We absorb the energy of the coil over itself through the bypass diode.

Example 2.2.

The AC Voltmeter, which measures the effective value connected to the input in the half-wave inductive loaded rectifier in Figure 17, shows 40 Volts. A voltmeter connected to the load terminals;

- a.) How many volts does volt-meter show for open A switch and $\beta=240^\circ$?
- b.) How many volts does volt-meter show when A switch is closed? (The threshold voltage value falling on the diode terminals will be neglected)

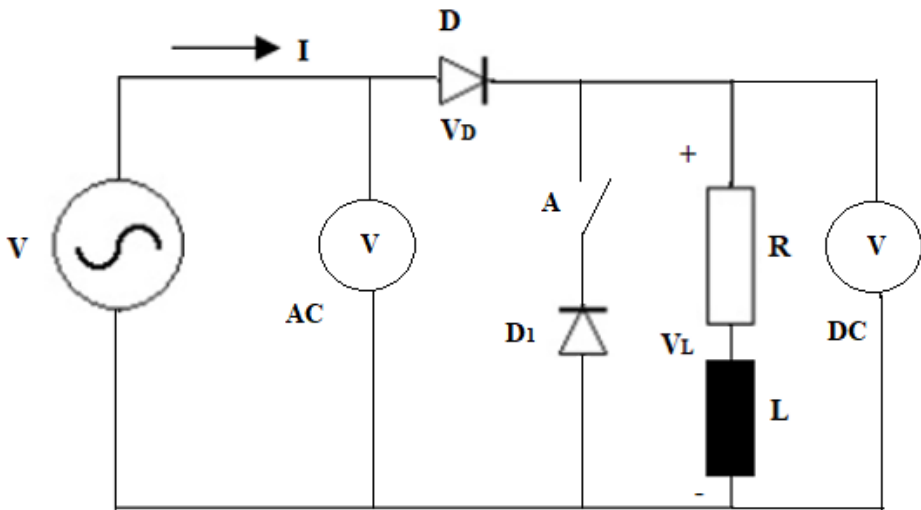


Figure 17. Inductive Half Wave Circuit

Solution

$$V_{\text{mean}} = \frac{V_m}{2\pi} (1 - \cos\beta) = \frac{40.1,41}{6,28} (1 - \cos 240^\circ) = \frac{56,4}{6,28} [1 - (-0,5)] =$$

a.) 13,47 Volt

$$V_{\text{mean}} = \frac{1}{T} \int_0^{\pi} V_m \sin \omega t dt = \frac{V_m}{\pi} = 0,318V_m = 0,318.56,4 = 17,93 \text{ Volt}$$

Here the reason for the increase in voltage is due to the self-induction being imparted to the load. By closing switch A, the voltage occurring at the load ends, and the current passing through the load increase.

Single Phase Ohmic Load Full Wave Rectifier

Full-wave or bridge rectifier circuit, which is used quite frequently for single-phase applications, is shown in Figure 18 (Karthikeyan and Amrutur, 2012). In the circuit consisting of four diodes, diodes D1 and D4 will pass the positive alternating voltage of the alternating voltage, and diodes D2 and D3 will actively rectify this region. As in the half-wave case, the source voltage and load resistance are of the same value. A full-wave circuit conducts a current through the circuit as in a half-wave, and the current in the load is also present in the second half-wave.

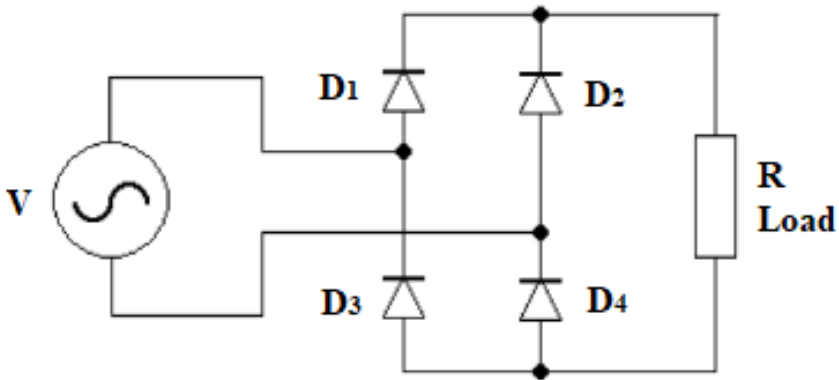


Figure 18. Single Phase Ohmic Load Full Wave Rectifier

In the single-phase bridge diode, the average and effective values of the load voltage and current are calculated by integrating them in the same way. Average and RMS values are found as is for the half-wave condition.

$$I_{mean} = \frac{1}{T} \int_0^T I_L t dt \quad (15)$$

$$I_{mean} = \frac{1}{T} \left[\int_0^{T/2} I_m \sin \omega t dt + \int_{T/2}^T -I_m \sin \omega t dt \right] = \left(\frac{2}{\pi} \right) I_m \quad (16)$$

Similarly, the following results are obtained in the equation for voltage.

$$V_{mean} = \frac{2V_m}{\pi} \quad (17)$$

$$V_{RMS} = \frac{V_m}{\sqrt{2}} \quad (18)$$

Since the waveforms of the currents and voltages are the same in the full wave case of the ohmic load, the current values given by the formulas can only be used for the ohmic loads. Current, voltage, and load waves at full-wave ohmic load are shown in Figure 19.

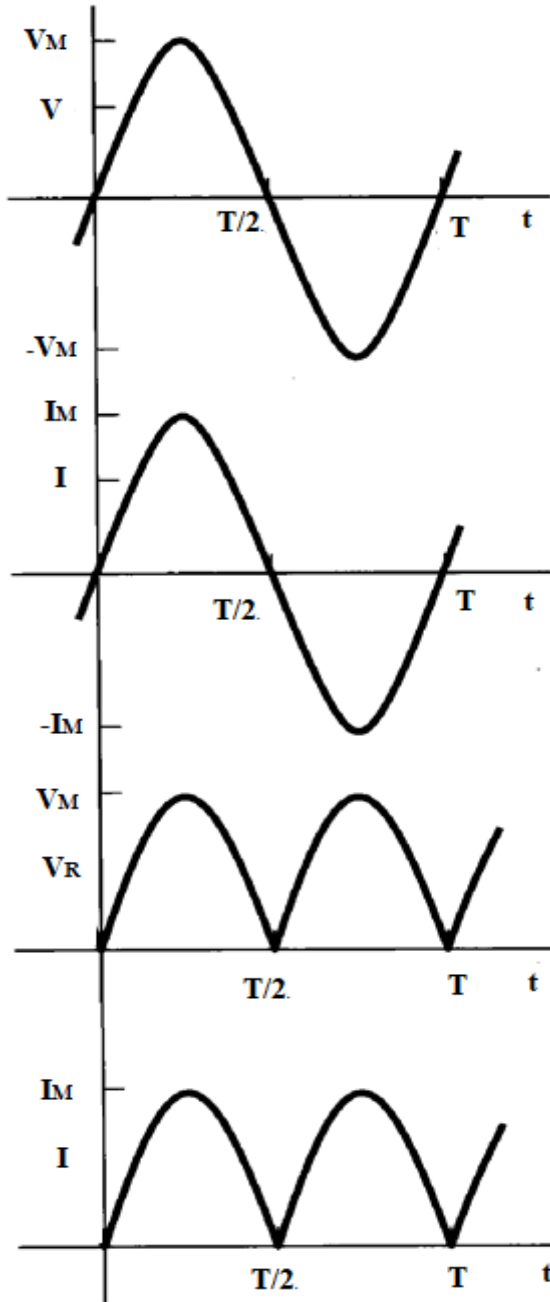


Figure 19. Ohmic Load Full Wave Current, Voltage, Load Waves

EXPERIMENTAL INVESTIGATION OF SINGLE PHASE UNCONTROLLED RECTIFIERS

In the experimental study of the ohmic-loaded full-wave rectifier, the waveform of the ohmic load is given in Figure 20.



Figure 20. Ohmic Full Wave Rectifier Circuit Load Voltage

Example 2.3

Since the input voltage is 40.04 V in the ohmic full-wave rectifier circuit in Figure 21, and 34.7 V is measured from the DC voltmeter that measures the average value connected to the load ends, how many volts does the AC voltmeter that measures the effective value at the output of the rectifier show? (Diode threshold voltage value V_D is neglected)

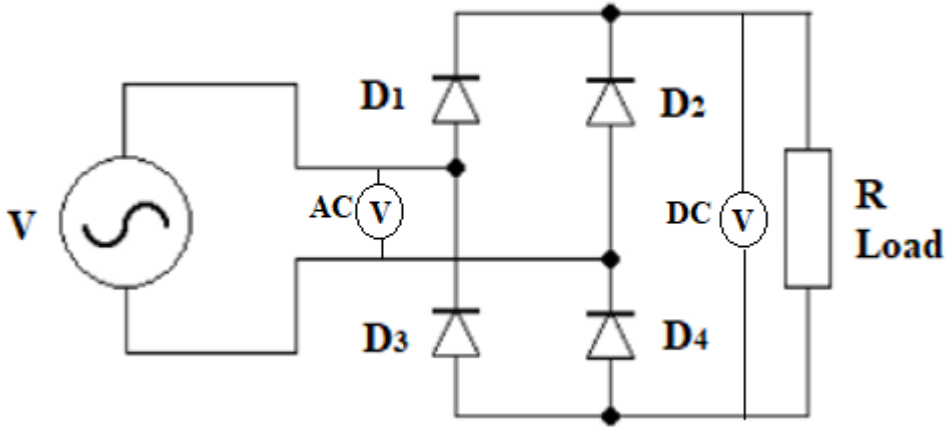


Figure 21. Ohmic Load Full Wave Rectifier

Solution

$$V_{mean} = \frac{1}{T} \int_0^{\pi} V_m \sin \omega t dt = \frac{2\sqrt{2}}{\pi} V = \left(\frac{2}{\pi}\right) V_m = \frac{2.1,41.40,04}{3.14} = 35,95 \text{ Volt}$$

Single Phase Inductive Load Uncontrolled Full Wave Rectifier

One phase full wave rectification circuit in inductive load is given in Figure 22. When the load is inductive, the current will fall behind the voltage, but the negative voltage situation observed in the half-wave rectifier will not occur in the bridge diode, since there is another diode in the positive voltage phase that will take the current. Connecting an inductance in series with a load resistor changes the waveform of the current. Waveforms for these are given in Figure 23.

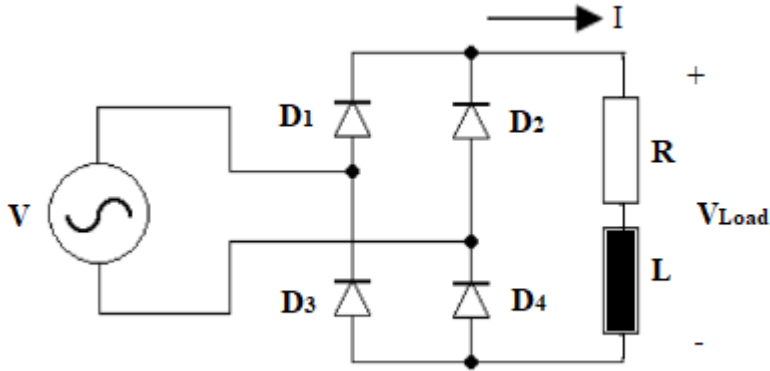


Figure 22. One-Phase Full-Wave Rectification Circuit in the Inductive Load

In the single-phase bridge diode, the average and effective values of the load voltage and current are calculated by integrating them in the same way.

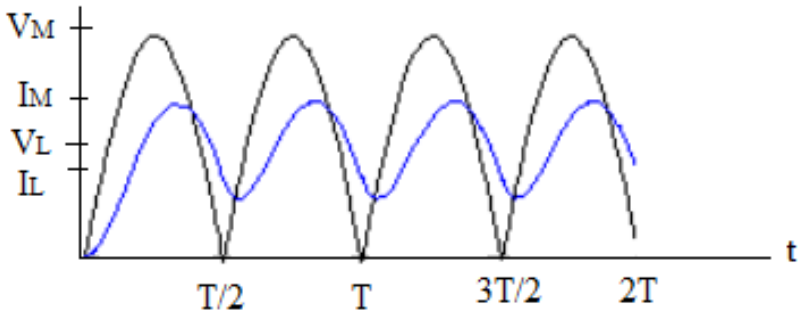


Figure 23. Inductive Load Full Wave Load Current, Voltage Waves

$$V_{Rmean} = V_{Lmean} = \left(\frac{2}{\pi}\right) V_m \quad (19)$$

$$I_{mean} = \frac{V_{Rmean}}{R} = \left(\frac{2}{\pi}\right) \left(\frac{V_m}{R}\right) \quad (20)$$

RMS effective and average values are constant due to constant load current. The inductive Full Wave Rectifier Experimental Circuit Load Voltage is shown in Figure 24.

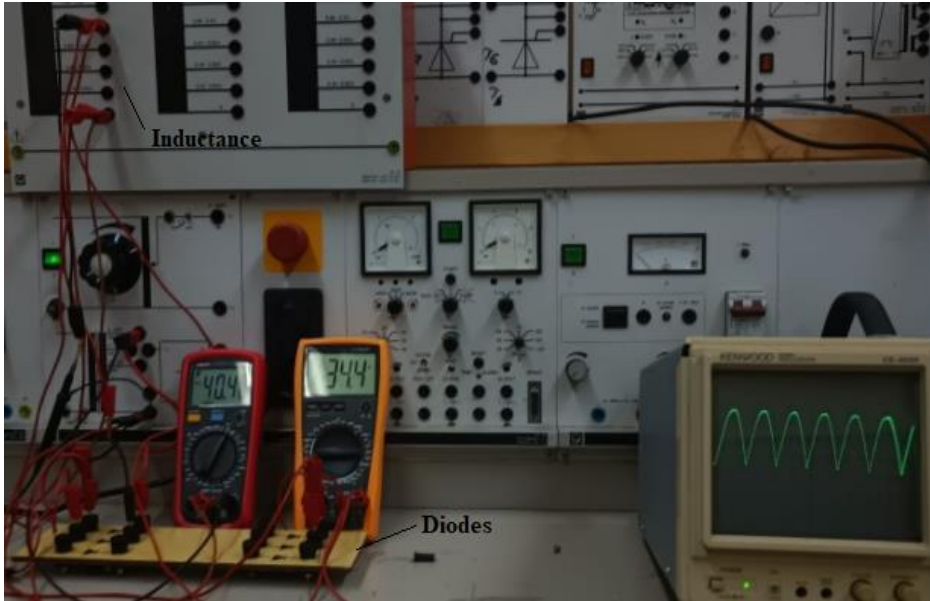


Figure 24. Inductive Full Wave Rectifier Circuit Load Voltage

When the coil inductance is $L=0.6$ Henry, the waveform of the Full Wave Rectifier Circuit Load Current is given in Figure 25. It is seen that the current becomes smoother as the inductance value increases due to the coil's ability to filter the current at the same time.

EXPERIMENTAL INVESTIGATION OF SINGLE PHASE UNCONTROLLED RECTIFIERS

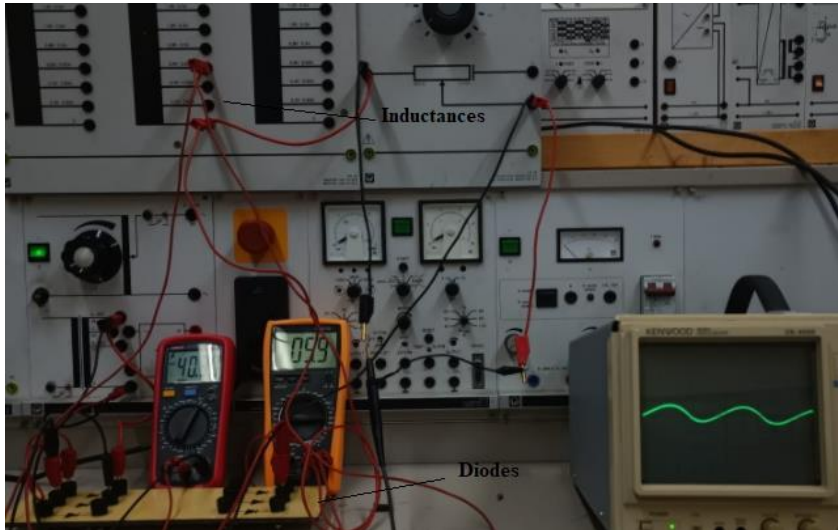
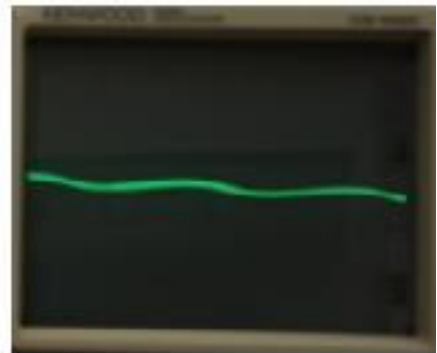


Figure 25. Inductive Full Wave Rectifier Circuit Load Current ($L=0.6$ Henry)

In Figure 26, current waveforms for 1 H and 2.4 H values of the coil are seen, as the inductance value increases, a smoother current form is obtained.



(a) $L=1H$



(b) $L=2.4H$

Figure 26. Inductive Full Wave Rectifier Circuit Load Current

Example 2.4.

The inductive uncontrolled full-wave rectifier circuit in Figure 27 feeds a highly inductive load. The DC voltmeter connected to the load

terminals shows 100 Volts. Since the ohmic resistance of the inductive load is 10Ω ;

- Find the maximum (I_m), effective (I_{rms}), and average (I_{mean}) values of the current
- Find the power consumed by the load
- How many volts does the voltmeter at the rectifier input show? (The diode threshold voltage will be neglected)

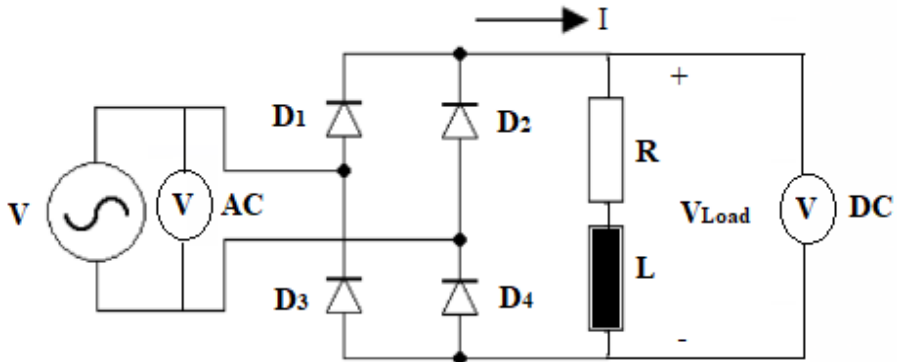


Figure 27. Inductive Full Wave Rectifier Circuit

Solution

$$a.) I_{mean} = I_{rms} = \frac{V_{mean}}{R} = \frac{100}{10} 10 A$$

The ripple in current is neglected when the inductance is large enough. $I_m = I_{rms} = I_{mean}$ is accepted.

$$b.) P = I_{rms}^2 \cdot R = 10^2 \cdot 10 = 1000 \text{ Watt}$$

$$c.) V_{mean} = \frac{1}{T} \int_0^{\pi} V_m \sin \omega t dt = \frac{2V_m}{\pi} = 0,636V_m$$

$$100 = 0,636 \cdot V_m \quad V_m = 157,23 \text{ Volt}$$

$$V_{rms} = \frac{V_m}{\sqrt{2}} = 0,707V_m = 0,707 \cdot 157,23 = 111,16 \text{ V}$$

Since diodes connected in parallel to the load act as bypass diodes in a single-phase bridge-type full-wave rectifier, there is no need for a separate bypass diode. Therefore, in ohmic and inductive loads, the voltage waveform at the load ends is the same. In ohmic loads, the voltage waveform and the current waveform are the same. However, in an inductive load, as the inductance of the load increases, its fluctuation in the current decreases. If the inductance is large enough, the ripple in the current is neglected.

CONCLUSION

In the study, the operation and behavior of single-phase uncontrolled diode rectifiers were investigated. At the same time, the purpose of controlled rectifiers is mentioned and the advantage of switching in obtaining high powers is shown in the concept of Efficiency. The basic power element used in uncontrolled rectifiers is the diode. This rectifier is given such a name because the diode is an uncontrolled power element. Single-phase uncontrolled diode rectifiers; It has been studied theoretically and experimentally in half-wave and full-wave scope. Theoretical and experimental studies were investigated under ohmic and inductive loads. In many power electronics applications, the input power is in the form of AC power at a frequency of 50 Hz or 60 Hz from the mains and converted to DC in applications. The general trend in terms of cost is to use diode rectifiers in applications that do not require controlled voltage or power transfer in industry and businesses. In diode rectifiers, the power flow from the grid to the load is only one-way. Diode rectifiers are preferred in DC power supply, AC motor drives, and many other areas. Since diode rectifiers rectify the voltage from the network, there are voltage oscillations on them at the frequency of the harmonics of the network, depending on the type of rectifier. To reduce them, a capacitor and inductor are added to the output before the load. Coils filter current, while capacitors filter voltage. For this, capacitors are connected in parallel to the load, and inductances are connected in series with the load and filter

operation. The larger the filter elements, the smaller the output voltage and current fluctuations.

One of the negative features of diode rectifiers is that they draw very high distortion currents from the network. Since this is limited by harmonic standards, diode rectifiers may not be used in all cases. Instead, controlled rectifiers are used to simulate the current with various control strategies. Diode rectifiers can be classified as single-phase, three-phase, half-wave rectifiers, and full-wave rectifiers. Half-wave rectifiers are generally not used because of their effects on the grid. Single-phase and three-phase bridge rectifiers are commonly used in single-phase and three-phase uncontrolled rectifiers and rectifier circuits.

It has been observed that the effect of ohmic loads in half-wave uncontrolled rectifiers is the same in current and voltage waveforms. In the inductive load, since there is a current storage situation, it has been examined that the effect of the current on the main diode continues in the negative alternate of AC. It has been experimentally proven that a bypass diode connected to the inductive load in reverse and parallel increases the output power. It has been shown that there is no need for a bypass diode in the full-wave rectifier since there are no diodes that conduct in negative alternate.

It has been observed that the effect of ohmic loads in full-wave uncontrolled rectifiers is the same in current and voltage waveforms. It has been shown from the waveforms that the inductive current lags the voltage and it has been seen that the inductive load makes the load current continuous. The effect of the inductance value on the increase in the continuity of the load current has been shown experimentally. It has been shown that the power transfer in full-wave rectifiers is higher than in half-wave and has smoother waveforms. As a result, it has been seen that the mathematical and experimental studies of single-phase rectifiers, which are widely used in AC-DC conversion, overlap with each other. It has been tried to contribute to a better understanding of the issue of un-

controlled rectifiers, which has an important place in power electronics systems. In the next study, controlled rectifiers will be examined theoretically and experimentally.

REFERENCES

- A. Emadi, S. S. Williamson and A. Khaligh. (2006). "Power electronics intensive solutions for advanced electric, hybrid electric, and fuel cell vehicular power systems," in *IEEE Transactions on Power Electronics*, vol. 21, no. 3, pp. 567-577, doi: 10.1109/TPEL.2006.872378.
- Azeem, A., Ansari, M. K., Tariq, M., Sarwar, A. & Ashraf, I. (2019). Design and Modeling of Solar Photovoltaic System Using Seven-Level Packed U-Cell (PUC) Multilevel Inverter and Zeta Converter for Off-Grid Application in India. *Electrica*, 19 (2), 101-102. Retrieved from <https://dergipark.org.tr/tr/pub/electrica/issue/46870/587716>
- Adak, S., Cangi, Hasan, Eid, B., & Yılmaz, A. S. (2021). Developed analytical expression for current harmonic distortion of the PV system s inverter in relation to the solar irradiance and temperature. *Electrical Engineering*, 103, 697–704.
- A. Eid, H. El-Kishky, M. Abdel-Salam and M. T. El-Mohandes. (2010). "On Power Quality of Variable-Speed Constant-Frequency Aircraft Electric Power Systems," in *IEEE Transactions on Power Delivery*, vol. 25, no. 1, pp. 55-65, doi: 10.1109/TPWRD.2009.2031672.
- G. Kkelis, D. C. Yates and P. D. Mitcheson. (2017). "Class-E Half-Wave Zero dv/dt Rectifiers for Inductive Power Transfer," in *IEEE Transactions on Power Electronics*, vol. 32, no. 11, pp. 8322-8337, doi: 10.1109/TPEL.2016.2641260.
- Gürdal, O. (2008). *Güç Elektroniği, Seçkin Yayıncılık*, ISBN:9789750207105
- Kılıç, E. (2019). DA-DA Yükselten Dönüştürücü İle Elektrikli Araç Batarya Şarj Cihazı Tasarımı. *Kahramanmaraş Sütçü İmam Üniversitesi Mühendislik Bilimleri Dergisi*, 22(4), 281-287.
- L. H. I. Lim, Z. Ye, J. Ye, D. Yang and H. Du. (2015). "A Linear Identification of Diode Models from Single I - V Characteristics of PV Panels," in *IEEE Transactions on Industrial Electronics*, vol. 62, no. 7, pp. 4181-4193, doi: 10.1109/TIE.2015.2390193.

L. Karthikeyan and B. Amrutur. (2012). "Signal-Powered Low-Drop-Diode Equivalent Circuit for Full-Wave Bridge Rectifier," in *IEEE Transactions on Power Electronics*, vol. 27, no. 10, pp. 4192-4201, doi: 10.1109/TPEL.2012.2190828.

M. B. Meier, S. Avelino da Silva, A. A. Badin, E. F. R. Romaneli and R. Gules. (2018). "Soft-Switching High Static Gain DC-DC Converter Without Auxiliary Switches," in *IEEE Transactions on Industrial Electronics*, vol. 65, no. 3, pp. 2335-2345, doi: 10.1109/TIE.2017.2739684.

M. Nour, G. Magdy, J. P. Chaves-Ávila, Á. Sánchez-Miralles and E. Petlenkov. (2022). "Automatic Generation Control of a Future Multisource Power System Considering High Renewables Penetration and Electric Vehicles: Egyptian Power System in 2035," in *IEEE Access*, vol. 10, pp. 51662-51681, doi: 10.1109/ACCESS.2022.3174080.

Özçelik, M. A. (2017). The Design and Implementation of PV -Based Intelligent Distributed Sensor LED Lighting in Daylight Exposed Room Environment. *Sustainable Computing: Informatics and Systems*, 13, 61-69.

Özçelik, M. A. (2018). The Design and Comparison of Central and Distributed Light Sensored Smart LED Lighting Systems. *International Journal of Photoenergy*, 2018, 1-14.

Özçelik, M. A., Utma, A., & Yilmaz, A. S. (2019). Micro PV Wind Hybrid Based Smart Energy Management System. *The International Journal of Materials and Engineering Technology*, 2(2), 54-59.

S. A. Q. Mohammed and J. -W. Jung. (2021). "A State-of-the-Art Review on Soft-Switching Techniques for DC-DC, DC-AC, AC-DC, and AC-AC Power Converters," in *IEEE Transactions on Industrial Informatics*, vol. 17, no. 10, pp. 6569-6582, doi: 10.1109/TII.2021.3058218.

S. -Y. Chan, T. -H. Yang and Y. -N. Chang. (2016). "Design of Electronic Ballast for Short-Arc Xenon Lamp With Interleaved Half-Wave Rectifier," in *IEEE Transactions on Power Electronics*, vol. 31, no. 7, pp. 5102-5112, doi: 10.1109/TPEL.2015.2480860.

X. Chen, Q. Xie, X. Bian and B. Shen .(2022). "Energy-saving superconducting magnetic energy storage (SMES) based interline DC dynamic voltage restorer," in *CSEE Journal of Power and Energy Systems*, vol. 8, no. 1, pp. 238-248, doi: 10.17775/CSEEJPES.2020.05440.

**EXPERIMENTAL INVESTIGATION OF SINGLE PHASE UNCONTROLLED
RECTIFIERS**

W. Kawamura, Y. Chiba, M. Hagiwara and H. Akagi. (2017). "Experimental Verification of an Electrical Drive Fed by a Modular Multilevel TSBC Converter When the Motor Frequency Gets Closer or Equal to the Supply Frequency," in *IEEE Transactions on Industry Applications*, vol. 53, no. 3, pp. 2297-2306, doi: 10.1109/TIA.2017.2665635.

Y. S. Kumar and G. Poddar.(2017). "Control of Medium-Voltage AC Motor Drive for Wide Speed Range Using Modular Multilevel Converter," in *IEEE Transactions on Industrial Electronics*, vol. 64, no. 4, pp. 2742-2749, doi: 10.1109/TIE.2016.2631118.

Yılmaz, M. (2016). Effect of Smart Grid on Electrical Distribution System Design. *European Journal of Technique*, 0-0.

Zhenxue Xu, Bo Zhang and A. Q. Huang. (2000). "An analysis and experimental approach to MOS controlled diodes behavior," in *IEEE Transactions on Power Electronics*, vol. 15, no. 5, pp. 916-922, doi: 10.1109/63.867681.

RADIATION SHIELDING PROPERTIES OF REINFORCED (BaSO₄ AND SiC) AZ91 MATERIALS

Gizem YALÇIN¹, Zübeyde ÖZKAN¹, Uğur GÖKMEN², Sema Bilge OCAK¹

Abstract: Today, ionizing radiation; is used in the diagnosis and treatment of diseases, in agriculture, for electricity generation in nuclear power plants, in the defense industry, etc. used in many fields. In addition to the benefits of radiation, it has many harmful effects on the environment and people. These include the storage of radioactive residues used and the spread of radiation to the environment as a result of attacks that may occur in nuclear power plants. For these reasons, radiation shielding has become increasingly important today. This study, it is the research of a shielding material that is compatible with the environment, which will be an alternative to the materials that are actively used today. For this reason, due to many reasons such as not wasting materials on the day, and providing convenience in the production of complex materials, the production of materials whose radiation properties will be theoretically investigated in the study was carried out using the powder metallurgy method. To determine the dust size distribution, which is one of the most important parameters in powder metallurgy, dust size analyses of the powders to be used in the Mastersizer 3000 device were performed. The radiation shielding properties of composite/hybrid materials reinforced with SiC and BaSO₄ at different rates (5-10-15%) were investigated with the Phy-x/ PSD program. It is aimed to reveal the absorption and scattering that occurs in the materi-

¹ Gazi University, Graduate School of Natural and Applied Sciences, Department of Advanced Technologies, 06500 Ankara / Türkiye, e-mail: sbocak@gazi.edu.tr

² Gazi University, Faculty of Technology, Department of Metallurgical and Materials Engineering, 06500 Ankara / Türkiye

als to be analyzed by running the program in the lower and upper energy levels of the program, 0,015 MeV and 15 MeV, respectively. Mean free path (MFP), linear attenuation coefficient (LAC), half value layer (HVL), mass attenuation coefficient (MAC), effective atomic number (Z_{eff}), tenth valuable layer (TVL), electron density (N_{eff}), effective conductivity (C_{eff}), fast neutron removal cross-sections values (FNRC), atomic cross-section (ACS) and the electronic cross section (ECS) parameters were investigated. The reinforcement materials added to the AZ91 matrix material increased the LAC value of the AZ91 matrix. The highest increase was realized in 15% BaSO₄ reinforced composite material. The material with the highest FNRC value was AZ91 with 5.932 cm⁻¹, while the highest FNRC value was AZ91+15% BaSO₄ composite material with 6.909 cm⁻¹. Among the materials analyzed, the most suitable material for both gamma and neutron shielding was Az91+15% BaSO₄ composite material.

Keywords: Magnesium Alloy, Gama Shielding, BaSO₄, Composite, Barium Sulfate, Silicon Carbide

INTRODUCTION

Radiation is defined as energy that can move through matter or space and has advantages and disadvantages. There are many disadvantages of nuclear application however, it is played an important role in recently some field such as medicine, agriculture and research and development studies. This application will be the essence of science in the next years. These applications can be hazardous to human health. Especially the use of gamma rays and neutron sources should be used with caution. Because of this, the shielding of gamma and neutron sources is more important for human health. There are three factors for the penetration degrees of gamma and neutron radiations; duration time, distance, and shielding (Gökmen et al., 2021)

The research on gamma radiation and its absorption is important due to use of gamma rays in medicine, industry, and agriculture which directly affect human health. Radiation shielding is simply a barrier pla-

ced between a radiation source and the person or area to be protected. The purpose of protection from radiation effects is to limit and control the rate of radiation exposure at the set point. The purpose of this radiation protection strategy is to cut down on time spent near the source of radiation. Radiation exposure has an exact proportional temporal relationship, which means that as the worker's exposure length grows, so does the amount of radiation he or she receives (Sayyed et al., 2018). Researchers have been extensively investigating the shielding factor recently. Radiation shielding is help to reduce the intensity of the incoming proton. That's why the materials which shield from radiation is interacted with radiation and reduce the radiation energy.

Many parameters are very important for calculating shielding effectiveness; MAC (mass energy absorption coefficient), Z_{eff} (effective atomic number), N_{eff} (density of electron), MFP (mean free path), TVL (tenth value layer) and HVL (half value layer). The researcher who studies in the shielding field used these parameters for understanding their physical properties on their effectiveness. The calculation of these parameters is required for shielding materials' behavior. MAC has known the mass energy absorption coefficient in the literature. It is the ratio of the first photon energy transferred to the material through ionization and excitation. The mean free path that is shown in MFP is mean the average distance that a particle moves between two successive collisions with other particles. The buildup factor is an important parameter in the calculation of a radiation shielding system. It can be observed that EBF and EABF parameters change significantly with photon energy and penetration depth. The half-value layers (HVL) and tenth-value layers (TVL) are known as the thickness of a shield that reduces the radiation level by half and one-tenth of the first level, respectively (Turan, 2018; Nagaraja et al. 2020). Some radiation shielding materials used commonly are lead bricks, and high-density concrete, and materials that included metals such as copper, steel, and tungsten as well as composites and alloys are used as a subject of research recently (Gökmen et al., 2021; Chilton et al.,

1984; Kurt, 2017). Neutrons are uncharged particles that can interact by various mechanisms with a medium such as a neutron capture, nuclear spallation, nuclear fission, and inelastic and elastic scattering. Fast neutron removal cross-section (FNRC) is a useful parameter for measuring any sample's ability for neutron attenuation.

The manufacturing of composite materials is very common recently. Especially metal matrix composite (MMC) materials are widely used in aerospace, marine, automotive and military industries expressing physical and mechanical properties such as low cost, low expansion coefficient, excellent dimensional stability, high corrosion resistance, high strength, and high hardness. One of the widely used composite materials is aluminum matrix composite (AMC). Commonly used techniques in the production of MMC materials are powder metallurgy, melt impregnation, pressure casting, mixing casting, ball milling, mechanical alloying, and semi-solid mixing. In these methods, the metallurgy method is preferred because of the simplicity of the process, low cost, and high mechanical properties. Types of research have been carried out on the production of MMCs for reinforcing materials such as Al₂O₃, TiC, MgO, and SiC and continue to do so (Srivinaset al., 2022). AZ91 is one of the matrix materials which has high purity alloy, super corrosion resistance, and good strength for MMC production. It is an element which is one of the Mg family. It is used commonly among cast magnesium alloy. The magnesium alloy AZ91 has main composition 9% aluminum, 1% zinc, and 0,3 manganese. The characteristics such as high strength-to-weight ratio, thermal conductivity, good machinability, high damping, easy recyclability, high specific strength, and good vibration absorption lead to the usage of Mg alloys in computer parts, household equipment, and implants, automotive and aerospace industries and biomaterials. Srinivas et al. studied AZ91 magnesium alloy. He has investigated these mechanical properties and he has obtained them by using die casting (Srivinaset al., 2022). Sriwognsa et al. researched the total and partial interaction, radiation shielding, and buildup factors properties of AM60 and AZ91

alloys. In conclusion, the AZ91 was found excellent radiation shielding and can be developed as a radiation shielding medium (Sriwongsa et al., 2021). Soy is studied in his thesis, pressure infiltration technique was used for the production of aluminum metal matrix composites. For this purpose, AlSi10Mg aluminum casting alloy was infiltrated into the open pore SiC, B₄C, and SiC/B₄C ceramic foams by using the pressure die casting method. An increase in the pore frequency of reinforcement has increased the tensile strength, bending strength, and elastic modulus of composites. In wear tests, as the sliding distance increases wear loss and friction coefficient have increased for both composite and unreinforced matrix alloy.

Thermal expansion and coefficient of thermal expansion values of composite have decreased for particle-reinforced composites by comparison of un-reinforced matrix alloy (Soy, 2009). In recent years, powder metal parts were more important than others because of their excellent properties. They are performed in many types of particle reinforced composites which are used in several applications. SiC is used commonly material in powder metallurgy manufacturing. Almisned is also studied on radiation shielding properties and they were used their study the composited where SiC and TiC added, were produced and radiation shielding performance was investigated. They were determined the best shielding performance using LAC, and MAC values. In this study composites where SiC and TiC were added, were produced and radiation shielding performance was investigated. The produced composites were formulated as (95-x) Al-5SiC-xTiC where x = 0, 5,10,15,20 (wt%). The results show that by increasing the TiC rate on the composite from S-0 to S-20, the ascending trend is observed for the linear attenuation coefficient (LAC, cm⁻¹) of the studied composites, and the best shielding performance is seen for S-20 (Almisned, 2022). Abdlhamed studied the radiation-shielding properties of composite materials. He was testing gamma-rays as the main goal of his thesis and composite materials used in this thesis were tested against gamma rays from Co(60) and Cs(137) sources at Su-

leyman Demirel University (Abdlhamed, 2018). Emikönel studied an investigation of radiation shielding properties in different areas which is fabric industries. She investigated the protective clothing against radiation to protect from radiation and she determined the radiation absorption characteristics of barite (BaSO₄) coated fabrics in different proportions (Emikönel, 2015). Akkaş is studied the same field which is the suggestion of a new hybrid composite radiation shielding material. Experimental works were performed on aluminum-boron carbide (Al-B₄C). The material in question contained B₄C compound in four different volume ratios (5%, 10%, 15%, 20%) and in five different particle sizes (average 3 µm, average 53µm, 75 to 150 µm, 150 to 250 µm, average 500 µm). The thesis arrives at the original finding that the results of the experiments performed for this study indicate that hybrid composite materials produced by adding WC by 5% to 10% in Al-B₄C composite material can be used as an efficient shielding material against fields of mixed radiations (Akkaş, 2015). Aydın is investigated the mechanical and corrosion properties of magnesium matrix composites with different reinforcements by powder metallurgy method. Productions were performed at 600 °C and 525 °C with 45 MPa under argon atmosphere for Mg and AZ91 matrix composites, respectively. The density, hardness, and microstructure analyzes were realized. After the microstructure characterization, homogeneous distribution of particles was seen. However, agglomeration of particles was seen with 30% reinforcement. After the measurements, porosity, hardness and wear resistance increased with increasing reinforcement content.

Generally, compression strength was increased up to 20 wt. % reinforcement. After the potentiodynamic and immersion tests, it is generally seen that the corrosion resistance of the samples was negatively affected by increasing reinforcement content (Aydın, 2018). Çavuşoğlu studied the production of B₄C particle reinforced AZ91 matrix alloy composites by using the stir casting method; and investigated mechanical properties of produced composites and mechanical properties with varying volume

fractions of B_4C reinforcement and The microstructural, chemical, and mechanical properties of composites were investigated. It was found from the experimental studies that as-produced samples presented relatively uniform particle distribution and relatively higher particle addition yields, mainly due to the formation of a Mn-C rich in-situ reaction layer on the matrix/reinforcement interface. Furthermore, an increase in particle volume fraction leads to an increase in hardness in Mg- B_4C composites. On the other hand, no significant differences were found in the compressive strength values between the unreinforced alloy and the 5% B_4C reinforced composites (Çavuşoğlu, 2013).

The aim of our study theoretically investigates the shielding properties of SiC and $BaSO_4$ particles reinforced AZ91 matrix composite materials in different compositions, 5% by weight, 10% by weight, and 15% by weight, using PSD software. These samples will be produced using many parameters such as TVL, HVL, MAC, and MFP calculated regarding the shielding properties used in space, industry, nuclear power plants, etc. It has been tried to determine the suitability for the areas.

MATERIAL and COMPUTATIONAL METHOD

Materials and Preparation of Shielding Materials

The AZ91 is the matrix material which is given the chemical composition in Table 1. It was used as matrix material and $BaSO_4$ and SiC powder were used as reinforcement material during the manufacturing of functionally graded composite materials. The size distribution of ceramic matrix powders is given in Figure 1-2, the D (50) value of the SiC ceramic material is 11 μm , the D (50) value of the $BaSO_4$ ceramic material is 3.85 μm . The reinforcement and matrix ratios in the composite/hybrid samples to be produced are given in Table 2.

**RADIATION SHIELDING PROPERTIES OF REINFORCED (BaSO₄ AND SiC)
AZ91 MATERIALS**

Table 1. Chemical Composition of AZ91

Element	Al	Mn	Zn	Si	Cu	Fe	Ni	Ot- hers	Mg
(%)	8.3- 9.7	0.15- 0.5	0.35- 1	0.1	0.0 3	0.00 5	0.00 2	0.02	Rema- inder

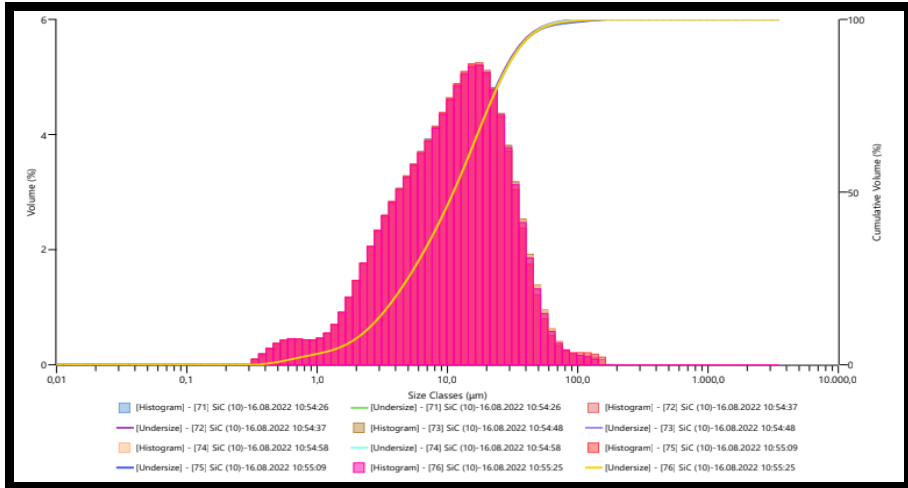


Figure 1. Grain Size of SiC

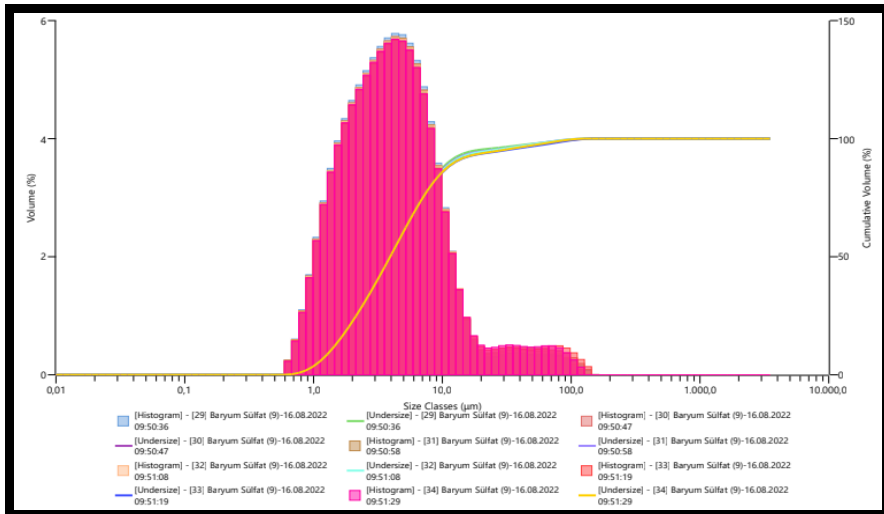


Figure 2. Grain Size of BaSO₄

The hybrid composite samples were produced by using the hot press method at X pressure at Y temperature by mixing the ratios given in Table 1 with a 3D mixer (Figure 3).

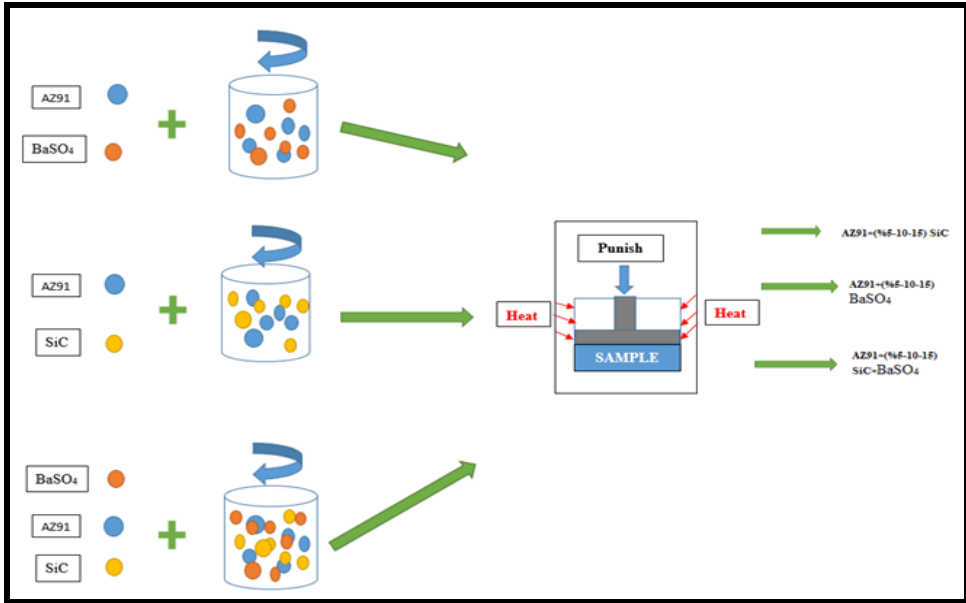


Figure 3. Production Scheme of SiC, BaSO₄ and SiC+BaSO₄ Composite/Hybrid Materials Reinforced into AZ91 at Different Rates (5%-10%-15%)

Table 2. Compositions And Theoretical Densities Of Composite/Hybrid Materials

SAMPLE ID	COMPOSITION	THEORIC DENSITY (g/cm ³)
A1	%100AZ91	1.81
A2	%95 AZ91+ %5 SiC	1.88
A3	%90 AZ91+ %10 SiC	1.95
A4	%85 AZ91+ %15 SiC	2.02
A5	%95 AZ91+ %5 BaSO ₄	1.944
A6	%90 AZ91+ %10 BaSO ₄	2.078
A7	%85 AZ91+ %15 BaSO ₄	2.212
A8	%95 AZ91+ %2,5SiC+%2,5 BaSO ₄	1.912

A9	%90 AZ91+ %5 SiC+%5 BaSO ₄	2.014
A10	%85 AZ91+ %7,5 SiC+%7,5 BaSO ₄	2.116

Linear-Mass Attenuation Coefficient

Many parameters are important for calculating shielding properties. The Beer- Lamber law is used to calculate the MAC and describe the below Equation 1 (Jalali and Mohammadi, 2008).

This law defined the between the concentration and the absorbance of the solution:

$$I = I_0 e^{-\mu x} \quad (1)$$

The x in equation 1 is the thickness of the material, μ is the LAC of the matter for radiation, I_0 presents the radiation intensity from the material, and I is represented in this equation the intensity of radiation passing through the material. The LAC is known that quantifies how much the weakened by the material it is passing through. The MAC is known as the mass attenuation coefficient which is the attenuation per unit mass. It is described as a mass of material that can be penetrated by energy or matter. The SI unit of MAC is the m²/kg. The material's MAC value is calculated in the Equation as follows:

$$\mu_m = \sum_{n=i} w_i \left(\frac{\mu}{\rho} \right) \quad (2)$$

In Equation 2, μ is denoted the LAC and depends on the incoming gamma-ray energy and ρ denotes the density of the material and w_i denotes for the weight fraction.

Mean Free Path, Half-Tenth Value Layer

The mean free path abbreviated MFP is the average distance traveled by a moving something such as an atom, unit, or photon before it changed its energy or direction. On the other hand, it is more successive collisions result. The half-value layers (HVL) and tenth-value layers (TVL)

are known as the thickness of a shield that reduces the radiation level by half and one-tenth of the first level, respectively. Their meanings are the thickness of a shielding material that reduces the radiation effect by one-half and one-tenth of the first level, respectively. The TVL value refers to the material thickness required to reduce the radiation intensity to 10% (Jalali and Mohammadi, 2008). The TVL, HVL, and MFP values are calculated in Equations 3-5.

$$\text{HVL} = \frac{\ln 2}{\mu} \quad (3)$$

$$\text{TVL} = \frac{\ln 10}{\mu} \quad (4)$$

$$\text{MFP} = \frac{1}{\mu} \quad (5)$$

Effective Atomic Number, Electron Density, And Effective Conductivity

Z_{eff} , which is as important a parameter as the others. The Z_{eff} value, which is also considered as the atomic number of the elements, defines the material composition and changes with the energy of the material (El-Sayed et al., 2003; Gerward et al, 2004; Harima 1993; Şakara et al., 2020). Its value is calculated the Equation (6):

$$Z_{\text{eff}} = \frac{\sigma_a}{\sigma_e} \quad (6)$$

In this equation (6), σ_a and σ_e values are the total atomic cross-section and the electronic cross-section, respectively. Their unit is cm^2g^{-1} . Afterward, they are calculated according to Equation (7) and Equation (8) (Şakara et al., 2020; Chiltan et al. 1984; Kaplan 1989).

$$\sigma_a = \frac{\mu_m}{[N_A \sum_i w_i A_i]} \quad (7)$$

$$\sigma_e = \frac{1}{N_A} \left[\sum_i \frac{f_i A_i (\mu_m)}{Z_i} \right] \quad (8)$$

Z_i is described as the atomic number of the i th element which is a specific number and in the composition of the material and then A_i is the meaning of the i th element and f_i is the atom number of the i th element reference to the total atom number in the composition. N_A is known the Avogadro's number (El-Sayed et al., 2003; Gerward et al., 2004; Harima 1993; Şakara et al., 2020). The electron density is calculated in the following Equation (9):

$$N_{\text{eff}} = \frac{N_A}{N} Z_{\text{eff}} \sum_i n_i \quad (9)$$

In Equation (9) the n_i is showed the electron number of each material in the composition. The C_{eff} is calculated (Equation 10) as follows:

$$C_{\text{eff}} = \left(\frac{N_{\text{eff}} \tau \epsilon^2 \rho}{\mu_e} \right) \times 10^3 \quad (10)$$

The ϵ is the electron's charge, μ_e is the electron's mass and τ is the electron's mean relaxation duration on the Fermi surface.

Fast Neutron Removal Cross-Section

Studies on neutron shielding are essential because of this indirect ionizing radiation behavior. The fast neutron removal cross-section (FNRCs) parameter, which is commonly used to compute the potentiality, is defined using the following Equation 11:

$$\Sigma_R = \sum_i \rho_i (\Sigma_R/\rho)_i \quad (11)$$

RESULTS

LAC-MAC

The LAC values of SiC and BaSO₄ and SiC+BaSO₄ composite/hybrid materials reinforced in AZ91 at different rates (5%-10%-15%) decrease depending on the energy increase of gamma radiation (Figure 4). The most important parameters in radiation shielding are the atomic number and density values of the shielding material. Since SiC (Si: 14 C:6) and BaSO₄ (Ba:56 S:16 O: 8) materials have different atomic numbers, their

transmittance values against radiation also differ. The LAC values of the analyzed samples decreased rapidly up to 0.02 MeV. In the 0.511 MeV<E<1.02 MeV energy range where Compton scattering occurs, the rate of decrease in LAC values decreased. Samples coded 0.081 MeV (133Ba) A1-A10 are respectively 36,157 cm⁻¹ - 37,578 cm⁻¹ - 39,00 cm⁻¹ - 40,425 cm⁻¹- 59.607 cm⁻¹- 85.922 cm⁻¹- 115,100 cm⁻¹. They took the values of 48,422 cm⁻¹ -61.778 cm⁻¹ -76,225 cm⁻¹. In the energy region of Compton scattering, the decrease in LAC values was less than that in the MAC region, since gamma radiation interacts with the atomic number of the material at the rate of Z².

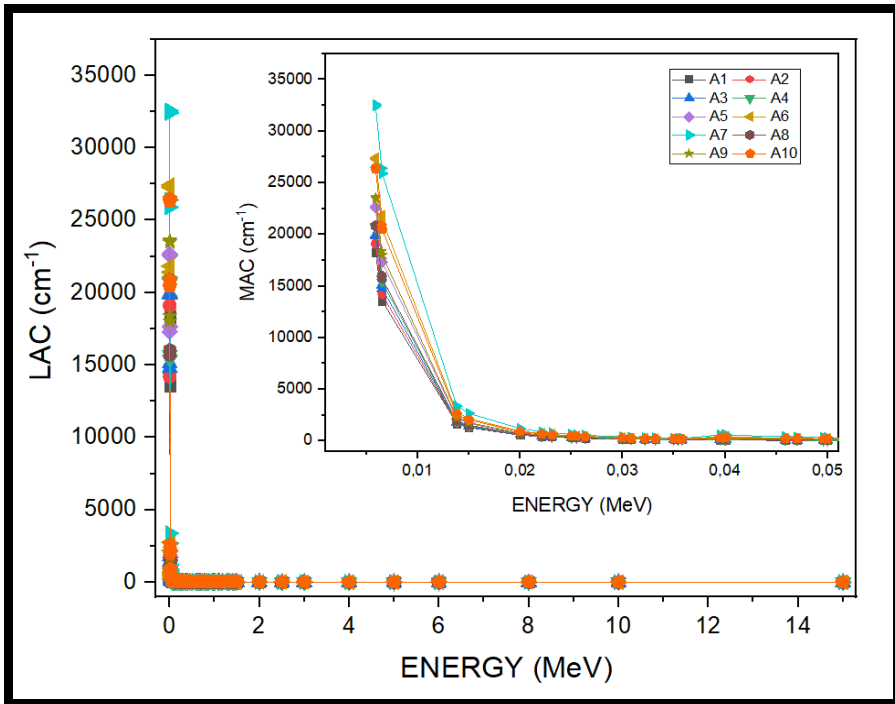


Figure 4. LAC Values of SiC and BaSO₄ Reinforced AZ91 Composite/Hybrid Material

In Figure 5, the MAC values of SiC and BaSO₄ and SiC+BaSO₄ composite/hybrid materials reinforced in AZ91 at different rates (5%-10%-15%) in the energy range of 0.015MeV-15 MeV are given. When the graph is examined, it is seen that the gamma radiation permeability va-

MAC values increase thanks to the reinforcement elements added into the AZ91 material. It is seen that the MAC values of the material increase at 15% reinforcement rates. While the highest increase was experienced with the addition of BaSO₄ ceramic, the least increase was experienced with the addition of SiC ceramic material. The main reason for this is that SiC (3.21 g/cm³) and BaSO₄ (4.49 g/cm³) ceramic powders added to AZ91 have different atomic numbers and density values. When the graph is examined, rapid decreases in MAC values have occurred due to the interaction of the photoelectric effective cross-section with the atomic number of the shielding material at a Z⁴ ratio in the energy region where the photoelectric effect (E<0.512MeV) occurs. 0,0221 MeV (⁴⁷Ag) in A1-A10 with the sequence of samples 238,637 cm²/g- 238,996 cm²/g- 239,356 cm²/g- 239,716 cm²/g- 297,094 cm²/g- 355,552 cm²/g- 414,010 cm²/g- 268,045 cm²/g-326,863 cm²/g values. In the energy region where Compton scattering occurs, the rate of decrease in the MAC values of the material becomes more linear. When the energy of gamma radiation reaches 3 MeV, the MAC values become more stable.

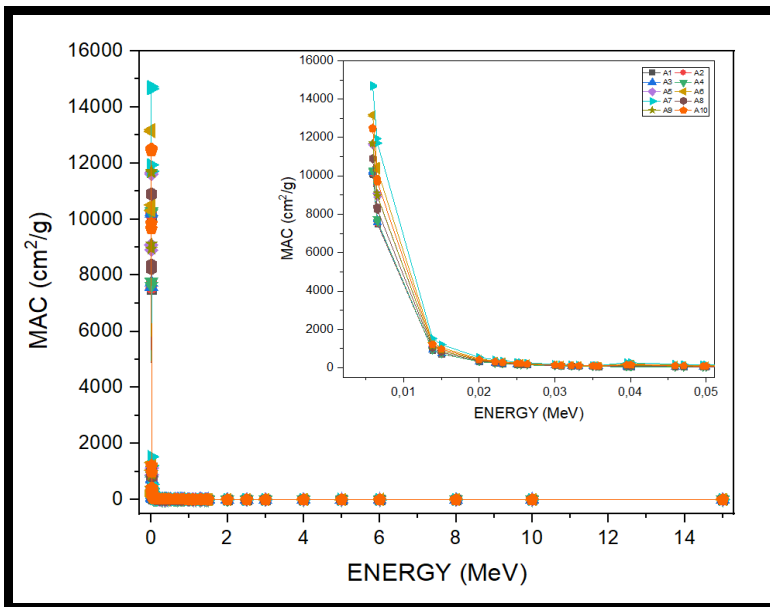


Figure 5. MAC Values of SiC and BaSO₄ Reinforced AZ91 Composite/Hybrid Material

3.2. MFP-HVL-TVL

When HVL (Figure 6) in the energy range of 0.015MeV-15 MeV of SiC and BaSO₄ and SiC+BaSO₄ composite/hybrid materials reinforced in AZ91 at different rates (5%-10%-15%) is examined, it is necessary to stop the gamma radiation of the material depending on the increasing energy. It is seen that the thickness of the material is increased. The AZ91 material, which has the lowest gamma shielding property, varies between 0.000 cm and 0.175 cm in the thickness required to reduce the intensity of the incident radiation to 1/2. The A7-coded AZ91+15% BaSO₄ material, which has the best gamma radiation transmittance value, takes values ranging from 0.000 cm to 0.132 cm. As indicated in Figure 2, materials with A1-A10 codes HVL values at 0.005888 MeV radiation energy AZ91 < AZ91+5% SiC < AZ91+10% SiC < AZ91+15% SiC < AZ91+5% BaSO₄ < AZ91+10% BaSO₄ < AZ91+15% BaSO₄ they take values as.

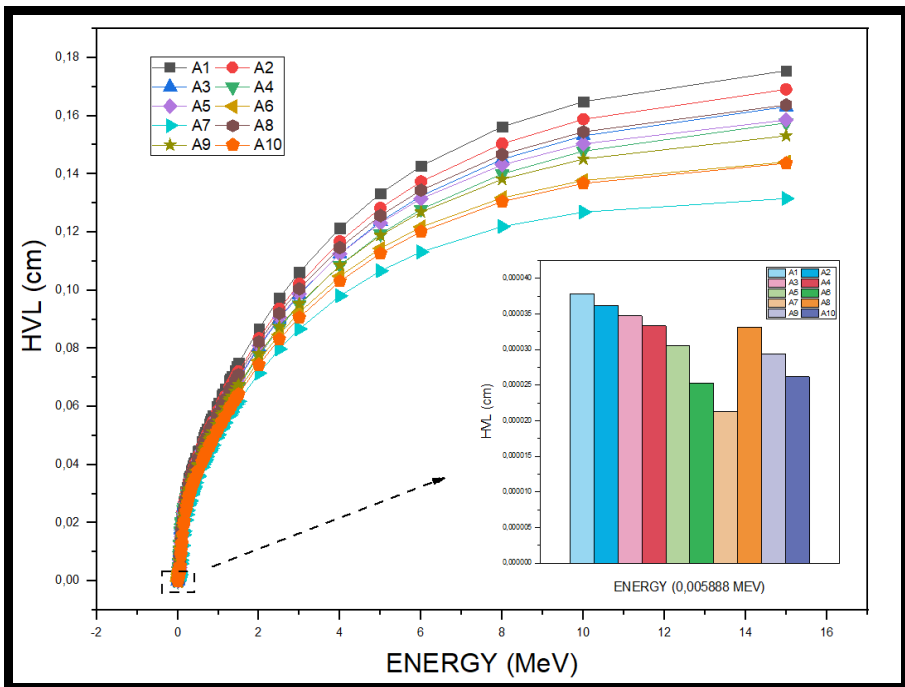


Figure 6. HVL Values of SiC and BaSO₄ Reinforced AZ91 Composite/Hybrid Material

**RADIATION SHIELDING PROPERTIES OF REINFORCED ($BaSO_4$ AND SiC)
AZ91 MATERIALS**

TVL value, which shows the material thickness required for the incoming radiation energy to decrease to 1/10 in the energy range of 0.015MeV-15 MeV, SiC and $BaSO_4$ and $SiC+BaSO_4$ composite / hybrid materials reinforced into AZ91 at different rates (5%-10%-15%) shown in Figure 7 Among the SiC and $BaSO_4$ and $SiC+BaSO_4$ reinforcement elements added to AZ91, the highest TVL values are seen in SiC -reinforced composites, while the lowest TVL values are seen in $BaSO_4$ reinforced composite materials. Materials with a 15% reinforcement ratio within each reinforcement group had the lowest TVL values. In the transition from the low energy region where the photoelectric effect occurs to the middle energy region where Compton scattering occurs, rapid increases in the TVL values of the material occurred. At 0.8261 MeV (^{60}Co) where Compton scattering predominantly occurs, the A1-A10 coded samples are 0.185cm- 0.178cm- 0.171cm- 0.165cm- 0.172cm- 0.161cm- 0.152cm- 0.175cm- 0.166cm- 0.158cm, respectively takes values. 2.51 MeV (^{60}Co) energy and energy occur as dominant for the formation of another pair in A1-A10 coded in the sequence of samples with 0,323cm - 0,311 cm - 0,299 cm - 0,289 cm - 0,301 cm-0,282 cm-0,265 cm-0,306 cm-0,290 cm- 0,276 cm values.

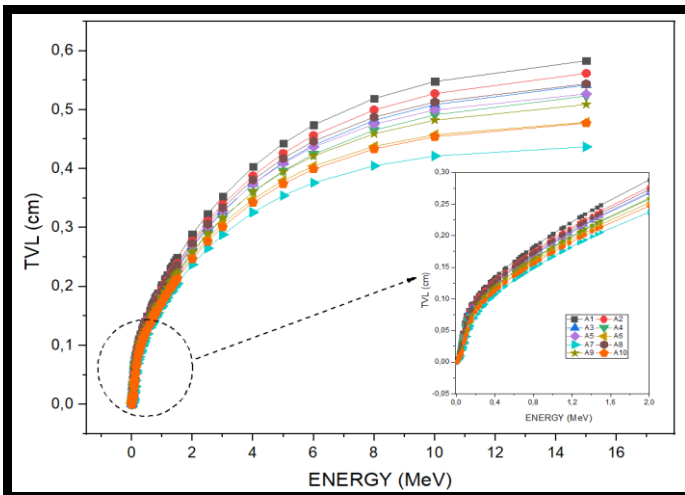


Figure 7. TVL Values of SiC and $BaSO_4$ Reinforced AZ91 Composite/Hybrid Material

The material thickness required for two consecutive interactions with a photon of SiC and BaSO₄ and SiC+BaSO₄ composite/hybrid materials reinforced in AZ91 encoded as A1-A10 at different rates (5%-10%-15%) is 0.015MeV in Figure 8. It is given for the energy range of -15 MeV. MFP values of hybrid/composite materials encoded with names A1-A10 are respectively 0.000-0.253cm/ 0.000-0.244cm/ 0.000-0.235cm/ 0.000-0.227cm/ 0.000-0.229cm/ 0.000-0.208cm/ 0.000-0.1190cm/ 0.000. They take values varying between-0.236cm/ 0.000-0.221cm/ 0.000-0.207cm. The lower the MFP value of a material, the better the radiation transmittance value of the material. The behavior of AZ91 reinforced composite/hybrid materials against photons is shown in Figures 6-7 and 8, where they are parallel in MFP, HVL, and TVL graphs. The MFP, HVL, and TVL values of a material vary depending on the atomic number and density of the material.

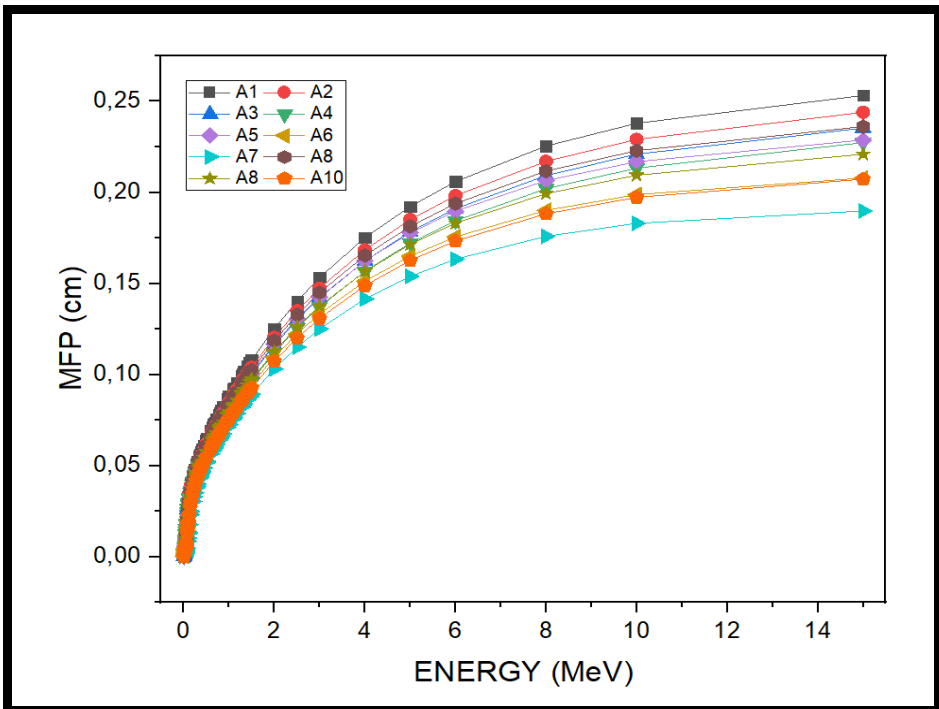


Figure 8. MFP Values of SiC and BaSO₄ Reinforced AZ91 Composite/Hybrid Material

Z_{eff}

Since composite/hybrid materials contain more than one element, it is impossible to express them with a single atomic number. For this reason, we use Z_{eff} to understand the average atomic numbers of composite/hybrid samples and their interactions with the photon. Atomic cross-sections of SiC and BaSO₄ and SiC+BaSO₄ composite/hybrid materials reinforced into AZ91 at different rates (5%-10%-15%) are shown in Figure 10. The material with the highest ACS value among composite/hybrid materials is the A7-coded sample. The reason for this is that the MAC value of the A7 coded sample is also at the highest value. A1-A10 coded samples at 0.005888 MeV energy are respectively 4.16E-21 cm²/g, 4.13E-21 cm²/g, 4.10E-21 cm²/g, 4.08E-21 cm²/g, 4.07E-21 cm²/g, 5.62E-21 cm²/g, 6.39E-21 cm²/g, 4.50E-21 cm²/g, 4.84E-21 cm²/g, 5.18 E-21cm²/g they take values.

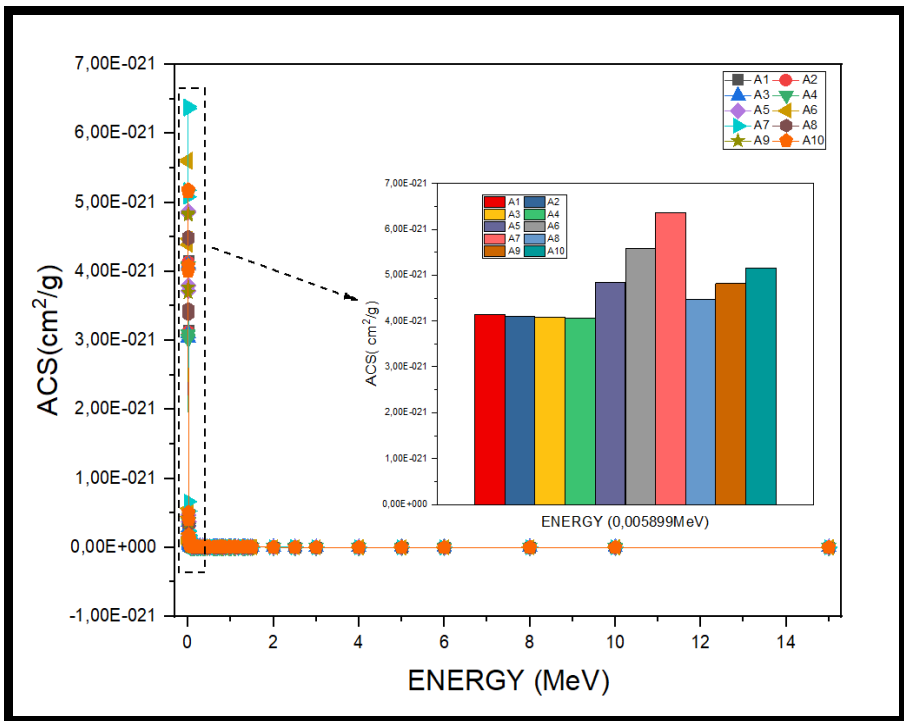


Figure 9. ACS Values of SiC and BaSO₄ Reinforced AZ91 Composite/Hybrid Material

It shows the total electric section of SiC and BaSO₄ and SiC+BaSO₄ composite/hybrid materials reinforced into AZ91 at different rates (5%-10%-15%) in the 0.015MeV-15 MeV energy range. While the ACS values of AZ91+(5-10-15%) SiC composite materials at 0.005899 MeV in the ACS graph (Figure 9) are very close to each other, in the ECS graph (Figure 10), which shows the total cross-section, the density values of the atomic number of the material are also included in the difference between the values due to its influence. The ECS values of the material decrease at increasing photon energies. The ECS values of SiC and BaSO₄ and SiC+BaSO₄ composite/hybrid materials reinforced in AZ91 at different rates (5%-10%-15%) became more stable after 4 MeV energy.

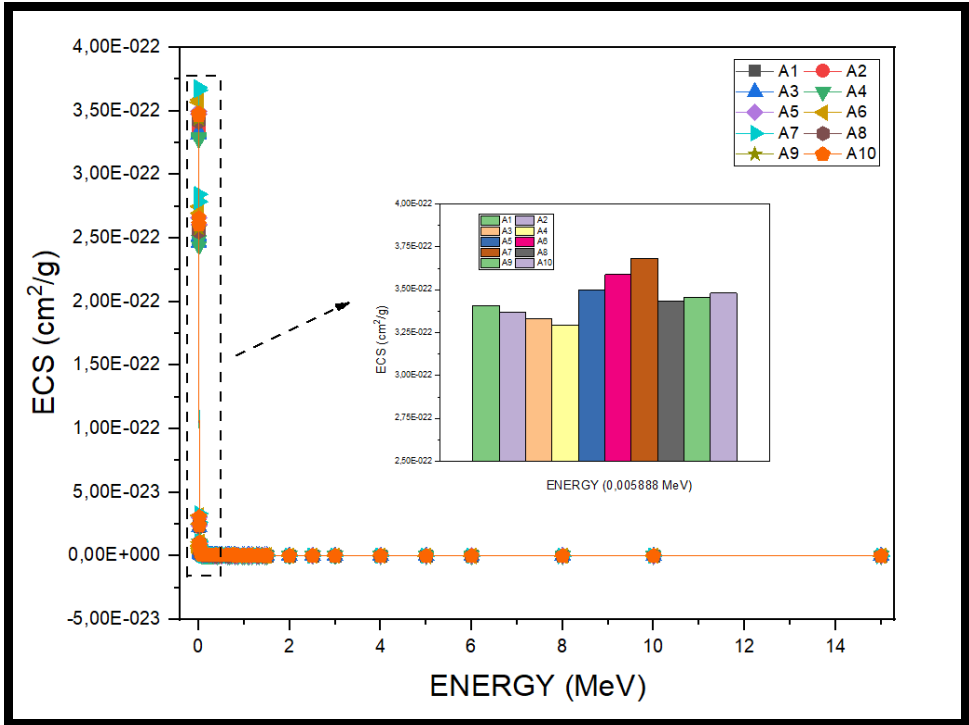


Figure 10. ECS Values of SiC and BaSO₄ Reinforced AZ91 Composite/Hybrid Material

It shows the total electric section of SiC and BaSO₄ and SiC+BaSO₄ composite/hybrid materials reinforced into AZ91 at different rates (5%-10%-15%) in the 0.015MeV-15 MeV energy range. While the ACS values

of AZ91+(5-10-15%) SiC composite materials at 0.005899 MeV in the ACS graph (Figure 10) are very close to each other, in the ECS graph (Figure 10), which shows the total cross-section, the density values of the atomic number of the material are also included in the difference between the values due to its influence. The ECS values of the material decrease at increasing photon energies. The ECS values of SiC and BaSO₄ and SiC+BaSO₄ composite/hybrid materials reinforced in AZ91 at different rates (5%-10%-15%) became more stable after 4 MeV energy.

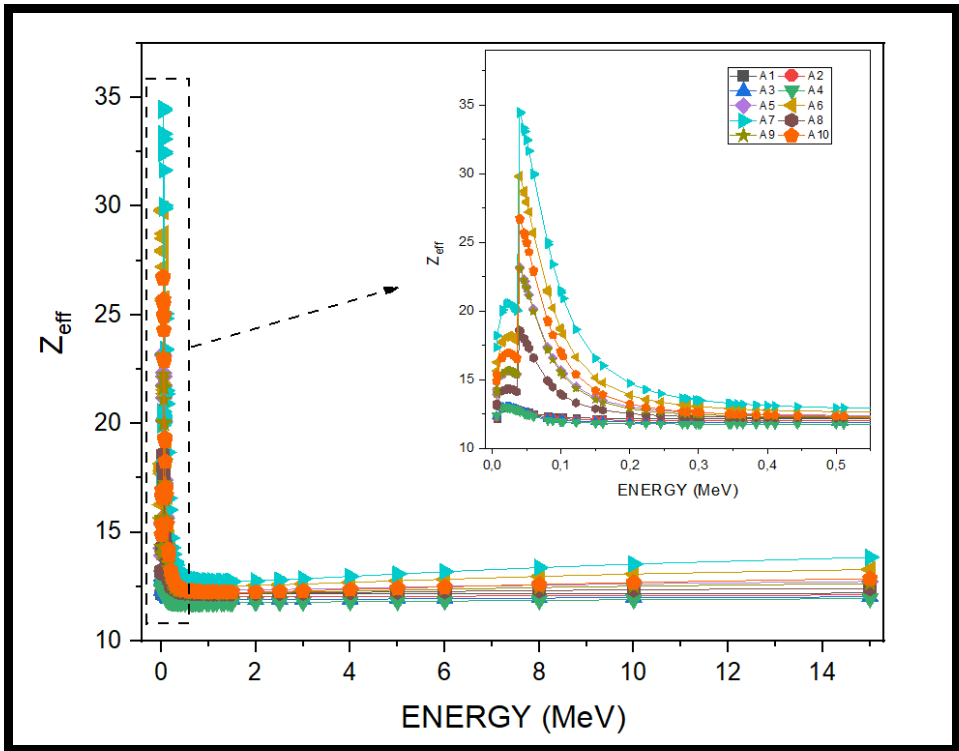


Figure 11. Z_{eff} Values of SiC and BaSO₄ Reinforced AZ91 Composite/Hybrid Material
 N_{eff}

The N_{eff} value, which is closely related to the Z_{eff} value, is about the electron density of SiC and BaSO₄ and SiC+BaSO₄ composite/hybrid materials reinforced into AZ91 at different rates (5-10%-15%) in the 0.015MeV-15 MeV energy range (Figure 12) provides information. In the

photoelectric effect, the electron that was released as a result of electron detachment at low energy levels of the atoms of the composite/hybrid samples increased the electron density of the material, while it remained constant due to the absence of any change in electrons during Compton scattering. In the energy region where pair formation is dominant, slight increases were observed due to the formation of positron and electron pairs. 1,50 E-02 MeV energy in A1-A10-coded in the sequence of samples with the 3,15 E+25 electron/g / -3,20 E+25 electron/g - 3,24 E+25 electron/g - 3,28 E+25 electron/g - 3,70 E+25 electron/g - 4,19 E+25 electron/g - 4,63 E+25 electron/g - 3,46 E+25 electron/g - 3,75 E+25 electron/g - 4,03 E+25 electron/g values they take. Thanks to the high atomic number of BaSO₄ ceramic material, the atomic number per mass has also increased.

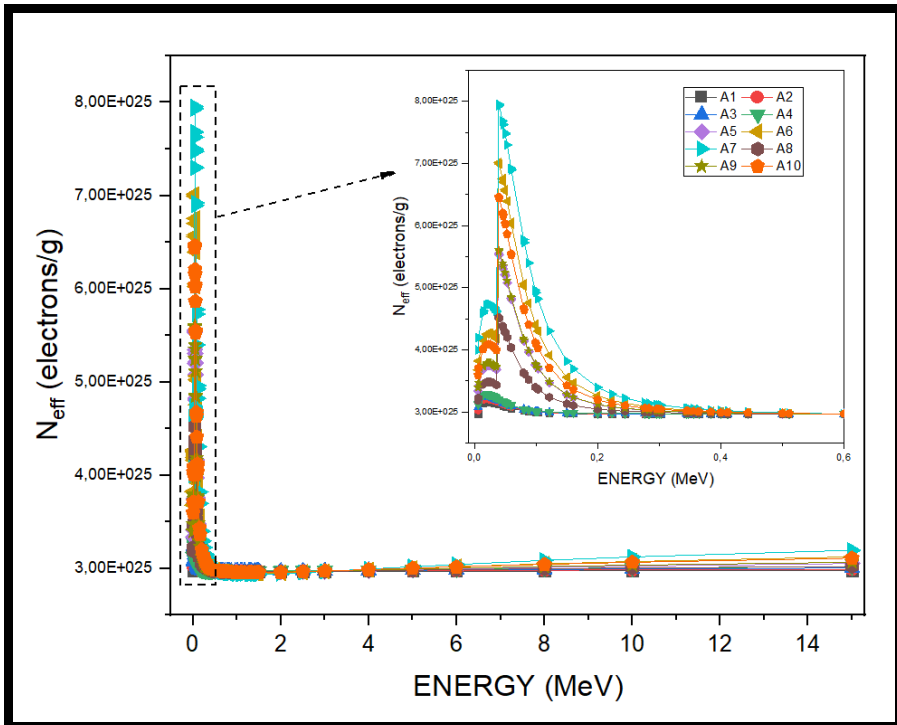


Figure 12. N_{eff} Values of SiC and BaSO₄ Reinforced AZ91 Composite/Hybrid Material

C_{eff}

As a result of the photon interacting with the material, free electrons are formed. The effective conductivity (C_{eff}) value, which is an indicator of free electrons, is in the 0.015MeV-15 MeV energy range for SiC and BaSO₄ and SiC+BaSO₄ composite/hybrid materials reinforced into AZ91 at different rates (5-10%-15%) has also been given. At 2.21E-02 MeV (⁴⁷Ag), the C_{eff} values of all composite//hybrid samples had their peak values. At 2.21E-02 MeV (⁴⁷Ag), A1-A10 coded samples are respectively 4.13E+10 S/m- 4.35E+10 S/m- 4.57E+10 S/m- 4.79E+10 S /m- 5.26E+10 S/m- 6.40E+10 S/m- 7.56E+10 S/m- 4.81E+10 S/m- 5.52E+10 S/m-6, They take the values of 25E+10 S/m. Samples with code A1-A10 in ⁶⁰Co source with 6.62E-01 energy, which is the most used in the industry, 3.87E+10 S/m- 4.03E+10 S/m- 4.18E+10 S/m- 4.33E+10 S /m- 4.16E+10 S/m- 4.44E+10 S/m- 4.73E+10 S/m- 4.09E+10 S/m- 4.31E+10 S/m, they take the values 53E+10 S/m.

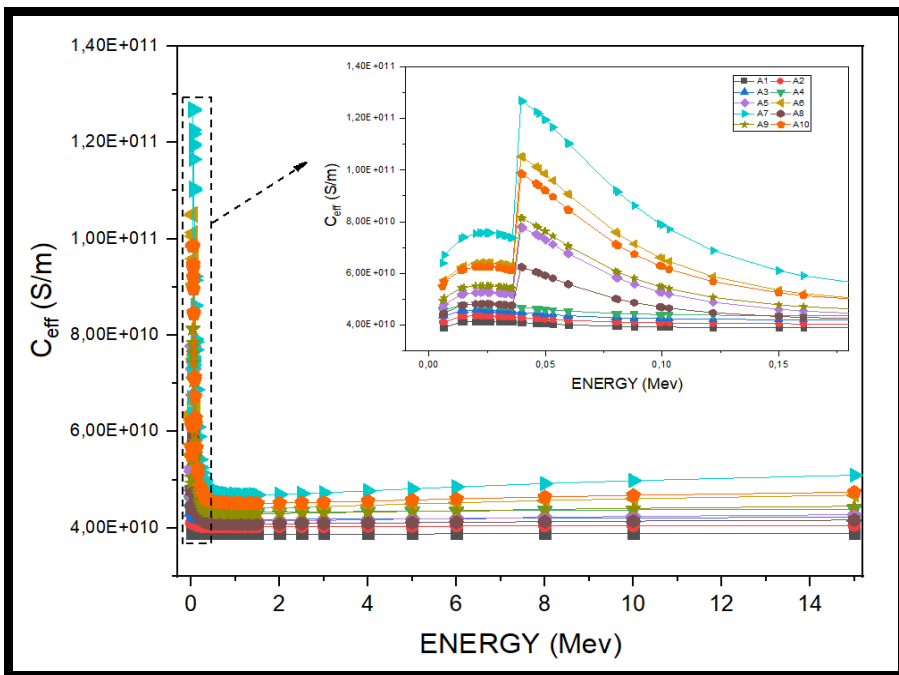


Figure 13. C_{eff} Values of SiC and BaSO₄ Reinforced AZ91 Composite/Hybrid Material

FNRC

Even at very low energies, the neutron can enter the nucleus without being affected by the Coulomb barrier and initiate nuclear reactions. For this reason, it is very difficult to stop neutrons. The neutron cross-section (ΣR) used in fast neutron shielding is a very important parameter in determining the neutron shielding properties of the materials to be used to intercept neutrons. ΣR parameters (Figure 14) were investigated in Am-241 radioactive source of SiC and BaSO₄ and SiC+BaSO₄ composite/hybrid materials at different ratios (5-10%-15%) to AZ91 by Phy-x/PSD program. Among the composite/hybrid samples, the material with the highest value was AZ91+15% BaSO₄ with 6,909cm⁻¹. A1-A10 coded samples are respectively 5,932cm⁻¹- 6,189cm⁻¹- 6,448cm⁻¹- 6,709cm⁻¹- 6,272cm⁻¹- 6,597cm⁻¹- 6,909cm⁻¹- 6,232cm⁻¹- 6,527cm⁻¹- 6,819cm⁻¹ they took the values of.

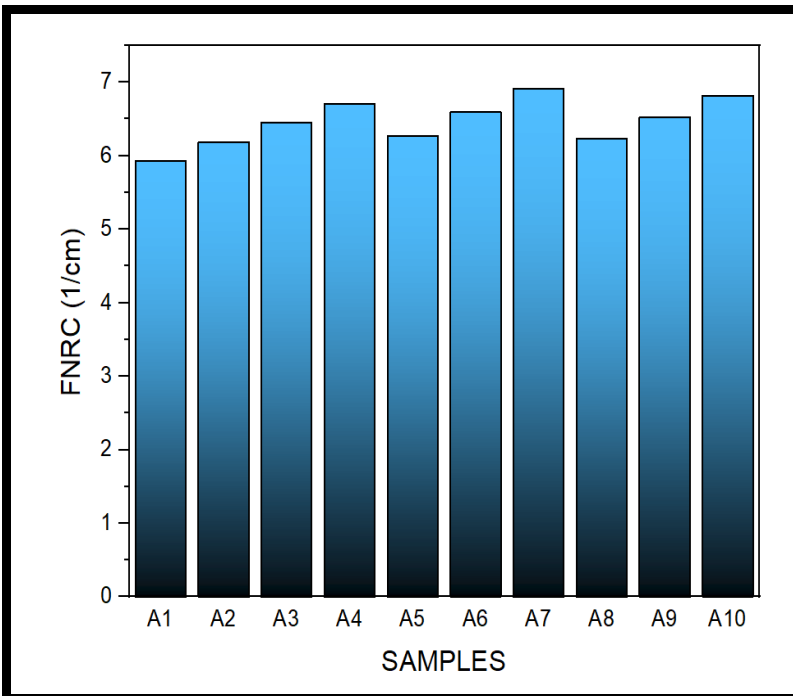


Figure 14. FNRC Values of SiC and BaSO₄ Reinforced AZ91 Composite/Hybrid Material

DISCUSSION

It is used in industry, power generation plants, medicine, and the defense industry. Radiation types are actively used in many application areas. Because of the increasing use of radiation, its effects are showing its effect day by day. For this reason, this study was carried out on a shielding material that will be an alternative to the shielding materials used today. Phy-x/PSD program was used to understand the behavior of SiC and BaSO₄ and SiC+BaSO₄ composite/hybrid materials reinforced into AZ91 at different rates (5%-10%-15%) in the 0.015MeV-15 MeV energy range against gamma rays and neutrons. LAC, HVL, TVL, MAC, ACS, Z_{eff} , ECS, MFP, N_{eff} , C_{eff} , and FNRC parameters were investigated. With the increase in the reinforcement ratio of BaSO₄ ceramic material added into the AZ91 matrix material, MAC and LAC values increased, while HVL, TVL, and MFP values decreased. This shows that the shielding ability of the material against gamma radiation improves depending on the increasing reinforcement ratio. Among the composite/hybrid materials, the material with the lowest Z_{eff} value was AZ91. Z values of composite/hybrid materials have increased with the added reinforcement elements. As the C_{eff} value, which is an indicator of the number of free electrons formed as a result of the interaction of the photon with the material, increases due to the increasing reinforcement ratio, the Z value of the material increases, and its highest value is obtained in AZ91+15% BaSO₄. The FNRC parameter, which is the indicator of the possibility of fast neutrons interacting with the material, took the lowest value of 5,932cm⁻¹ and became the AZ91 material. As a result of the analysis, it was determined that the most suitable material for use in gamma and neutron shielding is AZ91 + 15% BaSO₄ composite material.

ACKNOWLEDGEMENTS

We would like to thank Efe Barit mining for their contribution.

REFERENCES

Abdlhamed, F. (2018). Radiation Shielding Properties For Some Composite Materials. Isparta, 487819, 1-21

Almisned, F. (2022). Computer Simulation for Shielding Properties of SiC and TiC Reinforced Composites. October, <https://doi.org/10.21203/rs.3.rs-2076105/v1>

Akkaş, A. (2015). Shielding Effect of Boron Carbide Aluminium Metal Matrix Composite against Gamma and Neutron Radiation. Vol. 128, DOI: 10.12693/APhysPolA.128.B-176

Aydın, F. (2018). Investigation of Microstructure, Mechanical and Wear Behaviour of B4C Particulate Reinforced Magnesium Matrix Composites by Powder Metallurgy. 873-882

Chilton. A.B., Shultis. J.K., Faw. R.E. (1984). Principles of Radiation Shielding. Vol.5, No.3.

Çavuşoğlu, Ü. (2013). Production Of B4C Particle Reinforced Magnesium Matrix Composites. Yüksek Lisans Tezi. Yıldız Teknik Üniversitesi Fen Bilimleri Enstitüsü, İstanbul, 1-16

El-Sayed, A., Ali MA, Mand. and Ismail, MR. (2003). Natural fibre high-density poly-ethylene and lead oxide composites for radiation shielding. Radiat. Phys. Chem. 66 185-95. 10.1016/S0969-806X(02)00470-X

Emikönel, S. (2015). Investigation Of Radiation Shielding Properties Of Some Fabric Coated. Barite, Vol.128, DOI: 10.12693/APhysPolA.128.B-53

Gerward, L., Guilbert, N., Jensen, KB. and Levring, H. (2004). WinXcom-a program for calculating x-ray attenuation coefficients. J. Radiat. Phys. Chem. 71 653-4 DOI:10.1016/j.radphyschem.2004.04.040

Gökmen, U., Özkan, Z., Ocak, S. B. (2021). Impact of the gamma and neutron attenuation behaviors on the functionally graded composite materials. <https://doi.org/10.1088/1402-4896/ac41ef>

Harima, Y. (1993). An historical review and current status of buildup factor calculations and application. Radiat.Phys. Chem. 41 631-72. [https://doi.org/10.1016/0969-806X\(93\)90317-N](https://doi.org/10.1016/0969-806X(93)90317-N)

Jalali, M., Mohammadi, A. (2008). Gamma-ray attenuation coefficient measurement for neutron-absorbent materials. May, Vol.77, 523-527. <https://doi.org/10.1016/j.radphyschem.2007.12.014>

Kaplan, M.F. (1989). Concrete radiation shielding Longman scientific and

Technology. (England: Lonman Group UK, Limited, Essex)

Kurt, M. (2017). Investigation of production of Al-Mg composites reinforced by SiC ve Al₂O₃ through powder metallurgy method. Yüksek Lisans Tezi, Firat Üniversitesi Fen Bilimleri Enstitüsü, Elazığ, 484269, 3-73.

Manohara, S R., Hanagodimath, SM., Thind, KS. and Gerward, L. (2008). On the effective atomic number and electron density: A comprehensive set of formulas for all types of materials and energies above 1 keV. Nucl.Instrum. Methods Phys. Res. 266 3906-12.

<https://doi.org/10.1016/j.nimb.2008.06.034>

N, Nagaraja., H.C.Manjunatha., L.Seenappa., K.N.Sridhar., H.B.Ramalingam. (2020). Radiation shielding properties of silicon polymers. June, Volume 171, 108723.

<https://doi.org/10.1016/j.radphyschem.2020.108723>

Sayyed, M.I., Akman, F., Kumar, A., Kaçal, M.R. (2018). Evaluation of radioprotection properties of some selected ceramic samples. 11, 1100-1104. <https://doi.org/10.1016/j.rinp.2018.11.028>

Soy, U. (2009). Manufacturing Of SiC/B₄C Reinforced Metal Matrix Composites And Investigation Of Mechanical Properties. Yüksek Lisans Tezi. Sakarya Üniversitesi Fen Bilimleri Enstitüsü, Sakarya, 245239, 1-16

Srivinas, A., Pavan, D., Venkatesha, B.K., Rao, R. and Mohith, L. (2022). Study on Mechanical Properties of AZ91 Magnesium Alloy. Volume 54, Part 2, 291-294, <https://doi.org/10.1016/j.matpr.2021.09.171>

Sriwongsa, K., Glumglomchit, P., Suwannayuha, M., Kukuthapan, P., Sukkasame, N., Ravangvong, S. and Glumglomjit, S. (2021). The Interaction Radiation and Exposure Buildup Factors Properties of AM60 and AZ91 Alloys, 0858-7418, 9-19. <https://doi.org/10.14456/nujst.2021.22>

Şakara, E., Özpola. FÖ., Alım. B., Sayyed. MI. and Kurudirek, Mand. (2020). Development of a user-friendly online software for calculation of parameters relevant to radiation shielding and dosimetry. Radiat.Phys. Chem. 166 108496. <https://doi.org/10.1016/j.radphyschem.2019.108496>

Turan, M. E. (2018). Fabrication Of Nano Particle Reinforced Magnesium Matrix Composites Via Powder Metallurgy And Characterization. April, Volume 740, 1149-1158

SAVING ENERGY CONSUMPTION IN BUILDINGS BY ADVANCED CONTROL STRATEGIES

*Masoud TAGHAVI*¹

Abstract: This research shows an analysis of the relationship between the use of energy in the building and the equipment and performance of the control system in the building. A method for evaluating the potential of energy storage shows the progress in the building and equipment of the control system, which includes the effect of the use of software and hardware upgrades based on the evaluation of the level of sufficient energy design and the energy use of the building related to similar buildings. Sufficient energy design and energy use of the building is related to similar buildings with the energy use appendix for the building. This method introduces the building design appendix and the building equipment appendix to evaluate the energy performance of the building compared to similar buildings, and these indicators are used to evaluate the potential reserves and control the improvement of the system.

Keywords: Advanced Buildings, Optimization Of Energy Consumption, Efficiency, System Control, Design

INTRODUCTION

The importance of building energy consumption has been documented by clarifying the potential advantages of techniques to improve building energy efficiency. Pellet is one of the possible methods for the implementation of many related aspects, the arrangement of advanced materials, the development of intelligent components and systems. The stage

¹ Head of Mechanical Engineering Department, Faculty of Noshahr, Technical and Vocational University (TVU), Iran, e-mail: m-taghavi@tvu.ac.ir, Orcid No: 0000-0001-9794-2608

of designing, building and equipping the building with many components and technologies. Poor building performance is evident in many ways, including insufficient environmental conditions, energy use and cost, equipment and increased service calls. Many of these issues are directly related to the building control system, which have been created by examining the progress of the building control system performance from the progress of the building application.

Economic studies pay special attention to building control system planning and its activities. Hierarchy is that the design and implementation of the building control system needs to be investigated, because different buildings have different needs and characteristics of the unit and different solutions. On the contrary, increasing the performance of the building control system is described with this level, which requires the strengthening of the software and hardware elements of the control system, contrary to the original design goal. In the current state of the industry, achieving optimal control is time-consuming and costly. In any case, it is expected that the continuous progress in intelligent control strategies will create solutions that provide optimal control in an effective way. In this article, two issues related to control systems have been discussed. First, how the quality of potential reserves is related to the improvements in building equipment and control, secondly, how reserves are obtained in existing buildings.

Building Energy Use and Control System Performance

There are two statements that are generally accepted by the construction industry in the following ways:

- *Buildings are constantly using more energy than is reasonable.*
- *Building control systems are not continuously equipped.*

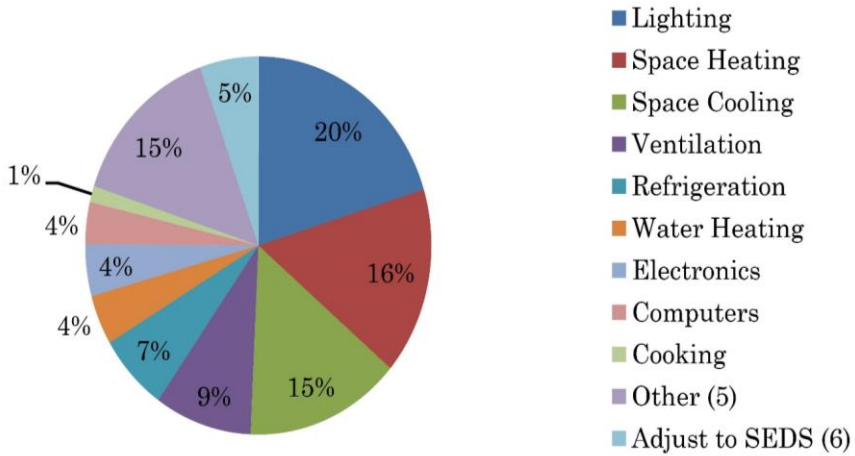


Figure 1. Maximum Energy Used for Commercial Buildings in 2021

There is a hypothesis that these two terms are related. The energy efficiency of the building is equal or equal when the equipment conditions of all sub-systems are equal or equal. This shows the challenge that buildings have more diversity than vehicles. In the sense that single and different solutions need to be developed and implemented.

The requirements of building systems are wider than vehicles, and accurate evaluations of energy storage potential require information from the progress of building control systems. Let's analyze some of the energy consumption based on the energy information reported in figure 1, commercial building energy usage is 20.2%, space heating is 16%, cooling space is 14.5%, ventilation is 9.1%, freezer is 6.6% and other cases. 33.6% is based on primary energy. This fact shows about 60% of the energy use (light, heating and cooling space, ventilation) which is related to the building control system. Studies show that optimal control strategies and misidentifications reduce energy loss and improve building energy efficiency.

SAVING ENERGY CONSUMPTION IN BUILDINGS BY ADVANCED CONTROL STRATEGIES

Table 1. Selection of Reported Control Resources Related to Energy Storage or Potential

Type of study	Storage %
a review	25-45% of the energy used in the HVAC system is wasted due to errors.
Comprehensive review based on information	20% - 4% of energy consumed by HVAC, lighting and larger refrigeration systems in a commercial building.
studied by simulation	Variable refrigerant flow air conditioning system can save 57.9% - 27.1% energy compared to AC system.
studied by simulation	Energy savings of up to 30.4% in summer using optimal set point control compared to fixed temperature set point.
studied by simulation	Centralized strategies and MPC distribution of energy consumption can reduce 13.4% compared to conventional P, PI, in off/on control (for a selected day).

A case study with EnergyMPC shows the extraction rule for control optimization in buildings that have the ability to save more than 40% of energy through relevant strategies.

Table 2. Annual Energy Effect of Defects Selected for Measurement by Roth and etc

Error	Error type	Percentage of error	Annual energy consumption
duct leakage	air distribution	30%	0.3
HVAC on the left, when the space is not occupied	HVAC	20%	0.2

Left light when the space is occupied	Lighting	18%	0.18
Unbalanced airflow	Air distribution	7%	0.07
Improper refrigerant change	Refrigeration circuits	7%	0.07
The damper is not working properly	Air distribution	6%	0.055
Insufficient evaporator airflow	Air distribution	4%	0.035
Improper setup or control	Control	2%	0.023
Control failure or destruction	Control	2%	0.023
Error in programming software	Control	1%	0.012
Improper hardware installation	Control	1%	0.01
Condenser path is closed with cold air	Refrigeration circuits	1%	0.008
Valve leakage	Water release	1%	0.007
Total	-	100%	1

Akinci and etc. briefly stated that 25-45% of the energy used in the HVAC system is wasted due to a series of mistakes that include strategy control. Roth and etc. colleagues evaluated 13 basic defects in commercial buildings. Based on the information, the study is carried out when the entire commercial building consumes approximately 17 parts of primary energy. The row of energy impact evaluation with a series of mistakes includes 0.24-0.88 parts and 11-20% of the total energy is consumed by commercial buildings. These authors concluded that these defects increase the primary energy consumption of commercial buildings by about 4-20% of the energy consumption of HVAC, lighting, and refrigeration systems in commercial buildings. Clearly, the progress of the control system performance reduces the energy consumption of the building and increases the environmental conditions and the internal environment conditions, which are as follows with the group's potential activities in 3 categories:

- *Storage of control system equipment for the purpose of design*
- *Implementation of conventional energy storage strategies such as energy recovery*
- *Increasing the ability of advanced control such as model prediction or adaptive control of steps for these matters*

Building Control System, Energy use and Energy Storage

The building control system is used to create points and the system components are used to maintain environmental conditions by switching on and off or modeling control signals. Depending on the control system, various sensor readings and logical phasing are used due to the equipment of the systems. The shape of the HVAC system of the building and the accumulation of components, if it is equipped appropriately, will become a row of energy applications, and the control points and signals are managed by the control system. There are buildings that perform well, but use a lot of energy because they

lack energy storage materials, control capabilities, and equipment. While the other building has energy storage features for energy use due to equipment issues. Figure 2 shows the energy use of normal building NBE in various stages of building design and equipment for simple building and high performance.

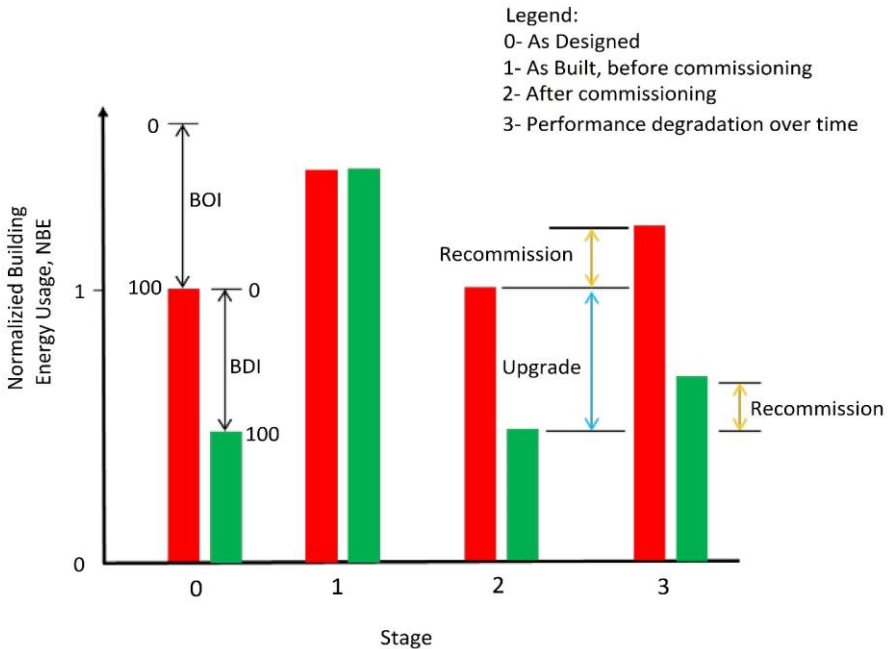


Figure 2. Normal Building Energy Use in Various Stages of Life in the Building

This energy use is different for these buildings because the shape of the AS bar has been reflected. As Built, the use of energy is more than the design values, while the extra energy is not added with a high performance building without proper equipment. The use of energy after the building is equal to the design goal. Energy usage increases as systems and components are rated. This examines that we represent a spectrum of building energy use for a floor of the building as the basis of the uncertainty of the design energy reserve and the degree to which the building is preferred and conforms to the design objective, which includes The primary dimension is the BDI building design appendix and the

term energy efficiency design is mentioned. The second dimension includes the addition of BOI building equipment with warnings that refer to aspects of building equipment and are related to energy use. According to Figure 3, the sample BDI scale with the performance structure based on the percentage defined by the difference between the two design goals are shown.

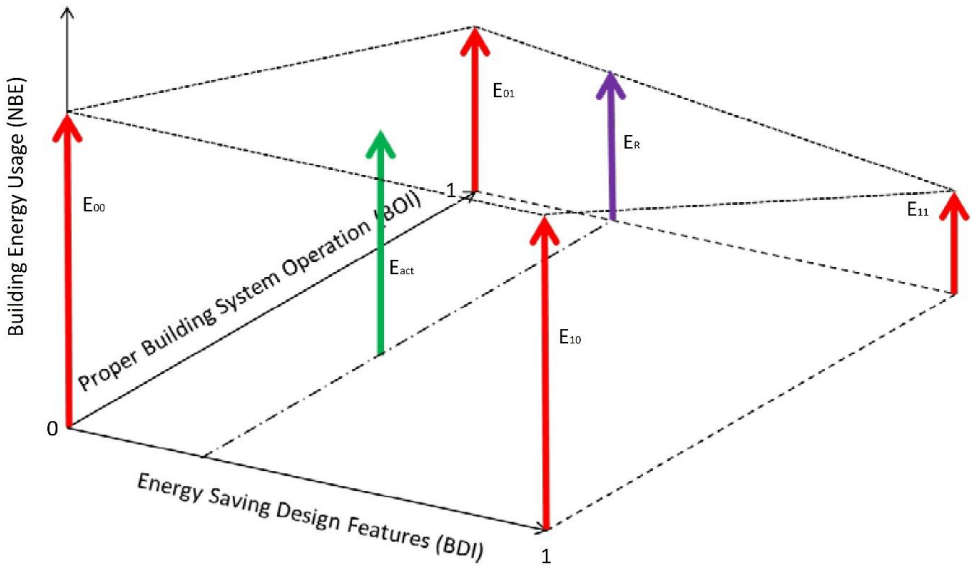


Figure 3. Building Energy Use as the Basis of Design and Equipment Indicators

The BOI scale of building equipment with a value of 100% is a response to the design goal, a value of 0% is a response to the amount of energy use limited by the use of As Built energy. Therefore, there is a possibility of incorrect energy performance. As shown in Figure 2, when a building is equipped with the discussed systems, its energy use increases according to the component and system shape change. The building stock needs a commission according to proper equipment, which includes physical and mechanical aspects. It is especially used to obtain the value of BOI at the level of 100%, while the reflection of the simple building with the high-performance building needs to be created in the BDI with a value of 100%. This con-

cept is shown in figure 3. In this form, it is less in the left area and the building is simple and does not show a good surface. It should be mentioned that a BOI of zero does not mean that the building is not equipped at all, but the probability of being equipped is low. On the contrary, BDI is responsive from zero in a simple building with the accumulation of basic equipment. BOI means that the building is equipped for equipment with limitations. The information related to the arrows in Figure 3 is as follows. The red arrows in the corners or angles show the use of normal building energy (NBE). E00 is a very weak or simple building, E01 shows the equipment of the same building and E10 shows the equipment of the building with high performance. It is assumed that the energy use of the building will decrease. As the design and equipment of the building increases, the buildings in the average values of the appendix respond to the energy use values in the average level with surface shape. The row of E11, E01 and E00 is reduced, as you repair the simple building and then you make it modern, you should make sure of the new systems you use. It is assumed that E10 is almost equal to E00, while advanced features do not provide advantages and lead to increased energy use. The green arrow shows the specific energy use of the Eact building. If BOI and BDI are used for the building, potential energy reserves are evaluated according to the style of the day. It is assumed that we know the participation of BOI and BDI, of course, according to the location of the green arrow, the potential of max energy storage is different according to the style of the day and between E11 and Eact, which consists of 2 parts, storage with which includes Eact minus ER and includes energy use for BDI without BOI, design day style reserves equal to ER minus E11. Therefore, 3 issues remain:

- *How the illumination of red arrows is determined*
- *How to determine the height between the red arrows*
- *How are BDI and BOI values determined?*

The explanation of these cases is based on the combination of analy-

tical, statistical, and innovative methods used to evaluate the connection of arrows. If it starts with E01, the simple building is fully equipped and the energy use value is designed, it needs to decide how much energy the building has used, and with E00 it becomes the style of the day and what The value decreases, if high performance is obtained by updating the building style (E11). We define the BOI scale by selecting E00 with several E01. The combination of the reported results shows one of these 2 factors that is responsible for showing the scale of the building equipment. In other words, the energy performance of the building has been graded and the energy use has been doubled with the purpose of its design, this result includes BOI of zero. Therefore, the buildings that have been investigated in the outer layers need special treatment. It is assumed that there is a linear relationship between BOI and NBE on the BOI axis, according to the figure that shows the linear relationship between E0 and E00. In another dimension, E11 shows the building. Surveys show that buildings with high performance are designed and equipped to use half of the energy of conventional buildings. The linear relationship between BDI and NBE assumed for BOI is equal to 1. Therefore, the slope in BOI path for BDI is equal to 1 greater than 4 boundaries and it is expected that all advanced features will be provided with great progress. It should be mentioned that the analytical method described below includes the relationship between the NBE values in the 4 corners so that these cases can be used based on specific information for one floor of the building. It is assumed that this surface is smooth, so the following formula shows the investigation of the quadratic form:

$$NBE = 0.5(BDI - BDI^2 + (BDI)(BOI)) - BOI + 2$$

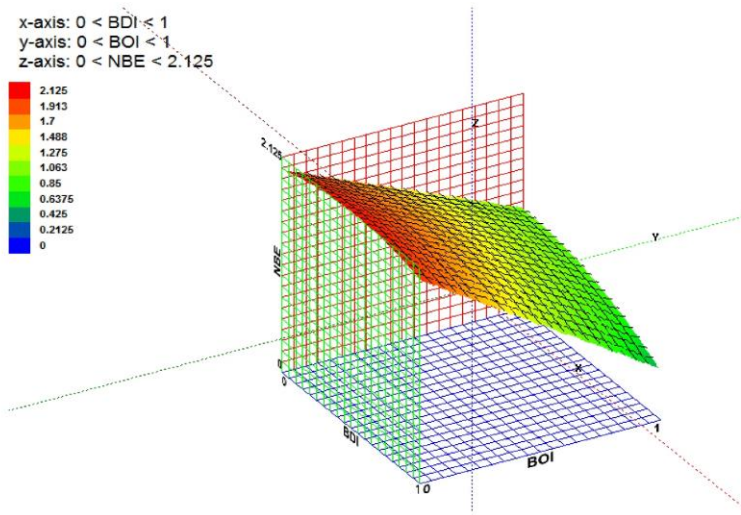


Figure 4. Normalization of the Energy Level Plan of the Building

Using this formula, according to Figure 4, the relationship between NBE and 2 indicators has been designed. The corner points have a transfer relative to the surface. There is a protrusion, because this surface needs the curvature of the borders. Figure 5 shows the surface information in the figure.

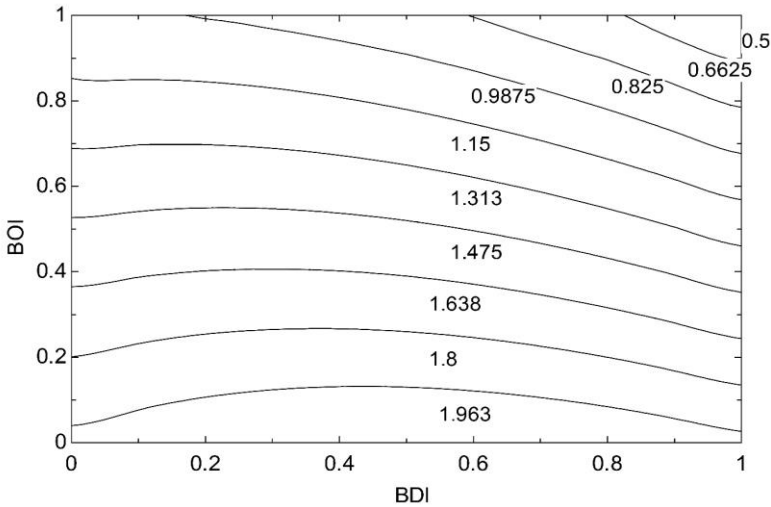


Figure 5. Normalization of Building Energy Use Controls

The level of NBE has been checked, with this method to determine the values of BOI and BDI for the specific building is started. First, BDI is calculated based on the evaluation of building ambiguity and system design with energy use. This evaluation is used with a meaningful scale and the knowledge in the field of building is evaluated with the energy efficiency of the building. The systems are designed into the following 4 groups:

- *Building equipment:*

wall - insulation - roofs - windows - mechanical and thermal electrical equipment - lighting

- *Shape or configuration of building systems:*

Stable air volume - stable or variable water flow - heating pumps - ground surface rings

- *Building ventilation:*

Variable and stable ventilation - energy saving - energy recovery - examination of outside air

- *Ability or ability to control the building:*

Maintenance of points - Seasonal points - Equipment planning - Real time dynamic equipment judgment - Control acceptance.

Now that the NBE level is determined. It can be investigated using the method to determine the BDI and boiler values for a specific building. First, BDI is calculated based on a subjective assessment of building evaluation and system design with respect to energy consumption.

Subjective evaluation using details, whereby someone knowledgeable about the building energy efficiency of the building and the design of the systems in four categories of points, as follows:

- *Building equipment:*

Wall - insulation - roof - thermal, mechanical and electrical equipment - lighting

- *Configuration of building systems:*

Constant or variable air volume - constant or variable water flow - heat pumps

- *Building air conditioning:*

Fixed, scheduled, variable or demand control ventilation - energy recovery - dedicated outdoor air

- *Ability to control the building:*

Fixed-seasonal.

Table 3. Staging of BDI Group

Credit %	Descriptive score	Score
0	By default years of technology, public	0
10	At least a little better	1
25	Relatively low, noticeably better, but below average	2
50	Standard sample product level	3
75	Above average, clearly better, but not the best	4
100	Exceptional, maximum performance	5

Each group of the above cases has been carefully investigated and each group is determined with numerical validity. The semantic scale is shown in Tables 3 and 4, and the weights of the BDI group and false parameters are determined. This evaluation is used to understand that the building is evaluated in all 4 groups to determine the BDI.

Table 4. BDI Group Weights and Incorrect Parameters

Category	Weight	Default parameters
Construction equipment	25	Outdated
Configuration of building systems	25	Constant air volume
Building air conditioning	25	Freezing air outdoors
Ability to control the building	25	Fixed setpoints
Total	100	Default parameters

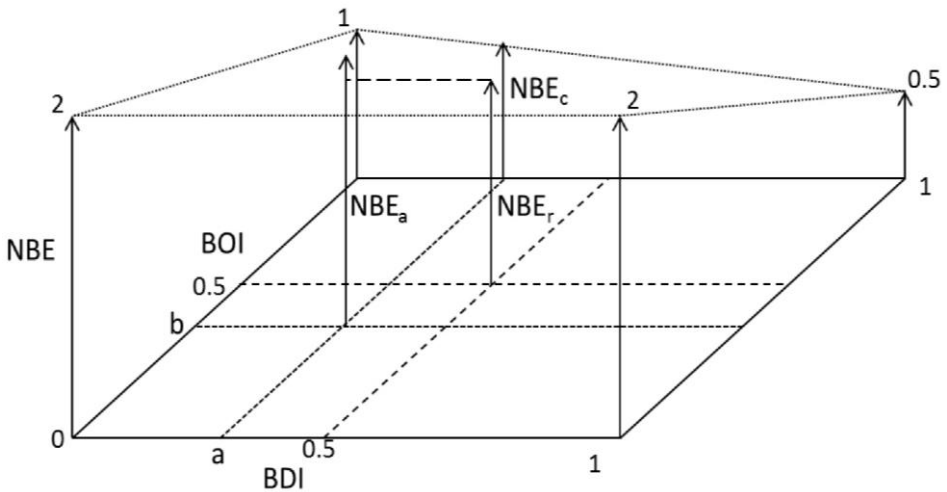


Figure 6. Determination of BOI from EUI Ratio

According to Figure 6, this NBE is used or proven to make a specific value of BDI, by showing the line “a” shown. For linear detection, a suitable value for BOI should be determined. This is implemented by using the building energy use appendix (EUI) parameter, which divides the total annual energy use by the floor area of the building and is basically collected, stored and built for many floors

and locations of the building. We can calculate the maximum energy storage potential etc. in the BOI-BDI space in Figure 7. Figure 7 examines that the building located in BOI and BDI, equal to 0.5, provides maximum energy reserves above 60%. Of course, the population of the building is variable in the performance characteristics of specific buildings.

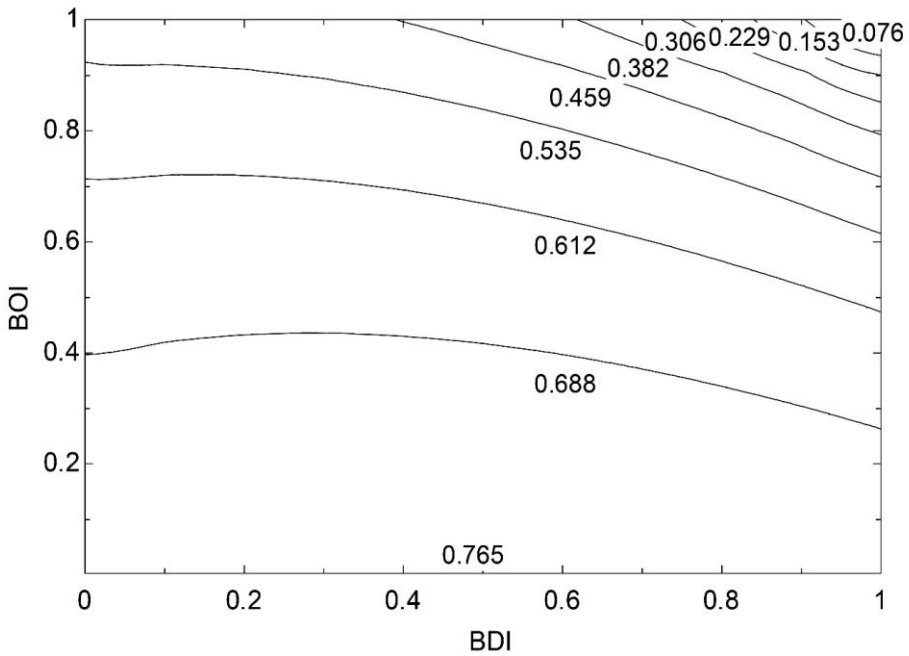


Figure 7. Maximum Energy Storage Potential of the ESPm Building

CONCLUSION

In general, to estimate the building, how the energy performance is placed in the spectrum of the building is important. There are 2 ways to do this:

1. Evaluating the energy performance of existing buildings in relation to similar buildings or groups of buildings (community, city, district, etc.) and defining energy performance in relation to design versus equipment. This information is invaluable for the owner of the building to enable the planning of energy performance improvement activities such as updating. Because advanced equipment and preparation have 2

separate groups with different economic costs and requirements. In addition, this methodology is used by the government or used to evaluate programs and improve energy efficiency for the region by enabling them to evaluate the building to obtain reasonable impacts.

2. The evaluation of the activities for a specific building by empowering the predicted or actual energy reserves with the maximum energy reserves. In this way, the evaluation becomes possible if additional evaluations are needed to obtain the energy storage potential of the building.

As a result, one of the biggest issues facing the building population is reducing the energy requirements of the building.

REFERENCES

U.S. Department of Energy (DOE), "Commercial Energy End-Use Splits, by Fuel Type (Quadrillion Btu)", In Building Energy Data Book; U.S. DOE: Washington, DC, USA, 2010.

Akinci, B.; Garrett, J.H.; Akin, Ö., "Identification of Functional Requirements and Possible Approaches for Self-Configuring Intelligent Building Systems", National Institute of Standards and Technology: Gaithersburg, MD, USA, 2011.

Roth, K.W.; Westphalen, D.; Feng, M.Y.; Llana, P.; Quartararo, L., "Energy Impact of Commercial Building Controls and Performance Diagnostics: Market Characterization, Energy Impact of Building Faults and Energy Savings Potential", A Report for Building Technologies Program: Cambridge, MA, USA, 2005.

Aynur, T.N.; Hwang, Y.H.; Radermacher, R., "Simulation comparison of VAV and VRF air conditioning systems in an existing building for the cooling season", *Energy Build* 41, 2009, pp. 1143-1150.

Mossolly, M.; Ghali, K.; Ghaddar, N., "Optimal control strategy for a multi-zone air conditioning system using a genetic algorithm", *Energy* 34, 2009, pp. 58-66.

Moroşan, P.D.; Bourdais, R.; Dumur, D.; Buisson, J., "Building temperature regulation using a distributed model predictive control", *Energy Build* 42, 2010, pp. 1445-1452.

May-Ostendorp, P.; Henze, G.P.; Corbin, C.D.; Rajagopalan, B.; Felsmann, C., "Model-predictive control of mixed-mode buildings with rule extraction", *Build. Environ* 46, 2011, pp. 428-437.

Hazyuk, I.; Ghiaus, C.; Penhouet, D., "Optimal temperature control of intermittently heated buildings using model predictive control: Part II—Control algorithm", *Build. Environ* 51, 2012, pp. 388-394.

Ma, Y.; Anderson, G.; Borrelli, F., "A Distributed Predictive Control Approach to Building Temperature Regulation", In *Proceedings of the 2011 American Control Conference (ACC)*, San Francisco, CA, USA, 29, 2011, pp. 2089-2094.

UNRELATED PARALLEL MACHINE SCHEDULING WITH SEQUENCE-DEPENDENT SETUP TIMES: AN APPLICATION TO AUTOMOBILE SPARE PART MANUFACTURER¹

*Muhammed SÜTÇÜ¹, İbrahim Tümay GÜLBAHAR², Yakup KAPAR³,
Fatih İNCE⁴, Nurettin ŞAHİN⁵*

Abstract: Production planning and scheduling play a significant role for a business in terms of meeting the demands and determining the optimal capacity to be able to complete the tasks on time. Moreover, scheduling the setup times and operation times of machines becomes a crucial need for operations management, which helps increase the company's profitability. As it becomes an important issue for manufacturing companies, there has been much research in the literature regarding scheduling with setup times. In most of the research on these problems, besides the problems have sequence-dependent setup times but the setup times of the processes were ignored, combined with the corresponding processing times, or studied as a not sequence-dependent problem to simplify the model. In the unrelated parallel machine scheduling problem, in which dependent setup times and machine availability are taken into account, a mathematical model is proposed that will decide both which machines will be used and which jobs will be produced in which order on the machines to be used. Also, the objectives of these problems are to minimize the number of machines to be used and the completion time of the last job. In this study, in addition to the manufacturing time and setup time, mold change times were also taken into account, with a methodology similar to the previous studies. In addition, another goal of this study is to work in 3

¹University, Faculty of Engineering, Kayseri / Türkiye, e-mail: muhammed.sutcu@agu.edu.tr, Orcid
No: 0000-0002-8523-9103

shifts in the company and we aim for minimum time loss in shift transitions. So, in this paper, the problem of spare parts manufacturing company's unrelated machines scheduling with sequence-dependent setup times in hot-upset forging department to minimize the makespan and setup time are studied. So, we propose a mixed-integer mathematical model in order to minimize total hours (makespan), changeover, and production time. The proposed mathematical model is run to find the optimum assignments of each work to machines in the hot-upset forging unit for a company that produces automobile spare parts. After running the model, the computational results show a 20 percent improvement in total production time for all shifts, and a 17 percent improvement in mold change and shift transition time.

Keywords: Unrelated Machine Scheduling, Mixed Integer Optimization, Automobile Spare Part Industry

INTRODUCTION

Scheduling is a decision-making process in which resources are assigned to activities to optimize one or more objectives over a period of time and are used frequently in many manufacturing and service businesses (Pinedo, 2012). In production-based businesses, scheduling is aimed at determining the order in which jobs will be assigned to machines and with what resources they will be produced (Mauergauz, 2016). One of the most important problems of companies in today's competitive environment is to create effective schedules that ensure the most efficient use of production resources such as machines and labor. Efficient schedules allow orders to be completed without delay, minimizing overtime costs. As the number of jobs in enterprises increases, it becomes difficult to create effective schedules. For this reason, there are many studies on the scheduling problem in the literature where the main aim of these studies is to create most effective schedules.

In classical machine scheduling problems, the number of machines is assumed to be constant, and all machines are scheduled to perform the jobs. However, in some sectors where molds are needed, such as the au-

tomobile spare part industry sector, putting into use of a machine leads to very serious energy consumption. Especially in mold changes, it is necessary to change the mold after it cools down and bring it to a certain temperature again. For this reason, it is preferable not to change the mold in a machine unless necessary in such sectors. In addition, for many other businesses, carrying out their work with fewer machines creates opportunities for machines that are not used in production to be rented to another company or to accept additional work as much as the capacity of idle machines. Therefore, in this study, it is aimed to minimize the number of machines to be used and their efficiency. Thus, the profitability and efficiency of the enterprises can be increased.

There are many studies in the literature dealing with the unrelated parallel machine scheduling problem. Retrievable from the studies conducted in the last 10 years on the unrelated parallel machine scheduling problem, in which setup times are addressed (Cota et. al., 2021; Kim and Kim, 2020; Lei et. al., 2020)

In addition to sequence-related setup times, machine availability constraints are also one of the constraints that have been taken into account in recent years (Hsu et.al., 2011; Kuo et.al., 2011; Lin et.al., 2011). These studies generally considered more than one objective function and heuristics or meta-heuristics were used as solution methods. When the multi-purpose studies are examined, it can be seen that the weighted sum method is generally used as the solution method. Moreover, stochastic optimization models are also used (Yıldız and Sutcu, 2022).

Production planning and scheduling are critical for a company's ability to fulfill demand and determine the best capacity for completing jobs on time. The time horizon of scheduling is short-term, like between one to eight weeks. The time horizon, on the other hand, of planning is mid-term, like three to twelve months. A private company producing spare parts such as tie rod, swing arm, etc., have not fixed orders due to different types and number of orders. Consequently, scheduling becomes a

crucial need for these kinds of businesses in order to increase their profit. To accomplish these, there are some approaches and applications. Optimization is one of the applications in order to schedule the production program properly. However, scheduling problems are considered as difficult problems, yet it could be gained some efficient solutions when it is applied properly. As it is seen in the literature, scheduling is a wide-open topic that needs to be taken into consideration for all businesses.

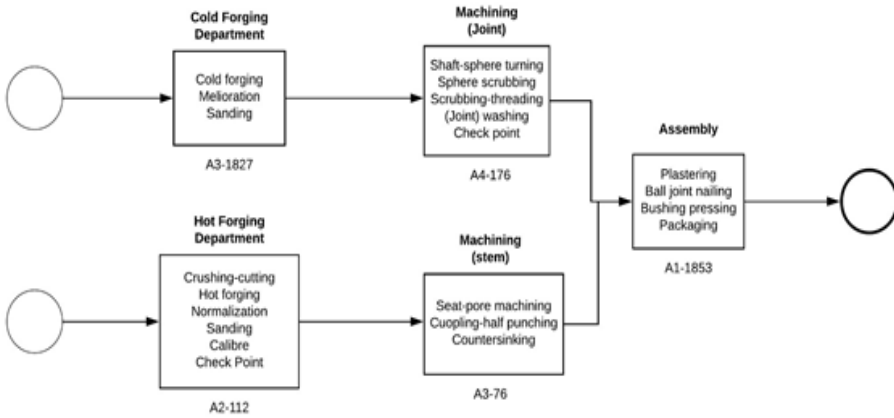


Figure 1. Automobile Spare Part Factory Layout

In the search of literature, there are some studies that are close to our study. Allahverdi and Soroush (2008) discuss the importance of modern production and service environments where timely delivery of reliable products/services and timing with installation times or installation costs. They also identify and highlight the importance, practices, and benefits of clearly taking into account the time/costs of installation in scheduling problems. In another study, Brauner et. al. (2014) deals with the production of iron bars used in reinforced concrete buildings and in this study, they plan the cutting of rods according to customers' orders by using greedy algorithm.

The importance of project management is also discussed by researchers in the literature especially on scheduling and production plan-

ning. For instance, Kerzner (2017) stresses the importance of techniques in achieving project objectives. They stress how successful implementation of techniques contributes to a successful project.

In the literature, the effects of behavioral operations in planning and scheduling are also discussed. Fransoo et. al. (2011) explains the importance of production planning and control in enterprises. Planning and scheduling activities are carried out to achieve high-quality products at very low cost, low inventory, and higher customer service levels within the enterprise and the entire supply chain. Another approach for solving production planning and scheduling is hierarchical integration. Hax and Meal (1975) describes the development of a hierarchical planning and scheduling system for multi-plant, multi-product, seasonal demand status. In this hierarchical structure, the most appropriate decisions at the total level of planning provide constraints for detailed decision-making timing and in their paper, this approach is solved by using mixed-integer programming.

Kreipl and Pinedo (2009) provide an overview of planning and scheduling theory and its application in supply chains. In their paper, they discuss how planning and scheduling models can be used in the design and development of decision support systems for planning and scheduling in supply chains. Also, the current trends in design and implementation have been focused on the implementation of planning and scheduling systems. Kruse et. al. (1996) develops a new strategy for column initiation and product replacement in production planning and scheduling. The purpose of these investigations is to minimize the time required from initial start-up or product change to steady-state study. Pinedo (2009) focuses on planning and scheduling applications in service industries especially in healthcare applications by using analytical techniques and heuristic methods.

Ruiz and Allahverdi (2007) discuss the problem of the non-wait flow workshop of the m-machine in order to minimize the maximum delay at

which the installation times are evaluated separately from the processing times and evaluated independently from the sequence. A dominance relationship has been developed for three machines and various heuristic scans and four new effective and efficient genetic algorithms have been proposed. In addition to advanced concepts such as genetic algorithms, steady-state and elitist belt schema, new rapid selection operators are also used. In another study, Stadler (2008) analyzes how production planning and scheduling is applied with a geographical focus in Switzerland and its environment in small and medium enterprises.

Behnamian et al. (2009) considered a scheduling problem with parallel machines and setup times that depend on the sequence. In that study, an effective hybrid of the population-based evolutionary searching ability of ant colony optimization with the local improvement ability of several variable neighborhood search and simulated annealing to balance exploration and exploitation was combined as the novel approach.

The study done by Tavakkoli-Moghaddam et al. (2009) proposes a two-level mixed-integer programming model for scheduling N jobs on M parallel machines that minimize bi-objectives, namely the number of late jobs and the total work completion time. They propose an efficient genetic algorithm to solve the bi-objective parallel machine scheduling problem.

In addition to all those studies, a different view can be offered as in the study done by Sütçü (2022).

Therefore, in this study, our aim is to schedule unrelated machines with sequence-dependent setup times in the hot-upset forging department to minimize the makespan and setup time. In the literature, there are studies that discuss the problem with sequence-dependent and sequence-dependent setup times. Our main difference is to schedule these models with sequence-dependent setup times by using mixed-integer programming while minimizing the makespan and setup time.

The remainder of this paper is organized as follows. Section 2 presents the problem definition of the proposed case study. Section 3 discusses the methodology and mathematical model of the proposed case study. Section 4 includes the findings of the study with application to the hot-upset forging department. Section 5 contains the concluding remarks.

PROBLEM DEFINITION

In this work, the optimum assignment for scheduling the machines of hot-forging units in the facility was studied. In the company, that the study has been carried out, even though the capacity of each machine in each unit is known, there is no systematic scheduling. In addition, the headworkers determine the assignment of the orders to the machines. In the hot-upset forging unit, the headworker assigns work to machines based on his experiences. In other words, scheduling is dependent on headworkers of the units. Consequently, it is doubtful that the assignments are optimum. In other words, based on the current situation, there could be an improvement for each unit in the company. Regarding this instinctual scheduling, the number of products produced is just determined by the daily production rate and this may cause problems for order fulfillment. Order fulfillment issues are important for any company due to these led up to a decrease in productivity and customer attrition. The capacity of production is based on machine/product ratio per hour and its set-up times for changing the mold between different product types. Also, as a constraint for the production schedule, the mold duration for the quantity of product produced from it and its maintenance duration is important for scheduling when it considers time slots.

Table 1. Production Capacity of Machines per Hour

Products	D65	Rus- D35	Manzoni-D46	D60	Beche- D62	D3	D1	D58
A2-904	240			227		134		
A2-6464	147						227	
A2-1925		80	134			134		
A2-2737		87	107		80			
A2-4078							267	
A2-220	267			267				
A3-2610			134					
A2-4065		80	107					
A2-1070	200			220				
A2-4576	187			174				

METHODOLOGY

In this section, we propose the mathematical modeling approach to solve the given problem. First, we introduce the sets, parameters, and decision variables. Then, we formulate the objective function with the given constraints by the company and theoretical constraints.

Table 2. Quantity of Demand and Produced Orders

Product	Demand	Produced
A2-904	2.807.000	2.847.000
A2-6464	1.968.000	2.097.000
A2-1925	1.290.000	1.340.000
A2-2737	1.196.000	1.228.000
A2-4078	1.076.000	1.335.000
A2-220	922.000	1.068.000
A3-2610	435.000	536.000
A2-4065	428.000	480.000
A2-1070	353.000	400.000
A2-4576	319.000	348.000

There is no production in machine D58 since the sample doesn't have a product that can be producible in the machine. According to hourly production capacity in machines table (Table 1), the products are assigned to the machines. Most of them can be produced in 2 or more machines besides some of them such as A2-4078 and A3-2610 can be produced in only one machine. The model is considered the situation and they assigned appropriate machine in a proper time period. Moreover, the weekly total quantity of order is considered and the demand is met (Table 2).

Mathematical Model

Sets

i = sample order $i = \{1, \dots, 70\}$

j = machines $j = \{1, \dots, 8\}$

k = parts $k = \{1, \dots, 30\}$

sub(k) subset of part k , sub(k) = $\{2, \dots, 30\}$

Parameters

A_i total quantity of order i (unit)

C_j setup time of machine j (hour)

Ka_{ij} maximum amount of product i that can be produced in machine j until a mold replacement (unit)

B_{ij} hourly production capacity in machine j for order i (unit/hour)

W_j total time that each machine operates (hours)

Decision Variables

x_{ijk} = total working hours of machine j to produce product i in part k

$y_{ijk} = \{1, \text{order } i \text{ is produced in machine } j \text{ in part } k; 0, \text{ otherwise}\}$

$setup_j$ = total setup time at machine j

r_j = total working hours of machine j

Formulation

Objective Function

The objective is to minimize total working hours and setup time of machines.

$$z^* = \text{Min } z = \sum_j (r_j + \text{setup}_j) \quad (1)$$

Constraints

$$1. \quad r_j = \sum_i \sum_k x_{ijk}, \quad \forall j \quad (2)$$

Variable r keeps the total working hours of each machine.

$$2. \quad \text{setup}_j = (\sum_i \sum_k y_{ijk} * C_j), \quad \forall j \quad (3)$$

Variable setup keeps the total amount of time spend for mold replacement in each machine.

$$3. \quad A_i = \sum_j \sum_k x_{ijk} * B_{ij}, \quad \forall i \quad (4)$$

Demand should be met.

$$4. \quad \sum_i \sum_k x_{ijk} + \sum_i \sum_k y_{ijk} * C_j \leq W_j, \quad \forall j \quad (5)$$

Total working hours and setup time of each machine cannot exceed total working hours.

$$5. \quad \sum_i y_{ijk} \leq 1, \quad \forall j, k \quad (6)$$

Only one order could be assigned to one part of a machine. This constraint prevents overlap.

$$6. \quad \sum_i y_{ijk} - y_{ij(k-1)} \leq 0, \quad \forall j, \text{sub}(k) \quad (7)$$

This constraint eliminates the problem of empty assignment by examining the relationship between parts of a machine.

$$7. \quad x_{ijk} * B_{ij} \leq K a_{ij} * y_{ijk}, \quad \forall i, j, k \quad (8)$$

This constraint indicates the relationship between x and y variables. If order i is produced by spending some time in machine j in part k , then y takes the value of 1 that product, machine, and part.

$$8. \quad y_{ijk} \in \{0,1\}, \quad \forall i, j, k \quad (9)$$

$$9. \quad x_{ijk} \geq 0, \quad \forall i, j, k \quad (10)$$

$$10. \quad \text{setup}_j \geq 0, \quad \forall j \quad (11)$$

$$11. \quad r_j \geq 0, \quad \forall j \quad (12)$$

Constraint 8, 9, 10, and 11 are variable definition constraints.

FINDINGS

The above model was solved by using CPLEX solver of the optimization software GAMS. The model is run for two weeks to compare with the intuitive schedule provided by production planning department. The orders and machine information are provided by the company for two-week schedule. After running the model for two weeks, the proposed schedule is given at Table 3. Table 3 illustrates the assignments of orders to machines with sorting. The ones that are highlighted with blue color represent the priority of the orders. In other words, the ones that are highlighted with blue color need to be processed as soon as possible rather than the white ones.

Table 3. A Division of the Schedule of Hot-Forging Unit for Two Weeks

Machine 1	Machine 2	Machine 3	Machine 4	Machine 5	Machine 6	Machine 7
A2-2797 (3.125h)	A2-904 (12.467h)	A2-6464 (14.981h)	A3-1991 (7.519h)	A2-3784 (4.615h)	A3-2610 (15.038h)	A2-2086 (4.615h)
A2-4271 (5.882h)	A2-7763 (20h)	A2-6464 (14.981h)	A2-3788 (7.143h)	A2-6297 (4.444h)	A2-6389 (10.526h)	A2-6537 (3.462h)
A2-473 (11.918h)	A2-7763 (20h)	A2-6464 (3.745h)	A2-5305 (7.353h)	A1-2128 (4h)	A2-1682 (6.5h)	A2-2257 (5.4545h)
A1-1007 (0.875h)	A2-7763 (20h)		A2-4385 (7.5h)	A2-4484 (2.25h)	A2-392 (24.815h)	A2-1940 (5.224h)
A2-2673 (5.376h)	A2-7763 (20h)		A2-3740 (7.692h)	A2-2172 (1.852h)	A2-5140 (0.893h)	A2-2478 (4h)
A2-7763 (20h)	A2-7763 (20h)		A2-3342 (7h)	A2-7112 (3.077h)	A2-6905 (6.875h)	A2-4263 (9.385h)
A2-7763 (20h)	A2-7763 (20h)		A2-3535 (0.885h)	A2-996 (10.448h)	A2-3757 (23.889h)	
A2-7763 (20h)	A2-7399 (19.893h)		A3-6963 (7.692h)	A1-5462 (2.2727h)	A2-7735 (6.596h)	
A2-7763 (20h)	A3-7112 (12.308h)		A3-1641 (7.143h)	A2-7481 (6.667h)	A2-998 (1.539h)	
A2-4332 (2h)	A3-7995 (7.692h)		A2-7200 (7.692h)	A2-3970 (2.778h)	A2-2475 (3.846h)	
A2-1278 (1.875h)	A3-2541 (5.385h)		A2-4609 (7.5h)	A2-3979 (2.857h)	A2-2390 (6.522h)	
A4-712 (11h)	A3-2597 (1.887h)		A2-4231 (7.857h)			
A2-1692 (5h)	A2-3516 (1.667h)		A2-4833 (7.5h)			
A2-1439 (5h)	A2-5055 (0.597h)		A3-3352 (7.519h)			
A4-461A (1.296h)			A2-865 (7.547h)			
A2-794 (0.75h)						
A2-2418 (0.926h)						
A3-3342 (1.075h)						

As long as the time spent for processing and changeover is shown in Table 4. As Table 4 is evaluated, it is seen that 747.279 hours is spent to meet the demands in total. 637.779 hours is the total working hours of machines without changeover time. In short, the machines totally work for 637.779 hours. In addition, 109.5 hours is spent for changeover. Apart from Machine 1 and 2, each machine has totally 150 hours because of operating 2 shifts, including both working and changeover time. Since Machine 1 and 2 are operated 3 shifts, the total time of these machines are 225 hours, indicated at the last row in Table 4.

Table 4. Total Time Spent for Processing and Changeover for Each Machine

	Machines (M)							
	M - 1	M - 2	M - 3	M - 4	M - 5	M - 6	M - 7	M - 8
Working Hours	176.099	144.97	33.71	105.54	31.74	116.44	29.28	637.779
Changeover Time	20	13	4.5	22.5	13.5	24	12	109.5
Total Time	196.099	157.97	38.21	128.04	45.24	140.44	41.28	747.279

As we compare our proposed mixed integer model with the intuitive schedule provided by production planning department, our model schedules the orders in 747.3 hours with changeover. The intuitive schedule provided by production planning department schedule the same orders in the same time period in 892.5 hours. So, on average, our model outperforms the current schedule around 19.4%.

CONCLUSION

Production planning is important in terms of meeting the optimum capacity and demands. Currently, many companies use intuitive methods for easy and fast decision making and cannot reach optimum values in terms of efficiency. Although the machine capacities were determined, no systematic program was used to use these capacities. Instead, the company employs a knowledgeable and experienced employee to do the plan and update when it is needed.

In the study, a mathematical model has been developed on order assignment to machines for the hot-upset forging unit which is one of the important parts of the factory. With this model, many criteria such as machines, production times, machine setting time have been taken into consideration. The model was written to meet the order as soon as possible and is coded with GAMS optimization tool.

Weekly scheduling for the actual order requirement of the factory was generated. The model has been updated and the result has been obtained in accordance with the priorities of the orders of the factory. A total of 747,279 hours of work plan was made in this sample, 109.5 hours of machine setting, and 637,779 hours were used to produce orders in machines. The results were evaluated by the relevant personnel of the company and the suitability of the appointments was approved. With the study done for the needs of the factory future studies will be carried out to use the model and program of the factory.

To sum up, scheduling in production line in DİTAŞ is done by headworkers, which means there is no professional approach in the production line. Therefore, having optimum production in an interval, like in a week, is a big question as long as efficiency of the production line is taken into consideration.

```
MIP Solution:          78.500000    (870162 iterations, 20614 nodes)
Final Solve:          78.500000    (0 iterations)

Best possible:        78.500000
Absolute gap:         0.000000
Relative gap:         0.000000
```

Figure 2. Objective Value for the Sample

In order to find the best assignments, we used optimization technique. We have written a mathematical model that minimizes total setup time and production time in Hot-up- set Forging Unit. After running the model on GAMS and receiving errors due to size of it, we chose a sample. Next, we applied the optimization technique to get results so that we could demonstrate GAMS, its input, and output. The reasons are to illustrate these to make sure that our model works correctly. After solving the model, it is seen that 78.5 hours of work could be completed within 11 hours, yet we do not know the current situation for the sample.

REFERENCES

- Allahverdi, A., & Soroush, H. M. (2008). The significance of reducing setup times/setup costs. *European Journal of Operational Research*, 187(3), 978-984.
- Behnamian, J., Zandieh, M., & Ghomi, S. F. (2009). Parallel-machine scheduling problems with sequence-dependent setup times using an ACO, SA and VNS hybrid algorithm. *Expert Systems with Applications*, 36(6), 9637-9644.
- Brauner, N., Finke, G., & Queyranne, M. (2014). *Production Planning*. In *Applications of Combinatorial Optimization: 2nd Edition* (Vol. 9781848216587, pp. 73-109). Wiley Blackwell.
- Cota, L.P., Coelho, V.N., Guimaraes, F. G., Bi-criteria formulation for green scheduling with unrelated parallel machines with sequence-dependent setup times, *International Transactions in Operational Research*, 28 (2), 996-1017, 2021.

**UNRELATED PARALLEL MACHINE SCHEDULING WITH SEQUENCE-DEPENDENT
SETUP TIMES: AN APPLICATION TO AUTOMOBILE SPARE PART
MANUFACTURER**

Fransoo, J. C., Wäfler, T., & Wilson, J. R. (2011). Behavioral Operations in Planning and Scheduling. *Behavioral Operations in Planning and Scheduling* (pp. 1-471). Springer Berlin Heidelberg.

Hax, A. C., & Meal, H. C. (1975). *Hierarchical Integration of Production Planning and Scheduling*. (M. Geisler, Ed.), Production (Vol. 1, Logisti, pp. 53-69). North Holland/Elsevier, New York.

Hsu, C.J., Kuo, W.H., Yang, D.L., Unrelated parallel machine scheduling with past sequence dependent setup times and learning effects, *Applied Mathematical Modelling*, 35, 1492-1496, 2011.

Kerzner, H. (2017). *Project management: a systems approach to planning, scheduling, and controlling*. 12th edition. John Wiley & Sons.

Kim, Y.H., Kim, R.S., Insertion of new idle time for unrelated parallel machine scheduling with job splitting and machine breakdowns, *Computers & Industrial Engineering*, 147, 2020.

Kreipl, S., & Pinedo, M. (2009). Planning and Scheduling in Supply Chains: An Overview of Issues in Practice. *Production and Operations Management*, 13(1), 77-92.

Kruse, C., Fieg, G., & Wozny, G. (1996). A New Time-Optimal Strategy for Column Startup and Product Changeover. *Journal of Process Control*, 6(2-3), 187-193.

Kuo, W.H., Hsu, C.J., Yang, D.L., Some unrelated parallel machine scheduling problems with past sequence dependent setup time and learning effects, *Computers & Industrial Engineering*, 61, 179-183, 2011.

Lei, D., Yuan, Y., Cai, J., An improved artificial bee colony for multi-objective distributed unrelated parallel machine scheduling, *International Journal of Production Research*, 2020.

Lin, S.W., Lu, C.C., Ying, K.C., Minimization of total tardiness on unrelated parallel machines with sequence and machine dependent setup times under due date constraints, *International Journal of Advanced Manufacturing Technology*, 53, 353-361, 2011.

Mauergauz, Y. (2016). *Advanced planning and scheduling in manufacturing and supply chains*. Springer.

Pinedo, M. L. (2009). *Project Planning and Scheduling. Planning and Scheduling in Manufacturing and Services*, 2, 53–81.

Pinedo, M. L. (2012). *Scheduling* (Vol. 29). New York: Springer.

Ruiz, R., & Allahverdi, A. (2007). No-Wait Flowshop with Separate Setup Times to Minimize Maximum Lateness. *International Journal of Advanced Manufacturing Technology*, 35(5–6), 551–565.

Stadtler, H. (2008). *Production Planning and Scheduling. In Supply Chain Management and Advanced Planning (Fourth Edition): Concepts, Models, Software, and Case Studies* (pp. 199–216). Springer Berlin Heidelberg.

Sütçü, M. (2022). Disutility Entropy in Multi-attribute Utility Analysis. *Computers & Industrial Engineering*, 169, 108189.

Tavakkoli-Moghaddam, R., Taheri, F., Bazzazi, M., Izadi, M., & Sassani, F. (2009). Design of a genetic algorithm for bi-objective unrelated parallel machines scheduling with sequence-dependent setup times and precedence constraints. *Computers & Operations Research*, 36(12), 3224–3230.

Yıldız, B., & Sütçü, M. (2022). A variant SDDP approach for periodic-review approximately optimal pricing of a slow-moving a item in a duopoly under price protection with end-of-life return and retail fixed markdown policy. *Expert Systems with Applications*, 118801.

**UNRELATED PARALLEL MACHINE SCHEDULING WITH SEQUENCE-DEPENDENT
SETUP TIMES: AN APPLICATION TO AUTOMOBILE SPARE PART
MANUFACTURER**

APPENDIX A

Gams Codes

```

OPTIONS RESLIM =18000,LIMROW =20,LIMCOL =0,DECIMALS=4,
        SYSOUT =ON,SOLPRINT=ON,LP=cplex,NLP=baron,MIP=cplex, MINLP=baron, OPTCR =0.0,
        OPTCA =0;

Set

i ürün /A2-2797, A2-4271, A2-473,A1-1007, A2-2673, A2-3516, A2-3535, A3-3342, A4-712, A4-461A, A2-1692,
A2-1278, A2-1439,A2-5055, A2-794, A2-2418, A2-4332, A2-6464, A2-904, A3-1991, A2-3788, A3-3352, A2-5305,
A2-4385,A2-3740,A2-3342,A2-4231, A2-4609,A3-6963,A3-1641,A2-4833,A2-7200, A2-865, A2-3784, A2-6297, A1-2128
A2-4484, A2-2172, A2-7112,A2-996, A1-5962, A2-3970, A2-3979, A2-7481, A2-7763,A2-7399, A3-7112, A3-7995,
A3-2541,A3-2597,A3-2610, A2-1682, A2-392, A2-5140, A2-6905, A2-3757, A2-998, A2-2390, A2-4263,A2-7735,
A2-2475, A2-6389,A2-2086, A2-6537, A2-2257,A2-1940, A2-2478/
j tezgah /RUS, Manzoni, D60, Beche, D3, D1, D58/
k kysym /1*30/
sub(k) /2*30/
;
    
```

```

Parameters

A(i) sipariş adedi
/
A2-2797 100
A2-4271 100
A2-473 870
A1-1007 70
A2-2673 500
A2-3516 100
A2-3535 100
A3-3342 100
A4-712 440
A4-461A 35
A2-1692 200
A2-1278 15
A2-1439 100
A2-5055 40
A2-794 15
A2-2418 25
A2-4332 40
A2-6464 9000
A2-904 2830
A3-1991 1000
A2-3788 50
A3-3352 1000
A2-5305 125
A2-4385 1950
A2-3740 100
A2-3342 35
A2-4231 55
A2-4609 45
A3-6963 100
A3-1641 50
A2-4833 15
A2-7200 100
A2-865 400
A2-3784 60
A2-6297 40
A1-2128 20
A2-4484 18
    
```

*Muhammed SÜTÇÜ, İbrahim Tümay GÜLBAHAR, Yakup KAPAR,
Fatih İNCE, Nurettin ŞAHİN*

A2-4484	18
A2-2172	50
A2-7112	40
A2-996	700
A1-5462	50
A2-3970	25
A2-3979	20
A2-7481	180
A2-7763	20000
A2-7399	1850
A3-7112	160
A3-7995	100
A3-2541	70
A3-2597	100
A3-2610	2000
A2-1682	650
A2-392	670
A2-5140	25
A2-6905	55
A2-3757	430
A2-998	20
A2-2390	150
A2-4263	122
A2-7735	310
A2-2475	50
A2-6389	1400
A2-2086	60
A2-6537	45
A2-2257	180
A2-1940	350
A2-2478	80
/	

C(j) tezgah ayar süresi (saat)	
/	
D1	1.5
D3	1.5
D60	1
Manzoni	2
Rus	2
Beche	1.5
D58	1
/	
Working(j)	
/	
D1	150
D3	150
D60	225
Manzoni	150
Rus	150
Beche	150
D58	225
/	

**UNRELATED PARALLEL MACHINE SCHEDULING WITH SEQUENCE-DEPENDENT
SETUP TIMES: AN APPLICATION TO AUTOMOBILE SPARE PART
MANUFACTURER**

Table Ka (i, j)							
	D58	D1	D60	D3	Beche	RUS	Manzoni
A2-2797	4000						
A2-4271	4000						
A2-473	4000						
A1-1007	4000						
A2-2673	4000						
A2-3516	4000		4000				
A2-3535	4000			4000			
A3-3342	4000						
A4-712	4000						
A4-461A	4000						
A2-1692	4000						
A2-1278	4000						
A2-1439	4000						
A2-5055	4000		4000				
A2-794	4000						
A2-2418	4000						
A2-4332	4000						
A2-6464		4000					
A2-904			4000	4000			
A3-1991			4000	4000			
A2-3788				4000			
A3-3352				4000			
A2-5305				4000			
A2-4385				4000			
A2-3740				4000			
A2-3342				4000			
A2-4231				4000			
A2-4609				4000			
A3-6963				4000			
A3-1641				4000			
A2-4833				4000			
A2-7200				4000			
A2-865				4000			
A2-3784					2500		
A2-6297					2500		
A1-2128					2500		
A2-4484					2500		
A2-2172					2500		
A2-7112			2500		2500		
A2-996					2500	2500	2500
A1-5462					2500		
A2-3970					2500		
A2-3979					2500		
A2-7481					2500		
A2-7763	2000		2000				
A2-7399			4000				
A3-7112			4000				
A3-7995			4000				
A3-2541			4000				
A3-2597			4000				
A3-2610							4000
A2-1682							4000
A2-392							4000
A2-5140							4000
A2-6905							4000
A2-3757						4000	4000
A2-998						4000	4000
A2-2390						4000	4000
A2-4263						4000	4000
A2-7735							4000
A2-2475							4000
A2-6389						4000	4000
A2-2086						4000	4000
A2-6537						4000	4000
A2-2257						4000	4000
A2-1940						4000	4000
A2-2478						4000	4000

**Muhammed SÜTÇÜ, İbrahim Tümay GÜLBAHAR, Yakup KAPAR,
Fatih İNCE, Nurettin ŞAHİN**

Table B(i, j)							
	D58	D1	D60	D3	Beche	RUS	Manzoni
A2-2797	32						
A2-4271	17						
A2-473	73						
A1-1007	80						
A2-2673	93						
A2-3516	53		60				
A2-3535	15			113			
A3-3342	93						
A4-712	40						
A4-461A	27						
A2-1692	40						
A2-1278	8						
A2-1439	20						
A2-5055	67		67				
A2-794	20						
A2-2418	27						
A2-4332	20						
A2-6464		267					
A2-904			227	133			
A3-1991			93	133			
A2-3788				7			
A3-3352				133			
A2-5305				17			
A2-4385				260			
A2-3740			93	13			
A2-3342				5			
A2-4231				7			
A2-4609				6			
A3-6963				13			
A3-1641				7			
A2-4833				2			
A2-7200				13			
A2-865				53			
A2-3784				13			
A2-6297				9			
A1-2128				5			
A2-4484				8			
A2-2172				27			
A2-7112		13		13			
A2-996				67	67	107	
A1-5462				22			
A2-3970				9			
A2-3979				7			
A2-7481				27			
A2-7763	100						
A2-7399		100					
A3-7112		93					
A3-7995		13					
A3-2541		13					
A3-2597		53					
A3-2610						133	
A2-1682		100				100	
A2-392						27	
A2-5140						28	
A2-6905						8	
A2-3757					13	18	
A2-998						13	
A2-2390					23	23	
A2-4263					13	13	
A2-7735						47	
A2-2475						13	
A2-6389					53	133	
A2-2086					13		
A2-6537					13		
A2-2257					33		
A2-1940					67		
A2-2478					20		
;							

**UNRELATED PARALLEL MACHINE SCHEDULING WITH SEQUENCE-DEPENDENT
SETUP TIMES: AN APPLICATION TO AUTOMOBILE SPARE PART
MANUFACTURER**

```

Variables
z
Binary Variable y(i,j,k);
Positive Variable x(i,j,k), tpi(i), tpj(j), tpijk(i,j,k), setup(j);

Equations

obj
atama          ayný tezagaha ayný saatte tek úrún atanması

sip           sipariş karbýlama

c4
c5
c6
c7
c8
c9
c10
;

obj..          z=e= sum(j, tpj(j) + setup(j));
atama(j,k)..  sum(i, y(i,j,k)) =l= 1;
c4(sub(k),j).. sum(i, y(i,j,k)- y(i,j,k-1)) =l= 0;
sip(i)..      A(i) =E= sum((j,k), x(i,j,k)*B(i,j));
c5(j)..      sum((i,k), x(i,j,k)) + sum((i,k), y(i,j,k)*C(j)) =L= Working(j);
c8(i,j,k)..  x(i,j,k)*B(i,j) =L= Ka(i,j)*y(i,j,k);
c6(i)..      tpi(i) =E= sum((j,k), x(i,j,k)*B(i,j));
c7(j)..      tpj(j) =E= sum((i,k), x(i,j,k));
c9(i,j,k)..  tpijk(i,j,k) =E= x(i,j,k)*B(i,j);
c10(j)..     setup(j) =E= sum((i,k), y(i,j,k)*C(j));

Model ditasdovme      /all/;

Solve ditasdovme using mip minimizing z;

Display z.l, x.l, y.l, tpi.l, tpj.l, setup.l, tpijk.l;

```

FUNDAMENTALS OF THE NEW CALCULATION METHOD OF THE HYDRODYNAMIC JOURNAL BEARINGS

Hüseyn MIRZAYEV¹

Abstract: Work is dedicated an estimation of the loading and resistance factors for journal bearings. It is established analytical dependence for a quantitative estimation of the loading and resistance factors. Schedules of dependence graphs of the angles of position, loading and resistance factors on relative eccentricity. The worked out method of calculation enables to choose the most efficient lubricant for a journal bearing under the given constructive and technological parameters what is of great practical importance in stage of design a new equipment. The work deals with analysis of an action regime of the bearing, motion trajectory of the journal in the bearing and hydrodynamic pressure distribution on the oil film. I have obtained the formulas of the angles characterizing arrangement of journal center relative to bearing. When eccentricity ratio (ϵ) changes in the interval [0; 1] the angle of position of the maximum film pressure symmetrical with the angle of position of the film thickness end, relative the eccentricity ratio $\epsilon = 0.5$. According to this hypothesis the analytical formulas for loading factor of the bearing (Sommerfeld number- S_o) and resistance factor of the rotation (ξ) are obtained and new calculation method of the hydrodynamic journal bearings have been worked out.

Keywords: Sliding Bearing, Journal Bearing, Hydrodynamic Bearing, Reynolds Equation, Loading Factor, Bearing Force, New Calculation Method

¹ Baku Engineering University, Mechanical Engineering Department, Baku, Khirdalan, Azerbaijan.
e-mail: humirzeyev@beu.edu.az, Orcid No 0000-0002-1977-3914

INTRODUCTION

The journal bearings are used in the constructions as a support of rotating axles and shafts in which an application of rolling bearings finds difficulty or is inadmissible for some reasons: high rotational speed, impact and vibratory loads; necessity of making diametral joint; operation in water and corrosive medium; an increase of requirements to accuracy and stability of the shaft's position; ensuring the energy-resources economy and etc. (Dwight G.B., 1983).

A number of shortcomings are typical for journal bearings as well, in particular, heavily loaded bearings $d=(140\div 1200)$ mm, with relative clearance $\varepsilon=0,0003\div 0,002$; $l/d=0,6\div 0,9$, operating at high rotational speed, in the range of relative velocities of sliding from 0,2 to 60 m/sec. need in formation of a wedge clearance between sliding surfaces; in positive supply of a lubricant of corresponding viscosity into wedge clearance; in generation of pressure ($p=5\div 25$ N/mm²) able of balancing external loading. Simultaneously, for maintaining the condition of fluid friction, removal of generated heat from zone of contact of a shaft and insert is of great importance.

Nevertheless, for constructive and economic reasons the journal bearings find a wide application in axle-box units of carriages in the supports of internal combustion engines, steam and gas turbines, rolling-mills, metal-cutting and wood-working machines, heavy reducers, centrifugal pumps, centrifuges and oth.

In the present work the specified calculation of journal bearings with use of analytic expressions of the loading and resistance factors is presented, a new methodological approach to creation of these mechanical systems with regard for features of the various machines and aggregates is considered.

THE INFINITELY LONG JOURNAL BEARING THEORY

The calculation of hydrodynamic bearings is based on the hydrodynamic theory of lubrication. The basic equation of hydrodynamics is taken as a basis for deriving the formulas that determine the load-carrying capacity and hydrodynamic pressure of the oil layer between the journal and the bearing.

Fig. 1 shows the surface elements of the shaft journal and the bearing separated from each other by the oil layer.

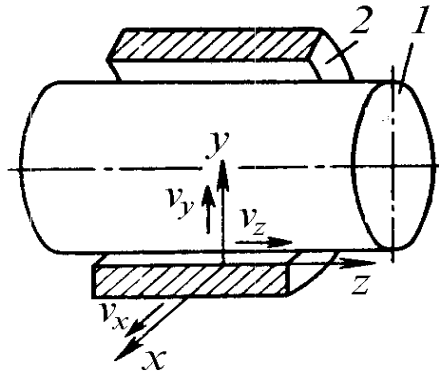


Figure. 1. Elements of the Surfaces of the Shaft Journal and Bearing Separated by A Layer of Oil

To determine the pressure generated in the oil layer, the generalized Reynolds equation written for any non-stationary case is used:

$$\frac{\partial}{\partial x} \left(h^3 \frac{\rho}{\mu} \frac{\partial p}{\partial x} \right) + \frac{\partial}{\partial z} \left(h^3 \frac{\rho}{\mu} \frac{\partial p}{\partial z} \right) = 12\rho v_x + 6 \frac{\partial}{\partial x} (\rho v_y h) + 6 \frac{\partial}{\partial z} (\rho v_z h) + 12h \frac{\partial p}{\partial z}, \quad (1)$$

This equation is written for any unsteady state of a viscous, compressible fluid. That is, the viscosity and density of the oil is not constant, it depends on the pressure, temperature and coordinates of the viewed point. In this case, the solution of equation (1) becomes extremely complicated. Therefore, solving the issue of the load-carrying capacity and

friction losses of sliding bearings in the fluid friction regime, as well as the distribution of hydrodynamic pressure, is associated with great difficulties. *To solve this problem, applying equation (1) to a normal cylindrical sleeve or bearing, the following simplifying conditions are accepted:*

1. *The load affecting the shaft is constant in value and direction: $F_r = \text{const}$;*
2. *The temperature and density of the lubricant are constant. $t = \text{const}$, $\rho = \text{const}$. In this case $\frac{\partial p}{\partial t} = 0$, the last part of the equation (1) loses its meaning, and the density (ρ) can be removed from both sides of the equation;*
3. *For the fixed operating mode of the journal at a constant rotation speed, the peripheral speed in the direction of the x axis is constant: $v_x = \text{const}$;*
4. *Then the eccentricity is considered constant: $e = \text{const}$;*
5. *Longitudinal and transverse displacement is excluded. Then the speed in the direction of the y axis can be taken as zero: $v_y = 0$;*
6. *The oil flow rate along the z -axis from the edges of the pad is much lower than in the direction of rotation, so $v_z = 0$ can be assumed as a first approximation. In other words, the size of the oil layer is not limited in the direction of the shaft axis: (infinitely long bearing $l = \infty$). Exclusion of external flow of oil from edges of bearing leads to planar flow;*
7. *The oil is a Newtonian oil, meaning that the pressure at any point is independent of direction, while the shear stress is proportional to the velocity gradient. Thus, oil viscosity is generally a function of temperature and pressure;*
8. *Surface layer structure and properties do not affect the adhesion of oil, its speed at the contacting surfaces is equal to the speed of these surfaces;*
9. *The movement of oil in the friction zone is laminar;*
10. *Due to the fact that the thickness of the oil layer along the y -axis is very small compared to its dimensions along the x - and z -axes, its curvature, the effect of gravity and inertial forces, capillarity properties and the variation of pressure across the thickness of the oil layer can be neglected;*

11. It is assumed that the working surfaces of the shaft and the insert are ideally smooth, and these structural elements are right circular cylinders with parallel axes.

These numbered conditions mathematically can be written as follows:

$$(2) \left\{ \begin{array}{l} F_r = \text{const}; t = \text{const}; \rho = \text{const}; \frac{\partial p}{\partial t} = 0; \mu = \text{const}; v_x = \text{const}; v_y = 0; \\ v_z = 0; \frac{\partial p}{\partial z} = 0; \tau = \mu \frac{\partial v}{\partial h}; \end{array} \right.$$

1. Derivation of the Basic Equation of Hydrodynamics

Let us look to the parallelepiped with sides of dx, dy, dz cutting off from the fluid flow moving in the working zone of the sliding bearing (Fig. 2, a).

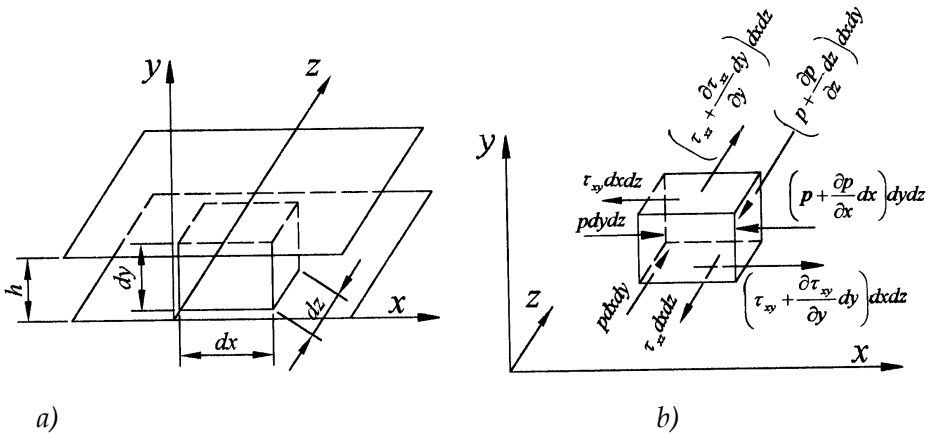


Figure 2. Elementary Parallelepiped Taking off from Oil Layer

Let's write the balance equations of the forces acting on the parallelepiped:

- from the forces acting in the x axis direction

$$\begin{aligned} \sum x &= p dydz - \tau_{xy} dx dz - \left(p + \frac{\partial p}{\partial x} dx \right) dy dz + \left(\tau_{xy} + \frac{\partial \tau_{xy}}{\partial y} dy \right) dx dz = \\ &= p dydz - \tau_{xy} dx dz - p dydz - \frac{\partial p}{\partial x} dx dy dz + \tau_{xy} dx dz + \frac{\partial \tau_{xy}}{\partial y} dx dy dz - \frac{\partial \tau_{xy}}{\partial y} dx dy dz - \frac{\partial p}{\partial x} dx dy dz = 0 \end{aligned}$$

If both sides of the equation divide by the product of $dx dy dz$, we write:

$$\sum x = \frac{\partial \tau_{xy}}{\partial y} - \frac{\partial p}{\partial x} = 0 \quad (1.1)$$

- from the forces acting in the y axis direction

$$\begin{aligned} \sum z &= p dx dy - \tau_{xz} dx dz + \left(\tau_{xz} + \frac{\partial \tau_{xz}}{\partial y} dy \right) dx dz - \left(p + \frac{\partial p}{\partial z} dz \right) dx dy = \\ &= p dx dy - \tau_{xz} dx dz + \tau_{xz} dx dz + \frac{\partial \tau_{xz}}{\partial y} dx dy dz - p dx dy - \frac{\partial p}{\partial z} dx dy dz = \frac{\partial \tau_{xz}}{\partial y} dx dy dz - \frac{\partial p}{\partial z} dx dy dz = 0 \end{aligned}$$

$$\sum z = \frac{\partial \tau_{xz}}{\partial y} - \frac{\partial p}{\partial z} = 0 \quad (1.2)$$

where

p is hydrodynamic pressure;

τ is the sliding resistance force of a viscous liquid.

According to Newton's law, we can write:

$$\tau_{xy} = \mu \frac{\partial v_x}{\partial y} \quad (1.3)$$

$$\tau_{xz} = \mu \frac{\partial v_z}{\partial y} \quad (1.4)$$

Consider (1.3) in (1.1) and (1.4) in (1.2)

$$\frac{\partial}{\partial y} \left(\mu \frac{\partial v_x}{\partial y} \right) = \frac{\partial p}{\partial x} \quad (1.5)$$

$$\frac{\partial}{\partial y} \left(\mu \frac{\partial v_z}{\partial y} \right) = \frac{\partial p}{\partial z} \quad (1.6)$$

Since the temperature changes very little at different points of the oil layer, and the pressure is generally small, it is possible to take its average value instead of the calculation value of the viscosity with some error. Then, dividing each side of equations (1.5) and (1.6) by μ , it can be written as follows:

$$\frac{\partial^2 v_x}{\partial y^2} = \frac{1}{\mu} \frac{\partial p}{\partial x} \quad (1.7)$$

$$\frac{\partial^2 v_z}{\partial y^2} = \frac{1}{\mu} \frac{\partial p}{\partial z} \quad (1.8)$$

Let's double integrate these equations.

Equation (1.7), first integration

$$\frac{\partial v_x}{\partial y} = y \frac{1}{\mu} \frac{\partial p}{\partial x} + C_1, \quad (1.9)$$

second integration

$$v_x = \frac{y^2}{2} \frac{1}{\mu} \frac{\partial p}{\partial x} + C_1 y + C_2. \quad (1.10)$$

Now let's double integrate equation (1.8):

first integration

$$\frac{\partial v_z}{\partial y} = y \frac{1}{\mu} \frac{\partial p}{\partial z} + C_3, \quad (1.11)$$

second integration

$$v_z = \frac{y^2}{2} \frac{1}{\mu} \frac{\partial p}{\partial z} + C_3 y + C_4. \quad (1.12)$$

Let's assume the following boundary conditions:

1) on a stationary surface $y = 0; v_x = 0; v_z = 0$

2) on a moving surface $y = h; v_x = v; v_z = 0$

Considering the first boundary condition in (1.10) and (1.12), we can find

$$C_2 = 0 \quad (1.13)$$

$$C_4 = 0 \quad (1.14)$$

consider the second boundary condition in (1.10) and (1.12).

$$v = \frac{h^2}{2} \frac{1}{\mu} \frac{\partial p}{\partial x} + C_1 \cdot h + C_2 \quad (1.15)$$

$$0 = \frac{h^2}{2} \frac{1}{\mu} \frac{\partial p}{\partial z} + C_3 \cdot h + C_4 \quad (1.16)$$

Consider (1.13) in (1.15).

$$v = \frac{h^2}{2} \frac{1}{\mu} \frac{\partial p}{\partial x} + C_1 \cdot h + 0$$

from here we find the first integral constant

$$C_1 = \frac{v}{h} - \frac{h}{2} \frac{1}{\mu} \frac{\partial p}{\partial x} \quad (1.17)$$

Correspondingly, writing (1.14) into (1.16), the third integral constant is found

$$C_3 = -\frac{h}{2} \frac{1}{\mu} \frac{\partial p}{\partial z} \quad (1.18)$$

Considering (1.13) and (1.17) in (1.10), let's simplify the expression

$$v_x = \frac{y^2}{2} \frac{1}{\mu} \frac{\partial p}{\partial x} + \left(\frac{v}{h} - \frac{h}{2} \frac{1}{\mu} \frac{\partial p}{\partial x} \right) \cdot y + 0 = \frac{y^2}{2} \frac{1}{\mu} \frac{\partial p}{\partial x} + \frac{v}{h} y - \frac{h y}{2} \frac{1}{\mu} \frac{\partial p}{\partial x} = \frac{v}{h} y + \frac{y}{2\mu} (y-h) \frac{\partial p}{\partial x}$$

Thus,

$$v_x = \frac{v}{h} y + \frac{y}{2\mu} (y-h) \frac{\partial p}{\partial x}. \quad (1.19)$$

Now consider (1.14) and (1.18) in (1.12) and simplify the expression

$$v_z = \frac{y^2}{2} \frac{1}{\mu} \frac{\partial p}{\partial z} - \frac{h y}{2 \mu} \frac{\partial p}{\partial z} + 0 = \frac{y}{2\mu} (y-h) \frac{\partial p}{\partial z}$$

$$v_z = \frac{y}{2\mu} (y-h) \frac{\partial p}{\partial z} \quad (1.20)$$

Due to the condition that the oil layer does not break, the amount of liquid flowing from the sides of the viewed parallelepiped at the same time should be the same (Figure 1.2).

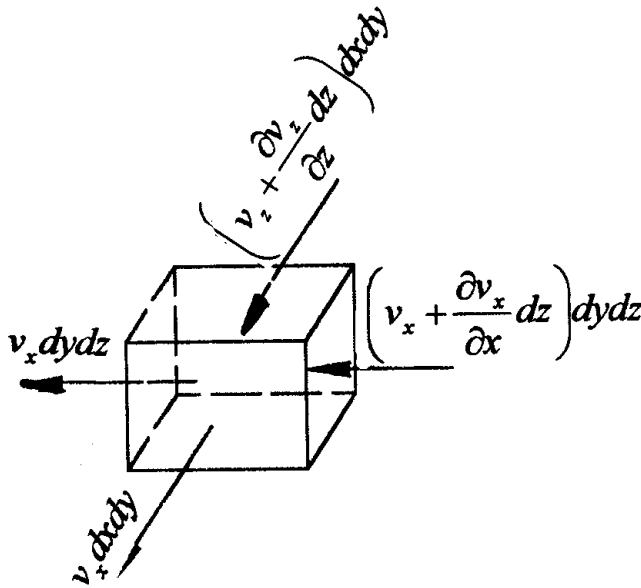


Figure 3. The Element of Oil

The corresponding volume can be written taking into account the signs:

$$\begin{aligned} & \left(v_x + \frac{\partial v_x}{\partial x} dx \right) dydz - v_x dydz + \left(v_x + \frac{\partial v_z}{\partial z} dz \right) dx dy - v_z dx dy = \\ & = v_x dydz + \frac{\partial v_x}{\partial x} dx dy dz - v_x dydz + v_z dx dy + \frac{\partial v_z}{\partial z} dx dy dz - v_z dx dy = \frac{\partial v_x}{\partial x} dx dy dz + \frac{\partial v_z}{\partial z} dx dy dz = 0 \end{aligned}$$

Thus, by dividing the equation by the product $dx dy dz$, we get

$$\frac{\partial v_x}{\partial x} + \frac{\partial v_z}{\partial z} = 0 \quad (1.21)$$

(1.21) can be written as follows, taking the flow rate W_x and W_z of the fluid flowing through the gap of unit width and height h in the direction of the x and z axes in a unit time:

$$\frac{\partial W_x}{\partial x} + \frac{\partial W_z}{\partial z} = 0 \quad (1.22)$$

Consumption of liquid flowing in x -axis direction W_x (1.19), flow rate W_z of the fluid flowing in the direction of the z axis and can be found taking into account (1.20):

$$W_x = \int_0^h v_x dy \quad (1.23)$$

$$W_z = \int_0^h v_z dy \quad (1.24)$$

Let's write (1.19) in (1.23) and open the integral

$$\begin{aligned} W_x &= \int_0^h \left(v \frac{y}{h} + \frac{y}{2\mu} (y-h) \frac{\partial p}{\partial x} \right) dy = \int_0^h v \frac{y}{h} dy + \int_0^h \frac{1}{2\mu} \frac{\partial p}{\partial x} y(y-h) dy = \frac{v}{h} \int_0^h y dy + \frac{1}{2\mu} \frac{\partial p}{\partial x} \int_0^h y(y-h) dy = \\ &= \frac{v}{h} \int_0^h y dy + \frac{1}{2\mu} \frac{\partial p}{\partial x} \int_0^h (y^2 - yh) dy = \frac{v}{h} \int_0^h y dy + \frac{1}{2\mu} \frac{\partial p}{\partial x} \left(\int_0^h y^2 dy - \int_0^h y h dy \right) = \\ &= \frac{v}{h} \frac{y^2}{2} \Big|_0^h + \frac{1}{2\mu} \frac{\partial p}{\partial x} \left(\frac{y^3}{3} \Big|_0^h - h \frac{y^2}{2} \Big|_0^h \right) = \frac{vh}{2} + \frac{1}{2\mu} \frac{\partial p}{\partial x} \left(\frac{h^3}{3} - \frac{h^3}{2} \right) = \frac{vh}{2} - \frac{1}{2\mu} \frac{\partial p}{\partial x} \frac{h^3}{6} \end{aligned}$$

Thus,

$$W_x = \frac{vh}{2} - \frac{h^3}{12\mu} \frac{\partial p}{\partial x} \quad (1.25)$$

Now, considering (1.20) in (1.24), let us open this integral:

$$\begin{aligned} W_z &= \int_0^h \left(\frac{y}{2\mu} (y-h) \frac{\partial p}{\partial z} \right) dy = \frac{1}{2\mu} \frac{\partial p}{\partial z} \int_0^h (y(y-h)) dy = \frac{1}{2\mu} \frac{\partial p}{\partial z} \int_0^h (y^2 - yh) dy = \frac{1}{2\mu} \frac{\partial p}{\partial z} \left(\int_0^h y^2 dy - \int_0^h y h dy \right) = \\ &= \frac{1}{2\mu} \frac{\partial p}{\partial z} \left(\frac{y^3}{3} \Big|_0^h - h \frac{y^2}{2} \Big|_0^h \right) = \frac{1}{2\mu} \frac{\partial p}{\partial z} \left(\frac{h^3}{3} - \frac{h^3}{2} \right) = -\frac{1}{2\mu} \frac{\partial p}{\partial z} \frac{h^3}{6} \end{aligned}$$

Thus,

$$W_z = -\frac{h^3}{12\mu} \frac{\partial p}{\partial z}. \quad (1.26)$$

Let us differentiate the equation (1.25).

$$\frac{\partial W_x}{\partial x} = \frac{v}{2} \frac{\partial h}{\partial x} - \frac{\partial}{\partial x} \left(\frac{h^3}{12\mu} \frac{\partial p}{\partial x} \right) \quad (1.27)$$

Let us also differentiate the equation (1.26).

$$\frac{\partial W_z}{\partial z} = \frac{\partial}{\partial z} \left(-\frac{h^3}{12\mu} \frac{\partial p}{\partial z} \right) \quad (1.28)$$

Considering equations (1.27) and (1.28) in (1.22), let's simplify:

$$\frac{v}{2} \frac{\partial h}{\partial x} - \frac{\partial}{\partial x} \left(\frac{h^3}{12\mu} \frac{\partial p}{\partial x} \right) - \frac{\partial}{\partial z} \left(\frac{h^3}{12\mu} \frac{\partial p}{\partial z} \right) = \frac{v}{2} \frac{\partial h}{\partial x} - \frac{1}{12\mu} \frac{\partial}{\partial x} \left(h^3 \frac{\partial p}{\partial x} \right) - \frac{1}{12\mu} \frac{\partial}{\partial z} \left(h^3 \frac{\partial p}{\partial z} \right) = 0$$

both sides of the last expression by (-12μ) :

$$-6\mu v \frac{\partial h}{\partial x} + \frac{\partial}{\partial x} \left(h^3 \frac{\partial p}{\partial x} \right) + \frac{\partial}{\partial z} \left(h^3 \frac{\partial p}{\partial z} \right) = 0 \quad (1.29)$$

This equation is called the basic equation of hydrodynamics - Osborn Reynolds equation. It is convenient to write it in the following way:

$$\frac{\partial}{\partial x} \left(h^3 \frac{\partial p}{\partial x} \right) + \frac{\partial}{\partial z} \left(h^3 \frac{\partial p}{\partial z} \right) - 6\mu v \frac{\partial h}{\partial x} = 0 \quad (1.30)$$

2. Determination of Hydrodynamic Pressure According to an Arbitrary Angle

Accepting the equation (1.30) , let's write in cylindrical coordinates: $\partial x = r \partial \varphi$

$$\frac{\partial}{r \partial \varphi} \left(h^3 \frac{\partial p}{r \partial \varphi} \right) + \frac{\partial}{\partial z} \left(h^3 \frac{\partial p}{\partial z} \right) - 6\nu\mu \frac{\partial h}{r \partial \varphi} = 0, \quad (2.1)$$

$$\frac{1}{r^2} \frac{\partial}{\partial \varphi} \left(h^3 \frac{\partial p}{\partial \varphi} \right) + \frac{\partial}{\partial z} \left(h^3 \frac{\partial p}{\partial z} \right) - 6\nu\mu \frac{v}{r} \frac{\partial h}{\partial \varphi} = 0, \quad (2.2)$$

where r is the radius of the journal.

Multiplying both sides of the equation (2.2) to r^2 :

$$\frac{\partial}{\partial \varphi} \left(h^3 \frac{\partial p}{\partial \varphi} \right) + \frac{\partial}{\partial z} \left(h^3 \frac{\partial p}{\partial z} \right) \cdot r^2 - 6\nu\mu v r \frac{\partial h}{\partial \varphi} = 0. \quad (2.3)$$

Reynolds equation written in this way $\frac{\partial p}{\partial z} = 0$, when integrated for an infinitely long bearing in the plane of oil motion, the equation and its integral become:

$$\frac{d}{d\varphi} \left(h^3 \frac{dp}{d\varphi} \right) - 6\mu\nu r \frac{dh}{d\varphi} = 0, \quad (2.4)$$

$$\frac{d}{d\varphi} \left(h^3 \frac{dp}{d\varphi} \right) = 6\mu\nu r \frac{dh}{d\varphi}, \quad (2.5)$$

$$h^3 \frac{dp}{d\varphi} = 6\mu\nu r h + C \quad (2.6)$$

The integral constant C can be found under the following conditions:

- in some value of the angle is $\varphi = \varphi_m$;
- at this time, the thickness of the oil layer is $h_{\varphi} = h_m$;
- and also $\frac{dp}{d\varphi} = 0$, correspondingly.

then it $C = -6\mu vr h_m$ is taken. Consider this equation in expression (2.6):

$$h^3 \frac{dp}{d\varphi} = 6\mu vr h - 6\mu vr h_m \text{ simplifying} \quad \text{divide}$$

$$h^3 \frac{dp}{d\varphi} = 6\mu vr (h - h_m) \text{ both sides by } h^3:$$

$$\frac{dp}{d\varphi} = 6\mu vr \frac{(h - h_m)}{h^3} \quad (2.7)$$

the thickness of the oil layer at any angle (φ) according to figure 2.1:

$$h = R - r \cos \gamma - e \cos(180^\circ - \varphi) \quad (2.8)$$

where R and r are the radii of the bearing and the journal, correspondingly; e - is eccentricity.

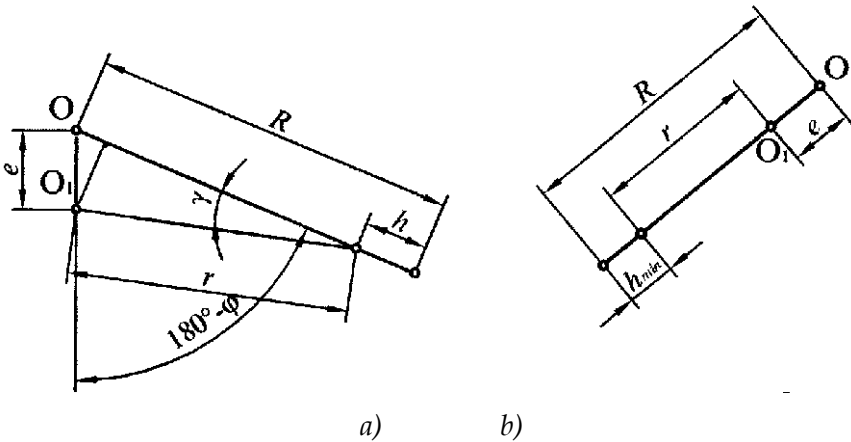


Figure 4. Determination of the Thickness of the Oil Layer

$\cos(\gamma) = 1$ due to the smallness of the angle (γ), the expression (2.8) will be simplified:

$$h = R - r + e \cos \varphi \quad (2.9)$$

$R - r = \delta$ and $e = \varepsilon \delta$ considering that

$$h = \delta + \delta \varepsilon \cos \varphi$$

thus

$$h = \delta(1 + \varepsilon \cos \varphi) \quad (2.10)$$

The minimum thickness of the oil layer occurs when $\varphi=180^\circ$ on the center line (Fig. 4, *b*):

$$h_{\min} = \delta(1 - \varepsilon) \quad (2.11)$$

the section with maximum pressure, φ the thickness of the oil layer at the angle = φ_m :

$$h_m = \delta(1 + \varepsilon \cos \varphi_m) \quad (2.12)$$

Let's write expressions (2.10) and (2.12) in (2.7):

$$\begin{aligned} \frac{dp}{d\varphi} &= 6\mu v r \frac{\delta(1 + \varepsilon \cos \varphi) - \delta(1 + \varepsilon \cos \varphi_m)}{\delta^3(1 + \varepsilon \cos \varphi)^3} = 6\mu v r \frac{\delta(1 + \varepsilon \cos \varphi - 1 - \varepsilon \cos \varphi_m)}{\delta^3(1 + \varepsilon \cos \varphi)^3} = \\ &= 6\mu v r \frac{\varepsilon \cos \varphi - \varepsilon \cos \varphi_m}{\delta^2(1 + \varepsilon \cos \varphi)^3} \end{aligned}$$

considering that $v = \omega r$ and $\delta = \psi r$

$$\begin{aligned} \frac{dp}{d\varphi} &= 6\mu v \omega r^2 \frac{\varepsilon(\cos \varphi - \cos \varphi_m)}{\psi^2 r^2 (1 + \varepsilon \cos \varphi)^3} \\ \frac{dp}{d\varphi} &= 6 \frac{\mu \omega}{\psi^2} \cdot \frac{\varepsilon(\cos \varphi - \cos \varphi_m)}{(1 + \varepsilon \cos \varphi)^3} \quad (2.13) \end{aligned}$$

To find the pressure in any section defined by the angle (φ), it is necessary to integrate the expression (2.13) along the arc from the beginning of the working zone:

$$p(\varphi) = 6 \frac{\mu \omega}{\psi^2} \int_{\varphi_1}^{\varphi_2} \frac{\varepsilon(\cos \varphi - \cos \varphi_m)}{(1 + \varepsilon \cos \varphi)^3} d\varphi \quad (2.14)$$

DETERMINATION of the SHEAR STRESS in the FLUID

The resistance to movement in the fluid friction regime is caused by the internal friction between the oil particles due to the viscosity of the lubricating material. According to Newton's law, the shear stress in the fluid is proportional to the rate of change of the velocity with respect to h :

$$\tau = \mu \frac{dv}{dh}. \quad (3.1)$$

If we apply this equation written for the movement of fluid between parallel infinite planes to a sliding friction bearing, we can write the shear stress on the surface of the for the working zone as follows:

$$\tau(\varphi) = \mu \left| \frac{dv_\tau}{dr} \right|, \quad (3.2)$$

where μ is oil dynamic viscosity; v_τ is speed of movement of liquid particles; r is the radius of the shaft journal.

Let's write the expression (1.19) as follows

$$v_x = \frac{v}{h} y + \frac{1}{2\mu} (y^2 - hy) \frac{dp}{dx} \quad (3.3)$$

us differentiate this expression with respect to y

$$\left(\frac{v}{h} y \right)' = \frac{v}{h} \text{ and } (y^2 - hy)' = 2y - h$$

Then we can write (3.3) as follows

$$\begin{aligned} \frac{dv_x}{dy} &= \frac{v}{h} + \frac{1}{2\mu} \frac{dp}{dx} (2y - h) \text{ or} \\ \frac{dv_x}{dy} &= \frac{v}{h} + \frac{y}{\mu} \frac{dp}{dx} - \frac{h}{2\mu} \frac{dp}{dx} \end{aligned} \quad (3.4)$$

where v is the circular velocity of the journal; h is the thickness of the oil layer.

Expression (3.4) in (1.3). consider if we get

$$\tau = \mu \frac{U}{h} + y \frac{dp}{dx} - \frac{h}{2} \frac{dp}{dx}$$

$y = h$ for the boundary condition

$$\tau = \mu \frac{U}{h} + h \frac{dp}{dx} - \frac{h}{2} \frac{dp}{dx} \text{ or } \tau = \mu \frac{U}{h} + \frac{h}{2} \frac{dp}{dx}$$

$v = \frac{\omega d}{2}$ and $dx = r d\varphi$ considering that in the last equation in polar coordinate:

$$\tau(\varphi) = \mu \frac{\omega d}{2h} + \frac{h}{2r} \frac{dp}{d\varphi}$$

last in Eq $2r = d$ substitution if we take we get :

$$\tau(\varphi) = \mu \frac{\omega d}{2h} + \frac{h}{d} \frac{dp}{d\varphi} \tag{3.5}$$

Consider expressions (2.10) and (2.13) in (3.5).

$$\begin{aligned} \tau(\varphi) &= \mu \frac{\omega d}{2\delta(1 + \varepsilon \cos \varphi)} + \frac{\delta(1 + \varepsilon \cos \varphi)}{d} 6\mu \frac{\omega}{\psi^2} \frac{\varepsilon(\cos \varphi - \cos \varphi_m)}{(1 + \varepsilon \cos \varphi)^3} = \\ &= \mu \omega \frac{d}{2\delta} \frac{1}{(1 + \varepsilon \cos \varphi)} + \frac{\delta}{d} 6\mu \omega \frac{1}{\psi^2} \frac{\varepsilon(\cos \varphi - \cos \varphi_m)}{(1 + \varepsilon \cos \varphi)^2} \end{aligned} \tag{3.6}$$

$\psi = \frac{2\delta}{d}$ Let's consider the substitutions obtained according to the

expression (3.6) $\frac{\delta}{d} = \frac{\psi}{2} \cdot \frac{d}{2\delta} = \frac{1}{\psi}$

$$\begin{aligned} \tau(\varphi) &= \mu\omega \frac{1}{\psi} \frac{1}{(1 + \varepsilon \cos \varphi)} + \frac{\psi}{2} 6\mu\omega \frac{1}{\psi^2} \frac{\varepsilon(\cos \varphi - \cos \varphi_m)}{(1 + \varepsilon \cos \varphi)^2} = \\ &= \frac{\mu\omega}{\psi} \frac{1}{(1 + \varepsilon \cos \varphi)} + 3 \frac{\mu\omega}{\psi} \frac{\varepsilon(\cos \varphi - \cos \varphi_m)}{(1 + \varepsilon \cos \varphi)^2} = \frac{\mu\omega}{\psi} \left(\frac{1}{(1 + \varepsilon \cos \varphi)} + \frac{3\varepsilon(\cos \varphi - \cos \varphi_m)}{(1 + \varepsilon \cos \varphi)^2} \right) = \\ &= \frac{\mu\omega}{\psi} \left(\frac{1 + \varepsilon \cos \varphi + 3\varepsilon \cos \varphi - 3\varepsilon \cos \varphi_m}{(1 + \varepsilon \cos \varphi)^2} \right) = \frac{\mu\omega}{\psi} \cdot \frac{1 - 3\varepsilon \cos \varphi + 4\varepsilon \cos \varphi_m}{(1 + \varepsilon \cos \varphi)^2} \end{aligned}$$

thus

$$\tau(\varphi) = \frac{\mu\omega}{\psi} \cdot \frac{1 - 3\varepsilon \cos \varphi + 4\varepsilon \cos \varphi_m}{(1 + \varepsilon \cos \varphi)^2} \quad (3.7)$$

In order to find the specific friction force on the surface of the entire working surface of the journal, it is necessary to integrate this expression according to the boundaries of the working zone.

$$\tau(\varphi) = \frac{\mu\omega}{\psi} \int_{\varphi_1}^{\varphi_2} \frac{1 - 3\varepsilon \cos \varphi + 4\varepsilon \cos \varphi_m}{(1 + \varepsilon \cos \varphi)^2} d\varphi \quad (3.8)$$

or

$$\tau(\varphi) = \frac{\mu\omega}{\psi} \cdot \xi \quad (3.9)$$

here

$$\xi = \int_{\varphi_1}^{\varphi_2} \frac{1 - 3\varepsilon \cos \varphi + 4\varepsilon \cos \varphi_m}{(1 + \varepsilon \cos \varphi)^2} d\varphi \quad (3.10)$$

- called resistance coefficient.

DETERMINATION of the ANALYTICAL EXPRESSION of the RESISTANCE COEFFICIENT

Let's open the integral (3.10).

**FUNDAMENTALS OF THE NEW CALCULATION METHOD OF THE
HYDRODYNAMIC JOURNAL BEARINGS**

$$\begin{aligned} \xi &= \int_{\varphi_1}^{\varphi_2} \frac{1 - 3\varepsilon \cos \varphi_m + 4\varepsilon \cos \varphi}{(1 + \varepsilon \cos \varphi)^2} d\varphi = \int_{\varphi_1}^{\varphi_2} \frac{1 + 3 - 3 - 3\varepsilon \cos \varphi_m + 4\varepsilon \cos \varphi}{(1 + \varepsilon \cos \varphi)^2} d\varphi = \\ &= \int_{\varphi_1}^{\varphi_2} \frac{4 + 4\varepsilon \cos \varphi_m - 3\varepsilon \cos \varphi - 3}{(1 + \varepsilon \cos \varphi)^2} d\varphi = \int_{\varphi_1}^{\varphi_2} \frac{4(1 + \varepsilon \cos \varphi) - 3(1 + \varepsilon \cos \varphi_m)}{(1 + \varepsilon \cos \varphi)^2} d\varphi = 4 \int_{\varphi_1}^{\varphi_2} \frac{1 + \varepsilon \cos \varphi}{(1 + \varepsilon \cos \varphi)^2} d\varphi - \\ &- 3(1 + \varepsilon \cos \varphi_m) \int_{\varphi_1}^{\varphi_2} \frac{d\varphi}{(1 + \varepsilon \cos \varphi)^2} = 4 \int_{\varphi_1}^{\varphi_2} \frac{d\varphi}{(1 + \varepsilon \cos \varphi)} - 3(1 + \varepsilon \cos \varphi_m) \int_{\varphi_1}^{\varphi_2} \frac{d\varphi}{(1 + \varepsilon \cos \varphi)^2} \end{aligned}$$

Let's look at the opening of each of the integrals included in the expression separately :

[1], according to integral 446.00

$$S = \int_{\varphi_1}^{\varphi_2} \frac{d\varphi}{1 + \varepsilon \cos \varphi} = \frac{2}{\sqrt{1 - \varepsilon^2}} \operatorname{arctg} \frac{(1 - \varepsilon) \operatorname{tg} \frac{\varphi}{2}}{\sqrt{1 - \varepsilon^2}} \Big|_{\varphi_1}^{\varphi_2} \quad (4.2)$$

[1], according to integral 446.03

$$S_{1.1} = \int_{\varphi_1}^{\varphi_2} \frac{d\varphi}{(1 + \varepsilon \cos \varphi)^2} = \frac{1}{1 - \varepsilon^2} \int_{\varphi_1}^{\varphi_2} \frac{d\varphi}{1 + \varepsilon \cos \varphi} - \frac{\varepsilon}{1 - \varepsilon^2} \frac{\sin \varphi}{1 + \varepsilon \cos \varphi} \Big|_{\varphi_1}^{\varphi_2} \quad (4.3)$$

Let's accept the above substitutions

$$e = 1 - \varepsilon^2; m = 1 + \varepsilon \cos \varphi_m$$

$$d = \frac{\varepsilon}{1 - \varepsilon^2} \left[\frac{\sin \varphi_2}{(1 + \varepsilon \cos \varphi_2)} - \frac{\sin \varphi_1}{(1 + \varepsilon \cos \varphi_1)} \right];$$

$$t = \frac{\pi}{180} \left[\left(180 - \operatorname{arctg} \frac{(1 - \varepsilon) \cdot \operatorname{tg} \frac{\varphi_2}{2}}{\sqrt{1 - \varepsilon^2}} \right) - \operatorname{arctg} \frac{(1 - \varepsilon) \cdot \operatorname{tg} \frac{\varphi_1}{2}}{\sqrt{1 - \varepsilon^2}} \right], \operatorname{ref}$$

Let's take these substitutions into account in (4.3) and write them instead in expression (4.1).

$$\xi = 4S - 3m \cdot \left(\frac{1}{e} \cdot S - d \right) = 4S - \frac{3m}{e} \cdot S + 3m \cdot d = \left(4 - \frac{3m}{e} \right) \cdot S + 3m \cdot d \quad (4.4)$$

If we substitute (4.2) in (4.4), we get an analytical expression to accurately calculate the resistance coefficient:

$$\xi = \left(4 - \frac{3(1 + \varepsilon \cos \varphi_m)}{1 - \varepsilon^2} \right) \cdot \frac{2 \cdot t}{\sqrt{1 - \varepsilon^2}} + 3d(1 + \varepsilon \cos \varphi_m). \quad (4.5)$$

When all substitutions are taken into account, the analytical expression is as follows:

$$\xi = \left(4 - \frac{3(1 + \varepsilon \cos \varphi_m)}{1 - \varepsilon^2} \right) \frac{2}{\sqrt{1 - \varepsilon^2}} \frac{\pi}{180} \left[\operatorname{arctg} \frac{(1 - \varepsilon) \operatorname{tg} \frac{\varphi_2}{2}}{\sqrt{1 - \varepsilon^2}} - \operatorname{arctg} \frac{(1 - \varepsilon) \operatorname{tg} \frac{\varphi_1}{2}}{\sqrt{1 - \varepsilon^2}} \right] + \quad (4.6)$$

$$+ 3(1 + \varepsilon \cos \varphi_m) \frac{\varepsilon}{1 - \varepsilon^2} \left(\frac{\sin \varphi_2}{1 + \varepsilon \cos \varphi_2} - \frac{\sin \varphi_1}{1 + \varepsilon \cos \varphi_1} \right)$$

THE RADIAL FORCE AFFECTING the on the BARING UNIT

The radial force characterized by the relative eccentricity and rotation angle, which characterizes the position of the sling in the casing and the bearing capacity of the cushion, can be determined from the balance equations of the sling. The hydrodynamic force acts on the surface of the shaft in the normal direction, that is, along the radius. This force can be divided into vertical and horizontal ones (Ryzhik I.M. and Gradshtein I.S., 2003). Only the vertical component of the hydrodynamic force lifts the propeller vertically above the casing and is directed in the opposite direction to the radial force. The horizontal component of the hydrodynamic force causes the displacement of the shaft in the bearing, as a result, the center line connecting the center of the shaft and the filling turns to the direction of the external force, that is, the radial force, by an angle

φ_e with respect to the vertical symmetrical axis of the bearing, and the eccentricity decreases (Fig. 5.1).

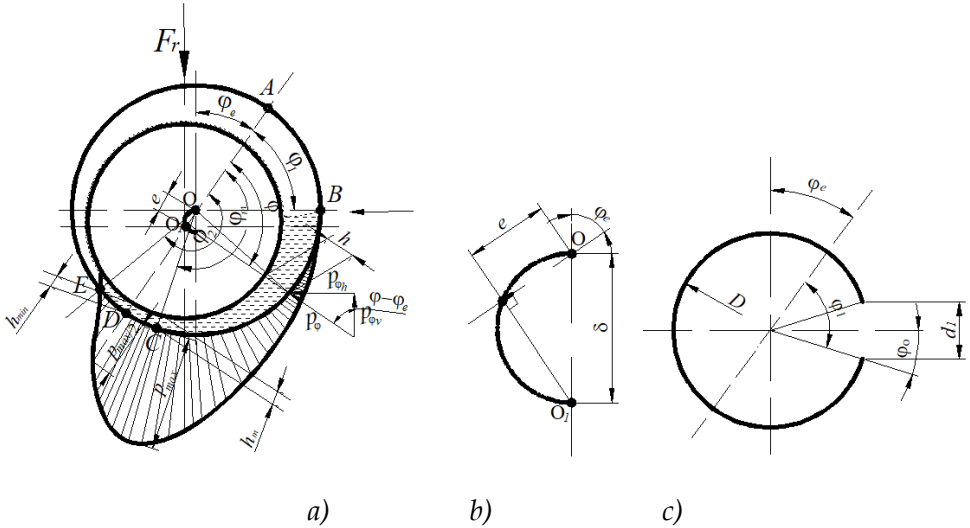


Fig. 5. The Calculation Scheme of the Hydrodynamic Journal Bearing

The radial force, characterized by the relative eccentricity and rotation angle, which characterizes the position of the shaft in the casing and the bearing capacity of the bearing, is determined from the equilibrium equations of the bearing (three equations for the plane problem). One of them - F_r . The sum of the projections of the forces acting on the journal in the direction of the force is expressed in the following way.

$$F_r = \frac{ld}{2} \int_{\varphi_1}^{\varphi_2} \{ p(\varphi) \cos[180^\circ - (\varphi + \varphi_e)] + \tau(\varphi) \sin[180^\circ - (\varphi + \varphi_e)] \} d\varphi \quad (5.1)$$

$$\cos[180^\circ - (\varphi + \varphi_e)] = -\cos(\varphi + \varphi_e) \text{ and } \sin[180^\circ - (\varphi + \varphi_e)] = \sin(\varphi + \varphi_e)$$

considering that (5.1) can be written as follows:

$$F_r = \frac{ld}{2} \int_{\varphi_1}^{\varphi_2} \{ p(\varphi) [-\cos(\varphi + \varphi_e)] + \tau(\varphi) \sin(\varphi + \varphi_e) \} d\varphi$$

or

$$F_r = \frac{ld}{2} \int_{\varphi_1}^{\varphi_2} (-p(\varphi)\cos(\varphi + \varphi_e)d\varphi + \tau(\varphi)\sin(\varphi + \varphi_e)d\varphi) \quad (5.2)$$

Substituting (2.14) and (3.8) in (5.2) and simplifying

$$F_r = \frac{ld}{2} \int_{\varphi_1}^{\varphi_2} \left(-6 \frac{\mu\omega}{\psi^2} \int_{\varphi_1}^{\varphi_2} \frac{\varepsilon(\cos \varphi - \cos \varphi_m)}{(1 + \varepsilon \cos \varphi)^3} d\varphi \cos(\varphi + \varphi_e)d\varphi + \frac{\mu\omega}{\psi} \int_{\varphi_1}^{\varphi_2} \frac{1 - 3\varepsilon \cos \varphi + 4\varepsilon \cos \varphi_m}{(1 + \varepsilon \cos \varphi)^2} d\varphi \sin(\varphi + \varphi_e)d\varphi \right)$$

$$F_r = -3ld \frac{\mu\omega}{\psi^2} \int_{\varphi_1}^{\varphi_2} \int_{\varphi_1}^{\varphi_2} \frac{\varepsilon(\cos \varphi - \cos \varphi_m)}{(1 + \varepsilon \cos \varphi)^3} \cdot \cos(\varphi + \varphi_e)d\varphi \cdot d\varphi + \frac{ld}{2} \frac{\mu\omega}{\psi} \int_{\varphi_1}^{\varphi_2} \int_{\varphi_1}^{\varphi_2} \frac{1 - 3\varepsilon \cos \varphi + 4\varepsilon \cos \varphi_m}{(1 + \varepsilon \cos \varphi)^2} \cdot \sin(\varphi + \varphi_e)d\varphi \cdot d\varphi$$

$$F_r = \frac{ld}{2} \frac{\mu\omega}{\psi^2} \left[-6 \int_{\varphi_1}^{\varphi_2} \frac{\varepsilon(\cos \varphi - \cos \varphi_m)}{(1 + \varepsilon \cos \varphi)^3} d\varphi \int_{\varphi_1}^{\varphi_2} \cos(\varphi + \varphi_e)d\varphi + \psi \int_{\varphi_1}^{\varphi_2} \frac{1 - 3\varepsilon \cos \varphi + 4\varepsilon \cos \varphi_m}{(1 + \varepsilon \cos \varphi)^2} d\varphi \int_{\varphi_1}^{\varphi_2} \sin(\varphi + \varphi_e)d\varphi \right]$$

So

$$F_r = \frac{ld}{2} \frac{\mu\omega}{\psi^2} S_0 \quad (5.3)$$

here

$$S_0 = -6 \int_{\varphi_1}^{\varphi_2} \frac{\varepsilon(\cos \varphi - \cos \varphi_m)}{(1 + \varepsilon \cos \varphi)^3} d\varphi \int_{\varphi_1}^{\varphi_2} \cos(\varphi + \varphi_e)d\varphi + \psi \int_{\varphi_1}^{\varphi_2} \frac{1 - 3\varepsilon \cos \varphi + 4\varepsilon \cos \varphi_m}{(1 + \varepsilon \cos \varphi)^2} d\varphi \int_{\varphi_1}^{\varphi_2} \sin(\varphi + \varphi_e)d\varphi \quad (5.4)$$

is a dimensionless coefficient and is called loading coefficient (Sommerfeld number).

Considering (3.10), (5.4) can be written as follows

$$S_0 = -6 \int_{\varphi_1}^{\varphi_2} \frac{\varepsilon(\cos \varphi - \cos \varphi_m)}{(1 + \varepsilon \cos \varphi)^3} d\varphi \int_{\varphi_1}^{\varphi_2} \cos(\varphi + \varphi_e)d\varphi + \psi \xi \int_{\varphi_1}^{\varphi_2} \sin(\varphi + \varphi_e)d\varphi \quad (5.5)$$

Here- φ_1 , φ_2 , φ_m and φ_e respectively, the initial, final, maximum pressure of the working zone and the turning angles of the geometric axis of the nozzle relative to the axis of the pillow (Figure 5.1); ψ -relative emptiness; ε - is the relative eccentricity, depends on the diametral gap and the minimum thickness of the oil layer

DETERMINATION of the ANALYTICAL EXPRESSION for the LOADING FACTOR

For simplification, let us accept the following substitutions in expression (5.5):

$$S_1 = \int_{\varphi_1}^{\varphi_2} \frac{\varepsilon(\cos \varphi - \cos \varphi_e)}{(1 + \varepsilon \cos \varphi)^3} d\varphi, \quad (6.1)$$

$$S_2 = \int_{\varphi_1}^{\varphi_2} \cos(\varphi + \varphi_e) d\varphi, \quad (6.2)$$

$$S_3 = \int_{\varphi_1}^{\varphi_2} \sin(\varphi + \varphi_e) d\varphi. \quad (6.3)$$

Let us write these substitutions in (5.5).

$$S_0 = -6 \cdot S_1 \cdot S_2 + \psi \cdot \xi \cdot S_3. \quad (6.4)$$

Now let's open the first integral, i.e. (6.1):

$$\begin{aligned} S_1 &= \int_{\varphi_1}^{\varphi_2} \frac{\varepsilon(\cos \varphi - \cos \varphi_m)}{(1 + \varepsilon \cos \varphi)^3} d\varphi = \int_{\varphi_1}^{\varphi_2} \frac{\varepsilon \cos \varphi - \varepsilon \cos \varphi_m}{(1 + \varepsilon \cos \varphi)^3} d\varphi = \int_{\varphi_1}^{\varphi_2} \frac{1 + \varepsilon \cos \varphi - 1 - \varepsilon \cos \varphi_m}{(1 + \varepsilon \cos \varphi)^3} d\varphi = \int_{\varphi_1}^{\varphi_2} \frac{1 + \varepsilon \cos \varphi}{(1 + \varepsilon \cos \varphi)^3} d\varphi - \\ &- (1 + \varepsilon \cos \varphi_m) \int_{\varphi_1}^{\varphi_2} \frac{d\varphi}{(1 + \varepsilon \cos \varphi)^3} = \int_{\varphi_1}^{\varphi_2} \frac{d\varphi}{(1 + \varepsilon \cos \varphi)^2} - (1 + \varepsilon \cos \varphi_m) \int_{\varphi_1}^{\varphi_2} \frac{d\varphi}{(1 + \varepsilon \cos \varphi)^3} \\ &. \end{aligned} \quad (6.5)$$

To simplify the expression, let us accept the following substitutions (see (4.3)):

$$S_{1.1} = \int_{\varphi_1}^{\varphi_2} \frac{d\varphi}{(1 + \varepsilon \cos \varphi)^2}, \quad (6.6)$$

$$S_{1.2} = \int_{\varphi_1}^{\varphi_2} \frac{d\varphi}{(1 + \varepsilon \cos \varphi)^3}, \quad (6.7)$$

$$m = 1 + \varepsilon \cos \varphi_m. \quad (6.8)$$

Considering these substitutions in the opening of the integral above, we can write the integral (6.5) as follows:

$$S_1 = S_{1.1} - m \cdot S_{1.2}. \quad (6.9)$$

Referring to [2], let's open the integral (2.452.11th integral) (6.7):

$$S_{1.2} = \int_{\varphi_1}^{\varphi_2} \frac{d\varphi}{(1 + \varepsilon \cos \varphi)^3} = -\frac{1}{2(1 - \varepsilon^2)} \left[\frac{\varepsilon \sin \varphi}{(1 + \varepsilon \cos \varphi)^2} \Big|_{\varphi_1}^{\varphi_2} - \int_{\varphi_1}^{\varphi_2} \frac{2 - \varepsilon \cos \varphi}{(1 + \varepsilon \cos \varphi)^2} d\varphi \right] \quad (6.10)$$

$e = 1 - \varepsilon^2$ simplify this expression by accepting

$$S_{1.2} = -\frac{\varepsilon \sin \varphi}{2e (1 + \varepsilon \cos \varphi)^2} \Big|_{\varphi_1}^{\varphi_2} + \frac{1}{2e} \int_{\varphi_1}^{\varphi_2} \frac{2 - \varepsilon \cos \varphi}{(1 + \varepsilon \cos \varphi)^2} d\varphi. \quad (6.11)$$

Considering (6.11) in (6.9), let's continue to open the integral:

$$\begin{aligned} S_1 &= S_{1.1} + \frac{m\varepsilon \sin \varphi}{2e (1 + \varepsilon \cos \varphi)^2} \Big|_{\varphi_1}^{\varphi_2} - \frac{m}{2e} \int_{\varphi_1}^{\varphi_2} \frac{2 - \varepsilon \cos \varphi}{(1 + \varepsilon \cos \varphi)^2} d\varphi = S_{1.1} + \frac{m\varepsilon \sin \varphi}{2e (1 + \varepsilon \cos \varphi)^2} \Big|_{\varphi_1}^{\varphi_2} + \frac{m}{2e} \int_{\varphi_1}^{\varphi_2} \frac{\varepsilon \cos \varphi - 2}{(1 + \varepsilon \cos \varphi)^2} d\varphi = \\ &= \frac{m\varepsilon \sin \varphi}{2e (1 + \varepsilon \cos \varphi)^2} \Big|_{\varphi_1}^{\varphi_2} + S_{1.1} + \frac{m}{2e} \int_{\varphi_1}^{\varphi_2} \frac{1 + \varepsilon \cos \varphi - 3}{(1 + \varepsilon \cos \varphi)^2} d\varphi = \frac{m\varepsilon \sin \varphi}{2e (1 + \varepsilon \cos \varphi)^2} \Big|_{\varphi_1}^{\varphi_2} + S_{1.1} + \frac{m}{2e} \left[\int_{\varphi_1}^{\varphi_2} \frac{1 + \varepsilon \cos \varphi}{(1 + \varepsilon \cos \varphi)^2} d\varphi - \right. \\ &\left. - 3 \int_{\varphi_1}^{\varphi_2} \frac{d\varphi}{(1 + \varepsilon \cos \varphi)^2} \right]. \quad (6.12) \end{aligned}$$

The last integral in this expression is the integral in (6.6), so let's consider that integral here:

$$\begin{aligned} S_1 &= \frac{m\varepsilon \sin \varphi}{2e (1 + \varepsilon \cos \varphi)^2} \Big|_{\varphi_1}^{\varphi_2} + S_{1.1} + \frac{m}{2e} \int_{\varphi_1}^{\varphi_2} \frac{d\varphi}{1 + \varepsilon \cos \varphi} - \frac{3m}{2e} \cdot S_{1.1} = \\ &= \frac{m\varepsilon \sin \varphi}{2e (1 + \varepsilon \cos \varphi)^2} \Big|_{\varphi_1}^{\varphi_2} + \left(1 - \frac{3m}{2e} \right) S_{1.1} + \frac{m}{2e} \int_{\varphi_1}^{\varphi_2} \frac{d\varphi}{1 + \varepsilon \cos \varphi} \quad (6.13) \end{aligned}$$

Consider (4.3) in (6.13):

$$\begin{aligned}
 S_1 &= \frac{m\varepsilon}{2e} \frac{\sin \varphi}{(1 + \varepsilon \cos \varphi)^2} \Big|_{\varphi_1}^{\varphi_2} + \left(1 - \frac{3m}{2e}\right) \cdot \left[\frac{1}{e} \int_{\varphi_1}^{\varphi_2} \frac{d\varphi}{1 + \varepsilon \cos \varphi} - \frac{\varepsilon}{e} \frac{\sin \varphi}{1 + \varepsilon \cos \varphi} \Big|_{\varphi_1}^{\varphi_2} \right] + \frac{m}{2e} \int_{\varphi_1}^{\varphi_2} \frac{d\varphi}{1 + \varepsilon \cos \varphi} = \\
 &= \frac{m\varepsilon}{2e} \frac{\sin \varphi}{(1 + \varepsilon \cos \varphi)^2} \Big|_{\varphi_1}^{\varphi_2} + \left(1 - \frac{3m}{2e}\right) \cdot \frac{1}{e} \int_{\varphi_1}^{\varphi_2} \frac{d\varphi}{1 + \varepsilon \cos \varphi} - \left(1 - \frac{3m}{2e}\right) \cdot \frac{\varepsilon}{e} \frac{\sin \varphi}{1 + \varepsilon \cos \varphi} \Big|_{\varphi_1}^{\varphi_2} + \frac{m}{2e} \int_{\varphi_1}^{\varphi_2} \frac{d\varphi}{1 + \varepsilon \cos \varphi} = \\
 &= \left[\left(1 - \frac{3m}{2e}\right) \cdot \frac{1}{e} + \frac{m}{2e} \right] \cdot \int_{\varphi_1}^{\varphi_2} \frac{d\varphi}{1 + \varepsilon \cos \varphi} + \frac{m\varepsilon}{2e} \frac{\sin \varphi}{(1 + \varepsilon \cos \varphi)^2} \Big|_{\varphi_1}^{\varphi_2} - \left(1 - \frac{3m}{2e}\right) \cdot \frac{\varepsilon}{e} \frac{\sin \varphi}{1 + \varepsilon \cos \varphi} \Big|_{\varphi_1}^{\varphi_2}
 \end{aligned} \tag{6.1}$$

4)

The opening of the integral included in this expression is given in (4.2).

For simplification, let us assume the following substitutions:

$$a = \frac{m\varepsilon}{2e} \frac{\sin \varphi}{(1 + \varepsilon \cos \varphi)^2} \Big|_{\varphi_1}^{\varphi_2} = \frac{m \cdot \varepsilon}{2 \cdot e} \left[\frac{\sin \varphi_2}{(1 + \varepsilon \cos \varphi_2)^2} - \frac{\sin \varphi_1}{(1 + \varepsilon \cos \varphi_1)^2} \right]; \tag{6.15}$$

$$b = 1 - \frac{3 \cdot m}{2 \cdot e}; \tag{6.16}$$

$$c = \frac{m}{2 \cdot e}; \tag{6.17}$$

$$d = \frac{\varepsilon}{1 - \varepsilon^2} \frac{\sin \varphi}{1 + \varepsilon \cos \varphi} \Big|_{\varphi_1}^{\varphi_2} = \frac{\varepsilon}{e} \left[\frac{\sin \varphi_2}{(1 + \varepsilon \cos \varphi_2)} - \frac{\sin \varphi_1}{(1 + \varepsilon \cos \varphi_1)} \right]; \tag{6.18}$$

$$t = \frac{\pi}{180} \left[\operatorname{arctg} \frac{(1 - \varepsilon) \cdot \operatorname{tg} \frac{\varphi_2}{2}}{\sqrt{e}} - \operatorname{arctg} \frac{(1 - \varepsilon) \cdot \operatorname{tg} \frac{\varphi_1}{2}}{\sqrt{e}} \right], \text{ ra} \tag{6.19}$$

these expressions $e = 1 - \varepsilon^2$ and $m = 1 + \varepsilon \cos \varphi_m$ their substitutions have already been accepted from the beginning.

Expression (6.19) only is true under the condition of $\varphi \leq 180^\circ$. If the angle is greater than 180° , this expression takes a different form. Specifically, for half journal bearing, which the bearing working zone are the 180° , angle φ_2 is taken to be greater than 180° (Figure 5.1), for this case expression (6.19) should be written as follows:

$$t = \frac{\pi}{180} \left[\left(180 - \left| \operatorname{arctg} \frac{(1-\varepsilon) \cdot \operatorname{tg} \frac{\varphi_2}{2}}{\sqrt{e}} \right| - \operatorname{arctg} \frac{(1-\varepsilon) \cdot \operatorname{tg} \frac{\varphi_1}{2}}{\sqrt{e}} \right), \operatorname{ref} \right] \quad (6.19^*)$$

The value of the angle in the expression is taken into account in degrees.

Let's write expressions (4.2), (6.15), (6.16), (6.17) and (6.18) in (6.14) and simplify the expression:

$$S_1 = a + b \cdot \left(\frac{1}{e} \cdot S - d \right) + c \cdot S = a + \frac{b}{e} \cdot S - b \cdot d + c \cdot S = a - b \cdot d + \left(\frac{b}{e} + c \right) \cdot S \quad (6.20)$$

(6.19*) with substitutions in (4.2), we can write it as

$$S = \frac{2 \cdot t}{\sqrt{e}} \quad (6.21)$$

Considering (6.21) in the expression (6.20), we can finally find the opening of the first integral (6.1):

$$S_1 = a - b \cdot d + \left(\frac{b}{e} + c \right) \cdot \frac{2 \cdot t}{\sqrt{e}} \quad (6.22)$$

Now let's open the second integral (6.2).

$$S_2 = \int_{\varphi_1}^{\varphi_2} \cos(\varphi + \varphi_e) d\varphi = \int_{\varphi_1}^{\varphi_2} \cos(\varphi + \varphi_e) d(\varphi + \varphi_e) = \sin(\varphi + \varphi_e) \Big|_{\varphi_1}^{\varphi_2}$$

$$S_2 = \sin(\varphi_2 + \varphi_e) - \sin(\varphi_1 + \varphi_e) \quad (6.23)$$

Now let's open the third integral, (6.3).

$$S_3 = \int_{\varphi_1}^{\varphi_2} \sin(\varphi + \varphi_e) d\varphi = \int_{\varphi_1}^{\varphi_2} \sin(\varphi + \varphi_e) d(\varphi + \varphi_e) = -\cos(\varphi + \varphi_e) \Big|_{\varphi_1}^{\varphi_2}$$

$$S_3 = \cos(\varphi_1 + \varphi_e) - \cos(\varphi_2 + \varphi_e) \quad (6.24)$$

Thus, by calculating the values of the expressions (6.22), (6.23), (6.24) and (4.6) and substituting them in (6.4), the load factor (Sommerfeld number) can be accurately calculated analytically. If we consider those mathematical expressions in (6.4), we get a new mathematical expression for calculating this coefficient:

$$S_0 = -6 \left[a - bd + \left(\frac{b}{e} + c \right) \frac{2 \cdot t}{\sqrt{e}} \right] [\sin(\varphi_2 + \varphi_e) - \sin(\varphi_1 + \varphi_e)] + \psi \xi [\cos(\varphi_1 + \varphi_e) - \cos(\varphi_2 + \varphi_e)] \quad (6.25)$$

Taking into account all substitutions, the mathematical expression obtained to calculate the exact value of Sommerfeld's equation is as follows:

$$\begin{aligned} S_0 = & -6 \left[\frac{\varepsilon(1 + \varepsilon \cos \varphi_m)}{2(1 - \varepsilon^2)} \left(\frac{\sin \varphi_2}{(1 + \varepsilon \cos \varphi_2)^2} - \frac{\sin \varphi_1}{(1 + \varepsilon \cos \varphi_1)^2} \right) - \left(1 - \frac{3(1 + \varepsilon \cos \varphi_m)}{2(1 - \varepsilon^2)} \right) \frac{\varepsilon}{1 - \varepsilon^2} \times \right. \\ & \times \left(\frac{\sin \varphi_2}{1 + \varepsilon \cos \varphi_2} - \frac{\sin \varphi_1}{1 + \varepsilon \cos \varphi_1} \right) + \left. \left(\left(1 - \frac{3(1 + \varepsilon \cos \varphi_m)}{2(1 - \varepsilon^2)} \right) \frac{1}{1 - \varepsilon^2} + \frac{1 + \varepsilon \cos \varphi_m}{2(1 - \varepsilon^2)} \right) \frac{2}{\sqrt{1 - \varepsilon^2}} \times \right. \\ & \times \left. \frac{\pi}{180} \left[\left(180 - \left| \arctg \frac{(1 - \varepsilon) \operatorname{tg} \frac{\varphi_2}{2}}{\sqrt{1 - \varepsilon^2}} \right| \right) - \arctg \frac{(1 - \varepsilon) \operatorname{tg} \frac{\varphi_2}{2}}{\sqrt{1 - \varepsilon^2}} \right] [\sin(\varphi_2 + \varphi_e) - \sin(\varphi_1 + \varphi_e)] + \right. \\ & + \psi \left[\left(4 - \frac{3(1 + \varepsilon \cos \varphi_m)}{1 - \varepsilon^2} \right) \frac{2}{\sqrt{1 - \varepsilon^2}} \frac{\pi}{180} \left[\left(180 - \left| \arctg \frac{(1 - \varepsilon) \operatorname{tg} \frac{\varphi_2}{2}}{\sqrt{1 - \varepsilon^2}} \right| \right) - \arctg \frac{(1 - \varepsilon) \operatorname{tg} \frac{\varphi_2}{2}}{\sqrt{1 - \varepsilon^2}} \right] + \right. \\ & \left. \left. + \frac{3\varepsilon}{1 - \varepsilon^2} (1 + \varepsilon \cos \varphi_m) \left(\frac{\sin \varphi_2}{1 + \varepsilon \cos \varphi_2} - \frac{\sin \varphi_1}{1 + \varepsilon \cos \varphi_1} \right) \right] [\cos(\varphi_1 + \varphi_e) - \cos(\varphi_2 + \varphi_e)] \right] \quad (6.26) \end{aligned}$$

It should be noted that during the calculation it is necessary to take the absolute value of the loading coefficient (Sommerfeld number) obtained by these formulas.

NEW CALCULATION METHOD of the HYDRODYNAMIC JOURNAL BEARINGS

Introduction

For the calculation of the hydrodynamic journal bearings (HJB) I have used the loading and resistance factor of the rotation (So & ξ).

These factors have been derived from the work condition in the bearing unit, influenced of the coefficient of friction. Therefore, it is very important to get correct calculation of these factors. Only in this case you may design the bearing units, which provides the required loading capacity, rotation frequency, durability and degree of reliability. In addition, it is important to choose the most suitable lubricant for the friction pair in maintenance and to keep maintenance parameters in rational intervals.

However, in the works (Mirzayev H.I., 2005) (Abdullayev A.H. and Mirzayev H.I., 2002) given empirical expressions, and some tables designed (Dimitriev V.A., 1970), (Reshetov D.N., 1989), (Chernavskiy S.A., 1963) (Koroychinskiy, 1959) according to these expressions the calculations of the HJB are not exactly accurate. Still using these expressions and tables, we may simplify calculation of the journal bearings. However, this method does not take into account the influence of all parameters, which characterize the maintenance regime of the bearing, so it is not compatible with modern requirements (Mirzayev H.I., 2005).

For the first time in works (Mirzayev H.I., 2005) (Abdullayev A.H. and Mirzayev H.I., 2002) (Abdullayev A.I etc., 2004) have used analytical expressions to determine loading and resistance factors depending on all parameters, such as eccentricity ratio (ϵ) and angles of position ($\varphi_1, \varphi_2, \varphi_e, \varphi_m$), influencing on the maintenance regime of the bearing. Using these analytical expressions and approach, I have worked out a new calculation method of the HJB.

Estimation

Analytical method of calculation of the HJB very complicated and calculations without using modern computer programs is much more difficult. On the other hand, while calculating relative eccentricity ratio changing interval [0 ... 1] after the half eccentricity ratio $\epsilon \geq 0.5$ value of the loading factor increases more than the values which given in (Dimi-

triev V.A., 1970), (Reshetov D.N., 1989), (Chernavskiy S.A., 1963), obtained with the empirical calculations.

In the calculation of the hydrodynamic journal $\alpha=\pi$ bearings with two half insert, according (Mirzayev H.I., 2005) (Dimitriev V.A., 1970), (Reshetov D.N., 1989) as a prerequisite, it has been accepted that, the sum of the angles of the start and end of the film thickness is equal to $\varphi_1+\varphi_2=\pi$ or according to the adopted calculation scheme $\varphi_2-\varphi_1=\pi$ (Fig.7). However, in the work (Chernavskiy S.A., 1963) these two conditions have further been adjusted and obtained and, actually $\varphi_2-\varphi_1=\pi$ equality correctly only in the value of the eccentricity ratio $\varepsilon = 0 \dots 0.5$. After the value of the eccentricity ratio $\varepsilon \geq 0.5$ dimensions of the working zone of the bearing gradually getting narrow and on the top $\varepsilon = 1.0$ not $\varphi_2-\varphi_1=\pi$, equality but $\varphi_2-\varphi_1=\pi/2$ it is true. To explain this opinion I have investigated the working process of the bearing.

2.3. Investigation of Working Process of the Bearing with Two Insert.

As being at rest the shaft due to the gravity forces of elements of bearing and external forces journal sitting on the bearing. At this time the lubrication, inlet to the bearing house at point A, on the perpendicular to the radial force may flow only to point B, and distributed to a maximum angle of 90 degrees field (Fig.6a).

When speed of the shaft generating hydrodynamic pressure on the oil film increases the journal raises, the eccentricity ratio decreases and theoretically approaching rotational speed infinity, it also approaches zero ($\omega \rightarrow \infty \Rightarrow \varepsilon \rightarrow 0$).

The center of the journal moved along the circle which its diameter equal to radial clearance at the top of the center of bearing and they situate as concentric circles and all clearance is equal to radial clearance ($h = \delta$) Fig.6b)

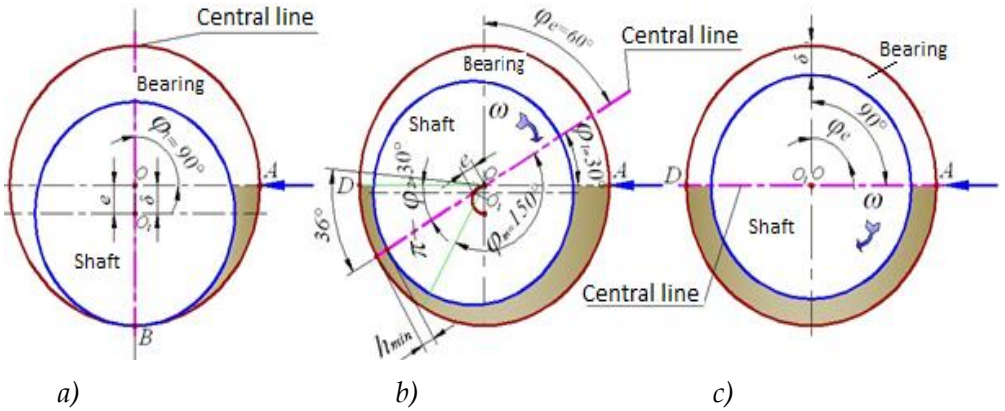


Figure 6. The Motion Maps of the Shaft in the Hydrodynamic Journal Bearing

Dimensions of the working zone, distributed by hydrodynamic pressure gradually growing and reaches the edges of the insert in the bearings with two half inserts (Fig. 6c). Thus, in the working process of the bearings, consisting of two parts, circumferential dimensions of the working zone may be change from 90° to 180°.

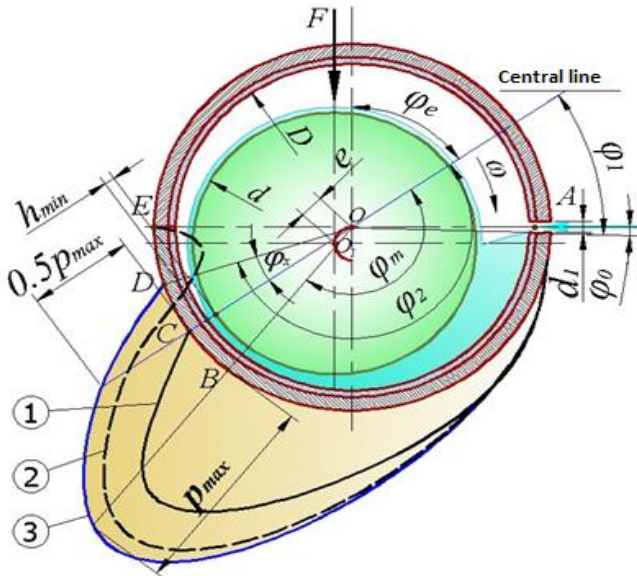


Figure 7. Schema of the Pressure Distribution in the Hydrodynamic Journal Bearings

1 –Half-Sommerfeld condition; 2 – Full-Sommerfeld condition; 3 –Reynolds boundary condition.

It is known that in the journal bearings, situated on the intermediate shaft neck consist of two half inserts. In this case, in the joint of the up and down inserts a little clearance arises. This clearance like that oil gaps designed as different configurations on the inner surface of the insert for the oil reservation.

Now, both the practice and the theory have confirmed that the hydrodynamic pressure decreases when there is oil gap (Dimitriev V.A., 1970), (Reshetov D.N., 1989), (Chernavskiy S.A., 1963) (Koroychinskiy, 1959). Therefore, in the loading zone, considered for the inner surface of the insert is not recommended to create the oil gaps and channels. From this point of view maximal area of the working zone in the two half inset HJB can be reproduced only according to the edges of the insert. Probably, Sommerfeld based on this logic received edges of the insert as the boundaries of the working zone (Mirzayev H.I., 2005) (Chernavskiy S.A., 1963) (Mirzayev H.I., Hashimov R.J., 2009)

On the other hand, as well as there was not used the oil pump in the hydrodynamic bearings, the lubrication, which inlet the bearing house at point A, on the perpendicular direction to the radial force may be self-flow only to point D situated on the opposite side in the same level, or until equalizing the level of lubrication (Fig.6).

Thus, I can confirm that in the two half inserts HJB hydrodynamic pressure may not be distributed out of edges of the inserts.

2.4. Symmetrical Calculation Method

I was used symmetrical calculation method for the determination of angle of end of the film thickness with correct mathematical appropriate.

The essence of this method was follows:

In the minimal and maximal values of the relative eccentricity ratio and the angle, characterized end of the film thickness (φ_2) received the

same values, equal to 180° . On the other hand in the middle value of the relative eccentricity ratio ($\varepsilon=0.5$) the angle φ_2 received its maximum value, which equal to 210° . Therefore, it may be suppose that, mathematically the angle, characterized by the end of the film which thickness is symmetric according to the middle value of the eccentricity ratio ($\varepsilon=0.5$).

According this approach, I have received the following formulas for the determination of angles, characterized by the position of the shaft in the bearing at the working process:

Angle of rotation

$$\varphi_\varepsilon = \arccos \varepsilon \quad (1)$$

Angle of the start of the film thickness

$$\varphi_1 = \frac{\pi}{2} - \arccos \varepsilon \quad (2)$$

Angle of the end of the film thickness:

$$\text{- at } \varepsilon \leq 0,5, \quad \varphi_2 = \frac{3\pi}{2} - \arccos \varepsilon \quad (3.1)$$

$$\text{- at } \varepsilon > 0,5, \quad \varphi_2 = \frac{3\pi}{2} - \arccos(1 - \varepsilon) \quad (3.2)$$

Angle of the position of the maximum film pressure

$$\text{- at } \varepsilon \leq 0,5, \quad \varphi_m = \frac{\pi}{2} + \arccos \varepsilon \quad (4.1)$$

$$\text{- at } \varepsilon > 0,5, \quad \varphi_m = \frac{\pi}{2} + \arccos(1 - \varepsilon) \quad (4.2)$$

In the specific calculation of angles of position has been used the both boundary conditions specifying Sommerfeld and Reynolds. Thus, determining the maximum value of the angle, characterizing end of the film thickness the Sommerfeld's, it symmetrical location with the angle of the position of the maximum film pressure based on Reynolds's boundary conditions.

Results

Variation of the angles of position with eccentricity ratio shown in Fig.8. These values of angles were determined according to the method of symmetrical calculation. Fig. 9 shows the comparison of the results

obtained by the symmetric calculation method with the results, which obtained by Kusayev, Kodnir and Phogelpol [9] for the angles of the position the shaft in the bearing (φ_1, φ_2).

Correctness of received theoretical results visually shown in Fig.9. As the new proposed, method is theoretical, so the suitable curves are more smoothly. Therefore, these cures are very close to each other shown according to that received results are very correct and consistent with the practice.

According to new formulas of angles of position obtained following new equations for loading and resistance factors for infinite journal bearings:

Loading factor (Sommerfeld number):

$$So = -12S_1, \text{ at } \varepsilon \leq 0,5; \quad (5.1)$$

$$So = -6S_1S_2 + \psi\xi S_3, \text{ at } \varepsilon > 0,5; \quad (5.2)$$

Resistance factor of the rotation (ξ):

$$\xi = (4 - 3a_1) \frac{2a_4}{\sqrt{1-\varepsilon^2}} + 3a_3(1 + \cos \varphi_m) \quad (6)$$

Where

$$S_1 = a_2 - (1 - 1,5a_1)a_3 + \left(\frac{1 - 1,5a_1}{1 - \varepsilon^2} + \frac{a_1}{2} \right) \left(\frac{2a_1}{\sqrt{1 - \varepsilon^2}} \right),$$

$$S_2 = -2, \text{ at } \varepsilon \leq 0,5; \quad S_2 = \sin(\varphi_2 + \varphi_\varepsilon), \text{ at } \varepsilon > 0,5;$$

$$S_3 = 0, \text{ at } \varepsilon \leq 0,5; \quad S_3 = -\cos(\varphi_2 + \varphi_\varepsilon), \text{ at } \varepsilon > 0,5;$$

$$a_1 = \frac{1 + \varepsilon \cos \varphi_m}{1 - \varepsilon^2}, \quad a_2 = \frac{a_1 \varepsilon}{2} \left[\frac{\sin \varphi_2}{(1 + \varepsilon \cos \varphi_2)^2} - \frac{\sin \varphi_1}{(1 + \varepsilon \cos \varphi_1)^2} \right],$$

$$a_3 = \frac{\varepsilon}{1 - \varepsilon^2} \left[\frac{\sin \varphi_2}{(1 + \varepsilon \cos \varphi_2)} - \frac{\sin \varphi_1}{(1 + \varepsilon \cos \varphi_1)} \right],$$

$$a_4 = \pi - \left| \arctg \left[\frac{(1 - \varepsilon) \operatorname{tg} \left(\frac{\varphi_2}{2} \right)}{\sqrt{1 - \varepsilon^2}} \right] \right| - \arctg \left[\frac{(1 - \varepsilon) \operatorname{tg} \left(\frac{\varphi_1}{2} \right)}{\sqrt{1 - \varepsilon^2}} \right], \text{ rad.}$$

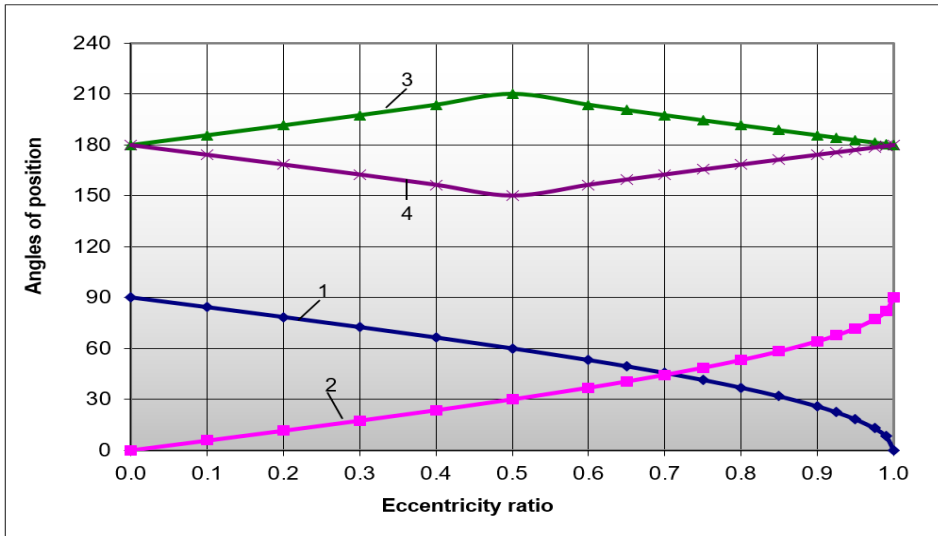


Figure 8. Variation of the Angles of Position with Eccentricity Ratio

1 – Angle of rotation (φ_e); 2 – start of the film thickness (φ_1); 3 – end of the film thickness (φ_2); 4- position of the maximum film pressure (φ_m).

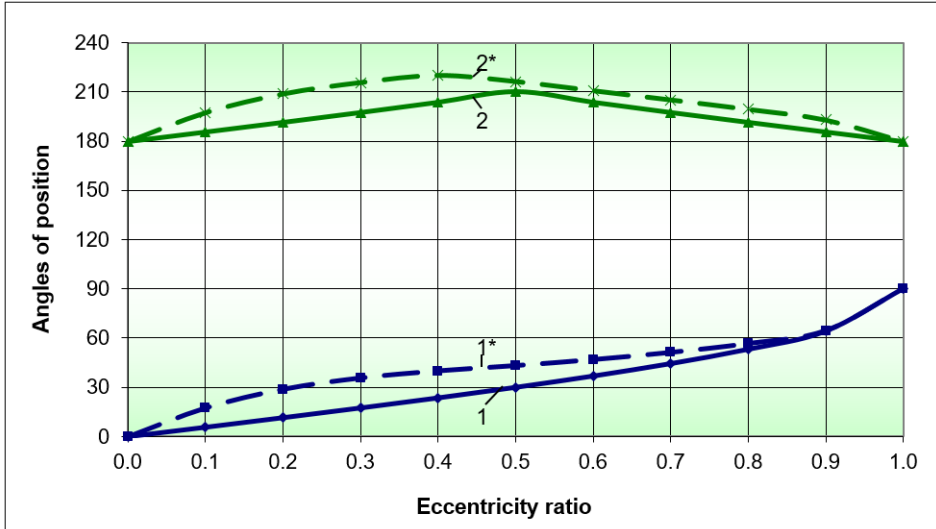


Figure 9. Comparison of Values of the Angles Start and End of the Film Thickness Calculating by the New Methods with the Values which Received by Corovchinsky (Reshetov, 1989)

**FUNDAMENTALS OF THE NEW CALCULATION METHOD OF THE
HYDRODYNAMIC JOURNAL BEARINGS**

1 – Start of the film thickness (φ_1); 2- end of the film thickness (φ_2); 1, 2- by the new calculation methods; 1, 2*-by the Corovchinsky*

Using MathCAD program pocket I have worked out special programs for calculation and analyzing of the loading factors according to equations (5.1), (5.2) and of the resistance factor of rotation (Dimitriev V.A., 1970). Using these programs, I have analyzed loading factor and resistance factor of the rotation in all values of relative eccentricity ratio. Below I have given the results of a MatCAD program for calculation of the loading factor (S_0) and the values of angles of position, loading factor and resistance factor of rotation (Tab. 1) and graphical dependences of loading and resistance factors with eccentricity ratio (Fig. 5 – 8).

The MathCAD program for calculation of the loading factor.

$$\begin{aligned}
 \text{So} := & \left\{ \begin{array}{l}
 \varepsilon \leftarrow 0.6 \\
 \varphi\varepsilon \leftarrow \arccos(\varepsilon) \\
 \varphi_1 \leftarrow \frac{\pi}{2} - \varphi\varepsilon \\
 \varphi_2 \leftarrow \begin{cases} \frac{3\pi}{2} - \arccos(\varepsilon) & \text{if } \varepsilon \leq 0.5 \\ \frac{3\pi}{2} - \arccos(1 - \varepsilon) & \text{if } \varepsilon > 0.5 \end{cases} \\
 \varphi m \leftarrow \begin{cases} \frac{\pi}{2} + \arccos(\varepsilon) & \text{if } \varepsilon \leq 0.5 \\ \frac{\pi}{2} + \arccos(1 - \varepsilon) & \text{if } \varepsilon > 0.5 \end{cases} \\
 a_1 \leftarrow \frac{1 + \varepsilon \cdot \cos(\varphi m)}{1 - \varepsilon^2} \\
 a_2 \leftarrow \frac{a_1 \cdot \varepsilon}{2} \cdot \left[\frac{\sin(\varphi_2)}{(1 + \varepsilon \cdot \cos(\varphi_2))^2} - \frac{\sin(\varphi_1)}{(1 + \varepsilon \cdot \cos(\varphi_1))^2} \right] \\
 a_3 \leftarrow \frac{\varepsilon}{1 - \varepsilon^2} \cdot \left(\frac{\sin(\varphi_2)}{1 + \varepsilon \cdot \cos(\varphi_2)} - \frac{\sin(\varphi_1)}{1 + \varepsilon \cdot \cos(\varphi_1)} \right) \\
 a_4 \leftarrow \pi - \left| \operatorname{atan} \left[\frac{(1 - \varepsilon) \cdot \tan\left(\frac{\varphi_2}{2}\right)}{\sqrt{1 - \varepsilon^2}} \right] \right| - \operatorname{atan} \left[\frac{(1 - \varepsilon) \cdot \tan\left(\frac{\varphi_1}{2}\right)}{\sqrt{1 - \varepsilon^2}} \right] \\
 \xi \leftarrow (4 - 3a_1) \cdot \frac{2 \cdot a_4}{\sqrt{1 - \varepsilon^2}} + 3 \cdot a_3 \cdot (1 + \varepsilon \cdot \cos(\varphi m)) \\
 S_1 \leftarrow a_2 - (1 - 1.5a_1) \cdot a_3 + \left(\frac{1 - 1.5a_1}{1 - \varepsilon^2} + \frac{a_1}{2} \right) \left(\frac{2 \cdot a_4}{\sqrt{1 - \varepsilon^2}} \right) \\
 S_2 \leftarrow \begin{cases} -2 & \text{if } \varepsilon \leq 0.5 \\ \sin(\varphi_2 + \varphi\varepsilon) & \text{if } \varepsilon > 0.5 \end{cases} \\
 S_3 \leftarrow \begin{cases} 0 & \text{if } \varepsilon \leq 0.5 \\ -\cos(\varphi_2 + \varphi\varepsilon) & \text{if } \varepsilon > 0.5 \end{cases} \\
 \psi \leftarrow \begin{cases} d \leftarrow 60 \\ D \leftarrow 60.2 \\ \frac{D - d}{d} \end{cases} \\
 12 \cdot S_1 & \text{if } \varepsilon \leq 0.5 \\
 -6 \cdot S_1 \cdot S_2 + \psi \cdot \xi \cdot S_3 & \text{if } \varepsilon > 0.5
 \end{array} \right.
 \end{aligned}$$

So = 3.836

**FUNDAMENTALS OF THE NEW CALCULATION METHOD OF THE
HYDRODYNAMIC JOURNAL BEARINGS**

In Table 1 shows, the values of angles of positions in degrees, calculated according equations (1) - (4), using Microsoft Excel program depending on eccentricity ratio. In this table also are given values of loading and resistance factors which calculated according equations (5) and (6) using MathCAD pocket programs.

Table 1. New values of the angles of position ($\varphi_1, \varphi_2, \varphi_e, \varphi_m$), loading factor (S_o) and resistance factor of the rotation (ξ) depending of the eccentricity ratio (ϵ)

ϵ	$\varphi_e, ^\circ$	$\varphi_1, ^\circ$	$\varphi_2, ^\circ$	$\varphi_m, ^\circ$	S_o	ξ
0,1	90	0	180	180	3,105	3,985
0,2	84,26083	5,73917	185,74	174,2608	5,274	4,684
0,3	78,46304	11,53696	191,54	168,463	6,754	5,287
0,4	72,5424	17,4576	197,46	162,5424	7,206	5,776
0,5	66,42182	23,57818	203,58	156,4218	4,832	6,012
0,55	60	30	210	150	3,041	6,404
0,6	56,63299	33,36701	213,37	146,633	3,836	6,873
0,65	53,1301	36,8699	203,58	156,4218	4,872	7,445
0,7	49,4584	40,5416	200,49	159,5127	6,265	8,159
0,725	45,573	44,427	197,46	162,5424	7,153	8,59
0,75	43,53115	46,46885	195,96	164,038	8,216	9,085
0,775	41,40962	48,59038	194,48	165,5225	9,51	9,662
0,8	39,19497	50,80503	193	166,9971	11,112	10,346
0,825	36,8699	53,1301	191,54	168,463	13,163	11,174
0,85	34,41151	55,58849	190,08	169,9213	15,86	12,203
0,875	31,78833	58,21167	188,63	171,3731	19,579	13,531
0,9	28,95502	61,04498	187,18	172,8192	25,059	15,334
0,925	25,84193	64,15807	185,74	174,2608	34	17,986
0,95	22,33165	67,66835	184,3	175,6988	51,443	22,455
0,975	18,19487	71,80513	182,87	177,134	102,208	32,602

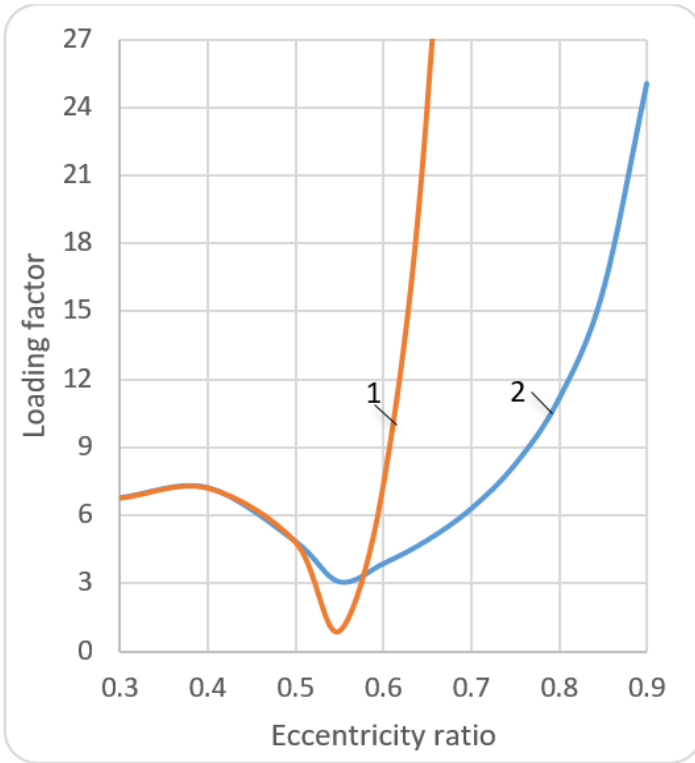


Figure 8. Comparison Values of the Loading Factor (Sommerfeld number) Calculating by the Old and New Methods

1 -by the old method, 2 - by the new method (symmetrical calculation method)

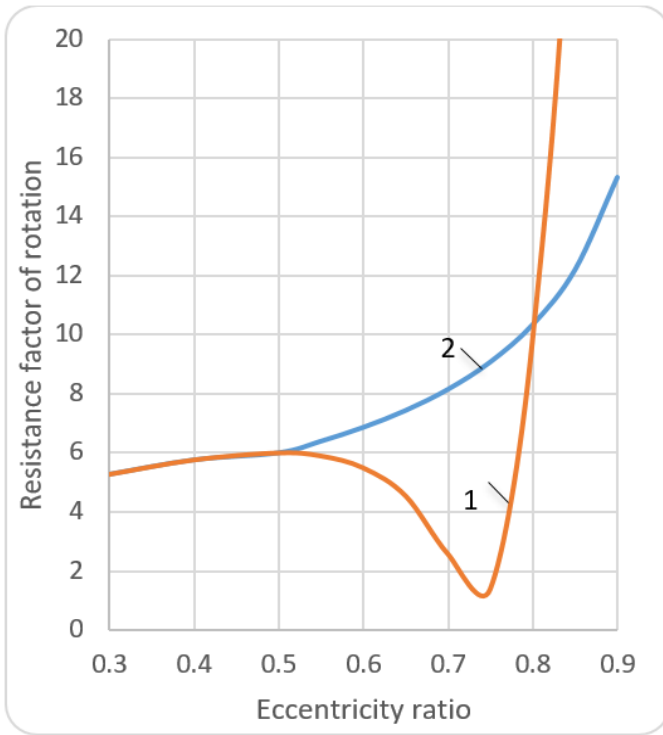


Figure 9. Comparison Values of the Resistance Factor of Rotation Calculating by the Old and New Methods

1 -by the old method, 2 - by the new method (symmetrical calculation method)

2.6. Analysis of results

Looking to figures 8 and 9 we can see that values got by using the new methods calculation completely overlap to the value of eccentricity ratio $\epsilon=0.5$, then from $\epsilon =0.6$ differs sharply. To see more clearly the difference in graphics I have enlarged branching parts. Looking to variation of the resistance factor in figure 6 we see that curves designed by the symmetrical calculation method is more fluent and accurate. Analysis of the results shows that this function is monotonously increasing. In the range $\epsilon=0.1...0.99$ from 3.9843 to 52.8628 consecutive increases. This in-

crease is even more acute after the value of relative eccentricity ratio equal to 0.6. However, I cannot say it for the change charts of the loading factor. Analyzing the values of the calculated loading factor using computer program for the values of eccentricity ratio from 0.1 to 0.99 with 0.01 steps, we can see that in the interval $\varepsilon=0.1\dots0.38$ loading factor increases from 3.1052 to 7.2489, and then gradually decreases to a minimum extreme value 2.5301 at $\varepsilon=0.51$ (Fig. 8). After that, it start to grow monotonously and increases up to 250.2856 at $\varepsilon=0.99$

After the value of eccentricity ratio at $\varepsilon=0.38$ the loading factor decreases until $\varepsilon=0.55$. Then it slowly increasing. After the value of eccentricity ratio is approximately $\varepsilon=0.8$ the loading factor already increasing dramatically.

In the Fig.10, variation of the loading and resistance factors with eccentricity ratio has been described. This chart allows comparing their values dependence on eccentricity ratio. On the analysis of the results of computer numerical experiment, I can say that, in the value of eccentricity ratio $\varepsilon=0.475$ and $\varepsilon=0.775$ the values of loading and resistance factors are approximately equal, in accordance with $S_o=5.91$ and $\xi=5.99$; $S_o=9.51$ and $\xi=9.66$. Taking into account that, coefficient of friction obtained with loading and resistance factors as

$$f = \psi \frac{\xi}{S_o}, \quad (7)$$

where ψ - relative clearance, this means that in these values of eccentricity ratio, coefficient of friction is equal to relative clearance.

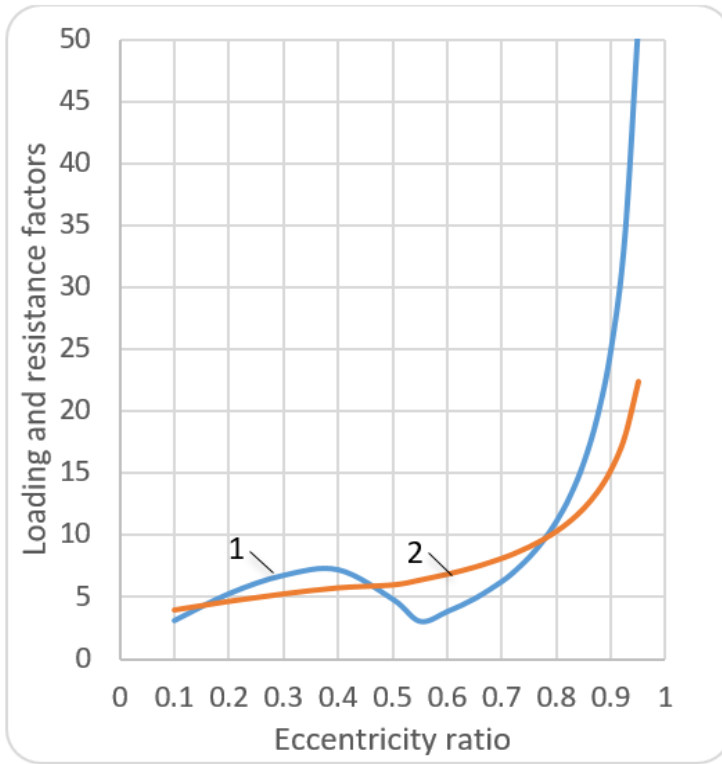


Figure 10. Variation of the Loading and Resistance Factor of the Rotation Torque with Eccentricity Ratio

1 – Loading factor (Sommerfeld number - S_o), 2 – resistance factor (ξ).

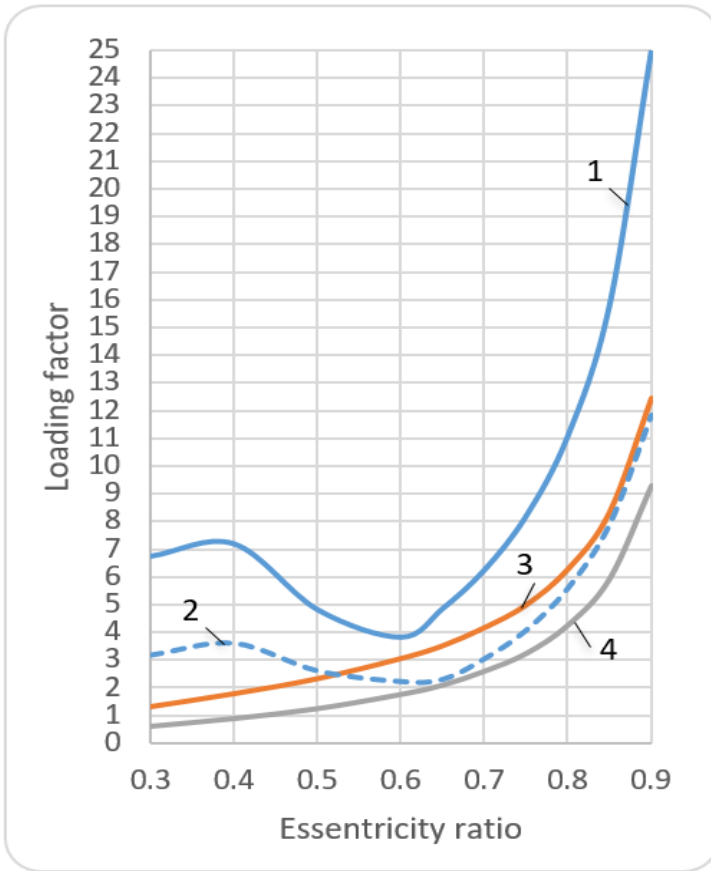


Figure 11. Variation of the Loading Factor with the Eccentricity Ratio

By the symmetrical calculation methods: 1 – for the infinite long bearing – $l/d=\infty$; 2 – for the long bearing – $l/d=1,5$; By the old calculation methods: 3 – by Korovchinsky; 4 – by Kodnir.

In Fig. 11 for the infinite ($l/d=\infty$) and a finite ($l/d=1,5$) journal bearings results of calculations of loading factor depending on eccentricity ratio by the new, symmetrical calculation methods and by Kodnir and Korovchinsky have been described. Results, receiving from both methods are consistent. If the value of eccentricity ratio equals 0.5, the results are matching. Therefore, this once again proves that new calculating method of the hydrodynamic journal bearings are correct.

CONCLUSIONS

In the first time worked out the full analytical method for calculation the regime factors as well as loading factor and resistance factor of rotation of the hydrodynamic journal bearings.

By using analytic expressions of the resistance and loading factors as well as constructive and technological parameters (of relative clearance ψ) specified expression for reduction coefficient of friction is established.

It is determined that with increase of relative eccentricity there takes place essential increase of the loading factor in comparison with the resistance factor. With this, reduction coefficient of friction decreases,

The worked out method of calculation enables to choose the most efficient lubricant for a journal bearing under the given constructive and technological parameters what is of great practical importance in stage of design a new equipment.

REFERENCES

Dwight G.B. Tables of integrals and other mathematical formulas. M : , Nauka, 1983, 176 p.

Ryzhik I.M. and Gradshteyn I.S. Tables of integral sums, rows and products. 2003

Mirzayev H.I. Development of scientific basis of a specified calculation of the hydrodynamic journal bearings. Ph.D. Dissertation (in Azerbaijani). Baku: 2005, pp.157

Abdullayev A.H., Mirzayev H.I. Analytical method of a choice of lubricant for plane bearings working in a condition of fluid friction (in Azerbaijani). Journal of Technique. Baku: 2002, No4, pp. 67 – 73.

Abdullayev A., Albert A., Mirzayev H., Najafov A. Determination Journal Bearings Clearance with Use of the Resistance Factor of the Rotation Torque and Sommerfeld Numbers / 11-th International Conference on Machine Design and Production, UMTİK 2004, Conference Proceedings, Antalya, 2004, v.II, pp. 771-782.

Dimitriev V.A. Machine design (in Russian). Leningrad: 1970, 792 p.

Reshetov D.N. Mashinedesign. Moscow:1989, 496 p.

Chernavskiy S.A. Journal bearings (in Russian). Moscow: 1963, 244 p.

Korovchinskiy (Коровчинский). Theoretical basis of working of the journal bearings (in Russian). Moscow, 1959, 404 p.

Mirzayev H.I., Hashimov R.J. Investigation of the working zone boundaries in the half-hydrodynamic bearings. Journal of Theoretic and Applied Mechanics. No. 2. Baku: 2009. pp. 6 - 12.

Mirzayev H.İ., Musaev Yu.A. Position parameters evaluation of shaft in friction bearing. «Bulletin of Engineering». No: 11, Moscow-2012. c.1, 41-42

Shigley J.E. Mechanical Engineering Design. Singapore National Printers Ltd., 3rd printing, 1988, 699 p.

H.İ.Mirzayev. New analytical calculation of the loading and resistance factors in the hydrodynamic journal bearings. Journal of "Mechanics-machine building" No2, Baku-2010. pp. 109 - 113.

SELECTION OF PLASTIC INJECTION MACHINE WITH AXIOMATIC DESIGN APPROACH

Gürcan ATAKÖK¹, İzzet ÖZBEK²

Abstract: Plastics are the materials with the most common usage area today. One of the various methods used in the production of plastics is the plastic injection method. Plastic injection methods and machines are difficult to choose and costly equipment. There are features to be considered in the selection of these machines. These features vary according to the material to be used, the part to be produced and the mold dimensions. It is a very difficult process to determine this. In this study, plastic injection machine selection was made by using the "Knowledge Axiom of Axiomatic Design Method", which is a method that will facilitate the selection of plastic injection machines and used in machine equipment selection before. Important criteria for machine selection were determined, a survey was conducted and questions with a high percentage of importance were selected with the Pareto analysis applied to the results. These questions were used in machine selection. Thus, the selection of the machine that can best meet the expectations among the different injection machine models available in the market has been made.

Keywords: Axiomatic Design, Injection Molding Machine Selection, Information Axiom

INTRODUCTION

Plastics, which have developed very rapidly until today, have now become superior to other materials in terms of many properties

¹ Marmara University, Faculty of Technology, Department of Mechanical Engineering, Istanbul / Türkiye, e-mail:gatakok@marmara.edu.tr, Orcid No: 0000-0002-5275-2429

² Marmara University Institute of Pure and Applied Sciences, Mechanical Engineering, İstanbul / Türkiye, e-mail: zetbek@hotmail.com

and have become the most preferred material type in almost every sector, especially in automotive, electronics and communication. Although it is the last material group to appear, it is one of the materials that enters our daily lives the most. The reason why they have become widespread and economically important in a short time can be shown as the change in the properties and diversity of plastics in a wide range (Akyüz, (1998).

Injection Molding Machines are the most suitable manufacturing machines for mass production, the injection molding method, which is generally applied to thermoplastics, can also be applied to thermosets by taking some precautions. Today, many polymers, especially PE, PS, PP, ABS, SAN, Nylon, are processed with this method and a wide variety of products are obtained. Generally, parts are obtained in three stages by injection method. These are: melting, filling the mold cavity, cooling and removing the part from the mold cavity. The heat required for injection is usually provided by electrical energy. Compared to metals, the thermal conductivity coefficient of plastics is very low (Akkurt, 1995).

In the Injection Unit, the main task of the Plastic unit is to melt the plastic material and inject the molten material into the mold cavity. In order to produce parts with the same characteristics, an equal amount of material of constant quality must be sent into the mold cavity in each cycle. Therefore, the plastic unit has to provide homogeneous molten material at a constant temperature. Locking Unit The locking unit is one of the most important units in injection molding machines. It ensures that sufficient force can be produced by opening and closing the molds and keeping the mold halves closed during injection (Akyüz, 1998).

A structural model was created to examine the relationship between the application of occupational health and safety management system and the operation and safety performance of construction projects (Yiu, 2019). In addition to the studies (Cebi, 2019) by the axiomatic design has become a more preferred method in many fields than in the past. When the studies conducted with axiomatic design are examined, it is seen that a significant part of the studies focus on "product design" and then on

"decision making" techniques (Aly, 2019; Benavides, 2019; Chen, 2019; Fagnoli, 2019; Goo, 2019). It has been observed that a limited number of studies have been conducted on the "system design", which is the subject of the study and the method is used (Ighravwe, 2019; Uzun, 2020; Yiu, 2019; Zhao, 2019).

AXIOMATIC DESIGN

In the literature, the Axiomatic Design (AD) technique and principles, developed by Suh and developing rapidly in recent years, have been applied in the design of systems in many areas such as software, quality, manufacturing, flexible manufacturing, cellular manufacturing and ergonomics. In addition, the Information axiom of AD, which is used as a multi-criteria decision-making technique, has been used to decide between alternatives by considering various criteria in areas such as equipment, transportation company and modern manufacturing systems.

The Design with Axioms method is a method developed by Nam Pyo Suh in order to put the design process on a scientific basis. The developed method enables the development of design activities by supporting the designer with logical and intelligent thinking processes. The basis of the method is 'WHAT will we achieve? - HOW do we get it?' there are questions (Özel, 2007).

Axiomatic design, as a design and method, was developed 20 years ago at the Massachusetts Institute of Technology and enabled the designers to focus on the problems that occur in bad designs. The owner of the theory, Prof. Nam P. Suh stated that the purpose of axiomatic design is to make design people more creative, to make research more efficient, to minimize the number of trial and error and to decide on the best design (Yavuz, 2010).

The axiom design method aims to form a basis for the design of systems, organizations and products. This goal is an important difference in the traditional design process created with experimental

and heuristic approaches. The field of design can never be systematized without scientific rules. The systematic approach has a facilitating effect on the understanding, coding, learning and implementation of designs (Çebi, 2008).

The Functional Requirement (FR_i) is a specified range for the features needed. The information content I during meeting a specified Functional Requirement (FR_i) is defined in terms of probability P_i as follows;

$$I_i = -\log_2 P_i \quad (2.1)$$

If the system range is unknown, we have to rely on previous designs and trained assumptions. Figure 1 graphically shows these two ranges. In this case, the information content is calculated as in equation (2.2).

$$I = \log_2 \left(\frac{1}{A_{cr}} \right) \quad (2.2)$$

Here A_{cr}=system interval Probability density function (oyf), customary interval=function on probability of success. From a statistical point of view, a FR can be considered a random variable on the FR sample space. If FR is a continuous random variable, the probability of reaching FR in the design range can be expressed as:

$$\int_{dr_1}^{dr_u} P_s(FR) dFR \quad (2.3)$$

Equation (2.3) gives the probability of success by integrating system oyf over the entire design range. That is, the lower limit of the design range dr₁, the upper limit of the design range dr_u) the shaded area in figure 1, the common range area A_{cr}, P is equal to the probability of success. Thus, the information content is as in equation (2.4) (Yavuz, 2010).

This equals to

$$I = -\log_2 P = -\log_2 \int_{dr_1}^{dr_u} P_s(FR) dFR \quad (2.4)$$

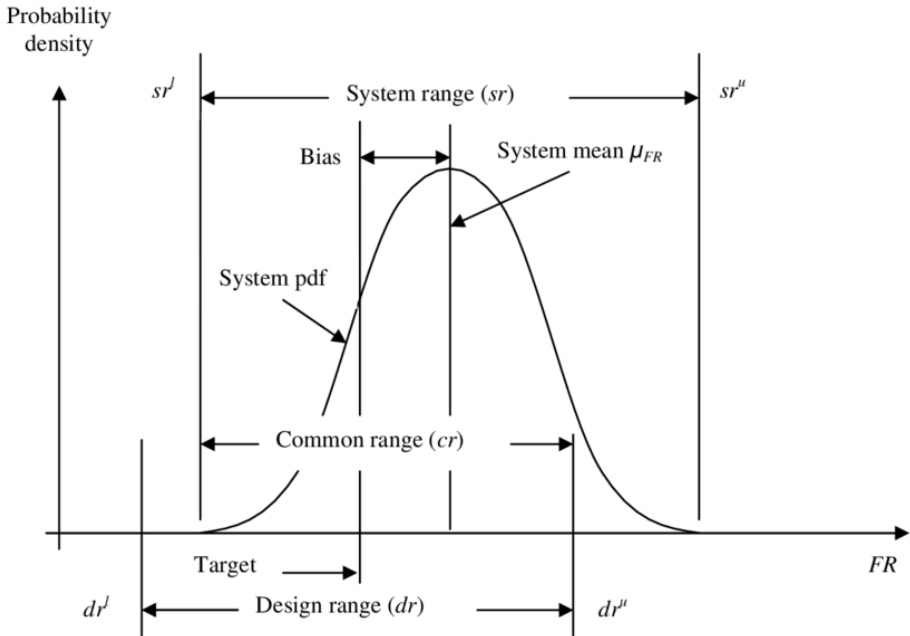


Figure 1. Design Range, System Range, Common Range, and Probability Density Function (ODF)

To minimize information content, we must eliminate bias and reduce variance so that the system range remains within the design range. Since the system range is completely within the design range, the probability of success is equal to 1.0 and therefore the information content is always zero. The most robust design always requires zero knowledge to meet FR with variation in DP and PVs tolerating (Suh, 2001; Erdem 2007).

MATERIAL and METHOD

Having experience and experience in Plastic Injection machines; A questionnaire was prepared to be conducted with the participation of machine manufacturers, suppliers and technical staff. In order to determine the Plastic Injection Molding Machine selection criteria and to determine which features should be considered while choos-

ing the machine, the results in Table 1 emerged as a result of the scores given by 25 participants to the criteria between 1-22.

Table 1. Survey Results

N o.	CRITERIA	%Im- portance	N o.	CRITERIA	%Im- portance
1	SCREW DIAMETER	78,8	12	COLUMN SHAFT DISTANCE	78,8
2	L/D RATIO	76,8	13	MAXIMUM MOLD THICKNESS	80,8
3	INJECTION WEIGHT	74,4	14	MINIMUM MOLD THICKNESS	75,2
4	INJECTION RATE	74,4	15	DRIVE STROKE	72
5	INJECTION PRESSURE	94,4	16	PUSHING FORCE	76,4
6	SCREW STROKE	78,8	17	MAXIMUM PUMP PRESSURE	83,2
7	SCREW SPEED	79,6	18	PUMP MOTOR POWER	82
8	INJECTION VOLUME	87,6	19	HEATER POWER	84,8
9	PLASTICIZING CAPACITY	82,8	20	OIL TANK CAPACITY	61,2
10	WISE FORCE	92	21	MACHINE DIMENSIONS	62,8
11	SCISSOR STROKE	82,8	22	MACHINE WEIGHT	50,4

Pareto analysis was applied to the results of the survey conducted to determine the evaluation criteria of Plastic Injection Molding Machines. Pareto analysis results are given in Table 2.

Table 2. Cronbach's Alpha Coefficient Result

Cronbach's Alpha	Item Count
0,8023	22

According to the 70-30 rule, criteria numbered 20, 21 and 22 were not taken into consideration because they remained within 30% in the application of the knowledge axiom. Decision-making was achieved with numerical solution by evaluating over 70% of them. For this, Pareto analysis was applied by taking into account the % importance values given to the evaluation criteria as a result of the survey and it was shown graphically. 22 criteria were ranked according to their % importance values, and the 70% limit was determined with the cumulative percentage.

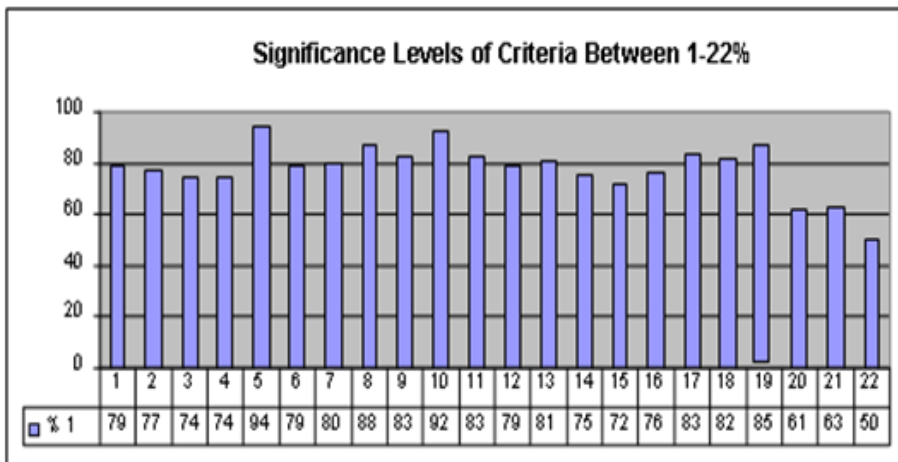


Figure 2. Representation of the Importance Levels of the Criteria in the Bar Chart

RESULTS and EVALUATION

Knowledge Axiom Application is made according to the results obtained in the survey, a table with technical specifications is handled on an example of current used plastic injection molding ma-

chines in Turkey, where the data are obtained from the internet and catalogues. In practice, the machines were ranked by considering the criteria determined according to the results obtained in the survey.

Exact values are calculated for the information content. Values have been exacted with no range. For this reason, we can use the satisfaction graph defined by Nakazawa to calculate the information content of all alternatives for each functional requirement. The abscissa of the graph is the functional requirements, and the ordinate is the level of satisfaction. The satisfaction level ranges from zero to one (Yavuz, 2010).

Taguchi's quality scale is used to calculate information content. M_s ; degree of satisfaction with the system, M_d ; is the target value and is taken as 1 in the formula. Since the system has exact values, the variance ($\sigma_s=0$) is zero. The coefficient C in the equation is the same for all alternatives and can be taken as 1.

X , the range of variation of was the random variable (a,b) . So the min that $a=X$ can take. value and the max. $b=X$ can take. get value. If the interval (a,b) is proportional to the probability of X , then this variable has a uniform distribution. With $a \leq X \leq b$, the probability density function of X is $f(x)=1/(b-a)$ (Yavuz, 2010).

The features that companies and participants give importance to in the survey are as follows; screw diameter, L/D ratio, injection weight, injection ratio, injection pressure, screw Stroke, screw speed, injection volume, plasticizing capacity, clamp force, scissor Stroke, column shaft distance, maximum mold thickness, minimum mold thickness, pusher Stroke.

The satisfaction level for screw diameter values is an example of the largest best type as shown in Figure 3. The horizontal axis of the graph is for the injection molding machine screw diameter and the vertical axis is for the degree of satisfaction. It is the lowest spindle speed value among the 25 mm alternatives and the satisfaction rating is 0. 48 mm is the highest value and the satisfaction rating is 1.

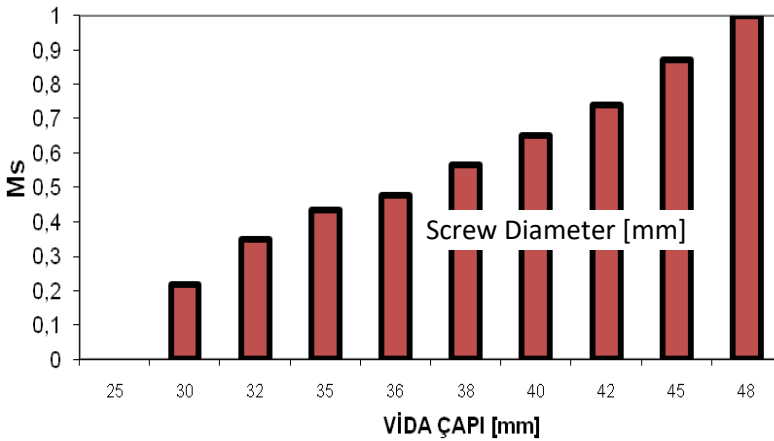


Figure 3. Screw Diameter Satisfaction Degree

In the Axiomatic Design application, in the graphs drawn as above, the vertical column shows the degree of satisfaction, while the horizontal column shows the values of the machine properties. Based on the results of the survey, the features considered to be important are; injection pressure, clamp force, injection volume, heater power, maximum pump pressure, plasticizing capacity, shear stroke, pump motor power, maximum mold thickness, screw speed, screw diameter, screw stroke, column shaft distance, l/d ratio, driving force, minimum mold thickness, injection weight, injection rate and ejector stroke are discussed separately. For these features, graphs were drawn separately according to their numerical data. Satisfaction degrees were obtained from the resulting graphics, the obtained satisfaction degrees were converted into axiomatic information content, and the best and worst machine was selected based on the sum of the information contents.

Table 5. Results of Satisfaction Degree and Information Content for Screw Diameter

No	Machine Model	Screw Diameter [mm]	Satisfaction Degree (Ms)	Information Content (I)	No	Machine Model	Screw Diameter [mm]	Satisfaction Degree (Ms)	Information Content (I)
1	EM-2C	48	1	0	2	EM-10B	36	0,47826	0,2722
2	EM-1C	45	0,8695652	0,0170132	2	EM-12B	36	0,47826	0,2722
3	EM-3C	45	0,8695652	0,0170132	3	EM-13A	36	0,47826	0,2722
4	EM-7C	45	0,8695652	0,0170132	2	EM-1A	35	0,43478	0,3194
5	EM-8C	45	0,8695652	0,0170132	3	EM-3A	35	0,43478	0,3194
6	EM-13C	45	0,8695652	0,0170132	2	EM-4B	35	0,43478	0,3194
7	EM-2B	42	0,7391304	0,0680529	2	EM-5C	35	0,43478	0,3194
8	EM-6C	42	0,7391304	0,0680529	3	EM-6A	35	0,43478	0,3194
9	EM-9C	42	0,7391304	0,0680529	0	EM-7A	35	0,43478	0,3194
10	EM-1B	40	0,6521739	0,1209829	3	EM-8A	35	0,43478	0,3194
11	EM-	40	0,6521739	0,1209829	3	EM-	35	0,43478	0,3194

SELECTION OF PLASTIC INJECTION MACHINE WITH AXIOMATIC DESIGN APPROACH

1	3B		13	87	2	9A		3	71
1	EM-7B	40	0,6521739	0,1209829	3	EM-14B	35	0,43478	0,3194
2	7B		13	87	3	14B		3	71
1	EM-8B	40	0,6521739	0,1209829	3	EM-11B	33	0,34782	0,4253
3	8B		13	87	4	11B		6	31
1	EM-12C	40	0,6521739	0,1209829	3	EM-4A	32	0,30434	0,4839
4	12C		13	87	5	4A		8	32
1	EM-13B	40	0,6521739	0,1209829	3	EM-10A	32	0,30434	0,4839
5	13B		13	87	6	10A		8	32
1	EM-2A	38	0,5652173	0,1890359	3	EM-12A	32	0,30434	0,4839
6	2A		91	17	7	12A		8	32
1	EM-4C	38	0,5652173	0,1890359	3	EM-14A	32	0,30434	0,4839
7	4C		91	17	8	14A		8	32
1	EM-6B	38	0,5652173	0,1890359	3	EM-5B	30	0,21739	0,6124
8	6B		91	17	9	5B		1	76
1	EM-9B	38	0,5652173	0,1890359	4	EM-11A	30	0,21739	0,6124
9	9B		91	17	0	11A		1	76
2	EM-11C	38	0,5652173	0,1890359	4	EM-10C	28	0,13043	0,7561
0	11C		91	17	1	10C		5	44
2	EM-14C	38	0,5652173	0,1890359	4	EM-5A	25	0	1
1	14C		91	17	2	5A		0	1

While the ones with the highest numerical values in the horizontal column were considered the best, the ones with the lowest numerical values were interpreted as the worst, and the value corresponding to each data in the vertical column was calculated as the degree of satisfaction. This process is described in detail below.

The satisfaction level and I information content of the EM-5 B

brand plastic injection molding machine with a screw diameter of 30 mm were calculated as in equation 4.1. The largest screw diameter is 48 mm, the lowest screw diameter is 25 mm. The screw diameter of the brand model to be calculated is 30 mm.

$$Ms_{30} = \frac{30 - 25}{48 - 25} = 0,217391304$$

$$I_{30} = 1 \times (0,217391304 - 1)^2 = 0,612476371$$

Using this formula, the features obtained from the survey results of all brands and models were calculated in the same way. The information content for the degrees of satisfaction and machine features obtained from the catalog data of all the machines and models to be selected were calculated and listed in the Microsoft Office Excel program.

Table 6. Total Information Contents

No.	Machine Model	Total of Interest Content	No.	Machine Model	Machine Model
1	EM-1C	5,23663	22	EM-11A	8,47718
2	EM-7C	5,3402	23	EM-9A	8,92608
3	EM-7B	5,48291	24	EM-4C	9,20831
4	EM-1B	5,54027	25	EM-2C	9,34904
5	EM-7A	6,00269	26	EM-4B	9,39732
6	EM-13C	6,16682	27	EM-3C	9,62972
7	EM-1A	6,32001	28	EM-3B	9,68079
8	EM-13B	6,54546	29	EM-4A	9,78536

**SELECTION OF PLASTIC INJECTION MACHINE WITH AXIOMATIC DESIGN
APPROACH**

9	EM-8C	6,69043	30	EM-2B	9,92011
10	EM-8B	6,7338	31	EM-14C	10,03969
11	EM-12C	6,95294	32	EM-14B	10,12719
12	EM-11C	7,00569	33	EM-3A	10,17399
13	EM-12B	7,24061	34	EM-14A	10,5068
14	EM-13A	7,32032	35	EM-10C	10,61035
15	EM-8A	7,37167	36	EM-6C	10,99224
16	EM-10B	7,71107	37	EM-6B	11,12937
17	EM-11B	7,84138	38	EM-6A	11,36671
18	EM-9C	7,98609	39	EM-2A	11,52816
19	EM-12A	8,18403	40	EM-5C	13,8839
20	EM-9B	8,30261	41	EM-5B	14,38497
21	EM-10A	8,45295	42	EM-5A	15,47775

In Suh's original axiom of knowledge technique, the information content of each functional requirement can easily be summed up in other terms without a weighting factor. The alternative with the smallest information content is the best design.

The application results according to the knowledge axiom are listed in Table 6. The optimum injection molding machine with the smallest information content was determined as EM-1C.

REFERENCES

Akkurt, S. (1995): *Plastic Materials Technology*, İ.T.Ü. Faculty of Machinery Offset Workshop İstanbul, 5-11.

Akyüz, Ö. F. (1998): *Introduction to Plastics and Plastic Injection Technolo-*

gy, PAGEV Publications Kaptan Offset İstanbul, 28-31,46-48,91-93,150-151.

Aly, A. ve Colton, J. (2019). The design and manufacturing of fluidic oscillators for composite aircraft structures, *Proceedings of the Institution of Mechanical Engineers Part B-Journal Of Engineering Manufacture*, Volume: 233, Issue: 4, Pages: 1250-1259.

Benavides, E. M., Lara-Rapp, O. (2019). Ideal output for a robust conceptual design process, *Journal Of Engineering Design*, Volume:30, Issue: 4-5, Pages: 103-154.

Cebi, S. ve Kahraman, C. (2019). A new weighted fuzzy information axiom method in production research, *Journal of Enterprise Information Management*, Volume: 32, Issue: 1 Pages: 170-190.

Çebi, S.; Çelik, M.; Kahraman, C. (2008): "Gemi Sistemleri İçin Entegre Bakım-Onarım Yönetimi Gereksiniminin Analizi", *Havacılık ve Uzay Teknolojileri Dergisi* Temmuz, 3, 4 17-24.

Chen, B., Hu, J., Chen, W. (2019). Dre-based semi-automation of the axiomatic design transformation: from the functional requirement to the design parameter, *Journal Of Engineering Design*, Volume: 30, Issue: 7, Pages: 255-287.

Erdem, V. , Belevi, M. & Koçhan, C. (2010). Taguchi Metodu ile Plastik Enjeksiyon Parçalarda Çarpılmanın En Aza İndirilmesi, *Dokuz Eylül Üniversitesi Mühendislik Fakültesi Fen ve Mühendislik Dergisi* , 12 (2) , 17-29.

Fargnoli, M., Haber, N., Sakao, T. (2019). PSS Modularisation: A customer-driven integrated approach, *International Journal Of Production Research*, Volume: 57, Issue:13, Pages:4061-4077.

Goo, B., Lee, J., Seo, S., vd. (2019). Design of reliability critical system using axiomatic design with FMECA, *International Journal of Naval Architecture and Ocean Engineering*, Volume: 11, Issue:1, Pages: 11-21.

Ighravwe, D. E., Oke, S.A. (2019). A multi-criteria decision-making framework for selecting a suitable maintenance strategy for public buildings using sustainability criteria, *Journal of Building Engineering*, Volume: 24, Article Number: Unsp 100753.

Özel, B.; Özyörük, B. (2007): "Bulanık Aksiyomatik Tasarım İle Tedarikçi Seçimi", *G.Ü.Müh.Mim. Fak Dergisi*, 3 415-423.

Slătineanu, L.; Coteață, M.; Hrițuc, A.; Dodun, O.; Nagîț, G. (2022); The use of some principles from axiomatic design in the case of an equipment for the study of electrochemical machining, *Nonconventional Technologies Review / Revista*

**SELECTION OF PLASTIC INJECTION MACHINE WITH AXIOMATIC DESIGN
APPROACH**

de Tehnologii Neconventionale, Vol. 26 Issue 3, p28-33

Suh, N.P. , (2001).: *Axiomatic Design – Advances and Applications*, Oxford University Press, New York.

Uzun, İ. M. (2020), *A New Model Proposal for The Design Of Occupational Health and Safety Management System With Axioms And Measurement of Performance Specific To The Construction Sector*, Doctorate Thesis, Yildiz Technical University, Institute of Pure and Applied Sciences.

Yavuz, M.; (2010). *Axiomatic Design Approach to Machine Equipment Selection*' Master Thesis, Marmara Uni. Institute of Pure and Applied Sciences, İstanbul, Türkiye

Yiu, N.S., Chan, D.W., Sze, N. N., vd. (2019). Implementation of safety management system for improving construction safety performance: a structural equation modelling approach, *Buildings*, 9, 89.

Zhao, Q., Cao, Y., Liu, T., vd. (2019). Tolerance specification of the plane feature based on the axiomatic design, *Proceedings Of The Institution Of Mechanical Engineers Part CJournal Of Mechanical Engineering Science*, Volume:233, Issue: 5 Pages: 1481-1492

FINE-KINNEY RISK ANALYSIS METHOD STUDY AT THE HAZARDOUS WORKPLACE MANUFACTURING METAL MATERIAL FOR THE DEFENSE INDUSTRY

Zehra Gülten YALÇIN¹, Muhammed Bora AKIN¹, Mustafa DAĞ¹

Abstract: A study was carried out to eliminate the existing risks using the Fine-Kinney method in a company in the hazardous workplace class that produces metal materials for the defense industry. This method enables to detect hazards in the current working environment before an accident occurs and to minimize or eliminate the possibility of an accident. In the Fine-Kinney method, risk assessment is the study of eliminating high risks by looking at decision and action levels. Accordingly, the risks between 0 and 20 are not considered. If there is no legal requirement for risks between 20 and 70, no precautions are taken. For the risks between 70 and 200, it is obligatory to carry out necessary precautionary studies. A short-term action plan should be taken for risks between 200 and 400. If it is over 400, the work should be interrupted, and necessary measures should be taken immediately. Existing hazards in the workplace are electrical leakage, absence of fire extinguishers at the designated points, absence of first aid certified personnel, electric shock and/or fire, use of plug and socket, grounding, cable mess, tripping, falling, electric shock and fire because of cables with worn insulation, use of ungrounded hand tools, hot burrs, using frayed cable insulation in humid and wet areas, the absence of insulation in the panels, the lack of panel grounding, the use of uninsulated

¹ Çankırı Karatekin University, Department of Chemical Engineering, Çankırı / Türkiye,
e-mail: zaltin@karatekin.edu.tr, Orcid No: 0000-0001-5460-289X
e-mail: mbakin@karatekin.edu.tr, Orcid No: 0000-0003-3841-1633
e-mail: mudag@karatekin.edu.tr, Orcid No: 0000-0001-9540-3475

sockets, maintenance by unauthorized persons, compressor maintenance by unauthorized persons, electrical parts, contact with electrical parts and/or installations, not determining the placement points of fire extinguishers, expired fire extinguishers has been determined as 480. In this study, the determinations made as "very high risk" with $R > 400$, there are also determinations made as "high risk" with $200 < R < 400$. As a result of the risk analysis study, measures to be taken to reduce very high and high risk results to acceptable risks were determined. Finally, the desired acceptable risk level was obtained by reaching the value of $R < 20$.

Keywords: Fine-Kinney Risk Analysis, Defense Industry, Hazardous Workplace

INTRODUCTION

The scope of the defense industry for a country consists of the studies carried out for the design and development of the equipment used in peacetime or war, whether strategic or not for weapons and similar materials. Defense industry closely follows the works also related to itself. Looking at the historical development of Turkish defense history, it is seen that from the establishment of the Ottoman Empire until the 17th century, studies were carried out in the field of defense industry. This process has come to a standstill since the 19th century and has fallen behind the many countries because it could not keep up with the start of industrialization in the world. With the proclamation of the republic in the country, the "General Directorate of Military Factories" was established, and this institution had a say in the development of the country's defense industry.

The establishment of small arms repair shops in Ankara was followed by the establishment of a military factory in Kırıkkale. Between the years 1933-1939, a new structuring was needed in the field of defense industry, with the acceleration of industrial studies, which are the basis of the defense industry. As a result of these needs, the Machinery and Chemical Industry Institution was established with the Law No. 5591

dated March 15, 1950 and a new structuring was made with the factories and facilities transferred from the General Directorate of Military Factories (Baran, 2018). The defense industry attaches great importance to industrial studies for the purpose of national security (Dunne vd., 2002). Turkey is a candidate to come to an important place in the future with the investments and developments it has made in the field of defense industry. Currently, the largest share of the defense industry and production is carried out in the USA. China, Russia, and the EU are considered among the important countries in the other defense industry in the world, respectively. Brazil, India, Israel and Turkey are new countries in the defense industry (Sezgin and Sezgin, 2018).

The practices made by considering the employee in working life in Turkey are seen in the "Dilaver Pasha Regulations" published in 1865 and the "Maadin Regulations" in 1869. In the Republican period, this issue was studied in all aspects in working life. In the literature research, it is seen that the Dilaver Pasha Regulations examine the rest and vacation times of Ereğli and Zonguldak coal basin workers, their accommodation needs, working hours and their health issues. On the other hand, it is seen that the legal regulations related to the work safety covering the people working in the mine are made in the Regulations of Mines. In the Maadin Regulations, some changes were made in the working time regarding the workers in the coal mine. In this period of compulsory working hours, this kind of change is the first example of humane treatment of working life. With the establishment of the Turkish Grand National Assembly, it is seen that studies related to employee health and working in a safe environment have been carried out. At a time when the National Struggle was most intense, the Law of Ereğli Havza-i Fahmiyesi Mine Workers (Law No. 151 on the Law of Ereğli Coal Basin Miners) was enacted on September 10, 1921, during the Sakarya War. The Labor Law No. 3008 enacted in 1936 covers basic occupational health and safety provisions. After the Second World War, the necessary regulations were not included in the working life for the employees. It is seen that the

same decisions were made in the Labor Law No. 931 enacted in 1967 and the Labor Law No. 1475 enacted in 1971. With the industrial revolution in a period of about 200 years, the Labor Law No. 1475 was deemed sufficient for a certain period of working life. At the end of the 20th century and the beginning of the 21st century, developments in the entire industrial field showed themselves with the developing technology. At the European Union's summit in December-1999, with the recognition of Turkey's candidacy status, the Labor Law No. 4857 was enacted in 2003.

The provisions of this Law regarding occupational health and safety, except perhaps a few articles, were transferred from the Labor Law No. 1475. However, the regulations that should be issued according to the Labor Law No. 4857 were harmonized according to the European Union's framework directive 89/391/EEC and other individual directives and were published consecutively in 2003 and 2004. Occupational Health and Safety Law No. 6331 was enacted on June 29, 2012 and put into effect as of January 1, 2013, and subsequently, the occupational health and safety legislation in our country has been equipped with modern provisions (Çiçek & Öçal, 2016). This new law differs from the previous law numbered 4857 with a proactive approach in line with the needs of working life (Altın vd., 2018).

A healthy and safe working environment was neglected in Turkey until 2012. Studies show that most accidents are caused by the behaviour of employees in an unsafe environment. It stated that about 10% was due to an insecure situation. In the light of these determinations, Law No. 6331 primarily required the employer to include the employees, together with a preventive, protective and remedial approach. To protect the employees from all kinds of hazards, the employer is obliged to determine the existing hazards in the workplace and to work on minimizing or eliminating them. Efforts are being made to ensure that employees participate in training and avoid all kinds of hazardous behaviours in the working environment (Dursun, 2013). The law, "health surveillance of

employees in the context of ensuring a healthy and safe working environment, must be prepared in advance for emergency situations, and in sufficient numbers, qualifications and appropriate personal protective equipment (PPE) and use of safety signs, workplace environment, supervision, etc. it obliges employers to take technical and administrative measures” (Occupational Health and Safety Law No. 6331, 2012) (Karahmetoğlu, 2019). 2012 No. 6331 Occupational Health and safety law which entered into force on the date of enterprises covering all of one of the most important sanctions of “risk assessment, or the obligation to do so” 28512 published in the Official Gazette numbered 29.12.2012 date risk assessment and the regulation entered into force (Özkılıç, 2005). Occupational Health and Safety Law No. 6331 covers all public-private employees. It has been prepared based on a proactive (preventive) approach.

Risk assessment is primarily the whole of the work done to protect the employee, the workplace, and the environment from harm. Risk assessment studies consist of identifying hazards in the workplace, identifying and analysing of risks, deciding on risk control measures, updating the documentation and studies, and renewing when necessary (Kacir and Taçgın, 2017).

Definitions Used in Risk Analysis

Hazard: It refers to the potential for harm or damage that exists in the workplace or may come from outside, which may affect the employee or the workplace.

Risk: The probability (combination of probability and severity) of loss, injury, or other harmful consequence resulting from a hazard.

Accident: It is an event that causes physical and mental discomfort to employees or those directly or indirectly related to the enterprise, immediately or afterwards, when faced with a hazard.

Near-miss: Events that occur without causing injury, ill-health or death are called “No-damage- Near-miss”.

Incident: A work-related action that causes or has the potential to cause injury, ill health, or death.

Risk assessment: It refers to the studies to be carried out in order to determine the hazards that exist in the workplace or that may come from outside, to analyze and rank the factors that cause the hazards to turn into risks and the risks arising from the hazards, and to decide on control measures.

Acceptable risk: It is the level of risk that will not cause loss or injury, in accordance with legal obligations and the workplace's prevention policy.

Prevention: It is the name given to the whole of the preventive works carried out to minimize or eliminate the risks that are high after risk analysis in the workplace.

Risk Management: It is all of the initiatives carried out to ensure, improve and maintain the health and safety conditions of an organization [2,3].

Risk Assessment Team

The risk assessment is carried out by a team formed by the employer.

- Employer or employer's representative, occupational safety specialists and occupational physicians who carry out health and safety services in the workplace, employee representatives in the workplace, support staff in the workplace.

The employer is obliged to meet all the necessary needs such as all kinds of tools, equipment, space, and time in order for the persons assigned in risk assessment studies to fulfil their duties. The employer can-

² <https://www.resmigazete.gov.tr/eskiler/2012/12/20121229-13.htm>, (Access Date: 10.10.2022)

³ <https://www.csgeb.gov.tr/yayinlar/raporlar/is-sagligi-ve-guvenligi/> (Access Date: 10.10.2022)

not restrict their rights and powers due to the execution of their duties. The persons assigned has to come together with the employees to represent all units in the workplace and conduct a risk assessment study (Boz Eravcı, 2019).

Employer/Employer's Attorney: It carries out a risk assessment in terms of occupational health and safety to ensure, maintain and improve the health and safety of the working environment and employees.

Occupational Safety Specialist: Engineers, architects, or technical staff, who are authorized by the Ministry to work in the field of occupational health and safety, and have occupational safety expertise, and participate in risk analysis studies.

Occupational Physician: They are authorized by the Ministry to work in the field of occupational health and safety, have an occupational medicine certificate and participate in risk analysis studies.

Employee representative: It is an employee who is elected unanimously or by appointment among the employees authorized to participate in the work related to occupational health and safety, to monitor the work, to request measures, to make proposals and to represent the employees.

All Directors: As a result of the risk assessment, it ensures that the proposed control measures are implemented according to the action plan. In cases such as the purchase of a new product, project, process, machine and in cases where it deems necessary, the employer requests the employer's representative to perform or repeat the risk assessment process.

Support staff: It refers to the person who has the appropriate equipment and sufficient training, who has been specially assigned in the fields of prevention, protection, evacuation, firefighting, first aid and similar issues related to occupational health and safety, in addition to his primary duty. Support staff participates in risk analysis studies.

Risk Assessment Steps

Risk assessment is carried out by following the stages of identifying hazards, identifying, and analyzing risks, deciding on risk control measures, updating documentation, updating the work done, and renewing when necessary, starting from the establishment stage in the workplace.

1. Identification of Hazards: It is the process of examining and analyzing all kinds of effects that may harm employees and workplace equipment in the working environment.

2. Evaluation of Hazards: In the first step, it is the evaluation process of the precautions to be taken in the process of identifying and evaluating the hazards for each unit in the company.

3. Identification and Analysis of Risks: In the second step, the weight ratios of the risks are calculated separately for each of the hazards for which risk grading is decided, the rating is made, and the risks are prioritized.

4. Implementation of Control Measures: It is the practice in which high risks are determined and preventive studies are carried out in the process of identifying and analyzing risks.

5. Inspection, Monitoring and Review: All stages and implementation of risk management in the workplace are regularly audited, monitored and deficiencies are reviewed. A suitable control period is determined for the high risk values to prevent them from reoccurring, where necessary preventive measures are taken. Implementation plans are made for non-urgent measures that require a certain cost and time (Ersoy and Çelenk Kaya, 2019).

Risk Assessment Method

1. Risk assessment is a study in which starting from the establishment stage in workplaces, identifying hazards, identifying, and analyz-

ing risks, deciding on risk control measures, documentation, updating the work done and renewing when necessary are followed.

2. While the risk assessment study of the employees is carried out, it is ensured that their opinions are taken by participating in the process at every needed stage.

3. Considering each of the identified hazards separately, it is determined how often the risks that may arise from these hazards may occur, and who, what, how and in what severity may be harmed by these risks. While making this determination, the effect of existing control measures is also taken into consideration.

4. The information and data collected from the risks determined in the light of the characteristics of the business activities in the workplace, and the workplace factors such as the nature of the risk or hazard or selected on the basis of the constraints of national or international standards will be analysed using a combination of one or more methods.

5. If the analysis is made for separate sections, it is handled and concluded as a whole, considering the interactions of the sections.

6. Analysed risks are listed and written down to decide on control measures, starting with the one with the highest risk level according to the magnitude and importance of their effects.

7. A planning is made to control the risks ranked according to the magnitude and importance of their effects.

8. To eliminate the risk completely, and if this is not possible, the following steps are applied to reduce the risk to an acceptable level.

1) Elimination of hazard or sources of hazard

2) Replacing the hazardous with a non-hazardous or less hazardous one.

3) Fighting risks at the source (Cündübeyoğlu and Kayabaşı, 2022).

The Fine-Kinney Method was used in the realization of these studies.

METHOD

Fine-Kinney risk analysis method

The Fine-Kinney risk analysis method is a frequently used risk method. With this method, analysis and prevention studies are carried out by classifying the risks separately for each department in the workplace.

Three parameters are used while working. The risk score is obtained by multiplying these three parameters and the risks are graded. Corrective and preventive actions are recommended according to the degree of risk (Altın vd., 2018). Risk scores are calculated by scoring and multiplying the probability of harm or damage, the frequency of exposure to the hazard, and the impact it will create even if the hazard occurs. The values to be given to these parameters are shown in Table 1. Table 2 is used to calculate the risk score and Table 3 is used for the risk assessment results. Table 4 contains the data in which the numerical value of the risk is interpreted.

This method is a method that ensures that the hazards in the working environment are detected before they cause an accident and that they are improved starting from the highest priority according to the risk score.

With the application, the risks that may cause work accidents and occupational diseases in the enterprise are evaluated and suggestions for improvement are made to prevent them (Bayram & Çelenk Kaya, 2022).

Risk Value calculated as

Risk Value = $I \times F \times D$.

Here I is probability, (between 0.2-10), F is frequency, (between 0.5-10) and D is degree of results.

Probability: The probability that harm or damage will occur over time.

Table 1. Fine Kinney Method Probability Scale (Altin vd., 2018; Bayram & Çelenk Kaya, 2022)

Severity Scale	Explanation
1	Must be considered (insignificant, harmless, or mild)
3	Important (minor damage, low loss of work, first aid may be required)
7	Serious (Loss of workforce, external treatment, significant damage)
15	Very serious (Environmental impact, loss of limb, disability)
40	Disaster (heavy environmental impact, total disability, death)
100	Catastrophe (Significant environmental disaster, multiple deaths)

Frequency: The frequency of exposure to hazard.

Table 2. Fine Kinney Method Frequency (exposure) scale (Altin vd., 2018)

Frequency Scale	Explanation
0.5	Very rare (less than once a year)
1	Extremely rare (once or several times a year)
2	Rare (once or several times a month)
3	Occasionally (once or several times a week)
6	Often (once or several times a day)
10	Continuous (continuous or multiple times per hour)

Degree: It is the severity of the damage or damage that the hazard will cause on people, workplace, and environment in case of realization.

Table 3. Fine Kinney Method Probability Values (Altin vd., 2018)

Probability value	Explanation
0.2	Practically meaningless
0.5	Weak probability
1	Pretty low probability
3	Rare but can happen
6	Strongly probable
10	Very strong probability

According to the risk value results between 0 and 20, control may not be required. In order to ensure that it does not pose a significant hazard, it is examined, and work can be carried out to take measures if necessary. The required trainings are given to the personnel.

Table 4. Fine Kinney Method Risk Assessment Result (Altin vd., 2018)

Risk Value	Explanation
R<20	Acceptable risk (may not require immediate action)
20<R<70	Definite risk (must be included in action plan)
70<R<200	Significant risk (must be included in the annual action plan and paid attention to)
200<R<400	High risk (must be included in short-term action plan)
R>400	Very High (precautions should be taken by interrupting work immediately)

For risk values between 20 and 70, if there is no legal requirement, there is no need to take precautions. However, control methods that ensure that the risk taken in the action plan is kept at this level should be implemented.

A corrective and preventive action must be planned for the risk values between 70 and 200. Preventive studies planned for risks with a score of 70 and above and those responsible should be determined.

A short-term action plan is made for risk values between 200 and 400. The convening of the board is ensured, and the improvement works are started within a few months.

In case of risks exceeding 400, the work should be interrupted, and necessary precautions should be taken. In this process, it may be necessary to stop the work, close the facility and the building against any work accident.

Scoring should be reviewed after remediation work is complete. For those whose score is still 70 and above after improvements, the measures should be revised and renewed. Despite all precautions, for studies that fall outside the acceptable risk values, the relevant persons should be notified about the subject and necessary precautions should be taken (Altın vd., 2018).

Renewal of Risk Assessment Study

Risk assessment made according to the hazard class:

In very hazardous workplaces, at the latest 2 years

In hazardous workplaces, at the latest 4 years

It should be renewed at least every 6 years in less hazardous workplaces.

The risk assessment is completely or partially renewed, considering that the new risks that may arise in the following situations affect the whole or a part of the workplace (Oturakçı vd., 2015).

Moving business or making changes to buildings.

Occurrence of work accident, occupational disease or near miss event.

Changes in technology, materials and equipment used in the workplace.

Changes in the production method.

Legislative changes regarding the limit values of the working environment.

Requirement based on the results of working environment measurement and health surveillance.

The emergence of a new hazard that originates from outside the workplace and may affect the workplace (Şengöz & Merdan, 2017).

RESULTS

Existing risks were determined by the Fine-Kinney method in the company that produces metal parts for the defense industry, and if the risk value is $R > 400$, it has been determined that it has a very high risk value. Current hazards are listed as electricity leakage, absence of fire extinguishers at designated points, lack of first aid certified personnel, electric shock and fire, use of plugs and sockets, tripping, falling, electric shock, fire, cables with worn insulation, and use of ungrounded hand tools, hot burrs, worn cable insulation, use in damp and wet areas, lack of insulation in the panels, not grounding the panel, use of uninsulated sockets, intervention of unauthorized persons, maintenance of the compressor by unauthorized persons, electrical parts and installation contact, the points where the fire extinguishers will be placed are not determined, the filling date of the fire extinguishers has passed. The precautions to be taken in the section where the risk is very high are listed as follows. Leakage current relays should be available and should be checked once a month. Use of insulating gloves, boots and helmets should be provided for electrical work. Fire extinguishers should be placed in designated places and warning signs should be hung on them. First aid certified personnel should be available as 1 person for every 10 personnel.

Electrical appliances should be checked monthly, body grounding should be done. It must be ensured that no one other than the electrician interferes with the defective tool. Personal protective equipment should be used. Workspace arrangement should be made. Training on working with electricity should be given. There should be residual current relays in the panels. Fire extinguishers should be available in certain parts of the working areas. There should be insulating mats in all places where there is a risk of electric shock and in front of electrical panels. All electrical systems must be in closed, locked panels, and warning signs must be hung. All panels must have a residual current relay. Cables should not be used directly by plugging into sockets, cable joints should be made with terminal blocks, and mobile cables should be passed from above in the spiral pipe. Plug and socket system suitable for the power of the voltage should be used.

Personal protective equipment should be used. Workspace arrangement should be made. Employees should be trained in working with electricity. Cables should not be routed through walkways. Worn out cables should not be used. All electrical work should be handled by a certified electrician. Worn out, deformed cables should not be used, no splices should be made. Grounding should be done, existing should be checked and reported annually. A visor should be used, and work should be done away from any flammable or combustible material. Damaged frayed cables should be replaced by a qualified electrician. If the working area is wet or humid, it should be worked after drying. If drying is not possible, it should be waited for drying and work should be started after that. Missing parts should be detected and completed by the electrical department. Grounding should be done by authorized electricians, once a year, the report should be kept.

Sockets should be checked and insulated and/or made. All kinds of electrical maintenance and repair activities should be done by authorized persons in electricity. Compressors should be maintained annually by

authorized technical personnel and a control report should be prepared. While the compressor is being installed, its contact with the electrical installation should be prevented. Access of unauthorized persons to the electrical equipment of the machines should be prevented. Electrical faults and adjustments must be made by authorized persons. At least 1 6 kg fire extinguisher should be placed in every 250 m² and its location should be marked so that it can be seen by the workers. Fire extinguishers whose filling date has passed should be filled once a year and visually inspected once in 6 months. With these protective measures, the risk value has been reduced to $7.5 < R < 20$. The risk level has been reduced also to $7.5 < R < 20$, with preventive studies carried out in the high-risk range of $200 < R < 400$.

The hazards identified as high risk are as follows: Putting the CNC machine on the metal stand, working in closed areas, ventilation, panel covers open, unauthorized intervention, absence of insulating mat in front of the panels, damaged electrical connections, interaction of sparks during grinding with electrical components, malfunction of foot pedal, stacking heavy materials, tripping, slipping, falling, heavy lifting, material falling, hand-foot sticking, throwing material into the work area, working with ladders, noise, removal of parts protecting from the machine, putting the hand under the mold while the machine is in operation, absence of personal protective equipment (PPE), not being used PPE, parts falling on workers' feet, not using shields of CNC, maintenance of CNC being carried out by unauthorized persons, absence of operating instructions, canceling the CNC two-hand use system, absence of personal protective equipment (PPE), not using of PPE, splashing burr pieces, absence of machine shields, absence of compressor operating instructions, inability to reach in a short time the worker who had an accident, use of chemical materials, failure to conduct an emergency drill. As can be seen in the Appendix, the risk value has been reduced to an acceptable risk by carrying out protective measures to minimize the existing hazards.

CONCLUSION and RECOMMENDATIONS

In the Fine-Kinney risk assessment study conducted in the company, which was determined as a hazardous workplace, the workplace was handled in sections and studies were carried out. The legal basis of the hazards and the existing hazards, risks, responsibilities, precautions to be taken and the maximum time required for the elimination of the hazards are determined.

The measures to be taken are determined according to the size of the existing risk values. Coloring was done on the risk analysis evaluation table in order of importance to eliminate the risks. Considering the current situation, the risks are listed in order of importance from the largest to the smallest. The risks that were determined above the acceptable risk level were reduced to the acceptable risk level after the employer took precautions and the work continued.

In the future work process, the risk analysis should also be renewed in case of revisions specified in the occupational health and safety risk assessment regulation. Since 2012, Turkey has seriously focused on occupational health and safety studies due to the increasing number of occupational accidents and the negative consequences of these accidents.

REFERENCES

- Altın, Z. G., Dag, M., Oz, A., & Aydogmus, E. (2018). Risk Analysis by FMEA Method in Hotel. *Physical Chemistry and Functional Materials (JPCFM)*, 1(1), 59-65.
- Baran, T. (2018). Türkiye’de Savunma Sanayi Sektörünü İncelenmesi ve Savunma Harcamalarının Ekonomi Üzerindeki Etkilerinin Değerlendirilmesi. *Uluslararası İktisadi ve İdari Bilimler Dergisi*, 4, 58-81. <https://doi.org/10.29131/uiibd.429369>
- Bayram, H., & Çelenk Kaya, E. (2022). Fine-Kinney Metodu İ le Risk Analizi : Trabzon Liman Örneği. *Gümüşhane Üniversitesi Sağlık Bilimleri Dergisi*, 11(2), 760-783.
- Boz Eravcı, D. (2019). 6331 Sayılı İş Sağlığı ve Güvenliği Kanunu İlgili

Yönetmelikleri Çerçevesinde İşverenİN Yükümlülükleri. *Hak İş Uluslararası Emek ve Toplum Dergisi*, 8(22), 330–355. <https://doi.org/10.31199/hakisderg.644319>

Cündübeyoğlu, İ., and Kayabaşı, R. (2022). Seramik Fabrikasında Fine-Kinney Yöntemi ile Risk Değerlendirmesi. *European Journal of Science and Technology*, 35, 633–642. <https://doi.org/10.31590/ejosat.1061103>

Çiçek, Ö., & Öçal, M. (2016). Dünyada Ve Türkiye’de İş Sağlığı Ve Güvenliğinin Tarihsel Gelişimi. *Hak İş Uluslararası Emek ve Toplum Dergisi*, 5(11), 106–129. <http://dergipark.gov.tr/hakisderg/issue/24441/259080>

Dunne, J. P., Alonso, M. G., Levine, P., & Smith, R. (2002). Concentration in the International Arms Industry. *Working Paper. Department of Accounting, Economics and Finance, Bristol Business School, University of the West of England, Bristol.*, 1–14. <http://ideas.repec.org/p/uwe/wpaper/0301.html>

Dursun, S. (2013). İş Güvenliği Kültürünün Çalışanların Güvenli Davranışları Üzerine Etkisi. *SGD-Sosyal Güvenlik Dergisi*, 3(2), 61–75.

Ersoy, S., and Çelenk Kaya, E. (2019). Bir Kamu Üniversitesi Gıda Mühendisliği Laboratuvarları Risk Analizi Uygulaması. *Gümüşhane Üniversitesi Sağlık Bilimleri Dergisi*, 8(4), 411–423.

Kacı, E., and Taçgın, E. (2017). 6331 Sayılı İş Sağlığı ve Güvenliği Kanunu kapsamında proaktif yaklaşım üzerine risk değerlendirme ve bazı öneriler. *The Journal of Marmara Social Research*, 12, 1–16.

Karahmetoğlu, A. (2019). 6331 Sayılı İş Sağlığı ve Güvenliği Kanunu Bağlamında Soma Madenlerinin İş Sağlığı ve Güvenliği Açısından Değerlendirilmesi. *Sosyal Siyaset Konferansları Dergisi/Journal of Social Policy Conferences*, 89–128. <https://doi.org/10.26650/jspc.2019.76.0005>

Oturakçı, M., Dağsuyu, C., & Kokangül, A. (2015). A New Approach to Fine Kinney Method and an Implementation Study. *Alphanumeric Journal*, 3(2), 83–92. <https://doi.org/10.17093/aj.2015.3.2.5000139953>

Özkılıç, Ö. (2005). Risk Değerlendirmesi. *İş Müfettişleri Dergisi*, 16–21.

Altın, Z. G., Dağ, M., Oz, A., & Aydogmus, E. (2018). Risk Analysis by FMEA Method in Hotel. *Physical Chemistry and Functional Materials (JPCFM)*, 1(1), 59–65.

Baran, T. (2018). Türkiye’de Savunma Sanayi Sektörünü İncelenmesi ve Savunma Harcamalarının Ekonomi Üzerindeki Etkilerinin Değerlendirilmesi.

Uluslararası İktisadi ve İdari Bilimler Dergisi, 4, 58-81.
<https://doi.org/10.29131/uiibd.429369>

Bayram, H., & Çelenk Kaya, E. (2022). Fine-Kinney Metodu İ le Risk Analizi: Trabzon Liman Örneği. Gümüşhane Üniversitesi Sağlık Bilimleri Dergisi, 11(2), 760-783.

Boz Eravcı, D. (2019). 6331 Sayılı İş Sağlığı ve Güvenliği Kanunu İlgili Yönetmelikler Çerçevesinde İşveren Yükümlülükleri. Hak İş Uluslararası Emek ve Toplum Dergisi, 8(22), 330-355. <https://doi.org/10.31199/hakisderg.644319>

Cündübeyoğlu, İ., and Kayabaşı, R. (2022). Seramik Fabrikasında Fine-Kinney Yöntemi ile Risk Değerlendirmesi. European Journal of Science and Technology, 35, 633-642. <https://doi.org/10.31590/ejosat.1061103>

Çiçek, Ö., & Öçal, M. (2016). Dünyada Ve Türkiye'de İş Sağlığı Ve Güvenliğinin Tarihsel Gelişimi. Hak İş Uluslararası Emek ve Toplum Dergisi, 5(11), 106-129. <http://dergipark.gov.tr/hakisderg/issue/24441/259080>

Dunne, J. P., Alonso, M. G., Levine, P., & Smith, R. (2002). Concentration in the International Arms Industry. Working Paper. Department of Accounting, Economics and Finance, Bristol Business School, University of the West of England, Bristol., 1-14. <http://ideas.repec.org/p/uwe/wpaper/0301.html>

Dursun, S. (2013). İş Güvenliği Kültürünün Çalışanların Güvenli Davranışları Üzerine Etkisi. SGD-Sosyal Güvenlik Dergisi, 3(2), 61-75.

Ersoy, S., and Çelenk Kaya, E. (2019). Bir Kamu Üniversitesi Gıda Mühendisliği Laboratuvarları Risk Analizi Uygulaması. Gümüşhane Üniversitesi Sağlık Bilimleri Dergisi, 8(4), 411-423.

Kacı, E., and Taçgın, E. (2017). 6331 Sayılı İş Sağlığı ve Güvenliği Kanunu kapsamında proaktif yaklaşım üzerine risk değerlendirme ve bazı öneriler. The Journal of Marmara Social Research, 12, 1-16.

Karaahmetoğlu, A. (2019). 6331 Sayılı İş Sağlığı ve Güvenliği Kanunu Bağlamında Soma Madenlerinin İş Sağlığı ve Güvenliği Açısından Değerlendirilmesi. Sosyal Siyaset Konferansları Dergisi/Journal of Social Policy Conferences, 89-128. <https://doi.org/10.26650/jspc.2019.76.0005>

Oturakçı, M., Dağsuyu, C., & Kokangül, A. (2015). A New Approach to Fine Kinney Method and an Implementation Study. Alphanumeric Journal, 3(2), 83-

92. <https://doi.org/10.17093/aj.2015.3.2.5000139953>

Özkılıç, Ö. (2005). Risk Değerlendirmesi. *İş Müfettişleri Dergisi*, 16–21.

Sezgin, Ş., and Sezgin, S. (2018). Defense industry in the world and in turkey: an overview. *Eurasian Journal of Researches in Social and Economics (EJRSE)*, 5(12), 1–19.

Şengöz, M. C., & Merdan, M. (2017). Fine-Kinney Risk Analizi Metoduyla, İş Yerlerinde Elektrik Nedenli Yangınların Önlenmesinde Yeni Bir Yöntem. *Gazi Mühendislik Bilimleri Dergisi (GMBD)*, 3(3), 74–82. .
<https://dergipark.org.tr/en/pub/gmbd/issue/31064/372670?publisher=gjeb>;

INTERNET SOURCES

Ministry of Labor and Social Security (2012). Occupational Health and Safety Risk Assessment Regulation. Official Gazette (Number: 28512). <https://www.resmigazete.gov.tr/eskiler/2012/12/20121229-13.htm> (Access Date: 10.10.2022).

Ministry of Labor and Social Security (2012). Occupational Health and Safety Law Report (Number 28339). <https://www.csgeb.gov.tr/yayinlar/raporlar/is-sagligi-ve-guvenligi/> (Access Date: 10.10.2022).

Appendix. Risk assessment report table

RISK ASSESSMENT REPORT														RA. Release Date				
														RA. Revision No.				
														RA. Revision Date				
														Page No				
-TABLE-																		
Company Name / Address:																		
No	Hazards	Risk	The Current Situation	Rating of Risk				Fine-Kinney Method: Decision Plan by Risk Level	Precautions to Take	Fine-Kinney Method: Deadline Plan by Risk Level	Rating of Risk After Taking Precautions				Correction date	Fine-Kinney Method: Decision Plan by Risk Level		
				Pos-sibility	Fre-quency	Effe-ct	Risk Value				Risk Level	Decision	Per-iod	Re-spon-sible			Pos-sibility	Fre-quency
1	Electric Leakage	Electrical Shock		6	3	40	720	R>400	Very High Risk	1. Leakage current relays should be available and should be checked once a month. 2. The use of insulating gloves, boots and hard hats should be provided in electrical work.	15-30 DAY	Employer	1	0.5	40	20	R<20	Acceptable Risk
2	Absence of Fire Extinguisher	Inability to Fight		6	2	40	480	R>400	Very High Risk	Fire extinguishers should be placed in	15-30 DAY	Employer	1	0.5	40	20	R<20	Acceptable Risk

**FINE-KINNEY RISK ANALYSIS METHOD STUDY AT THE HAZARDOUS
WORKPLACE MANUFACTURING METAL MATERIAL FOR THE DEFENSE IN-
DUSTRY**

	at the Determined Points	ht the Fires							k	designated places and warning signs should be hung on them.									k
3	Absence of First Aid Certified Personnel	Inability to Respond to Emergencies	6	2	40	480	R>400	Very High Risk	First aid certified personnel should be available for 1 person for every 10 personnel.	15-30 DAY	Employer	1	0.5	40	20	R<20	Acceptable Risk		
4	Electrical Shock and/or Fire	Injury and/or Death	6	2	40	480	R>400	Very High Risk	1. Electrical tools should be checked monthly, body grounding should be done. 2. It must be ensured that no one other than the electrician interferes with the defective tool. 3. Personal protective equipment should be used. 4. The work area should be arranged. 5. Training on working with electricity should be	15-30 DAY	Employer	1	0.5	40	20	R<20	Acceptable Risk		

**FINE-KINNEY RISK ANALYSIS METHOD STUDY AT THE HAZARDOUS
WORKPLACE MANUFACTURING METAL MATERIAL FOR THE DEFENSE IN-
DUSTRY**

									and warning signs must be hung. All panels must have a leakage current relay. Cables should not be used directly by plugging into sockets, cable joints should be made with terminal blocks, and mobile cables should be passed from above in the spiral pipe. Plug and socket system suitable for the power of the voltage should be used.									
6	Trip, Fall, Electrical Shock, Fire	Injury and/or Death	6	2	40	480	R>400	Very High Risk	1. Personal protective equipment should be used 2. Work area arrangement should be made. 3. Training should	15-30 DAY	Employer	1	0.5	40	20	R<20	Acceptable Risk	

**FINE-KINNEY RISK ANALYSIS METHOD STUDY AT THE HAZARDOUS
WORKPLACE MANUFACTURING METAL MATERIAL FOR THE DEFENSE IN-
DUSTRY**

		tact with Flammable Gases or Liquids																	
10	Worn Cable Insulation	Electrical Shock	6	2	40	480	R>400	Very High Risk	Damaged and frayed cables should be replaced by a qualified electrician.	15-30 DAY	Employer	1	0.5	40	20		R<20	Acceptable Risk	
11	Usage of Device in Humid and/or Wet Areas	Electrical Shock	6	2	40	480	R>400	Very High Risk	If the working area is wet or humid, it should be worked after drying. If drying is not possible, it should be waited for drying itself and work should be started after that.	15-30 DAY	Employer	1	0.5	40	20		R<20	Acceptable Risk	
12	Absence of Insulation in Electric Panels	Electrical Shock	6	2	40	480	R>400	Very High Risk	The missing ones should be determined and completed by the Electricity Unit.	15-30 DAY	Employer	1	0.5	40	20		R<20	Acceptable Risk	
13	Absence of Grounding of	Electrical Shock	6	2	40	480	R>400	Very High Risk	Grounding should be done by authorized	15-30 DAY	Employer	1	0.5	40	20		R<20	Acceptable Risk	

**FINE-KINNEY RISK ANALYSIS METHOD STUDY AT THE HAZARDOUS
WORKPLACE MANUFACTURING METAL MATERIAL FOR THE DEFENSE IN-
DUSTRY**

17	Contact with Electrical Parts and/or Installations	Fire , Injury and /or Death	6	2	40	480	R>400	Very High Risk	report should be prepared. 1. While the compressor is being installed, its contact with the electrical installation should be prevented. 2. Access to the electrical equipment of the machines by unauthorized persons should be prevented. 3. Electrical repairs and adjustments should be made by authorized persons.	15-30 DAY	Employer	1	0.5	40	20	R<20	Acceptable Risk
18	Failure to Determine the Points Where the Fire Extinguishers will be Located	Inability to Respond to Fire in Emergency Situations	6	2	40	480	R>400	Very High Risk	At least one 6 kg fire extinguisher should be placed for every 250 m2 and its location should be marked so that it can be seen by the workers.	15-30 DAY	Employer	1	0.5	15	7.5	R<20	Acceptable Risk

19	Being Out of Date of Expiration Date of the Fire Extinguishers	In-ability to Respond to Fire in Emergency Situations		6	2	40	480	R>400	Very High Risk	Fire extinguishers whose filling date has passed should be filled once a year and visually inspected once in 6 months.	15-30 DAY	Employer	1	0.5	15	7.5	R<20	Acceptable Risk
20	Inserting the sheet metal stand into the CNC machine	Injury, Amputation		3	3	40	360	200<R<400	High Risk	It should be ensured that the system stops automatically when the hand reaches out during the operation of the machine.	3 MONTH	Employer	1	3	3	9	R<20	Acceptable Risk
21	Working in Confined Areas, Ventilation	Poisoning		3	3	40	360	200<R<400	High Risk	1. When working with chemical substances in closed areas, the working areas should be ventilated mandatory and masks should be used. 2. In single person works, the working area should be	3 MONTH	Employer	1	0.5	40	20	R<20	Acceptable Risk

**FINE-KINNEY RISK ANALYSIS METHOD STUDY AT THE HAZARDOUS
WORKPLACE MANUFACTURING METAL MATERIAL FOR THE DEFENSE IN-
DUSTRY**

										checked at appropriate time intervals.								
22	Having Panel Covers Open	Electrical Shock, Injury and /or Death		3	3	40	360	200 < R < 400	High Risk	Panel covers should always be kept closed.	3 MONTH	Employer	1	0.5	40	20	R < 20	Acceptable Risk
23	Intervention by Unauthorized Persons	Electrical Shock		3	3	40	360	200 < R < 400	High Risk	Information of authorized persons should be written on the board, and workers should be made aware of this.	3 MONTH	Employer	1	0.5	40	20	R < 20	Acceptable Risk
24	Absence of Insulating Mats in Front of Electrical Panels	Electrical Shock		3	3	40	360	200 < R < 400	High Risk	Insulating mats should be available in front of all panels.	3 MONTH	Employer	1	0.5	40	20	R < 20	Acceptable Risk

No	Hazards	Risk	Th e C urrent Situation	Rating of Risk				Fine-Kinney Method: Decision Plan by Risk Level		Precautions to Take	Fine-Kinney Method: Deadline Plan by Risk Level		Rating of Risk After Taking Precautions				C or re cti on date	Fine-Kinney Method: Decision Plan by Risk Level	
				Pos sibility	Fre quency	E ff ect	Ri sk V al	Ris k Level	De cision		Pe-ri-od	Re-spo-nsi-ble	Pos sibility	Fre quency	E ff ect	Ri sk V		Ris k Level	De cision

25	Damaged Electrical Connections	Electrical Shock	3	3	40	360	200 < R < 400	High Risk	Plug-socket connections must be intact, broken and damaged parts must be repaired by persons competent in electricity.	3 MONTH	Employer	1	0.5	40	20	R < 20	Acceptable Risk
26	Interaction of Sparks Emitted During Grinding with Electrical Components	Fire	3	3	40	360	200 < R < 400	High Risk	The placement of the bench grinder should be done in such a way that it does not interact with the electrical components.	3 MONTH	Employer	1	0.5	40	20	R < 20	Acceptable Risk
27	Broken foot pedal	Injury, Amputation	3	3	40	360	200 < R < 400	High Risk	The top of the foot pedal should be covered, and it should be constantly checked that the pedal is working properly. No one other than the operator should use it.	3 MONTH	Employer	1	3	3	9	R < 20	Acceptable Risk
28	Stacking of In-	In-	6	3	15	270	200 < R < 400	High	1. The height of	3 M	Em plo	1	0.5	15	7.5	R < 20	Ac ce

**FINE-KINNEY RISK ANALYSIS METHOD STUDY AT THE HAZARDOUS
WORKPLACE MANUFACTURING METAL MATERIAL FOR THE DEFENSE IN-
DUSTRY**

	Heavy Materials	jury due to Falling Materials					R<400	Risk	the stacking should not exceed 3 meters 2. While stacking, stacking should be done by entering inward as the level increases in the form of a pyramid.	ON TH	yer						pta ble Risk
29	Trip, Slip, Fall, Heavy Lifting, Material Drop, Hand and Foot Impingement	Injury	6	3	15	270	200<R<400	Hig h Risk	1. The work area should be organized and unused materials should not be kept in the work area. 2. Personal protective equipment should be used. 3. Necessary training should be given to the employee. 4. Penetrating objects such as nails should be removed from the work area.	3 M ON TH	Em plo yer	1	0.5	15	7.5	R<20	Ac ce pta ble Risk
30	Throwing Material	Injury	6	3	15	270	200<R<400	Hig h Risk	Material throws should be controlled	3 M ON TH	Em plo yer	1	0.5	15	7.5	R<20	Ac ce pta ble

	into the Work Area						0		in the work area.									Risk
31	Work with Ladder	Injury and /or Death from Falling from a Ladder	6	3	15	270	200<R<400	High Risk	Stairs should be worked with a 3-point contact system, double-winged ladders should be used, and the stair steps should be solid.	3 MONTH	Employer	1	0.5	15	7.5		R<20	Acceptable Risk
32	Fall due to Slide	Injury	6	3	15	270	200<R<400	High Risk	Railings should be made on the stairs and the steps should be wide enough.	3 MONTH	Employer	1	0.5	15	7.5		R<20	Acceptable Risk
33	Noise	Hearing Losses	6	3	15	270	200<R<400	High Risk	Ear protector should be used while working.	3 MONTH	Employer	1	0.5	15	7.5		R<20	Acceptable Risk
34	Removing Machine Guards	Injury	6	3	15	270	200<R<400	High Risk	The machine whose guard has been removed must not be started or used.	3 MONTH	Employer	1	0.5	15	7.5		R<20	Acceptable Risk
35	Putting the Hand Under the Mold While the Machine	Injury, Amputation	6	3	15	270	200<R<400	High Risk	Hands should be kept away from the molds while the machine is running.	3 MONTH	Employer	1	0.5	15	7.5		R<20	Acceptable Risk

**FINE-KINNEY RISK ANALYSIS METHOD STUDY AT THE HAZARDOUS
WORKPLACE MANUFACTURING METAL MATERIAL FOR THE DEFENSE IN-
DUSTRY**

	Is Working																	
36	Absence of Personal Protective Equipment (PPE), Not Used	Injury		6	3	15	270	200<R<400	High Risk	Personal protective equipment should be provided and used.	3 MONTH	Employer	1	0.5	15	7.5	R<20	Acceptable Risk

No	Hazards	Risk	The Current Situation	Rating of Risk				Fine-Kinney Method: Decision Plan by Risk Level	Precautions to Take	Fine-Kinney Method: Deadline Plan by Risk Level	Rating of Risk After Taking Precautions				Corrective Action Date	Fine-Kinney Method: Decision Plan by Risk Level		
				Possibility	Frequency	Effect	Risk Value				Period	Responsibility	Possibility	Frequency			Effect	Risk Value
37	Falling of Work-piece onto Feet	Injury		6	3	15	270	200<R<400	High Risk	The worker working with the corner press machine should be provided with steel-toed shoes that will protect her feet in case of a falling piece and he should be made to use it.	3 MONTH	Employer	1	0.5	15	7.5	R<20	Acceptable Risk
38	Not Using CNC	Amputa-		6	3	15	270	200<R<400	High Risk	The machine whose	3 MONTH	Employer	1	0.5	15	7.5	R<20	Acceptable Risk

	Machine Guards	tion , In-jury					400	k	guard has been removed must not be started or used.	TH								ble Risk
39	Maintenance of CNC by Unauthorized Persons	In-jury	6	3	15	270	200<R<400	Hig h Risk	Machine maintenance should be done by authorized technical personnel or have it do by authorized someone else.	3 MONTH	Employer	1	0.5	15	7.5		R<20	Acceptable Risk
40	Absence of Operating Instructions	In-jury	6	3	15	270	200<R<400	Hig h Risk	1. The operating instructions of the machine to be worked on should be prepared and hung in a place where it can be seen easily. 2. The worker must be informed and complied with.	3 MONTH	Employer	1	0.5	15	7.5		R<20	Acceptable Risk
41	Cancellation of Two-Hand Operation System on CNC	In-jury	6	3	15	270	200<R<400	Hig h Risk	The machine usage instructions should be followed and no external intervention should be	3 MONTH	Employer	1	0.5	15	7.5		R<20	Acceptable Risk

**FINE-KINNEY RISK ANALYSIS METHOD STUDY AT THE HAZARDOUS
WORKPLACE MANUFACTURING METAL MATERIAL FOR THE DEFENSE IN-
DUSTRY**

									allowed.										
42	Absence of Personal Protective Equipment (PPE), Not Used	Injury	6	3	15	270	200 < R < 400	High Risk	Personal protective equipment should be provided and used.	3 MONTH	Employer	1	0.5	15	7.5		R < 20	Acceptable Risk	
43	Splashing of Burr	Injury	6	3	15	270	200 < R < 400	High Risk	Machine guards should not be removed, goggles or visors should be used.	3 MONTH	Employer	1	0.5	15	7.5		R < 20	Acceptable Risk	
44	Not Using Machine Guards	Amputation, Injury	6	3	15	270	200 < R < 400	High Risk	The machine whose guard has been removed must not be started or used.	3 MONTH	Employer	1	0.5	15	7.5		R < 20	Acceptable Risk	
45	Absence of Operating Instructions	Injury	6	3	15	270	200 < R < 400	High Risk	1. The operating instructions of the machine should be prepared and hung at a point where it can be seen easily. 2. The worker must be informed and complied with.	3 MONTH	Employer	1	0.5	15	7.5		R < 20	Acceptable Risk	
46	Splashing of	Injury	6	3	15	270	200 < R < 400	High Risk	Work clothes,	3 M	Employer	1	0.5	15	7.5		R < 20	Acceptable Risk	

	Work-piece						R<400	Risk	glasses or a visor should be provided to the worker working with a circular saw and should be made to use it.	ON TH	yer						pta ble Risk	
47	Not Using Machine Guards	Injury		6	3	15	270	High Risk	The machine whose guard has been removed must not be started or used.	3 MONTH	Employer	1	0.5	15	7.5		R<20	Acceptable Risk

No	Hazards	Risk	The Current Situation	Rating of Risk				Fine-Kinney Method: Decision Plan by Risk Level		Precautions to Take	Fine-Kinney Method: Deadline Plan by Risk Level		Rating of Risk After Taking Precautions				Correction date	Fine-Kinney Method: Decision Plan by Risk Level	
				Posi-bility	Fre-quency	Eff-ect	Risk Value	Risk Level	Decision		Pe-ri-od	Re-spo-n-sible	Posi-bility	Fre-quency	Eff-ect	Risk Value		Risk Level	Decision
48	Absence of Compressor Operating Instructions	Injury and/or Death		3	2	40	240	High Risk	1. Compressor usage instructions should be prepared. 2. It should be hung in a point where the employee can see it easily. 3. The	3 MONTH	Employer	1	0.5	40	20		R<20	Acceptable Risk	

**FINE-KINNEY RISK ANALYSIS METHOD STUDY AT THE HAZARDOUS
WORKPLACE MANUFACTURING METAL MATERIAL FOR THE DEFENSE IN-
DUSTRY**

49	Failure to Reach in a Short Time the Worker Who Had an Accident	Injury or Death	3	2	40	240	200 < R < 400	High Risk	The worker should be informed about this issue. The worker should never be worked alone.	3 MONTH	Employer	1	0.5	40	20	R < 20	Acceptable Risk
50	Using Chemical Materials	Exposure to Chemicals (Poisoning, Injury, Occupational Disease)	3	2	40	240	200 < R < 400	High Risk	1. Material safety data sheets should be announced to the relevant persons. 2. Forms should be kept in the work area. 3. Employees should be given training on the subject.	3 MONTH	Employer	1	0.5	40	20	R < 20	Acceptable Risk
51	Emergency Drill	Failure to Intervene Effectively in Emergency	3	2	40	240	200 < R < 400	High Risk	Emergency drills should be conducted and reported at regular intervals every year.	3 MONTH	Employer	1	0.5	40	20	R < 20	Acceptable Risk

